(Unclassified)

PRELIMINARY DESIGN AND EXPERIMENTAL INVESTIGATION
OF THE FDL-5A UNMANNED HIGH L/D SPACECRAFT
Part II - Parametric Configuration Development and Evaluation

C. F. Ehrlich and F. L. Guard

*** Export controls have been removed ***

> DOWNGRADED AT 3 YEAR INTERVALS;
> DECLASSIFIED AFTER 12 YEARS.
> DOD DIR 5200.10

This document is subject to special export controls and each transmittal to foreign giverments or foreign nationals may be made only with prior approval of the Air Force Flight Dynamics Laboratory, Wright-Patterson Air Force Base, Ohio.

(U) FOREWORD

(U) This is the final report of work performed under Contract No. AF33(615)-5241, "Preliminary Design of Two Volumetrically Efficient High L/D Unmanned Flight Test Vehicles". This report was prepared under Project 1366, "Aerodynamics and Flight Mechanics", Task 136616, "Synthesis of Hypersonic Vehicles".

(U) The work was sponsored by the Aerospace Vehicle Branch, Flight Mechanics Division, Air Force Flight Dynamics Laboratory. The research investigation was performed under the direction of the Air Force Project Engineer Mr. Thomas R. Sieron. Mr. C. J. Cosenza and Mr. A. C. Draper of AFFDL provided overall technical guidance.

(U) The work was accomplished by the Lockheed-California Company, Burbank, California and the report is also identified as LR 21204.

(U) This is Part II of a five part report:

Part I	Summary
Part II	Parametric Configuration Development and Evolution
Part III	Aerodynamics
Part IV	Aerothermodynamics
Part V	Vehicle Design

(U) This manuscript was released by the authors for publication in January 1968.

(U) The contributions of the following individuals to this report are gratefully acknowledged:

> H. D. Schultz
>
> C. P. Valery
>
> H. H. Drosdadt
>
> F. X. Hurley

(U) This technical report has been reviewed and is approved.

Philip P. Antonatos
Chief, Flight Mechanics Division
Air Force Flight Dynamics Laboratory

ii

(U) ABSTRACT

(U) The derivation of two volumetric efficient high L/D entry vehicles is
described. Parametric trades in the areas of aerodynamics and aerothermo-
dynamics are discussed and selected parameters are identified. Alternate
modes of vehicle recovery are described and the effect on vehicle design
determined. The evolution of the FDL-5 configuration selected for wind tunnel
testing is described through the presentation of a series of intermediate
configurations.

(U) This report is subject to special export controls and each transmittal
to foreign governments or foreign nationals may be made only with prior
approval of the Air Force Flight Dynamics Laboratory (FDMS) Wright-Patterson
Air Force Base, Ohio 45433.

(REVERSE SIDE IS BLANK)

CONTENTS

v

CONTENTS (Continued)

LIST OF FIGURES

UNCLASSIFIED

LIST OF FIGURES (Continued)

LIST OF FIGURES   (Continued)

LIST OF FIGURES (Continued)

LIST OF FIGURES (Concluded)

LIST OF TABLES

(U)   LIST OF SYMBOLS

a   major semi-axis of ellipse

b   minor semi-axis of ellipse

C_D drag force coefficient

C_L lift force coefficient

C_N normal force coefficient

C_ℓ rolling moment coefficient

C_m pitching moment coefficient

C_n yawing moment coefficient

H   altitude, ft

K   roll-out angle of fin or lateral surface, degrees

L   length, ft

L/D   lift-drag ratio

M   Mach number

P   pressure, lb/ft^2

q   heating rate, Btu/ft^2-sec

R   radius, ft

Re   Reynolds number

S   distance from leading edge, ft; area, ft^2

$\overline{S}$ ratio of area to reference area, S/S_{REF}

T   temperature, $^\circ F$

V   velocity, ft/sec, or volume, ft^3

X   characteristic dimension, ft

Y   lateral distance, ft

α vehicle angle of attack, degrees

β vehicle yaw angle, degrees

Γ dihedral angle, degrees

δ flow expansion or surface inclination angle, degrees

ϵ delta wing semi-apex angle, degrees or emissivity

ϵ_p dihedral wing panel angle, degrees

θ upper angle or boat-tail angle, degrees

Λ sweepback angle, degrees

τ fin toe-in angle, degrees

ϕ circumferential angle or fin roll-out angle, degrees

ϕ_s body side angle, degrees

Subscripts

c   chord

bt   boat tail

e   local value external to boundary layer or elevon

eff effective

f   flap

fin fin

fr   forward ramp

le   leading edge

N   nose lower ramp

REF reference

sl   stagnation line

TE   trailing edge

∞ freestream

(REVERSE SIDE IS BLANK)

SECTION 1

(U) INTRODUCTION AND APPROACH

(U) This preliminary design study of two volumetrically efficient high L/D unmanned flight test vehicles is a part of the continuing USAF Flight Dynamics Laboratory program to conduct basic research on hypersonic vehicle systems.

(U) This contract followed an earlier study title "Preliminary Design of Hypersonic High L/D Test Vehicles"(Ref. 1). In the earlier study, six high L/D entry vehicles were analyzed to establish the size, weight, and system requirements for conducting free flight research on high performance entry systems from orbital speed to landing.

(U) The present study was then focused on improving the hypersonic geometry and properties of a high L/D research vehicle. Specifically, the objectives were to configure an unmanned entry research vehicle having a hypersonic L/D of 3.0 at 20,000 fps and 200,000 feet altitude; and to confirm the vehicle performance through wind tunnel test. In addition to this requirement, the vehicle was to be designed for maximum volume with the relationship between volume and L/D to be identified. Horizontal recovery was the primary recovery mode, but alternate recovery concepts were to be investigated. A structure concept and the vehicle subsystems were to be selected based on earlier work and the experience gained in other USAF programs including ASSET, ASCEP, and PRIME.

(U) The contract effort was divided into two phases: the analytical phase consisted of the development of the parameters affecting the selection of candidate configurations; the experimental phase included supersonic and hypersonic wind tunnel testing of one candidate configuratic and selection of the structure and subsystems.

(U) In the analytical phase parametric study, over 200 relationships among configuration geometry, volume, aerodynamic heating, and aerodynamic perform, ance and stability were evolved. These data trends were based on hypersonic theories, results of ASSET flight data, and results of USAF AFFDL and Lockheed in-house wind tunnel tests of high performance lifting bodies. The sources for each of these data are documented in this final report. The purpose in developing these parameters was to provide the rationale for selecting the test geometry for the experimental phase.

(U) Two classes of configurations emerged from analytical phase studies: (1)a finned high volume geometry designated the HDL-35 series (a modification of

the F-5 geometry developed in the earlier study), and (2) a finless high volume geometry designated as the FDL-5 series.

(U) The FDL-5 was selected for wind tunnel testing and structure design during the experimental phase. Its size was varied during the study from 30 to 35 ft in length.

SECTION 2

(U) AERODYNAMICS

(U) This section describes the definition of aerodynamic effects due to
parametric perturbations of geometry about a baseline configuration. These
parametric variations were defined to assist in the selection and eventually
the development of the test configuration. They were principally determined
by using the analysis of subsonic, supersonic, and hypersonic wind tunnel
tests of the F-5 configuration (Refs. 2 and 3). Where test data were
inadequate for parametric evaluation, they were complemented by analytical
estimates. In all, 25 geometric parameters were varied. Table 1
identifies the vehicle characteristics which were evaluated as functions
of the geometric parameters. Variations in vehicle characteristics which
were negligible or not applicable (by inspection) were not evaluated. Many
of the vehicle characteristic trades require the consideration of several
parametric variations. This is particularly true of the stability and control
parameters, where control surface variables must be evaluated as well as
those of vehicle geometry and vehicle attitude. The following discussion
reviews the development of the parametric curves and the results of these
studies.

2.1 (U) DEVELOPMENT OF THE PARAMETRICS

(U) Aerodynamic data for the development of the parametric curves have been
obtained from experimental data and analytical estimates. The parametric
curves presented in this section have been developed from these data by deter-
mining the changes in the aerodynamic characteristics due to the geometric
variations. The curves were prepared by plotting either the data increments
or absolute magnitude as functions of the geometric variations.

2.1.1 (U) Geometric Variations

(U) The geometric properties varied were those judged to have effects on
vehicle aerodynamic characteristics. The geometric parameters considered are
defined in Section 2.2. The primary aerodynamic effects evaluated include
changes in L/D, C_m, C_{n_β}, and C_{l_β}. The effects on vehicle volume were estimated
for selected geometric variations and are presented in this section for
convenience.

2.1.2 (U) Wind Tunnel Data

(U) The experimental data utilized for developing the parametrics were obtained
from wind tunnel tests of the F-5 configuration, Figure 1. The development
of this vehicle concept is fully documented in Ref. 1 "Preliminary Design
of Hypersonic High L/D Test Vehicles." Supersonic data were obtained from
extensive tests (Ref. 2) in the Arnold Engineering Development Center (AEDC)

Table 1

(C) AERODYNAMIC TRADES

	L/D			C_m			C_{n_β}			C_{l_β}			VOL
	Sub	Super	Hyp	Sub	Super	Hyp	Sub	Super	Hyp	Sub	Super	Hyp	Ft^3
FINS:													
Toe-in, τ (Deg.)	+.102	-.018	-.046	*	*	*	-.00006	+.00019	+.00019	-.00006	-.0001	-.0001	2.64
Roll-out, K (Deg.)	+.042	0	A	*	*	*	-.00006	+.00002	+.00002	-.00006	-.00002	-.00002	.333
Camber, (% Chord)	+.11	A	A	*	A	A	-.00031	A	A	+.00006	A	A	A
Area, $\bar{S}$ (% Planform)	C	C	-.014	*	*	*	+.0006	C	D	-.0008	C	D	A
LE Sweepback, Λ_{Fin} (Deg.)	A	C	+.01	A	*	*	A	A	A	A	A	A	A
LE Radius, LER$_{Fin}$ (In.)	A	C	-.07	A	*	*	A	A	A	A	A	A	A
$\in$ Fir Area, $\bar{S}_\in$ (% Planform)	A	A	A	A	A	A	+.059	+.004	+.002	-.043	-.002	-.001	A
UPPER BODY:													
Length, L (Feet)	A	C	+.036	B	B	B	B	B	B	B	B	B	25.38
LE Sweepback, Λ_{Body} (Deg.)	A	C	+.007	A	A	A	A	A	A	A	A	A	-19.7
Side Roll-out, ϕ (Deg.)	A	0	C	A	*	*	A	C	*	A	C	+.00001	2.87
LE Radius, LER$_{Body}$ (In.)	A	0	0	A	A	A	A	A	A	A	A	A	A
Profile Angle, θ (Deg.)	C	C	0	A	*	*	A	0	0	A	0	0	17.15
Base Area, $\bar{S}_{Base}$ (% Planform)	-.17	A	A	B	B	B	B	B	B	B	B	B	6.53
Flap Area, $\bar{S}_F$ (% Planform)	-.19	-.02	0	*	*	B	B	B	B	B	B	B	B
Flap Deflection, δ_F (Deg.)	-.033	-.006	0	*	*	B	B	B	B	B	B	B	B
Elevon Area, $\bar{S}_E$ (% Planform)	-.06	C	+.0055	*	C	*	B	B	B	B	B	B	B
Elevon Deflection, δ_E (Deg.)	+.041	0	0	*	*	*	B	B	B	B	B	B	B
Fin Ramps, δ_R (Deg.)	A	-.045	-.045	D	B	*	A	A	A	A	A	A	2.11
Ailerons, δ_A (Deg.)	B	B	B	B	B	B	B	B	B	*	*	*	B
Nose Cap Radius, R (In.)	A	-.036	-.036	A	A	A	A	A	A	A	A	A	A
LOWER SURFACE:													
Nose Ramp Area, $\bar{S}$ (% Planform)	A	C	D	A	*	*	A	A	A	A	A	A	A
Nose Ramp Angle, δ_N (Deg.)	A	C	-.07	A	*	*	A	C	+.00008	A	C	-.000008	A
Dihedral Bottom, Γ (Deg.)	-.016	C	-.018	A	*	*	A	C	-.000036	A	C	-.00003	3.33
Curved Bottom, Γ Vol. Equiv. (Deg.)	-.016	C	-.018	A	*	*	A	C	-.000024	A	C	-.000026	3.33
Boat Tail	-.016	C	-.045	*	*	*	D	A	A	A	A	A	*

NOTE.

A. Negligible C. Hypersonic and Supersonic Trends Similar

B. Not Applicable D. Not Determined

(*) Complex Trade

Wind Tunnels A, B, and D at M = 2.5 to 8.0 in conjunction with AFFDL in-house studies. Subsonic data were obtained from tests (Ref. 3) in the Lockheed-California Company Low Speed Wind Tunnel at M = .26.

(U) These test programs were designed to determine the aerodynamic characteristics of the F-5 configuration, including the elevon and upper body flap effectiveness, toe-in and roll-out effects of the vertical fins, and, at low speed, the effects of landing gear and lower surface geometry. The tests were conducted in pitch and yaw at angles of attack up to a maximum of 60 degrees for the M = 8.0 tests, and for yaw angles up to 10 degrees; combined pitch and yaw data were obtained at all test Mach numbers. Additional knowledge of the aerodynamic characteristics of the F-5 configuration was obtained through the use of tufts on the subsonic model, and through oil flow visualization techniques on the supersonic model.

2.1.3 (U) Analytical Estimates

(U) The analytical techniques described in Ref. 1, have been employed in this study. They include the use of oblique-shock/Prandtl-Meyer expansion flow theory at supersonic and hypersonic speeds in combination with the viscous interaction skin friction analyses. Where appropriate, as indicated by the test results, tangent-cone or tangent-wedge prediction methods have been employed for estimating the local pressure coefficients. The low speed prediction methods include those outlined in the USAF DATCOM, Ref. 4. Since no data at M = 20 exists for the F-5 configuration, the analytical techniques for hypersonic velocities were substantiated by correlation with data from tests of The F-4 configuration (Figure 2) in the Cornell 96-inch shock tunnel at M = 19.2, (Ref. 5). As in the F-5 tests, data were obtained in pitch and yaw with elevon deflection. These data were correlated with analytical estimates in order to determine and evaluate the reliability of the analytical techniques which have been used.

(U) Variations in the viscous forces on the individual geometric elements are in general negligibly small for the parametric ranges considered. Consequently, the evaluation of the vast majority of the parametric changes was accomplished through application of easily mechanized pressure theories such as Newtonian. (Where viscous effects were significant, as in the case of the effect of length on L/D, they were included in the analysis.) These analyses were accomplished with the aid of the IBM 360 Arbitrary Body Computer Program which was developed from one furnished by AFFDL, Ref. 6. The method of describing the vehicle geometry to the program through the use of semi-automatically produced vehicle coordinates enabled the detailed description of specific configurations. From the configuration coordinate inputs the program determines local surface normals and pressure coefficients. These coefficients are then integrated to determine the total vehicle aerodynamic properties in pitch and yaw.

(U) Generally, the parametric data presented were developed employing a single analysis approach (i.e.: hand-calculated or computer-calculated). In certain cases, these approaches were combined to include the full advantages of each.

(Figure 32 of Section 2.2.2 is an example of this type of combined presentation.) The $\delta_N = 3$ degrees nose ramp curve was estimated using the detailed analytical techniques of Ref. 4. The aerodynamic increments (ΔC_N and ΔC_m) due to variation of δ_N about the nominal value were developed from the computer program. The combined predictions provide a very practical and useful illustration of trade-off effects.

2.2 (U) DISCUSSION OF THE PARAMETRIC RESULTS

(U) Results of the trade-off studies are summarized in Table 1. The values presented in this table are the slopes of the parametric curves at the F-5 design point, and may be considered as partial derivatives. Due to the nonlinearity of most of the data, these values are valid only for small perturbations and should not be considered much beyond the design point values. They do, however, provide a rapid assessment of the relative importance of each geometric parameter to L/D, stability, and volume. The parameters, Figure 3, are regrouped for discussion into two general areas: L/D and stability (longitudinal and lateral). Volume trades are also discussed with respect to the appropriate geometry.

2.2.1 (U) L/D Trades

2.2.1.1 (C) Equivalent Nose Radius. The trade-off was calculated using a hemispherical nose cap to represent the actual 2:1 elliptical inclined cap. Figure 4 shows that L/D_{max} decreases as effective nose radius increases. This reduction amounts to about .05 in L/D for the first 3 inches of radius, but as the nose cap becomes larger it becomes a more significant portion of the vehicle drag. As a result, the L/D penalty becomes significantly greater for further increases in nose radius. Cross plotting nose radius L/D increments from this figure with temperature increments (see Section 3.1.1) provides the curve of Figure 5. It is evident that further reduction of nose radius from 3 inches leads to undesirable increases in temperature for only small gains in L/D while the converse is true for increased radius.

2.2.1.2 (C) Leading Edge Radius and Sweep. At the reference leading edge sweep angle of 81.5 degrees and radius of 1.5 inches, Figure 6 shows that L/D varies about .005 per degree of sweep or per inch radius. As the sweep angle is decreased to gain volume and aspect ratio, the increments due to radius become more significant; for instance, at 78 degrees sweep the L/D decreases about .015 per inch radius. The increased leading edge heating associated with decreased sweep will, therefore, compound the L/D loss through the required increases in radii.

(U) A second effect of changes in leading edge sweepback is the corresponding change in configuration volume. Figure 7 shows the resulting variation of configuration volume with leading edge sweep angle for a 30 ft configuration length with a fixed body side angle of 58 degrees. The variation of volume and L/D with leading edge sweep is discussed under Body Length below.

2.2.1.3 (U) <u>Body Side Angle</u>. Variation of the body side angle about the nominal value of 58 degrees results in changes in L/D and longitudinal stability as seen in Figures 8 and 9. For $\phi < 58$ degrees, and $\Lambda_{LE} = 81.5$ degrees, the surface is out of the flow in the Newtonian sense, and so does not influence the aerodynamic characteristics. For larger angles, the high sweep angle ($\Lambda_{LE} = 81.5$ degrees) results in small drag and longitudinal moment increments. The lateral derivatives, C_{n_β} and C_{ℓ_β} however, are sensitive to body side angle as shown in Figure 10, since yawing induces destabilizing pressures with relatively large moment arms on the side surfaces.

(U) Cross plotting incremental L/D and volume side angle parametrics in Figure 11 reveals that volume increases through side angle increases are achieved at the expense of rapidly decreasing L/D.

2.2.1.4 (C) <u>Body Profile Angle</u>. Perturbations of the body profile angle also yield only small variations in the aerodynamic effects as noted in Figures 12, 13 and 14. While Newtonian theory predicts zero variation in L/D, cone theory indicates about .017 decrease in L/D per degree with increasing angle (Figure 12). The actual trend of the tradeoff lies between these limiting approaches. The L/D variation due to change in the body profile angle is a nearly linear function of volume as shown in Figure 15.

2.2.1.5 (C) <u>Equivalent Dihedral Angle</u>. The equivalent dihedral angle, (Γ), Figure 3, is based on the definition that the curved surface represented has the same volume as an equivalent dihedral surface with the indicated angle. The influence of lower surface perturbations has been reported in Ref. 7. For equivalent dihedral angles less than 10 degrees, small decrements on the order of .05 in L/D_{max} are experienced; increasing L/D penalties are realized with dihedral angles above 10 degrees. The influence of equivalent dihedral angle of L/D_{max} is shown in Figure 16. When the L/D and volume trades are cross-plotted, the knee in the curve apparent in Figure 16 is much more pronounced, as shown in Figure 17. Whereas initial designs considered 20 degree equivalent dihedral angles, the present analysis clearly indicates a more suitable compromise of 10 degrees.

2.2.1.6 (C) <u>Base Area</u>. The base area has little effect on hypersonic lift-to-drag ratio (since the base pressure coefficient varies approximately as $1/M^2$) but has a significant effect on aerodynamic drag, and consequently L/D, at subsonic and transonic speeds. The effect is readily apparent from Figure 18 in which the drag coefficient at L/D_{max} is shown to increase rapidly with increasing base area. In the wind tunnel data from the F-5 configuration tests, the base drag contributed about 30 percent of the total drag at L/D_{max}. These data are described in Ref. 8. Increasing the configuration volume by fairing to a larger base reduces the L/D_{max} value by approximately 1.0 for each 40 cubic feet in volume gained. Volume gained in this manner will therefore have a large impact on subsonic L/D. (Care must be taken when fairing to small base areas, however, to avoid premature flow separation and consequent drag increase.)

2.2.1.7 (C) Body Length. The variation of L/D_{max} with body length is primarily a function of the Reynolds number, since the skin friction increment is reduced as vehicle length increases. Figure 19 shows that to provide L/D_{max} of 3.0 for hypersonic flight, the F-5 design length must be increased to about 36 feet. It is significant that vehicle length is the only parameter for which an increase yields increased volume and increased L/D simultaneously. These effects assume that the boundary layer remains laminar. This is shown in Figures 20 and 21.

2.2.1.8 (C) The loss of L/D_{max}, with increased vehicle volume, is clearly illustrated in Figure 21 which superimposes early high L/D vehicles on a summary plot of vehicle geometry traits. Trends with specific parameter variations are also shown in this figure with the F-5 configuration as a base point.

2.2.2 (U) Stability Trade

(U) Discussion of the results of the parametric studies has thus far considered only the geometry trades necessary to maximize hypersonic L/D and volume. The remainder of the discussion will review the stability trades necessary to achieve a stable and controllable vehicle at hypersonic and subsonic speeds.

2.2.2.1 (C) Fin Toe-In and Roll-Out. The vertical fin toe-in and roll-out trade results are presented in Figures 1 through 11 of Reference 8. The influences on L/D_{max}, pitching moment, and directional stability as determined from test data, are shown in these figures. A qualitative assessment of the general trends is represented in Table 2. A trend favoring the selection of 5-degree toe-in was noted from the supersonic and hypersonic data: increased heating and loss of L/D limits the use of higher values, while a stability decrease limits the use of lower values of toe-in. At subsonic speeds, increased toe-in and roll-out angles provided increased L/D. Considerations of the trim requirements at L/D_{max} suggest an increase in toe-in and roll-out angles at supersonic and hypersonic speeds and a reduction in roll-out angles at subsonic speeds. However, at subsonic speeds, decreased toe-in and roll-out angles contributed to early pitch up. Slightly improved subsonic C_{m_O} characteristics were noted for increased roll-out angles. Conversely, at the same speeds, reduced toe-in angles improved C_{m_O}.

(C) Considerations of $C_{n\beta}$ and $C_{\ell\beta}$ revealed a mixed trend towards larger toe-in angles although the toe-in variation maximized L/D at $\tau = 6$ degrees at supersonic speeds. Roll-out angles, on the other hand, revealed a weak trend toward smaller angles. A knee in the curve for $C_{n\beta}$ versus roll-out angle at K = 25 degrees was noted, indicating that a reduced advantage would be gained from larger angles. Heating considerations present a strong justification to minimize toe-in and roll-out angles.

2.2.2.2 (C) Fin Leading Edge Sweep Angle. Both L/D and heating considerations demonstrate the favorable effect of increased sweep angles at hypersonic speeds. Figure 22 shows that L/D increments of about .01 per degree sweep may be expected at M = 20. At low speeds, increased sweep angles are expected to decrease the influence of the fins on the subsonic C_{m_O}.

Table 2

(c) TRENDS IN τ, K REQUIRED BY AERO PARAMETERS

	L/D	$C_{m_o}, C_{m_{L/D_{max}}}$	$C_{n\beta}$	$C_{\ell\beta}$	TEMP.
Toe-In (τ)					
Subsonic	large	small* (5° knee) (C_{m_o})	large (weak)	small (weak)	N/A
Supersonic	5° peak	large $(C_{m_{L/D_{max}}})$	large (limit 6°)	large	N/A
Hypersonic	small (5° knee)	ditto	ditto	ditto	small
Roll-Out (K)					
Subsonic	large	large (C_{m_o}) small* $(C_{m_{L/D_{max}}})$	small	small	N/A
Supersonic	N/A	large $(C_{m_{L/D_{max}}})$	25° knee	large	N/A
Hypersonic	N/A	ditto	ditto	ditto	small

* promotes unstable break in C_m/C_N curve at lower angles of attack

9

2.2.2.3 (C) <u>Fin Leading Edge Radius</u>. Figure 23 shows that about .05 in L/D at M = 20 may be realized by decreasing the leading edge radius to 1 inch from the design point of 1.5 inches. The increased heating which would normally be expected for this radius decrease may be avoided by simultaneously increasing the sweep angle as discussed above.

2.2.2.4 (C) <u>Fin Camber</u>. While no influence of fin camber on L/D at hypersonic or supersonic speeds is expected, significant effects are revealed at subsonic speeds by the test data as shown in Figures 12 and 13 of Reference 8. These data indicate the desirability of retaining positive camber.

2.2.2.5 (C) <u>Outboard Fin Area</u>. Outboard fin area significantly affects both L/D and stability at subsonic and hypersonic speeds. At low speeds, reduced fin area reduces the trim requirements on the elevons and upper body flaps although a degradation in L/D_{max} is noted. Corresponding decreases in $C_{n\beta}$ and $C_{\ell\beta}$ were also noted with decreasing fin area at low speeds. The low speed data are presented in Figures 14 and 15 of Reference 8. At hypersonic speeds, reduced fin area provides modest improvement in L/D_{max} due to the reduced axial force and significant variations in stability as shown in Figures 24 and 25. Trends noted from detailed study of the subsonic and supersonic wind tunnel test data toward a reference center of gravity of 64% of body length provide the criteria for required fin size. Figure 25 reveals that a fin size of 12.5% of the reference area will provide self-trimming capability at hypersonic speeds.

2.2.2.6 (C) <u>Outboard Fin Height</u>. The vertical position of the outboard fins on the body, in the absence of body upwash, is not expected to have significant effect on normal force, L/D, or pitching moment. The primary effect of position is expected to be a geometric increase of the fin moment arm about the longitudinal axis as shown in Figure 26. The resulting changes in rolling moment then are seen to be functions of geometry rather than flow properties. The effects on $C_{\ell\beta}$ and the dutch roll parameter, $C_{n\beta}/C_{\ell\beta}$, are illustrated in Figure 27. It is seen that the $C_{\ell\beta}$ increases with fin height; this is undesirable at subsonic speeds due to the already high $C_{\ell\beta}$. In addition, the dutch roll parameter decreases in magnitude from the F-5 value of -3. Thus, it is seen that increasing fin height shows no immediate advantage for the basic configuration.

2.2.2.7 (C) <u>Elevon Area</u>. While increases in exposed elevon area at hypersonic speeds are seen in Figure 28 to result in slightly increased values of L/D_{max}, they also yield increases in longitudinal stability (Figure 29). The L/D increases result from increased normal force due to the larger planform area with negligible increases in axial force. Similar variations are seen at subsonic speeds from test data as shown in Reference 3. These elevon size effectiveness data have been estimated assuming a linear variation in elevon effectiveness with area and fixed elevon deflection. No change was recommended from the F-5 geometry since decreased elevon size will be destabilizing hypersonically and increasing exposed elevon area will add a negative C_{m_O} increment subsonically (for $\delta_e = 0°$). However, subsonic C_{m_O} is sensitive to elevon area when configuration, installation geometry, and upward deflections are considered.

2.2.2.8 (C) <u>Nose Ramp Area</u>. The ramp size was determined from studies summarized in Reference 1, and presented in Figure 30. The results indicate a maximum ramp effectiveness at a ramp-to-planform area ratio of about .40.

2.2.2.9 (C) <u>Nose Ramp Deflection</u>. The effect of nose ramp angle on L/D_{max} at $M = 20$ is seen in Figure 31 to be negligible up to about 3 degrees. Beyond 3 degrees, increasing reduction of L/D_{max} is apparent. The effect of nose ramp angle on longitudinal stability is illustrated in Figure 32 which has been developed through a combination of analytical and Newtonian calculations. It may be seen from this figure that considerable flexibility in establishing longitudinal stability is available through variations in nose ramp angle. Similar flexibility was seen earlier through variations in elevon size and fin size. However, no increases in ramp angle from the F-5 value were desired since stability considerations show that the vehicle was self-trimming at high speeds, that is, L/D_{max} trimmed was obtained with zero elevon deflection. Conversely, decreased ramp angles would add an undesirable negative increment to C_{m_O}.

2.2.3 (U) <u>Aft Body Shaping Parametric Analysis</u>

(U) The preceding parametric trades coupled with the aerothermodynamic trades described in the next section, led to the derivation of the initial study configuration, designated HLD-35-1. After evaluation of this finned lifting body configuration, consideration was given to generating a true lifting body configuration without protruding fins for hypersonic stabilization. The evolution of the configuration is described in Section 5 of this volume. The following paragraphs describe the parametric trades made on the configuration afterbody shaping.

(U) To parametrically evaluate the aerodynamic effects of the aft body fairing on this class of configuration, it was necessary to systematically perturb the aft body geometry, maintaining the forebody geometry of the F-5 configuration. Several sets of alternate geometries were derived for three series of parametric variations. These geometries were programmed for analysis by the Arbitrary Body Computer Program to determine their aerodynamic characteristics.

2.2.3.1 (U) Series A. The first series of configurations considered, Series A, was one in which the aft side surfaces of the vehicle were gradually warped outward from a basic body shape to define various trailing edge roll-out angles (K_{TE}) (Figure 33). Three configurations thus generated were evaluated. These confined the variations to the area aft of station 280 as shown in Figures 34, 35 and 36. Alternate No. 1 eliminates the upper shoulder line sweep out by keeping the sides parallel. Alternate No. 2 increases the upper shoulder line sweep to K_{TE} value of plus 15 degrees at station 420. Alternate No. 3 retains the upper geometry but clipped the bottom planform from station 280 aft parallel to centerline.

(C) The L/D variations of these configurations are presented in Figure 37 for a constant angle of attack of 10 degrees (to simplify vehicle performance comparisons). A constant increment in C_A of .0104 for a 30-foot vehicle at M = 20, H = 200,000 ft was included in the L/D calculations to provide for skin friction forces. This increment was derived from the analysis of the 30 ft F-5 vehicle which had a similar wetted area (Reference 1). (L/D) max occurs at about α = 10 degrees for all configurations considered. Figure 37 shows the rapid degradation of L/D which occurred as K_{T_E} was increased from the basic body configuration which has planar body side surfaces with K_{T_E} = -33 degrees.

(C) Variations in the yaw stability parameter, $C_{n\beta}$, for the above configurations are shown in Figure 38 as a function of angle of attack. It can be seen from this figure that as K_{T_E} increases, the level of $C_{n\beta}$ increases (but at the expense of L/D as noted from Figure 37). The variations with angle of attack indicate, however, that the yaw stability of this series of configurations decreases significantly as α is increased.

(C) The longitudinal stability characteristics of these configurations are shown in Figure 39. It can be seen from this figure that the "A" series of vehicles fell within a narrow band which was both stable and trimmable for CG = .62L. It should be noted that the values presented are for Newtonian flow and will change as experimentally verified shock-expansion pressures are used. The use of two-dimensional, tangent-wedge pressure theory yields results which are different than those obtained using Newtonian flow theory. These differences are of great importance in the evaluation of vehicle longitudinal stability characteristics. Figure 40 presents the characteristics of the F-5 vehicle for both theories. Conversion to theoretically calculate tangent-wedge pressures yields a decrease in $+C_{m_O}$ and an increase in vehicle static margin.

(C) In an effort to maintain a hypersonic L/D value of about 3.0 while achieving adequate $C_{n\beta}$ at operational angles of attack, it was noted that some combination of the HLD 35-1 aft body with one of the A-series where $K_{T_E} \sim -25$ degrees would be desirable. This consideration led to the second series of configurations which were evaluated.

2.2.3.2 (U) Series "B". The second series of configuration variables which was evaluated is illustrated in Figure 41. This series is characterized by toed-in, rolled-out, lower aft surfaces (τ = 5 degrees, K = 25 degrees in combination with warped upper surfaces, where h/H (shoulder height to base height) was variable). The minimum h/H incorporated the A-series K_{T_E} = -25 configuration.

(U) This geometry comprises a "compression sharing" concept in which compression forces are shared by the upper and lower aft sides at low angles of attack. At higher angles of attack, the lower sides become more effective and the upper surfaces become less effective. This concept was evolved from the A-series and the previously-developed fin parametric variations.

(C) The L/D values of these three configurations (at α = 10 degrees) are shown in Figure 42. They are seen to be relatively high and constant for the values of h/H evaluated. The yaw stability characteristics of the vehicles, as a function of angle of attack, are presented in Figure 43. It can be seen from this figure that the B-4 configuration possesses a desirable level of yaw stability that is relatively constant with angle of attack.

(C) This second series of vehicles are longitudinally stable and trimmable for CG = .62I based on Newtonian flow pressures. These longitudinal stability results are shown in Figure 44.

2.3 (U) COMPRESSION-SHARING PARAMETRIC VARIATIONS

(U) A third series of parametric analyses of the lifting body vehicle was conducted. This series (Series "C") is based on the B-4 configuration discussed above. The purposes of this study were to more fully evaluate the aerodynamic influence of the vehicle surfaces involved in the compression sharing concept and to provide a ready reference for analyses of wind tunnel test data and subsequent configuration modification.

(U) The variables included in the parametric series are defined in Figure 45 and the ranges of values of each one set forth in Table 3. The C-1 configuration represents the B-4 configuration. In all cases, the nose cap and forward sections are common. The results shown in Figures 46 through 49 were estimated using the Arbitrary Body Computer Program.

Table 3

(C) "C" - SERIES OF AFT BODY PARAMETRIC VARIATIONS

Parameter	Lowest Values	Nominal Values	Highest Values
τ	4°	6°	8°
K	10°	20°	30°
h/H	0.50	0.75	1.00
b/B	0.70	0.85	1.00

2.3.1 (C) L/D$_{max}$ - (Figure 46)

(C) No strong influences on L/D$_{max}$ were noted for the toe-in, roll-out, and span parameters. The height parameter, h/H, did exhibit a substantial loss for values above 0.75; a slight "knee" in the curve appears at that point.

2.3.2 (C) Longitudinal Stability - (Figure 47)

(C) The variations show slight increases in stability for increases in
parameter values with the exception of the span parameter, b/B, where no
variation is noted. The slight variations of the trim point ($C_m = 0$) may be
a useful degree of freedom in later configuration modifications if the
accompanying variations in $C_{n\beta}$ are acceptable.

2.3.3 (C) Directional Stability - (Figure 48)

(C) The values of toe-in and roll-out for the C-1 geometry are near optimum
since variations tend to decrease $C_{n\beta}$. The substantial increase due to height
is achieved at the expense of L/D. Similarly, the increased $C_{n\beta}$ at low
angles of attack gained from increased shoulder span are at the expense of
subsonic L/D.

2.3.4 (C) Roll Parameter - (Figure 49)

No significant variations are noted. The configuration $C_{\ell\beta}$ is shown to be
sensitive to vertical C.G. Location.

(U) The preceding parametric data formed the basis for the configuration
evolution discussed in Section 5.

SECTION 3

(U) AEROTHERMODYNAMICS

(U) An investigation was conducted to determine the effects of vehicle geometry and attitude parameters on equilibrium surface temperature levels. The objective of the parametric study was to provide temperature data which, when used in conjunction with aerodynamic and structural considerations, would lead to the logical selection of a high-volume, high L/D configuration. As such, the temperature parametric data serve primarily as constraints due to material design limits.

(U) The scope of the aerothermodynamic parametric studies is shown in Table 4. For the various configuration elements this table lists the change in temperature per unit change in the parameter listed in the left hand column. Calculations were not performed where it was determined that a design change has a second order effect on the heating rate.

(U) The high lift-to-drag ratio configuration under study is characterized by a high fineness ratio delta wing planform. Figure 50 illustrates the significant geometric properties of the configuration and also serves to define the nomenclature used in the aerothermodynamic analysis. To achieve increased volume, various lower surface geometries were investigated including flat, curved and dihedral. Depending on the particular geometry, the lower surface is therefore defined at each station by a radius of curvature or a dihedral angle (Γ). A lower surface forward ramp is employed for stability purposes and is defined by the angle α_{fr}. A final lower surface parameter which was considered is the boattail angle, θ_{bt}, shown in Figure 50.

(U) A constant-radius cylindrical leading edge and an ellipsoidal nose cap were assumed. The ratio of the minor-to-major axes of the ellipse (aspect ratio) was assumed as 0.5. Leading edge orientation is specified by the quantity $\alpha_{\ell e}$ which is defined as the acute angle between the leading edge geometric stagnation line and the vehicle longitudinal axis.

(U) As shown in Figure 50, significant upper body geometric variables are the profile angle, θ, and the body side panel angle, ϕ_s. Fin parameters include the leading edge sweep angle (Λ_{fin}), toe-in angle (τ), and the rollout angle (ϕ).

(U) The aerothermodynamic parametric studies are based on a flight velocity and altitude of 21,000 fps and 200,000 feet for laminar flow; and 18,000 fps and 180,000 feet for turbulent flow. For the geometries and wing loadings of

15

interest, these two trajectory points approximate entry conditions during peak laminar and peak turbulent heating, respectively. Methods used to predict aerodynamic heating rates are described in Part IV. All temperatures and heating rates are based on radiation equilibrium conditions assuming a surface emissivity of 0.7. In the majority of the parametric studies, the design variations are considered to be perturbations of the baseline F-5 (Fig. 1) configuration at a design attitude of ten degrees angle of attack and zero yaw. Where appropriate, the F-5 design point is indicated on the figures by a circle on the curve or by an arrow on the abscissa.

3.1 (U) FIN PARAMETERS

(U) Figure 51 shows the effects of sweepback, roll-out, and toe-in on the fin stagnation line temperatures for a vehicle angle of attack of 10 degrees and a leading-edge radius of 1.5 inches. Near the F-5 design sweepback of 63 degrees, the stagnation line temperature decreases approximately 35°F for each degree of increased sweep. Increasing the roll-out angle from zero to 40 degrees increases the stagnation line temperature by about 150°F at zero toe-in and by 300°F at 10 degrees toe-in. Increasing the toe-in from zero to 10 degrees increases the temperature by 100°F for zero roll-out and by 250°F at 40 degrees roll-out.

(U) Figure 52 illustrates the effect of fin toe-in on the outboard panel temperature. The vehicle was assumed at zero yaw with a fin roll-out angle of 25 degrees. Temperatures are presented at a location of 3 feet measured along the direction of flow from the fin leading-edge stagnation line. For a toe-in angle of 5 degrees, the panel temperature is 1820°F and increases by approximately 40°F per degree increase in toe-in angle.

(U) Figure 53 shows the effect of roll-out angle on the fin outboard panel temperature at a distance of 3 feet along the panel surface in the direction of flow from the fin stagnation line. Heating rates were computed by laminar strip theory, and the effective angle of attack was determined from Eq. 6 (Part IV) assuming a toe-in angle of 5 degrees and zero yaw. A roll-out angle of 25 degrees increases the temperature by 225°F from the zero degree roll-out position. Throughout the range of roll-out angles investigated, the temperatures fall between 1600 and 1900°F which precludes the use of superalloy (assuming a 1500°F capability) for the outboard fin panels.

(U) The effect of leading-edge radius on fin stagnation line temperatures is shown in Figure 54. The effective sweepback angle is based on the F-5 design parameters listed on the figure. For a radius of 1.5 inches, the stagnation line temperature is 3230°F, and the rate of change is -300°F/inch.

(U) Of the fin geometric parameters investigated, toe-in angle is most significant for vehicle design since this variable exerts a dominant influence on the fin side panel temperature. Leading-edge sweep angle and radius are less important, as the stagnation line temperatures are generally within the capability of the material considered for use at this location (tantalum). Use of superalloy material in the fin side panels limits the toe-in angle to a value

of about two degrees, if the requirement of a 25-degree roll-out angle is maintained.

3.2 (U) WING LEADING EDGE PARAMETERS

(U) Figure 55 shows the effect of body sweepback angle on the leading edge stagnation line temperatures for a radius of 1.5 inches. For the range of sweep angles of interest, stagnation line temperatures decrease by about 37°F per degree of sweepback. The equilibrium temperature for the F-5 design (Λ = 81.5°) is 2870°F. Shown in Figure 56 is the effect of radius on leading-edge stagnation line temperatures, for a sweep angle of 81.5 degrees. At the design radius of 1.5 inches, the temperature slope is approximately -280°F/inch.

(U) The effect of leading-edge sweepback angle on flat lower surface center-line temperature is shown in Figure 57. The ratio of predicted temperature divided by the laminar strip value is plotted for angles of attack of 10 and 20 degrees. This analysis is based on the assumption that the only effect of leading-edge sweep is to vary the outflow correction factor which is applied to flat bottom delta configurations. For the F-5 design angle of attack (10 degrees), the effects of sweep are small on lower surface centerline temperature. The sweepback angle is assumed to have no effect on the center-line temperature of a curved lower surface since the heating rates are based on swept cylinder theory.

(U) Figure 58 shows the effect of nose radius on stagnation point tempera-tures. Calculations were performed for both a hemispherical nose and for an elliptical nose with a 2:1 aspect ratio, such as the F-5 design employs. The elliptical nose is about 300°F cooler than a hemispherical nose whose radius is equal to the major axis of the ellipse. For the F-5 design the stagnation point temperature is 4300°F.

(U) Small changes in wing leading-edge parameters are anticipated to have a negligible effect on material selection and structural concept for the base-line F-5 design and trajectory. For a flat lower surface, this is not true if the vehicle is required to operate at higher angles of attack near peak heat-ing due to the coupling between leading-edge sweep angle and lower surface temperature. For example, at 20 degrees angle of attack, if the sweep angle is increased from 81.5 to 83 degrees, the lower surface centerline temperature will increase approximately 10 percent. At the higher angle of attack, a similar temperature increase will result from the effect of lift coefficient variation on equilibrium glide altitude (Figure 344, Ref. 1). The combined temperature increase could preclude the use of coated columbium at forward lower surface locations.

3.3 (U) UPPER SURFACE PARAMETERS

(U) The effect of the body side angle on the upper side panel surface temper-ature is shown in Figures 59, 60, and 61. The flow deflection angle of the side panels is plotted in Figure 59 as a function of the vehicle angle of attack and the body side angle, ϕ_s, defined by the sketch. The deflection

angles were computed from Eq. 3 (Part IV) assuming a sweepback angle of 81.5 degrees, a forward ramp angle of 3 degrees, and zero yaw. The assumed effect of flow deflection angle on the side panel surface temperature one foot aft of the leading edge stagnation line is shown in Figure 60.

(U) Figure 61 illustrates the effect of the body side angle on the side panel temperatures, based on the flow deflection angles and temperature predictions of Figures 59 and 60. Temperatures are shown for vehicle angles of attack of 10, 15, and 20 degrees. This figure illustrates the rapid increase in surface temperature as the side panels change from expansion to compression surfaces. At a vehicle angle of attack of 10 degrees, the temperature one foot aft of the leading edge increases from 1230°F to 1640°F as the angle ϕ_s is increased from 55 to 65 degrees.

(U) Shown in Figure 62 is the effect of the profile angle θ on the upper body centerline temperatures. As was the case with the side panels, the predicted temperatures are a strong function of the flow deflection angle. As indicated by the arrow on the abscissa, the F-5 design employs a profile angle of six degrees, which results in a leeward surface throughout the angle of attack range of interest.

(U) Figure 63 shows the effects of the fin ramp angle on the ramp surface temperature distribution. As the ramp angle is increased above the vehicle angle of attack, this surface becomes windward and the temperature increases by approximately 100°F per degree of flow deflection. This analysis neglects localized problems such as the effects of shock wave-boundary layer interaction or a reduced radiation view factor to space, due to the presence of the fins and the body.

3.4 (U) CONTROL SURFACE PARAMETERS

(U) Figure 64 shows the effect of elevon deflection on the maximum elevon surface temperatures for a vehicle angle of attack of ten degrees. Temperatures are shown for attached laminar flow and for the reattachment point of separated laminar flow. The elevon deflection required for incipient separation was estimated from the data correlations of Popinski and Ehrlich (Ref. 9) and of Needham and Strollery (Ref. 10). The criteria proposed by these two sources predict separation for deflection angles greater than about 5 and 10 degrees, respectively. For these calculations, the flow upstream of the ramp was assumed to be generated by a sharp 10-degree wedge. The Reynolds number was based on a characteristic dimension of 12 feet (average distance to the leading edge). The ratio of peak heat transfer coefficient at reattachment to the laminar attached flow value on the deflected control surface was calculated by the empirical relation proposed in Reference 11. Attached flow is desirable to reduce the elevon heat transfer and to maintain control surface effectiveness. At a deflection angle of only 5 degrees, the elevon temperatures may exceed the capability of coated columbium if the upstream flow separates and reattaches on the elevon.

(U) Although not indicated on the figure, additional analyses were performed to predict the temperatures on the elevons for attached turbulent flow at a

flight velocity and altitude of 18,000 fps and 180,000 ft, which approximates the peak turbulent heating condition. Temperatures of 2220°F and 2710°F are predicted for deflection angles of zero and five degrees, respectively. For the assumed flight conditions and vehicle attitude, the local tangent wedge Reynolds number at the hinge line is 1.2 x 10^6. Although the flow would probably be laminar for zero elevon deflection, transition would probably occur at a deflection angle of five degrees due to the adverse pressure gradient.

3.5 (U) LOWER SURFACE PARAMETERS

(U) Figure 65 shows the effect of forward ramp angle on the body leading-edge stagnation line temperatures for an edge radius of 1.5 inches, a sweepback angle of 81.5 degrees, and a vehicle angle of attack of 10 degrees. Heating rates were computed assuming that the only effect of increasing the forward ramp angle is to decrease the effective sweep angle of the leading edge. A temperature increase of about 55°F per degree increase in forward ramp angle is predicted. The actual temperature increase is probably less than indicated because, at large angles of attack, the leading edge becomes (in the sense of airflow direction) a trailing edge. When this occurs, the heating rates are generally lower than swept-cylinder values.

(U) Figure 66 shows the effect of the forward ramp angle on the lower surface centerline temperature distribution. Heating rates shown are based on the F-5 radius distribution along the lower surface centerline. At a forward ramp angle of 1.5 degrees the temperature at a longitudinal distance of 5 feet is 1965°F and increases by about 50°F per degree increase in forward ramp angle.

(U) Figures 67, 68 and 69 show a comparison of heating distributions over curved and dihedraled lower surfaces. The configurations which were compared are drawn to scale in Figure 67 and include (1) a 60-inch radius lower surface, (2) a 20-degree dihedral with a 20-inch radius keel, (3) a 120-inch radius lower surface, and (4) a 10-degree dihedral with a 20-inch radius keel. Configurations 1 and 2 have approximately equal volumes as do configurations 3 and 4. A 1.5-inch leading-edge radius was assumed for each configuration. Heating distributions over the four lower surfaces are shown in Figures 68 and 69 for vehicle angles of attack of 10 and 20 degrees, respectively.

(U) In general, the heating rates over the curved lower surfaces vary less in the spanwise direction and are of lower magnitude compared to the dihedraled surfaces. On the lower surface centerline the dihedraled surface heating rates are considerably higher due to the smaller edge radius. Near the leading edge, the 10-degree dihedraled panel experiences higher heating than the 20-degree dihedraled panel, although the effective angle of attack of the latter is larger. This is a result of the assumed flow direction in which the boundary layer origin is the leading edge for $\Gamma = 10°$ and the keel line for $\Gamma = 20°$.

(U) Although the heating distributions over the curved lower surfaces are approximate, they are of sufficient accuracy to conclude that, based on

temperature and thermal stress considerations, the curved lower surface is slightly superior to a dihedraled surface.

(U) Shown in Figure 70 is the effect of the lower surface boat-tail angle on aft lower surface temperatures. The temperatures are normalized with respect to the temperature for a zero-degree boat-tail configuration. The temperatures decrease by approximately 2.1 percent per degree of boat-tail angle on a curved lower surface and by 2.6 percent per degree on a flat lower surface.

3.6 (U) VEHICLE ATTITUDE PARAMETERS

(U) Figure 71 shows the effect of vehicle angle of attack on the fin leading-edge stagnation line temperatures. Temperatures were computed assuming 5 degrees toe-in, 63 degrees sweepback, 25 degrees roll-out, zero yaw, and a 1.5-inch radius. At $\alpha = 10°$, the temperature is 3230°F and decreases by 32°F per degree angle of attack.

(U) The effect of vehicle angle of attack on the fin outboard panel temperature is shown in Figure 72. Temperatures are presented for a distance of 3 feet aft of the fin stagnation line measured in the flow direction. The effective panel angle of attack was computed from Eq. 6 (Part IV), assuming $\tau = 5°$, $\phi = 25°$, and $\beta = 0°$. At $\alpha = 10°$, the temperature at X = 3 ft is 1820°F and increases by 22°F per degree angle of attack.

(U) Figure 73 shows the effect of angle of attack on the body leading edge stagnation line temperature. When the plane through the leading edge is at an angle of attack of 13 degrees, the stagnation line temperature is 2870°F and increases by 52°F per degree angle of attack.

(U) Figure 74 shows the effect of angle of attack on lower surface centerline temperatures. Calculations were performed for a curved lower surface assuming a radius of 37 inches, which corresponds to the F-5A configuration at station 120. The assumed effective angle of attack of the centerline was the vehicle angle of attack plus four degrees to account for the forward ramp angle. Temperatures are presented for both laminar and turbulent heating based on the flight parameters listed on the figure. At $\alpha = 10°$, the temperature for laminar flow is 1785°F and increases by 42°F per degree angle of attack; the temperature for turbulent flow is 2220°F and increases by 66°F per degree. The local Reynolds number based on tangent wedge flow properties and wetted distance from the nose (X = 10 ft) is approximately 1.0×10^6 for the assumed peak turbulent heating conditions, so it is doubtful if the boundary layer would be turbulent at this vehicle location.

(U) The effect of vehicle yaw angle on fin stagnation line temperature is shown in Figure 75. The temperature increases from 3230°F to 3375°F as the yaw angle is increased from zero to five degrees. The effect on the fin outboard panel temperatures is shown in Figure 76. At X = 3 ft, the temperature increases by approximately 35°F per degree angle of yaw. Figure 77 shows the yaw angle effect on the body leading-edge stagnation line temperatures. The temperature increases by about 40°F per degree of yaw from the zero yaw value of 2870°F.

(U) Figures 78, 79 and 80 demonstrate the effect of yaw on the body side panel temperatures. Figure 78 shows the side panel flow deflection angle as a function of yaw angle for vehicle angles of attack of 10, 15, and 20 degrees. The flow deflection angles were computed by Eq. 3 (Part IV) assuming a sweepback of 81.5 degrees, a forward ramp angle of 3 degrees, and a body side angle of 57 degrees. The latter results in zero flow deflection for $\alpha = 10°$ and $\beta = 0°$. Body side panel surface temperatures one foot aft of the leading-edge stagnation line measured in the flow direction are plotted as a function of yaw angle in Figure 79. These temperatures are based on the flow deflection angles of Figure 78 and the temperature versus deflection angle plot of Figure 60. For a vehicle angle of attack of 10 degrees, the temperature increases from 1300°F to 1850°F as the yaw angle is increased from zero to 5 degrees. The effect of body side angle on the surface temperature one foot aft of the leading-edge stagnation line is shown in Figure 80, for yaw angles of zero and five degrees. This figure illustrates the rapid increase in temperature as the body side angle and the yaw angle are increased.

(U) The effect of vehicle yaw on lower surface temperature for a flat bottom delta wing is shown in Figure 81. Temperatures are at a point 5 feet aft of the leading edge measured in a direction parallel to the lower surface centerline. It was assumed that the only effect of yaw angle was to decrease the local boundary-layer thickness and thereby increase the heat transfer. Characteristic dimensions were measured from the leading edge in a direction parallel to the projection of the freestream velocity vector into the plane of the wing lower surface. The temperature at $\beta = 0$ degrees is 1950°F and increases by 30°F per degree of yaw.

3.7 (U) PARAMETRIC SUMMARY

(U) The results of the aerothermodynamic parametric studies are summarized in Table 4 which lists the approximate change in temperature per unit change in the design parameter. Configuration elements are listed in the top row along with predicted temperatures at each location for the F-5 baseline design. Various geometric and vehicle attitude parameters which influence the design are listed vertically. Where appropriate, baseline F-5 values are also shown for the various parameters. All temperature derivations are in °F/degree or °F/inch.

(U) As shown in the table, fin leading-edge stagnation line temperatures are most sensitive to changes in radius and fin rollout angle. Moderate changes in any of the fin parameters should not affect the design, however, as the predicted temperature level at this location is well within the assumed material capability. Fin rollout angle and vehicle yaw exert a major influence on the fin side panel material selection. To construct this panel of superalloy limits the toe-in angle and yaw angle to about two and zero degrees, respectively, for the baseline F-5 design and reference trajectory.

(U) Body leading-edge temperature for the baseline F-5 is predicted at approximately 2900°F. As with the fin leading edge, minor changes in the design parameters are not expected to alter the material selection at this location.

Table 4

(U) AEROTHERMODYNAMIC SENSITIVITY SUMMARY

Parameter	F-5 Design Value	Predicted F-5 Temperatures (°F)						
		Fin Stagnation Line 3230	Fin Outboard Panel (X=3 ft) 1830	Wing Stagnation Line 2870	Body Upper Surface 1300(a) 780(b) 1400(c)	Lower Surface Centerline (X=10 ft) 1780	Elevons 2200	Nose Stagnation Point 4300
		ΔT/Δ Parameter (°F/degree or °F/in.)						
Fin Toe-in Angle	5 deg	25	41					
Fin Roll-out	25 deg	80	5					
Fin Leading-edge Sweep Angle	63 deg	-35						
Leading-edge Radius	1.5 in.	-300						
Leading-edge Sweepback Angle	81.5 deg			-37				
Leading-edge Radius	1.5 in.			-280				
Body Side Angle	57 deg				38(a)			
Profile Angle	6 deg				0			
Fin Ramp Angle	10 deg				100(c)			
Elevon Deflection Angle	5 deg						200(a)	
Nose semi-major axis	2.7 in.							-200
Forward Ramp Angle	3 deg			55		50		
Lower Surface Curvature								
Dihedral Angle	0							
Boattail Angle	0							
Angle of Attack	10 deg	-32	22	52	38(a)	42(e)		
Yaw Angle	0	40	35	40	170(a)	30		

(a) Side Panel, X = 1 ft
(b) Upper Forebody Centerline, X = 5 ft
(c) Fin Ramp, X = 1 ft

(d) Assuming Separated Flow
(e) Laminar Flow

(U) Rapid increases in surface temperature are predicted as locations on the upper surface become windward. It is therefore desirable that these surfaces remain leeward with respect to the freestream flow. As shown in Table 4, body side panel temperature is most sensitive to vehicle yaw and less dependent on effective leading edge angle and vehicle angle of attack. It should be noted that in addition to constraining vehicle yaw to limit this temperature, other alternatives are possible, such as increasing the vehicle angle of attack (Figure 78) or reducing the vehicle bank angle at peak heating.

(U) Temperature levels on the lower surface are nearly equally influenced by changes in ramp angle and vehicle attitude. On a flat lower surface, signif- icant temperature increases can result from increased leading edge sweep when combined with large angles of attack. A curved lower surface geometry was determined to be superior compared to a dihedral, as a result of the nonuni- form heating experienced by the latter.

SECTION 4

(U) VEHICLE RECOVERY

(U) Selection of recovery mode for the high L/D research vehicle has a
significant impact on the vehicle configuration. Decoupled mode devices, for
example, can provide greater freedom to configure for maximum L/D and maximum
volume. Horizontal glide landing without wings or engines, on the other hand,
requires careful boattailing and contouring of the aft surfaces with attendance
reduction in internal volume.

(U) This section describes ten alternate modes of recovery that were considered
during the study. Horizontal landing with rocket engines was selected. Alter-
nate recovery modes for an unmanned research vehicle are compared on the basis
of weight, and tradeoffs are presented to show the variation of weight with
design requirement. The special case of horizontal landing penalties with a
rocket engine to overcome base drag is compared with booster adapter weight
penalties.

(U) Qualitative factors influenced the decision to configure the unmanned
research vehicle for hoirozntal landing using rocket engines. These factors
include:

1. (U) Low weight and maximum vehicle volume (study objectives)

2. (U) Achievement of unmanned low speed and landing research through the
       use of horizontal landing as the basic recovery mode

3. (U) Use of the vehicle in repetitive low speed research flights by
       adaptation to carrier aircraft

4. (U) Maximum reuse potential and reusable structure research through
       horizontal recovery

5. (U) Availability of ground control recovery avionics developed for
       the X-20 program

6. (U) Proven value of rocket motors in landing of lifting body vehicles

7. (U) Lowest system cost.

4.1 (U) WEIGHT TRADES FOR ALTERNATE RECOVERY MODES

(U) Weights of the alternate recovery systems shown in Figure 82 have been
evaluated and are compared in Table 5. Horizontal landing with no aids is
the lightest system, but this mode is subject to high landing damage risk due

24

Table 5

(U) ALTERNATE LANDING SYSTEMS

System	Weight/Horizontal Landing Weight*	Comments
Horizontal Landing	1.00	Lowest weight. However, with no thrust available to offset the high base drag, the sink speed may be too high for reasonable landing gear design.
Horizontal Landing W/Thrust	1.05	This system is based on ground contact at V_v = 10 ft/sec and thrust time of approximately 20 sec.
Vertical Descent Recovery (All)		Landing thrust and horizontal-type landing gear not required.
Parachute + honeycomb shock strut	1.09	Figure 83 shows the lightest weight of this combination occurs when parachute decelerates vehicle to 25 fps. Honeycomb shock strut then decelerates vehicle to zero fps.
Parachute (water recovery)	1.05	This system may operate with high vertical descent, 30 fps, if vehicle is allowed to enter water nose first.
Parachute (air snatch)	1.01	This system is sized with a parachute system to decelerate vehicle to 25 fps.
Parachute (reel)	1.04	Reel system to wind parachute lines rapidly just before touchdown can be rocket-powered.
Parachute + retrorockets	1.07	Figure 83 shows that the lowest weight of this combination occurs when parachute decelerates vehicle to 26 fps. Retrorockets are fired just before touchdown.
Paraballoon	1.11	This system was sized to hover at an assumed altitude of 5000 ft.
Rotor	1.13	System sized for vehicle simulating horizontal landing at an altitude, then deploying rotors to obtain an average descent of 25 fps and adding collective pitch just before impact to reduce descent rate to 8 fps.
Paraglider	1.17	Information in reference 14 was used to ratio paraglider system weight for this vehicle.
Horizontal Landing (Variable Geometry)	1.20	Originally sized in Ref. 1, and later refined for the maximum volume configuration. Weight based on 4g load factor and use of wing flaps, aelerons, and slots.

*Based on 5000-lb vehicle

UNCLASSIFIED

to the inherently low landing performance of lifting bodies. The recommended landing system using rocket engines is 5 percent heavier.

(U) Parachute devices which avoid landing attenuation requirements (air snatch, inertial reel, or water impact) are also lightweight but were discarded for the qualitative reasons cited earlier.

(U) Figures 83 through 91 summarize the parametric recovery system weight data used in Table 5. Figure 83 summarizes the combined weight of 5 shock attenuation devices used in combination with parachutes. The parachute weight data and attenuation devices data are shown separately in Figure 84 and were obtained from References 12, 13 and 14. Minimum system weight occurs with a descent rate of from 20 to 25 fps.

(U) The crushable structure weight shown in Figure 85 is based on 80% efficiency and was taken from Reference 14.

(U) The novel paravulcoon concept shown in Figure 82 offers the greatest flexibility for vehicle recovery and least structure tankage risk. Its weight is summarized in Figure 86 as a function of landing system weight. The weight data are based on studies of Saturn recovery systems (Ref. 15) and are scaled down to the high L/D research vehicle. This system is one of the heaviest alternates considered.

(U) Propulsion system weights to compensate for base drag and improve landing performance are compared in Figure 87. For short thrust times (less than one minute) the solid or high thrust/weight ratio rockets offer the least system weights. Turbojet engine installations are heavy and cannot compete with rockets unless the thrust time is greater than one minute (go-around or cruise capability).

(U) Rotor recovery system weight values were obtained from Reference 16 and are shown in Figure 88. The system is assumed to be a single aluminum rotor with a disk loading of 7.5 psf. Descent is assumed to start at zero fps and with autorotation to attain an average descent rate of 25 fps. The touchdown descent rate of 8 fps is obtained through use of collective pitch and conversion of rotor energy to lift.

(U) Horizontal landing gear weight and landing gear plus structure support weights are summarized in Figures 89 and 90. The solid lines in Figure 89 represent the band of weights for various high performance aircraft. The dashed lines are the median ranges used for the high L/D research vehicle.

(U) Figure 91 shows the water recovery system weights used in the recovery comparisons. The descent rate is assumed to be 30 fps.

4.2 (U) BASE AREA TRADES

(C) Base area has little effect on hypersonic lift-to-drag ratio, but has a great effect on aerodynamic drag (and consequently L/D) at landing velocities. Figure 92 shows that a base area 13.2% as great as the planform area

($\bar{S}$ = 0.132) will double the drag (at L/D_{max}) of the same vehicle with no base area, and reduce the L/D by 50%. This base drag effect normally leads to attempts to reduce base area in entry vehicle designs.

(U) Base area reduction, while improving landing L/D, presents two additional problems. First, the volume of the configuration is reduced to allow a reasonable aerodynamic fairing to the base cross section, and second, the smaller base area requires a larger and heavier adapter for booster attachment. This is shown in Figure 92.

(U) If the adapter is considered to be a frustum of a cone, the surface area is defined by

$$S = A_2/ \sin \theta \ (1 - A_1/A_2) \tag{1}$$

where:

A_1 = Cross section of the small circular end (vehicle base area)

A_2 = Cross section of the large circular end (booster cross section area)

θ = Cone half angle

(U) For a given structural weight per unit area, the weight of the adapter is defined by the surface area.

(U) It is apparent that the unit structural weight of an adapter (pounds per square foot of surface area) will vary with the complexity of the design and load to be boosted. A cursory review was made of available data on adapter weights to determine realistic adapter unit structural weights. While the complexity of a specific adapter design for a lifting vehicle is a function of many factors, it was found that a reasonable correlation could be obtained using the ratio of lifting area-to-base area of the payload as the correlating parameter. Figure 93 shows the correlation. Data for this figure were taken from References 17, 18, and 19. The structural weight of each transition element was determined as was the ratio of lifting area to vehicle base area involved in booster attachment (excluding fin trailing edge area, etc.). As indicated on the figure, some of the adapters were two piece units, one a retro section, and one a cargo module. Each unit was considered separately. The resulting trend is sufficiently defined to estimate the unit structural weight as a function of the base attachment area-to-lifting surface area.

(C) From Eq. (1) and Figure 93 a trend in adapter weight can be established for a given installation. Figure 94 shows such a trend. The figure is based on a Titan series of installations, diameter = 10 ft, $A_2 = 78.5$ ft^2, with a cone half angle of 20°. The upper curve represents the relative

adapter weight for a vehicle with 300 square feet of lifting area, while the lower curve represents the relative adapter weight for a vehicle with 141 square feet. These areas typify the lifting areas of high L/D mission vehicles and test vehicles respectively. Transition section weight is shown as a function of vehicle base area divided by booster cross section area, A_1/A_2. The weights were calculated using the middle of the band of unit structural weights in Figure 93. It is interesting to note in Figure 94 that when the base area of the vehicle equals the cross section area of the booster, the adapter weight can theoretically be zero, i.e., direct attachment can be made.

(U) Figure 95 is the same as 94, except the adapter weight is given as a function of base area.

(C) Since vehicle L/D decreases with increasing base area and adapter weight decreases, there is a possible trade where part of the decrease in adapter weight could be used as fuel for propulsion to regain a higher effective L/D. Such a trade is shown in Figure 96. This figure shows the combined adapter and solid rocket weight for a small (test) vehicle as a function of base area for various effective L/D-time combinations. It is obvious that for some conditions there is a flat but distinct optimum base area for minimum adapter-motor weight. This trade discounts the intuitive desire for minimum base area if a rocket can be used to regain L/D lost with the larger base area. The base area of the high L/D research vehicle lies in the favorable range of values of base area from 20 to 30 ft^2.

SECTION 5

(U) CONFIGURATION EVOLUTION

5.1 (U) HLD-35 EVOLUTION

(U) The parametric trade-off studies presented in Sections 2 and 3 of this report and in Reference 7 were used to evolve the basic study configurations. Consideration of the parametrics and their interrelationship resulted in the recommended values for the basic configuration geometry and stability variables presented in Tables 6 and 7, respectively. In addition to the magnitude of each variable, the effects of increasing or decreasing the recommended value is also shown.

(C) The resulting initial configuration, designated HLD-35-1, is shown in Figure 97. Its planform is defined by the highly swept body leading edge, $\Lambda = 81.5^{\circ}$, and the fin toe-in angle of 5° resulting in a wing sweep of 85° on the aft body leading edge. The nose of the configuration is a segment of 2:1 ellipsoid with an equivalent radius at the stagnation point of 3 inches. Body leading edge radii are 1.5 inches. Two vertical fins are attached, one to either side of the outside rear of the configuration. The fins are attached to the body along the aft body leading edge and are rolled outward about the attachment line 25° from true vertical. The fin leading edges are swept back 73° (at $\alpha = 0^{\circ}$) and have a radius of 1 inch. The aft portion or base of the body is closed by two flat vertical panels coincident with the swept hinge line of the elevons, and an additional vertical panel normal to the body centerline. The fins extend beyond the base to form a rudder area, although the requirement for a rudder was not defined. (Consequently, neither rudder hinge line nor area have been defined.) The fin trailing edge is swept 7 degrees. The fin has a root chord of 127 inches, and a tip chord of 15 inches. The lower edge of the fin extension beyond the base has been swept upward 24 degrees to prevent forming a leading edge on that surface at angle of attack.

(U) Aerodynamic control of the configuration is accomplished by the two lower elevons attached at the base of the vehicle flush with the lower surface (when in the zero deflection position), and with an upper surface flap which is flush with the top surface of the vehicle. The cross section of the body is defined by (1) a shallow arc segment on the lower surface, (2) rolled-in straight sides, and (3) a varying arc-to-straight line segment for the upper surface. Between the body and the fins, fillets have been added to prevent a deep trough with the associated high heating at the body-fin junctions.

(U) Each configuration element has been selected as a result of compromises between aerodynamic efficiency, stability, internal volume, and aerodynamic

29

Table 6

(U) GEOMETRY TRADES

Geometry	Effect of Increase	Recommended Values	Effect of Decrease
Equivalent Nose Radius	Decreased Heating	3 in.	Increased Hypersonic L/D
Leading Edge Radius	Decreased Heating	1.5 in.	Increased Hypersonic L/D
Leading Edge Sweep	Decreased Fin Toe-in/CP Movement Side Surface Heating	81 1/2°	Increased Volume Decreased Side Surface Heating to Yaw and Volume Sensitivity
Side Angle	Increased Volume	58°	Increased Yaw Stability Increased Hypersonic L/D Decreased Heating
Profile Angle	Increased Volume	5°	Increased Hypersonic L/D Increased Yaw Stability
Equivalent Dihedral Angle	Increased Volume Increased Depth	10°	Increased Hypersonic L/D Increased Yaw Stability
Base Area	Increased Hypersonic L/D (Lwr. Surf.) Decreased Adapter Weight	24 Ft.²	Increased Subsonic L/D
Length	Increased Volume Increased Hypersonic L/D	30 Ft.	Decreased Weight

UNCLASSIFIED

Table 7

(U) STABILITY TRADES

Geometry	Effect of Decrease	Recommended Value	Effect of Increase
Fins:			
Toe-in	[Low pitch-up (sub)]	5 deg.	excessive heating (hyp)
Roll-out	[pos $\Delta\ C_m$ (hyp)]	25 deg.	exc. heating (hyp); loss $C_{n\beta}\ C_{\ell\beta}$ (sub)
LE Sweep	Neg Δ L/D, incr. temp (hyp)	73 deg.	effectiveness loss (sub)
LE Radius	excessive heating (hyp)	1 in.	neg. Δ L/D (hyp)
Camber	Neg $\Delta\ C_m$, Δ L/D (sub)	2 %	neg. $\Delta\ C_{n\beta}$ (sub)
Area	Pos $\Delta\ C_m$, loss $C_{n\beta}$, $C_{\ell\beta}$	12.5 %	excess static margin (all speeds)
Height	N/A	low	$C_{n\beta}$, $C_{\ell\beta}$ loss (hyp)
Elevons:			
Area	destablizing (hyp)	9 %	neg $\Delta\ C_{m_o}$ (sub)
Nose Ramp:			
Deflection	Neg $\Delta\ C_{m_o}$ (sub)	3 deg.	destabilizing (hyp)
Area	Neg $\Delta\ C_m$ (hyp)	40 %	neg $\Delta\ C_m$ (hyp)
Lower Surface:			
Eq. Dihedral	small vol increase	10 deg.	excessive hyp L/D loss

heating. The previously discussed trade-offs which contributed to the selection of the basic configuration elements are shown in Table 6. Only the principal trades are shown.

(C) The effective nose radius of 3 inches was selected as a compromise between heating and L/D. Heating restricts reduction of the body leading-edge radius below 1.5 inches, but no strong constraint clearly inhibits a slight increase in that parameter. Center of pressure movement and heating restrict a reduction in body sweep angle, 81.5 degrees, while loss of volume restricts an increase in that parameter. The body side angle, 58°, was selected such that the side surface is aligned with the free stream flow when the vehicle is at the angle of attack for maximum L/D. A decrease in this value causes a rapid loss in configuration volume. Increasing this angle reduces directional stability and hypersonic L/D, and increases the heating of the body sides. The upper profile angle and contour of the vehicle have no discrete criteria to specify the 5 degree angle and contour shown. However, a reduction of this angle causes a reduction of the configuration volume. An increase in this angle and the possible addition of a cockpit would result in a small reduction in hypersonic L/D, and possibly yaw stability, depending upon the nature of the modification. The curved lower surface of the vehicle provides additional cross-section area equivalent to a straight 10° dihedral bottom. Reducing the depth of the lower surface arc results in decreased configuration depth and volume, while hypersonic L/D and yaw stability are degraded with a deeper arc segment. The base area, 24 ft^2, is primarily a result of the selection of the other configuration parameters. There is, however, a direct trade between the base area and subsonic L/D. Reducing the base by boat-tailing the lower surface can have an adverse effect on hypersonic L/D, and excessive reduction of base area can result in a rapid increase in booster adapter weight, as discussed in Section 4. Also, reducing the base area by reducing the height of the base, i.e., boat-tailing the upper surface downward, can lead to an adverse negative C_{m_o} increment at subsonic speeds. Fairing of the sides of the base does seem to be possible, since this approach trades volume directly for subsonic L/D. The configuration in Figure 97 would employ a rocket motor to assure landability. The vehicle length assumed for aerodynamic analysis is 30 feet.

(C) The key stability trades are shown in Table 7. The stability trades are somewhat more complex than the basic geometry trades, and have been discussed in Section 2.2.2. One significant observation which can be drawn from the stability and geometry trades is the dominance of hypersonic constraints. It is apparent that even if the requirement to horizontally land the vehicle were removed, only small configuration changes would be made.

(U) The characteristics of the HLD-35-1 configuration developed from the parametric study are as follows:

Length	= 30 ft
Span	= 8 ft

$$\text{Volume} = 308.7 \text{ ft}^3$$

$$\text{Planform Area} = 144.2 \text{ ft}^3$$

$$V^{2/3}/S_{(plan)} = 0.317$$

$$V^{2/3}/S_{(wet)} = 0.122$$

$$\text{Weight} = 4987 \text{ lb}$$

(C) The subsonic L/D variation with α is shown in Figure 98. The untrimmed L/D_{max} is seen to be 3.2. If the elevons and hinged flap are used to trim the vehicle, the resulting L/D_{max} is 1.84. Alternate means of trimming the configuration with less trim penalty are also possible. Subsonic trim characteristics of the configuration are shown in Figure 99. Both the elevons and flap are required to trim the configuration.

(C) The hypersonic L/D variation with α is shown in Figure 100. Maximum L/D occurs at $\alpha = 12°$. Untrimmed L/D_{max} is approximately 2.9. Trim requirements as shown in Figure 101 are expected to reduce the trimmed L/D_{max} to between 2.8 and 2.9 for the 30-foot length. A trimmed hypersonic L/D_{max} of 3.0 is expected for a vehicle with a length between 35 to 36 feet, using a geometric growth version of the configuration.

5.2 (U) FDL-5 EVOLUTION

(U) Continued analyses of the HLD-35-1 configuration (Figure 97), revealed the need for improvement in vehicle performance capabilities. These analyses resulted in a series of improved configurations and, ultimately, an entirely new configuration concept, identified by the term "compression sharing." These improvements and the concept development are described in the following paragraphs, and reflect the adoption of the following goals suggested by the AFFDL Project Engineer:

L/D = 3.0 @ V = 20,000 fps, h = 200,000 ft

L/D = 3.0 @ V = 450 fps, h = 1,000 ft

Length = 33 ft

Controllable and stable throughout the flight regime

Trimmable for $5° \leq \alpha \leq 30°$ hypersonically

Trimmable for $5° \leq \alpha \leq 20°$ supersonically

33

Trimmable for $3^\circ \leq \alpha \leq 15 - 20^\circ$ subsonically

Maximum usable volume forward of CG

Design to accommodate a 75 percentile man

Basic geometry compatible with booster/human requirements

(C) The HLD-35-1 configuration exhibited generally poor predicted low-speed performance. As seen in Figure 99, the configuration was capable of only unstable trim at high angles of attack. This condition required large deflections of both the elevons and upper body flaps to overcome the large negative C_{m_o} values induced by the adverse flow effects of the leading edge vortices in the body-ramp-fin channel. Large drag increments induced by the resulting control deflection requirements decreased trimmed L/D_{max} to 1.0 - 1.5, Figure 98. This effect was revealed in Lockheed subsonic tests of the F-5 configuration, Figure 1, (Reference 3).

(U) To relieve these performance deficiencies, the HLD-35-1 configuration was modified to the HLD-35-2 (Figure 102). The approach used to develop this configuration involved removing the volume between the fin and the body, and boattailing the lower surface. The resulting design exhibited discrete wing and fin geometries; it closely resembled the earlier F-4 vehicle described in Reference 6.

(C) The base area was reduced from 16.7% of planform area to 5.6% to substantially reduce the low speed zero-lift drag (subsonic zero-lift drag is primarily composed of skin friction and base drag with minor increments of pressure drag and momentum loss through the wing-body channel). The parametric data presented in Figure 18 indicates a potential L/D increase of 1.0 to 2.5.

(U) Control deflection requirements for trimming are also expected to decrease since the trailing edge elevons are in flow for both positive (TE down) and negative (TE up) deflections. These reduced deflections for trimming are expected to result in increased L/D.

(U) Subsequent review of this configuration revealed potentially undesirable characteristics of the wing-fin geometry. The suspected high heating rates on the inner and outer surfaces of the fin, upper and lower wing, and adjacent body surfaces impose serious structural design and weight penalties to accommodate these rates.

(U) A pure lifting body approach with no distinct hypersonic fins was recommended by AFFDL for configuration evaluation. This approach was followed in revising the HLD-35-1 configuration to the HLD-35-3 configuration shown in Figure 103. Following the goals recommended by AFFDL, this configuration is 33 feet long. A canopy is added to explore the adaptability to accommodate a

pilot, and the upper profile angle is modified to 6 degrees. The bottom aft area is boattailed to provide a horizontal elevon hinge line. The outboard fins are eliminated, and the fin ramps are enlarged, increasing side area for direction stability. A center fin is added for subsonic directional stability and two upper flaps replace the single upper flap used on the HLD-35-1.

(U) An additional approach to the pure lifting body concept is shown in Figure 104. This configuration was developed from a model supplied by AFFDL with an accompanying sketch. The overall length of this arrangement is 35 feet. It has a delta planform of 205 square feet. The nose section is very similar to the HLD-35-1 configuration, with a sweep of 81 degrees and top ramp angle of 6 degrees. The bottom nose ramp has been replaced by the 3-degree aft boattail which provides the same effect. The upper shoulder line aft of station 280 fairs out to 90 degrees at station 420. This eliminates the former fin ramps. A 40-degree lower aft ramp provides space within the aft body for deflecting the elevons. The upper surface of the aft body flattens out to provide for the upper trim flaps. A center fin is added and the outboard fins practically eliminated. Provisions for a manned cockpit are shown in phantom lines.

(U) It is apparent from Figures 102, 103, and 104 that all of these concepts share essentially the same forward body configuration; the significant variations are restricted to the rear half. At this point in the configuration evolution the previously discussed aft body shape parametric analysis (Section 2.2.3) was performed, resulting in the FDL-5A configuration.

(U) The FDL-5A configuration, Figure 105, is a refinement of the B_4 or C_1 geometry (Section 2). The upper-aft surfaces have been modified in an effort to reduce the base area and increase subsonic L/D. Since this fairing tends to reduce the exposed side area of the aft body, the body toe-in angle, τ, has been increased to six degrees and lower side surface roll-out angle K_{TE} has been set at 20 degrees to maintain adequate yaw stability as suggested by the earlier parametric analyses.

(C) A review of the predicted characteristics of the FDL-5 configuration, relative to the goals established by AFFDL led to the selection of the configuration for extensive wind tunnel testing at the Arnold Engineering Test Center (AEDC). The wind tunnel tests were designed to verify the following predicted characteristics of the FDL-5 configuration.

$$L/D = 3.0 \text{ for length} \cong 35 \text{ ft, } H = 200,000, V = 20,000 \text{ fps}$$

Controllable and stable throughout the flight regime:

$$5° \le \alpha \le 30° \text{ hypersonically}$$

$$5° \le \alpha \le 20° \text{ supersonically}$$

(U) This vehicle configuration was approved by AFFDL for experimental study at AEDC. The aerodynamic and aerothermodynamic test data are presented in Parts III and IV, as are the data-theory correlations and the verified characteristics of the FDL-5 configuration.

REFERENCES

1. J. T. Lloyd, et al, Preliminary Design of Hypersonic High L/D Test Vehicles, AFFDL-TR-66-12, May 1966 (C)

2. C. P. Valery and C. M. Onspaugh, Summary Results of Wind Tunnel Tests of the AMR F-5 Configuration at Mach Numbers of 2.5, 3.5, 6.0, and 8.0 (U), LR 20112, Lockheed-California Company, October 1966 (C)

3. C. P. Valery and C. M. Onspaugh, Summary Results of Wind Tunnel Tests of the AMR F-5 Configuration at a Mach .26 (U), LR 20113, Lockheed-California Company, November 1966 (C)

4. USAF Stability and Control DATCOM, 1960

5. C. P. Valery and C. M. Onspaugh, Wind Tunnel Test Results of the AMR F-4 Configuration at M = 19.2 (U), LR 19747, Lockheed-California Company, June 1966 (C)

6. V. Dahlem, A Digital Computation Method for Determining the Hypersonic Aerodynamic Characteristics of Arbitrary Bodies, AFFDL-ASRMDF-TM-62-61, September 1966

7. H. H. Drosdat and F. X. Hurley, The Effect of Dihedral and Cross-Sectional Shape on High L/D Entry Vehicles, LR 19782, Lockheed-California Company, June 1966

8. J. T. Lloyd, et al, Preliminary Design and Experimental Investigation for High L/D, High Volume Flight Test Vehicles (U), Monthly Progress Report, LR 20067, Lockheed-California Company, 20 September 1966 (C)

9. Z. Popinski and C. F. Ehrlich, Development of Design Methods for Predicting Hypersonic Aerodynamic Control Characteristics, Lockheed-California Company, LR 19460, April 1966

10. D. Needham and J. Stollery, Boundary Layer Separation in Hypersonic Flow, AIAA Paper 66-455, Presented at the 4th Aerospace Sciences Meeting, June 27-29, 1966, Los Angeles, California

11. Aerothermodynamic Analysis Report (U), Boeing Airplane Company Document No. D2-8108, August 10, 1961 (C)

12. Douglas Aircraft Company, Parametric Study of Logistics-Type Entry Vehicle, SM 48785, Vol III, September 1965

13. Proceedings of the Recovery of Space Vehicles Symposium, Los Angeles, California, August 3 - Sept 1, 1960, sponsored by the Institute of the Aeronautical Sciences and the ARDC Regional Office at Los Angeles

14. Lockheed-California Company, Final Report Study of a Ballistics Reentry Type Logistics Spacecraft (U), Vol. 3, for NASA Manned Spacecraft Center Houston, Texas, LR 17477, 12 February 1964 (C)

15. The Boeing Company, Study of Saturn S-1C Recovery and Reusability, D2-23233-1, Vol I, 1 September 1964

16. Lockheed-California Company and Lockheed-Georgia Company, V/STOL Concepts for Short Haul Transport Aircraft (U), LR 19585, Vol. 3, 30 March 1966 (C)

17. The Boeing Company, Weight Analysis Report, Model X-20, Vol. 1, D2-81264-2, July 10, 1964

18. "Apollo Weight Estimated at 98,000 Lb," Aviation Week, Page 26, August 15, 1966

19. Mission Requirements of Lifting Systems-Engineering Aspects (U), McDonnell Report No. B831, 27 August 1965 (C)
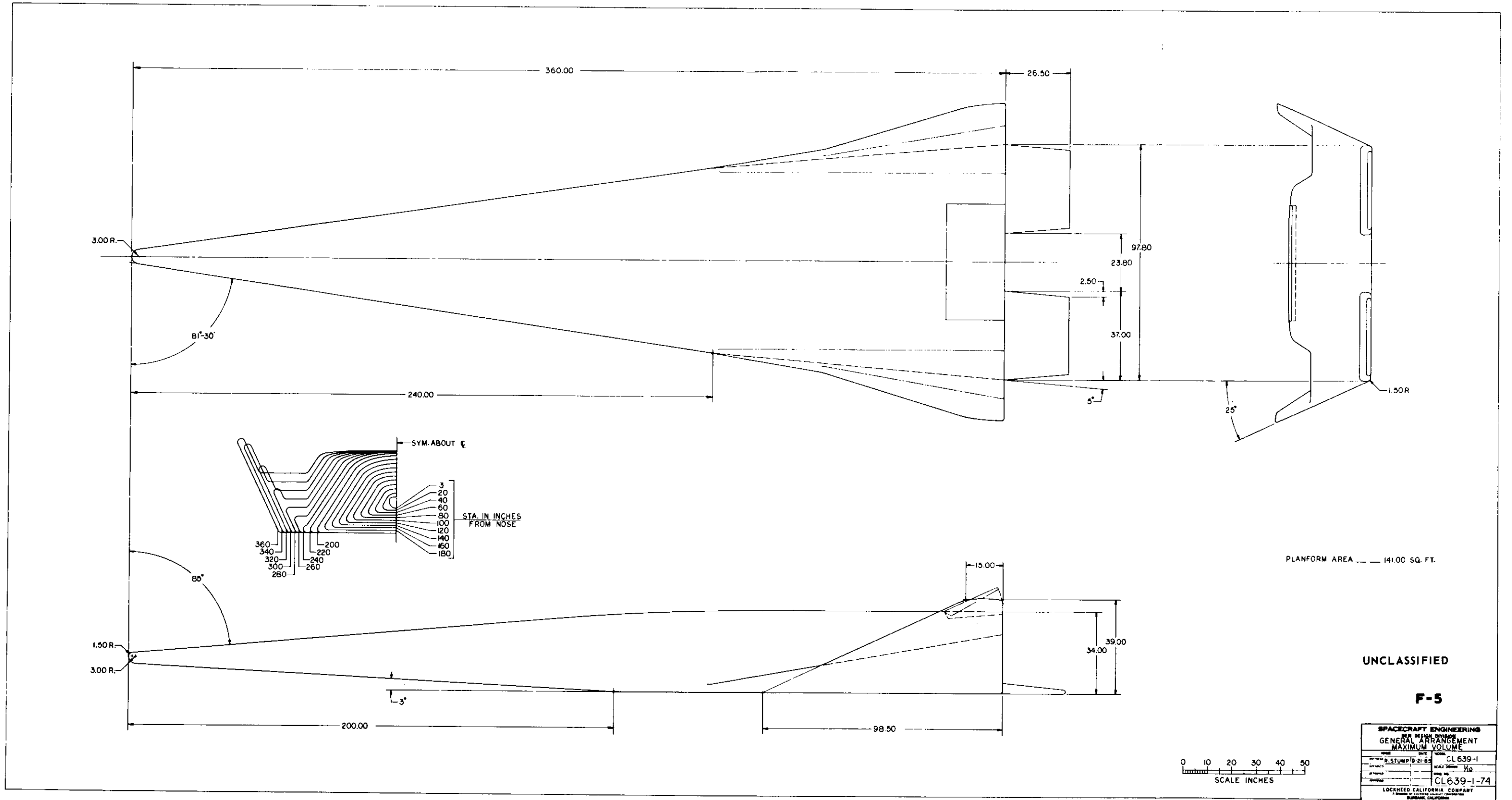
FIGURE 1   (U) F-5 GENERAL ARRANGEMENT
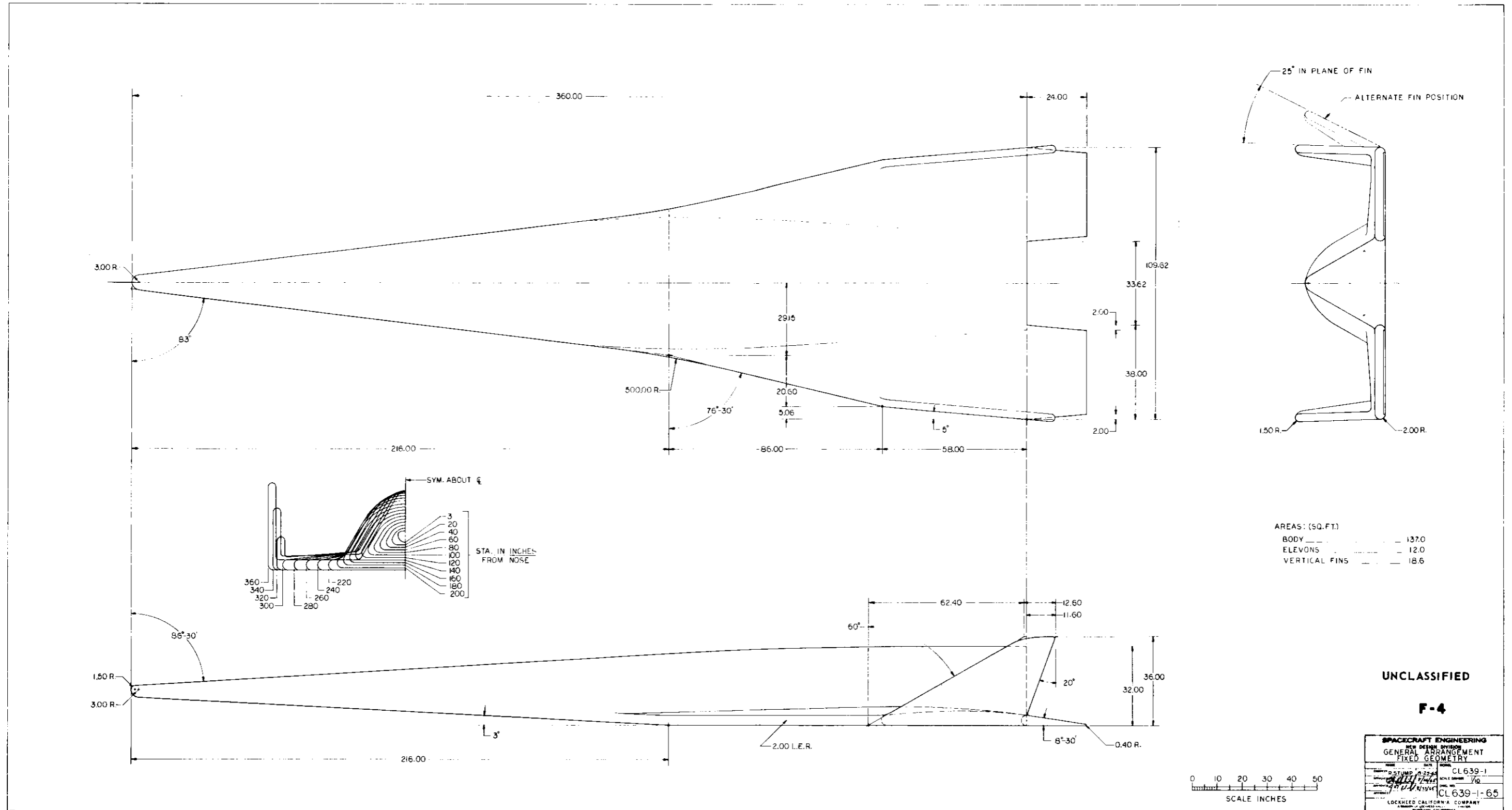
FIGURE 2   (U) F-4 GENERAL ARRANGEMENT

FIGURE 3   (U) AERODYNAMIC CONFIGURATION PARAMETERS
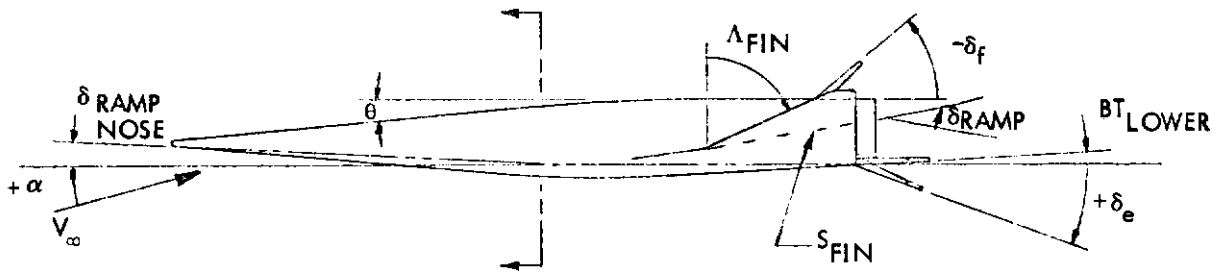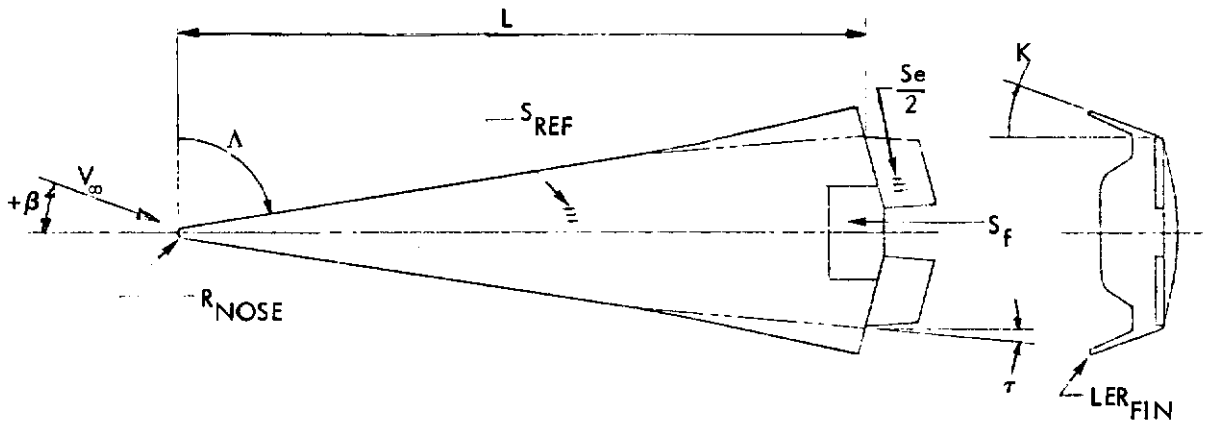
PITCH CONTROL: $\delta_p = \delta_{el} + \delta_{er}$

AILERON CONTROL: $\delta_A = \delta_{el} - \delta_{er}$

UNCLASSIFIED

43

F-5
M = 20
H = 200,000(FT)
L = 30(FT)
$\tau = 5^{\circ}$, K = 25°

F-5 BASE POINT

$(L/D)_{MAX}$

R_{NOSE} (in.)
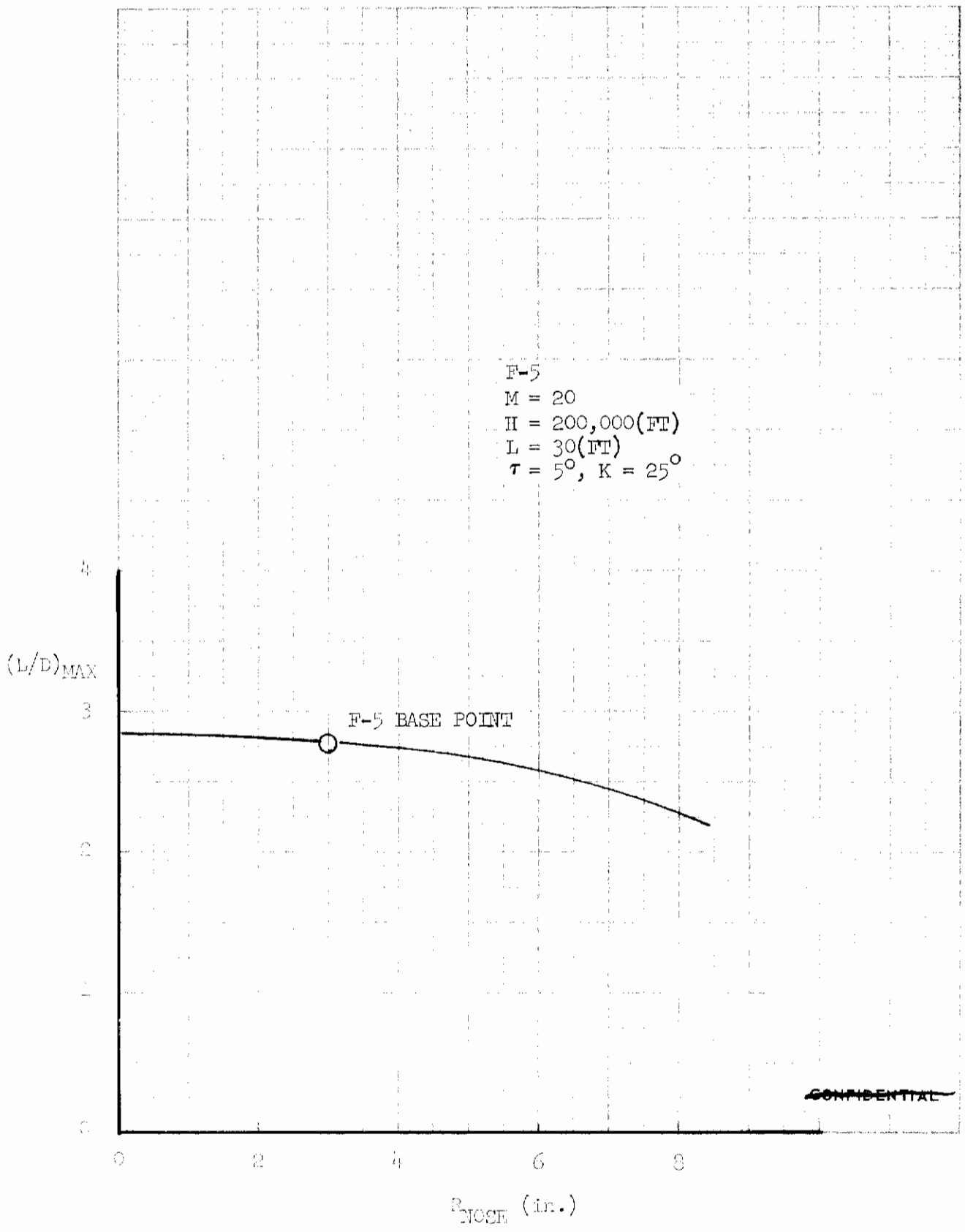
FIGURE 4   (U) VARIATION OF $(L/D)_{MAX}$ WITH NOSE RADIUS AT M = 20
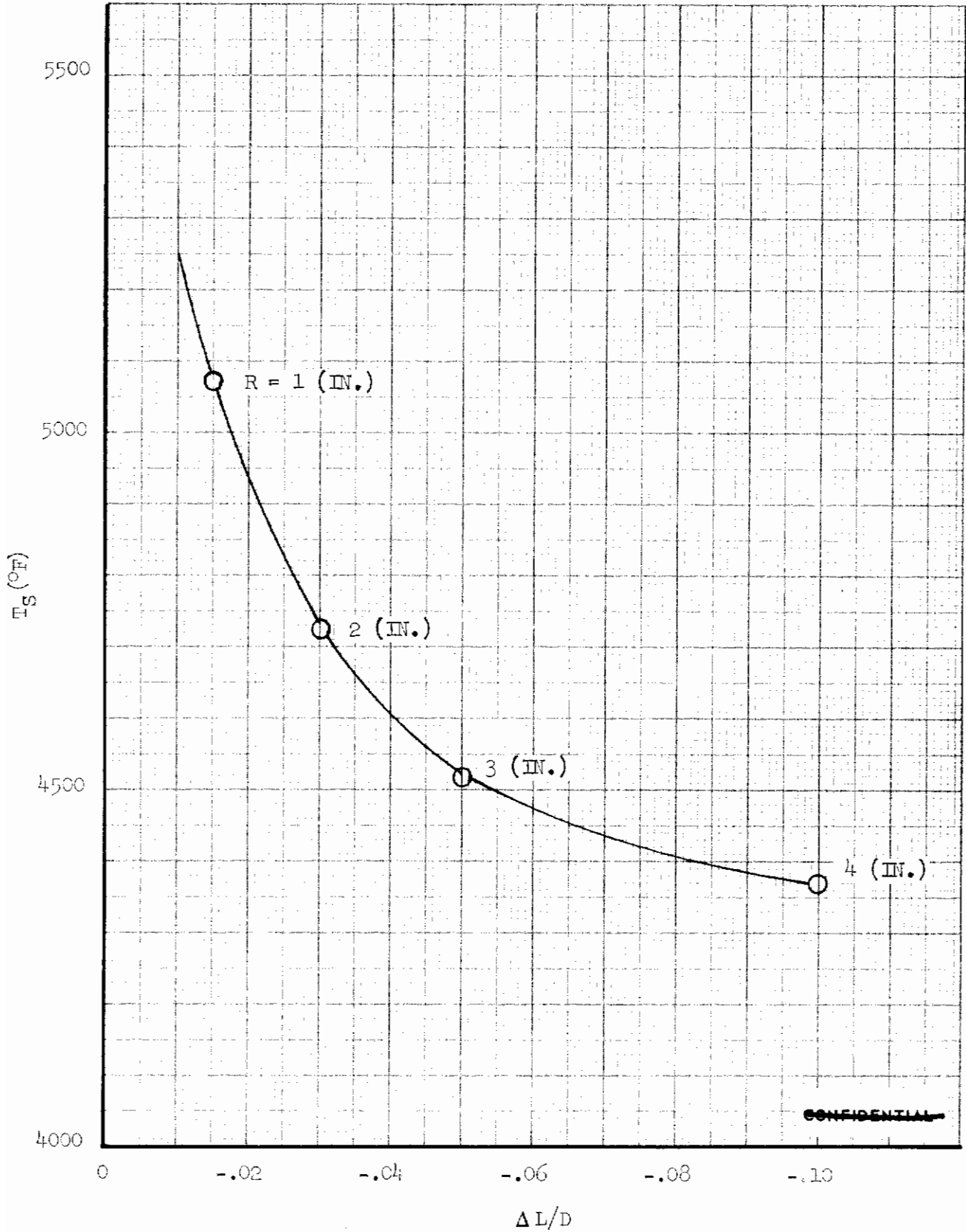
FIGURE 5   (U) NOSE RADIUS TRADE

45

SWEPT CYLINDER DRAG THEORY
(REFERENCED TO F-5 BASE POINT)

F-5 BASE POINT

LER
(IN.)
.75
1.5
3.0

$(L/D)_{MAX}$

Λ (deg)
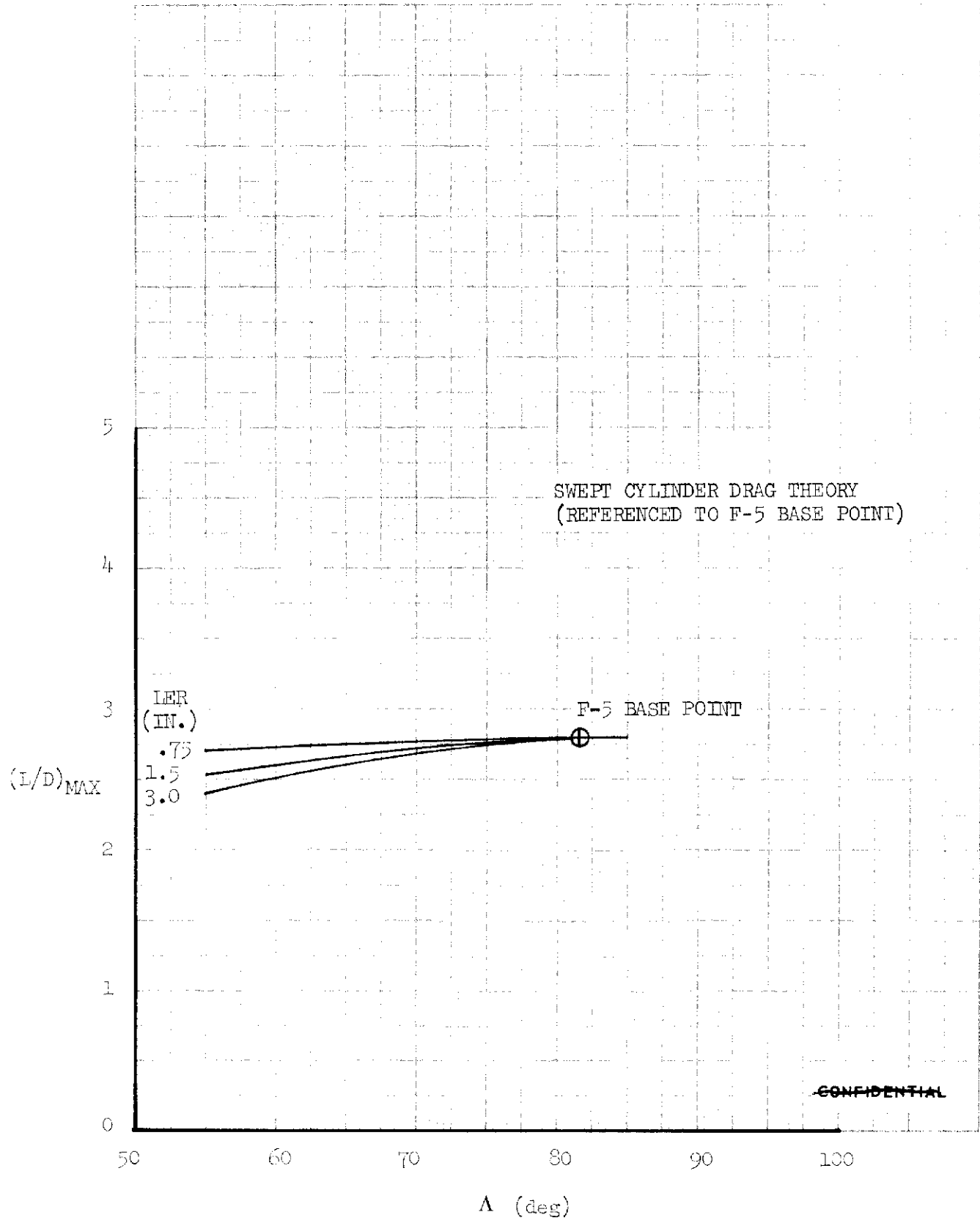
FIGURE 6 (U) VARIATION OF $(L/D)_{MAX}$ WITH BODY SWEEP ANGLE AT M = 20

46
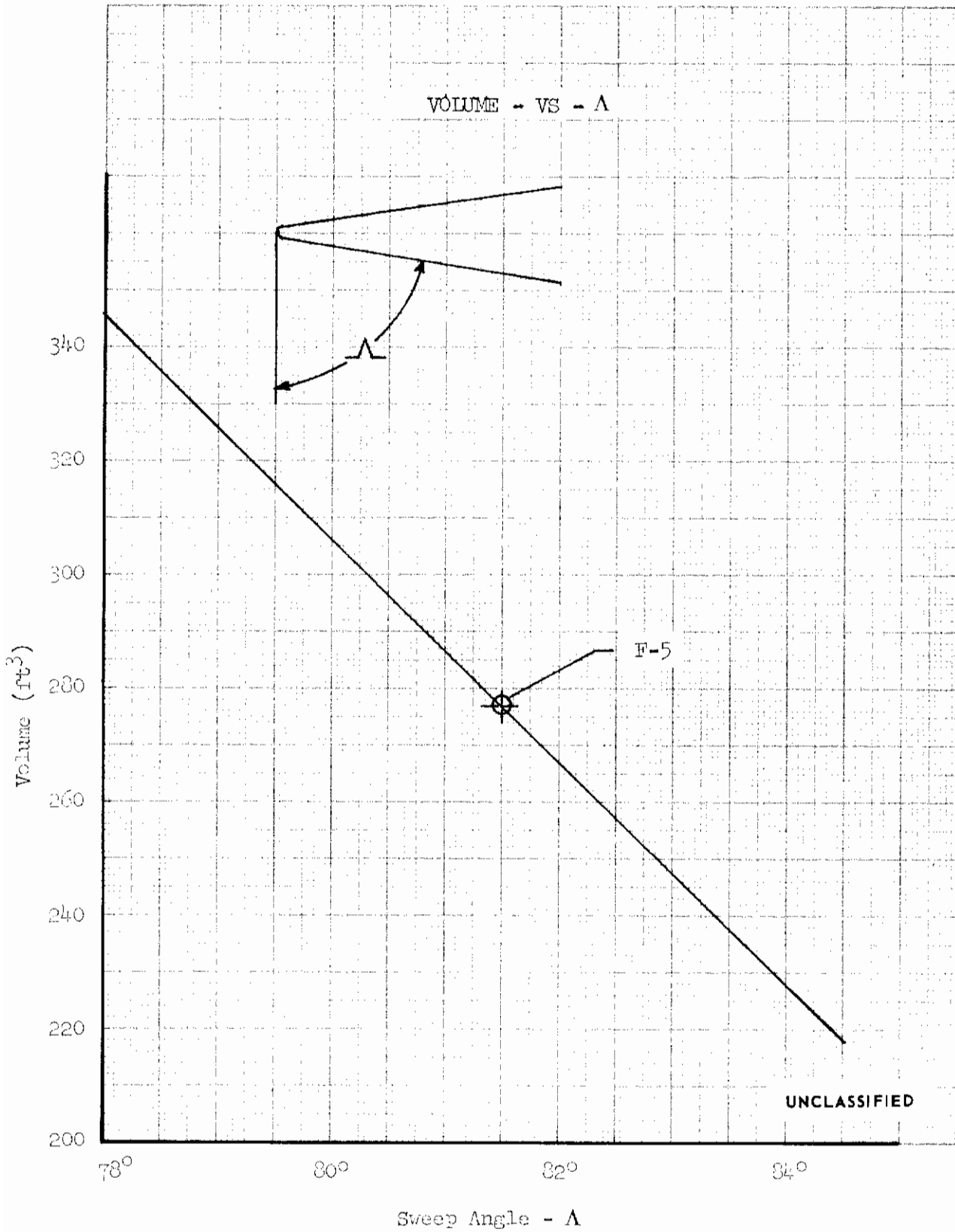
FIGURE 7 (U) VARIATION OF VOLUME WITH LEADING EDGE SWEEP ANGLE - LENGTH = 30 (FT)

NEWTONIAN FLOW THEORY, K = 20
(F-5A, FLAT BOTTOM, BODY ONLY)

$\alpha = 12^{\circ}$
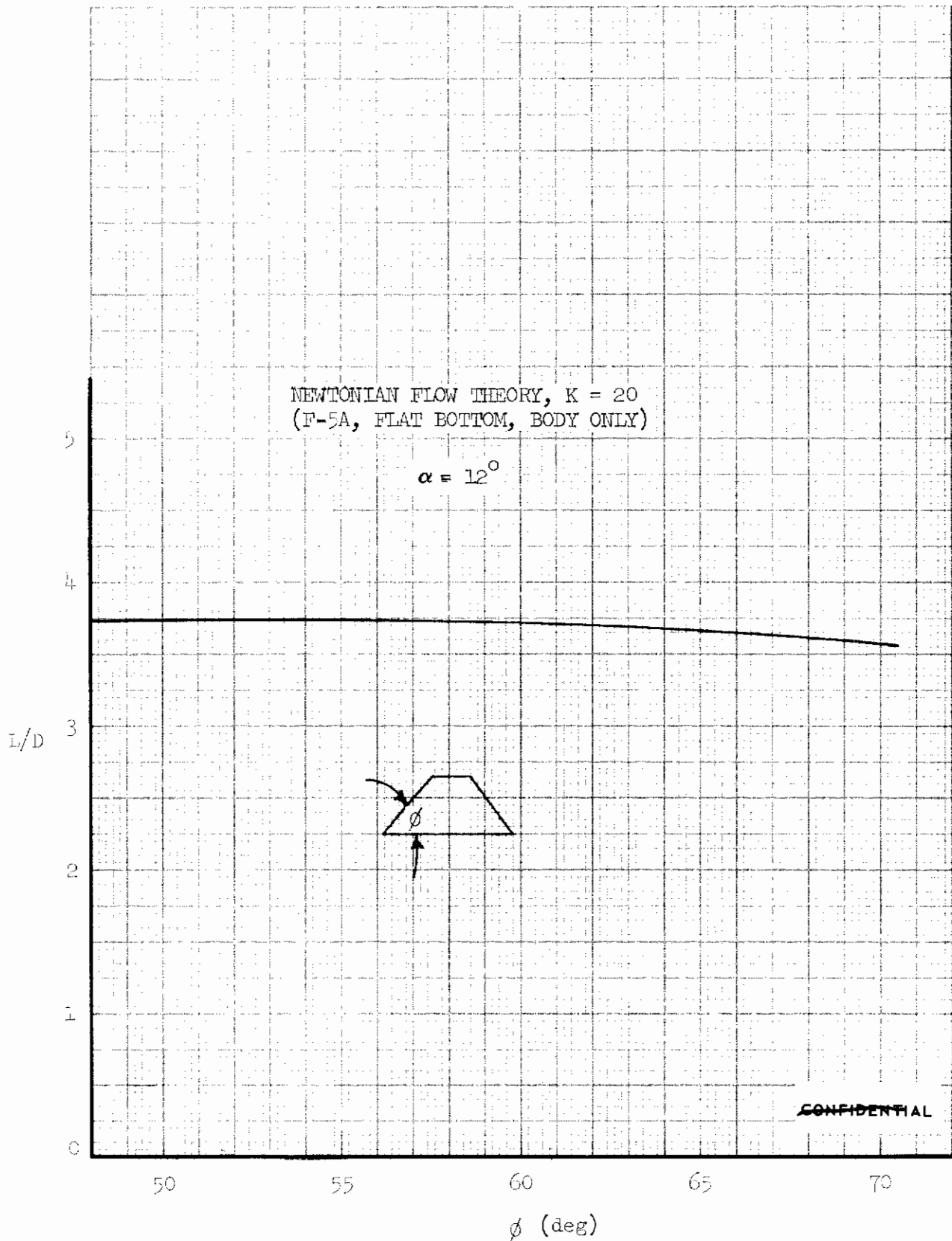
FIGURE 8   (U) EFFECT OF SIDE ANGLE VARIATION ON L/D_{MAX}

48
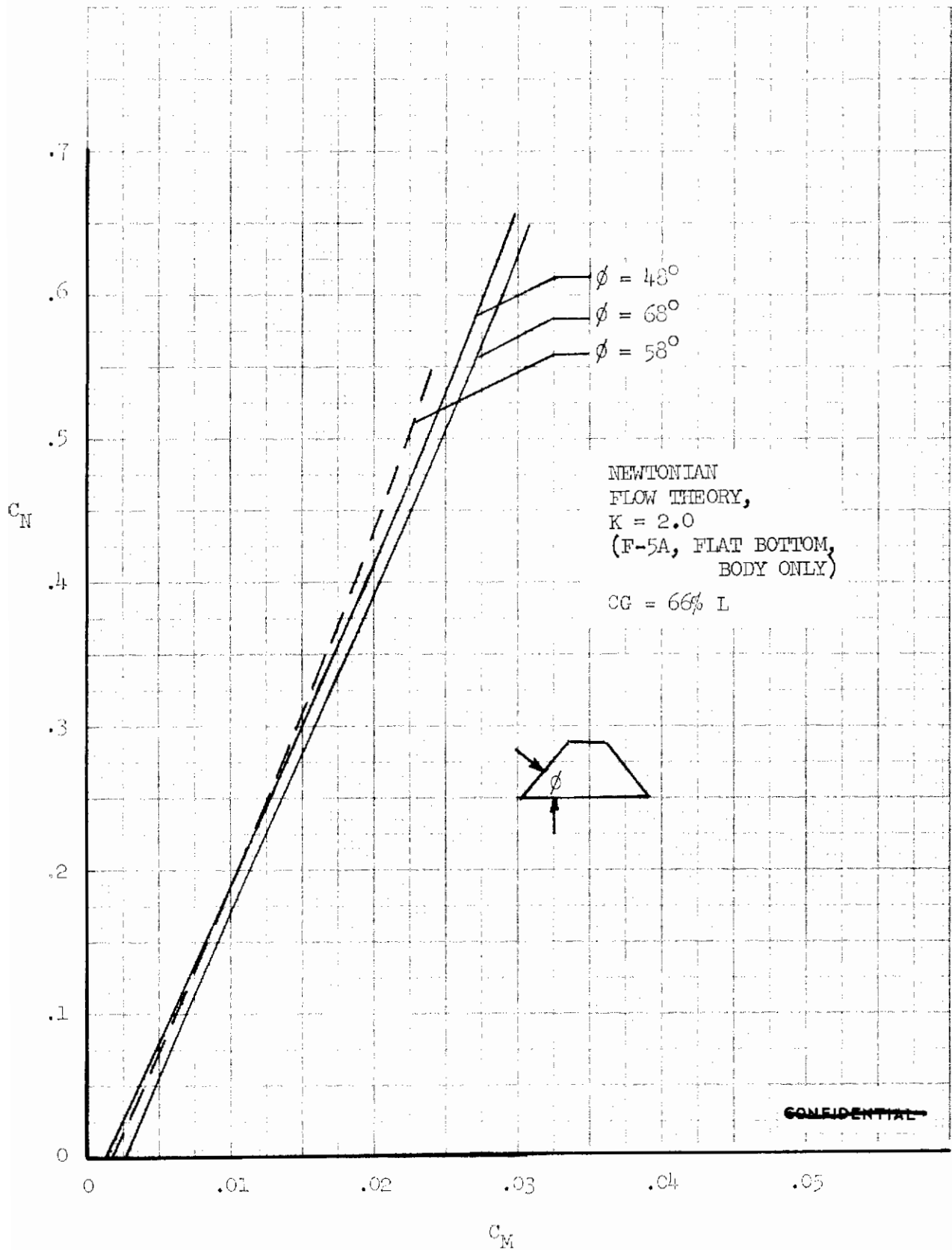
FIGURE 9   (U) EFFECT OF SIDE ANGLE ON LONGITUDINAL STABILITY

49
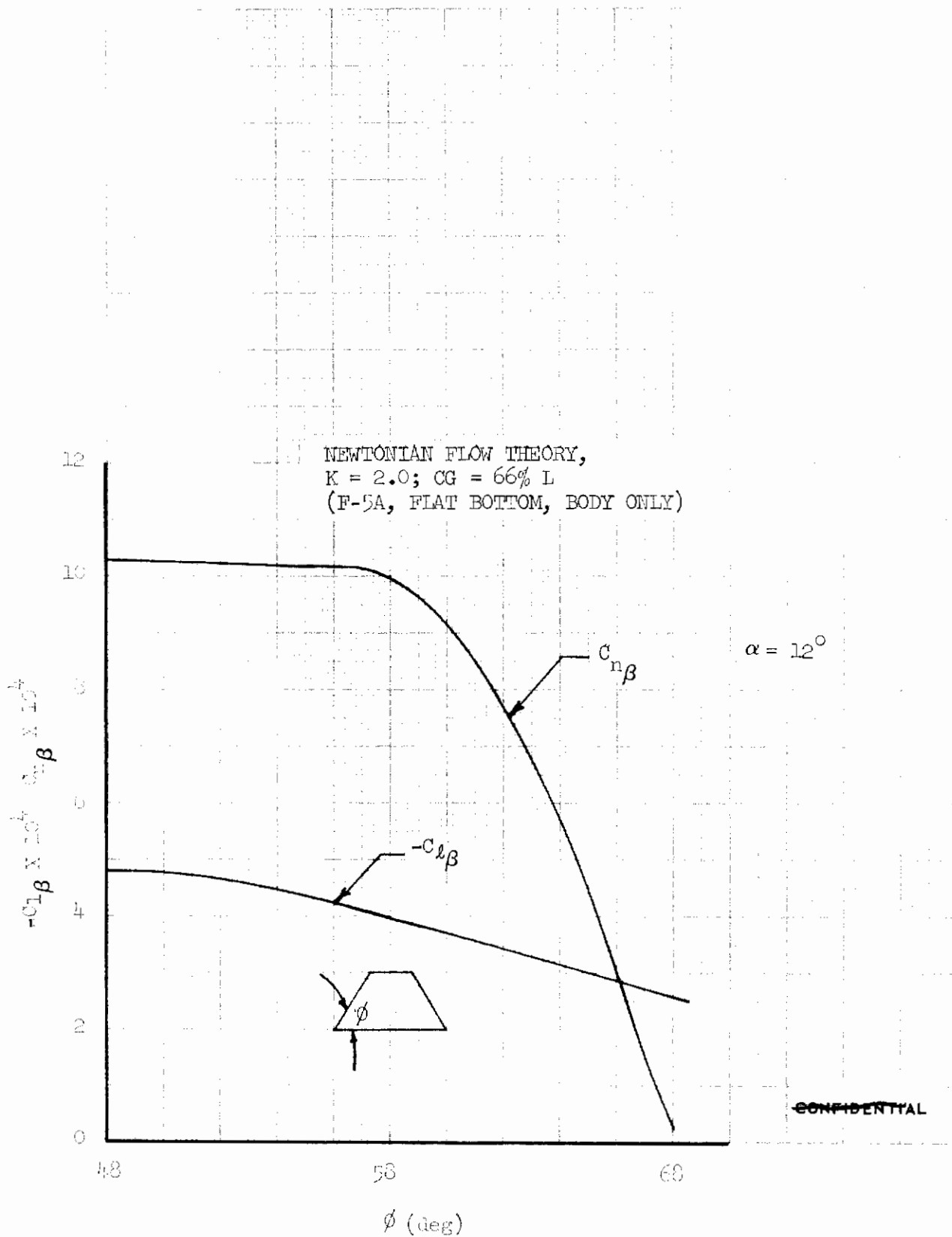
FIGURE 10   (U) EFFECT OF SIDE ANGLE VARIATION ON THE LATERAL STABILITY
DERIVATIVES

50
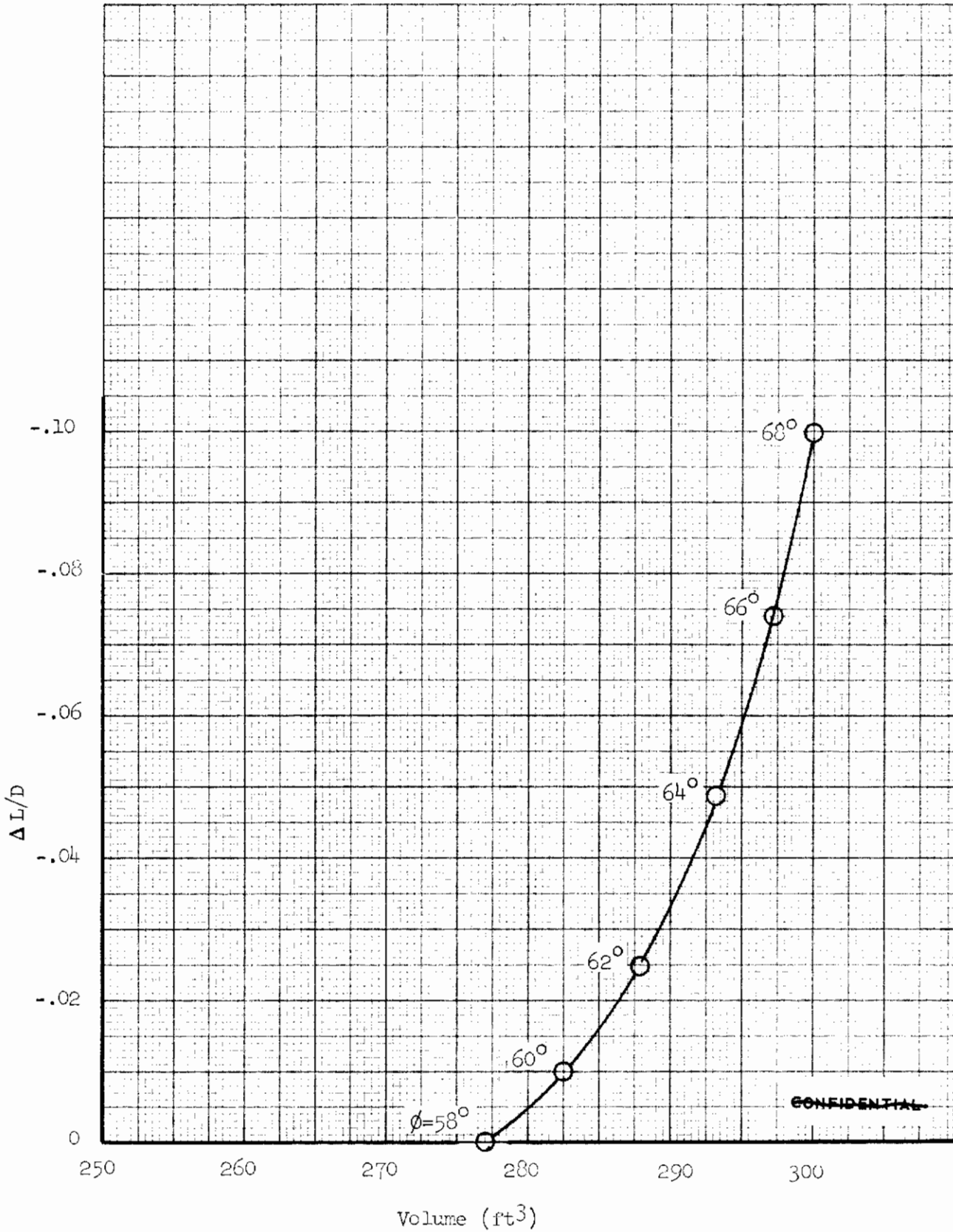
FIGURE 11 (U) BODY SIDE ANGLE TRADE

M = 20
H = 200,000 (FT)
L = 30 (FT)
τ = 5°
K = 25°

$(L/D)_{MAX}$

DESIGN POINT

NEWTONIAN THEORY

CONE THEORY

θ (deg)
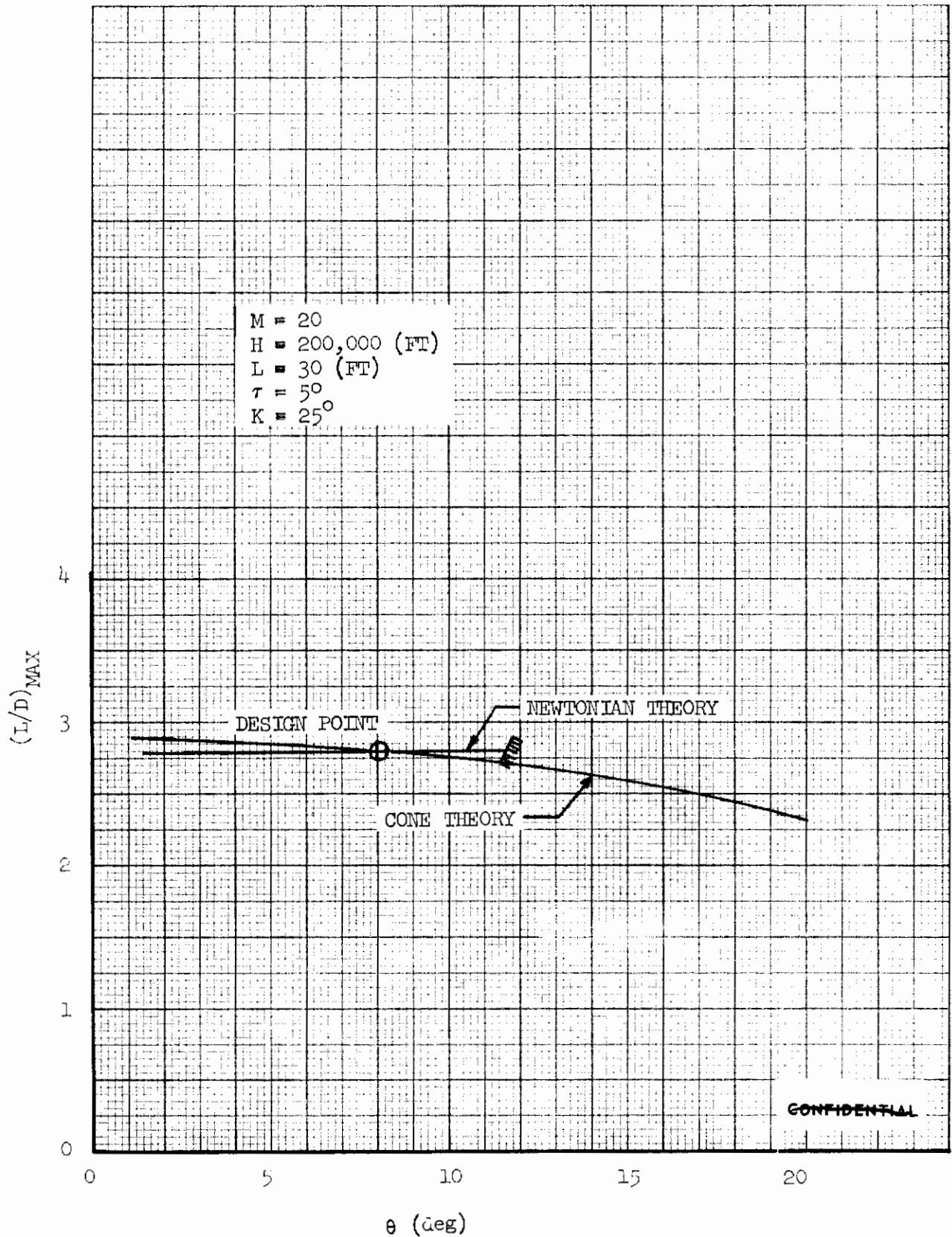
FIGURE 12 (U) VARIATION OF $(L/D)_{MAX}$ WITH BODY PROFILE ANGLE AT M = 20
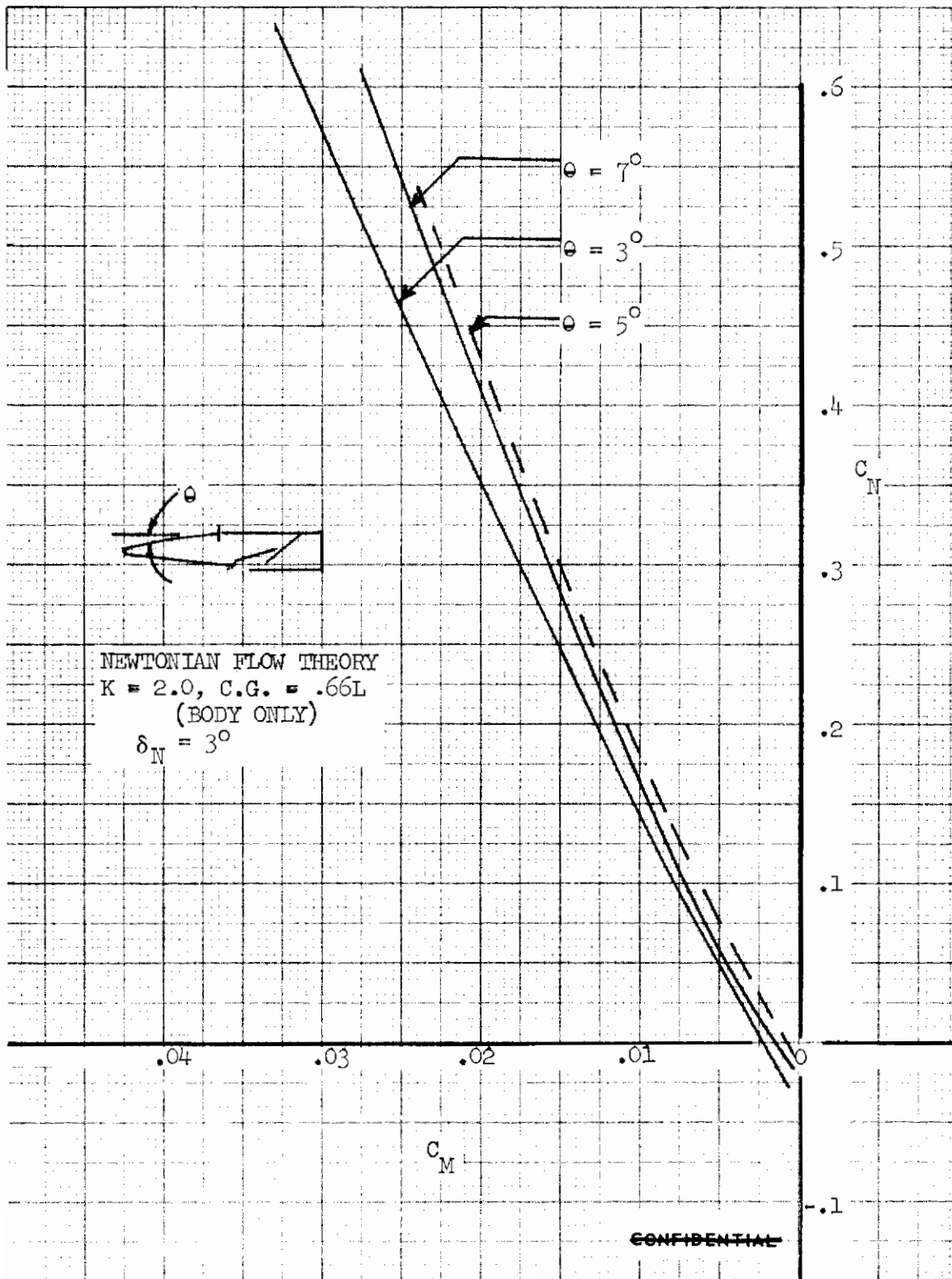
FIGURE 13 (U) EFFECT OF BODY PROFILE ANGLE ON LONGITUDINAL STABILITY

NEWTONIAN FLOW THEORY
K = 2, C.G. .66L
(F-5A, FLAT BOTTOM,
BODY ONLY)
$\delta_N = 3^\circ$, $\alpha = 10^\circ$

c_{n_β}

c_{l_β}

θ (deg)

$- c_{l_\beta} \times 10^4$ & $c_{n_\beta} \times 10^4$
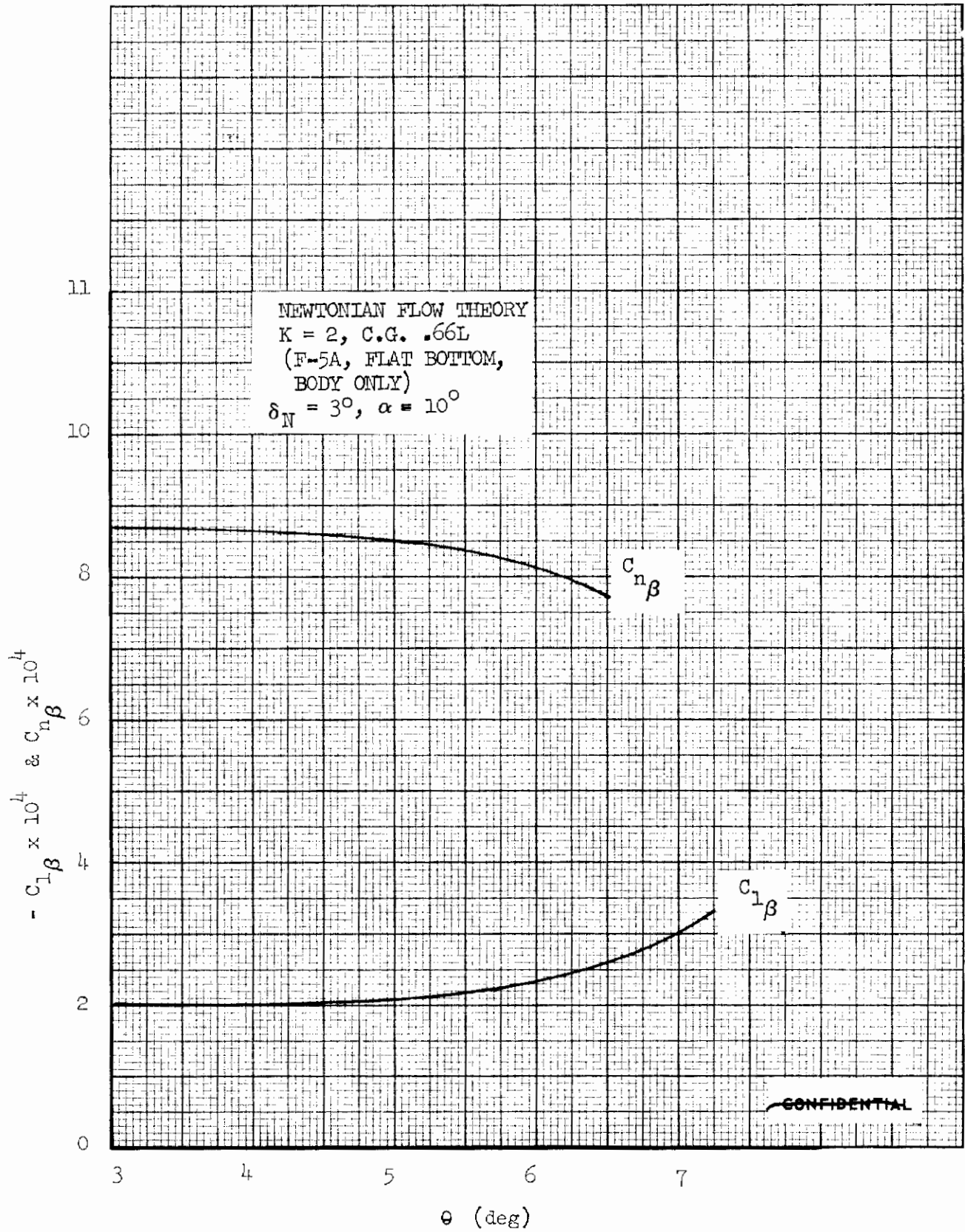
FIGURE 14   (U) EFFECT OF BODY PROFILE ANGLE ON THE LATERAL STABILITY
            DERIVATIVES

54
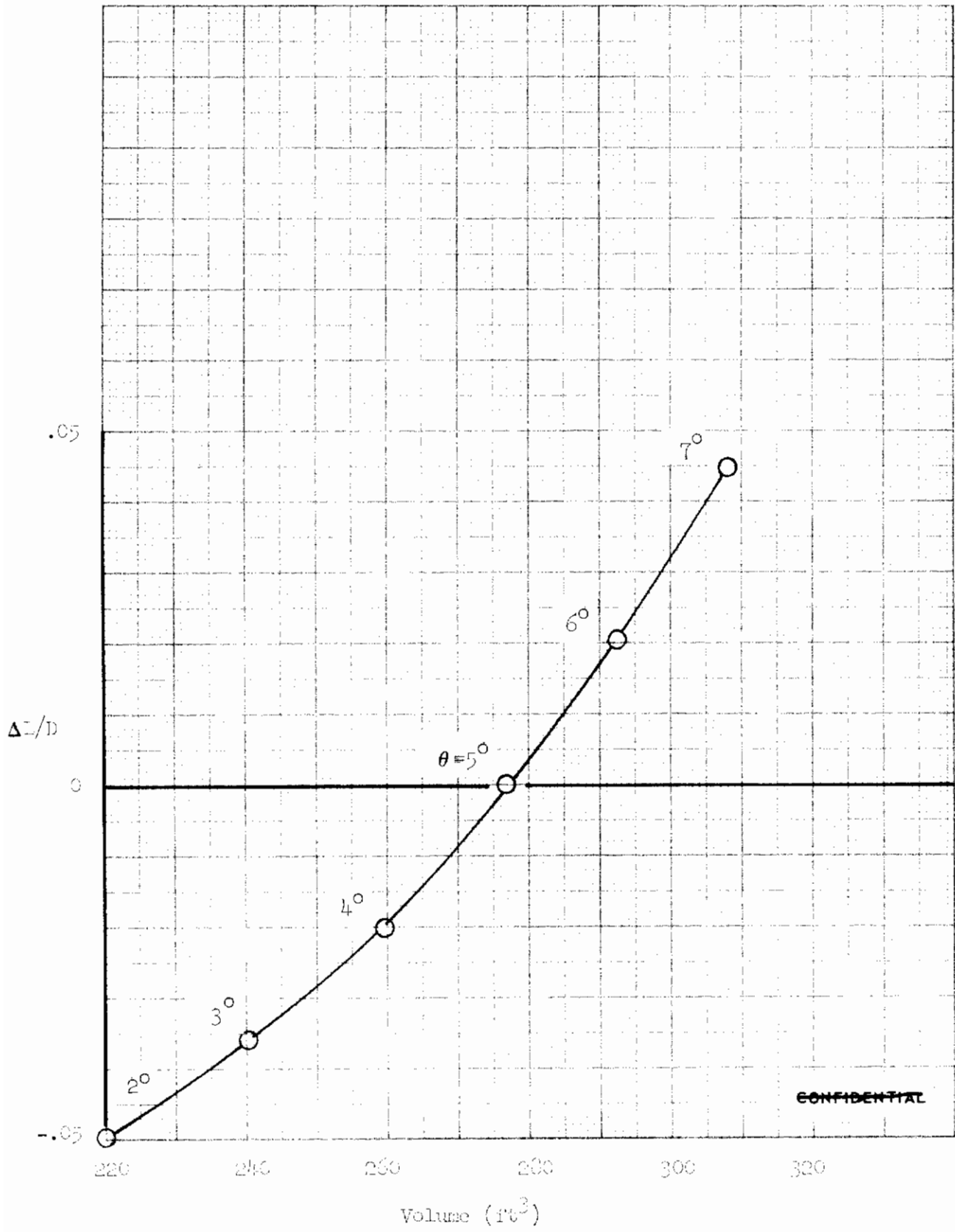
FIGURE 15   (U) BODY PROFILE ANGLE TRADE

55

NEWTONIAN FLOW THEORY, K = 2.0

L/D_{MAX}

$\Gamma_{(Volume\ Equivalent)}$ (deg)
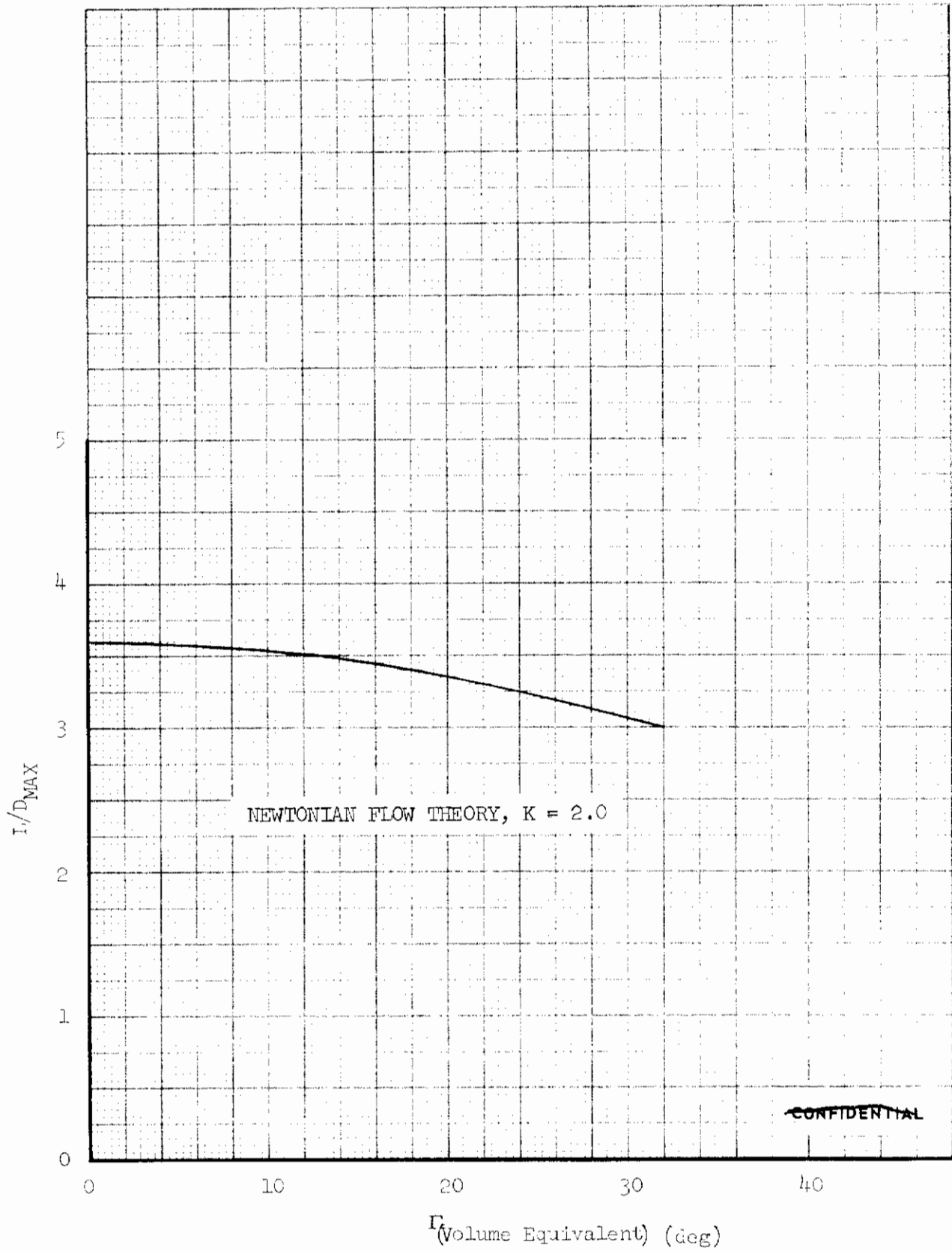
FIGURE 16 (U) EFFECT OF BOTTOM GEOMETRY ON L/D_{MAX} (F-5A, CURVED BOTTOM, BODY ONLY)

56
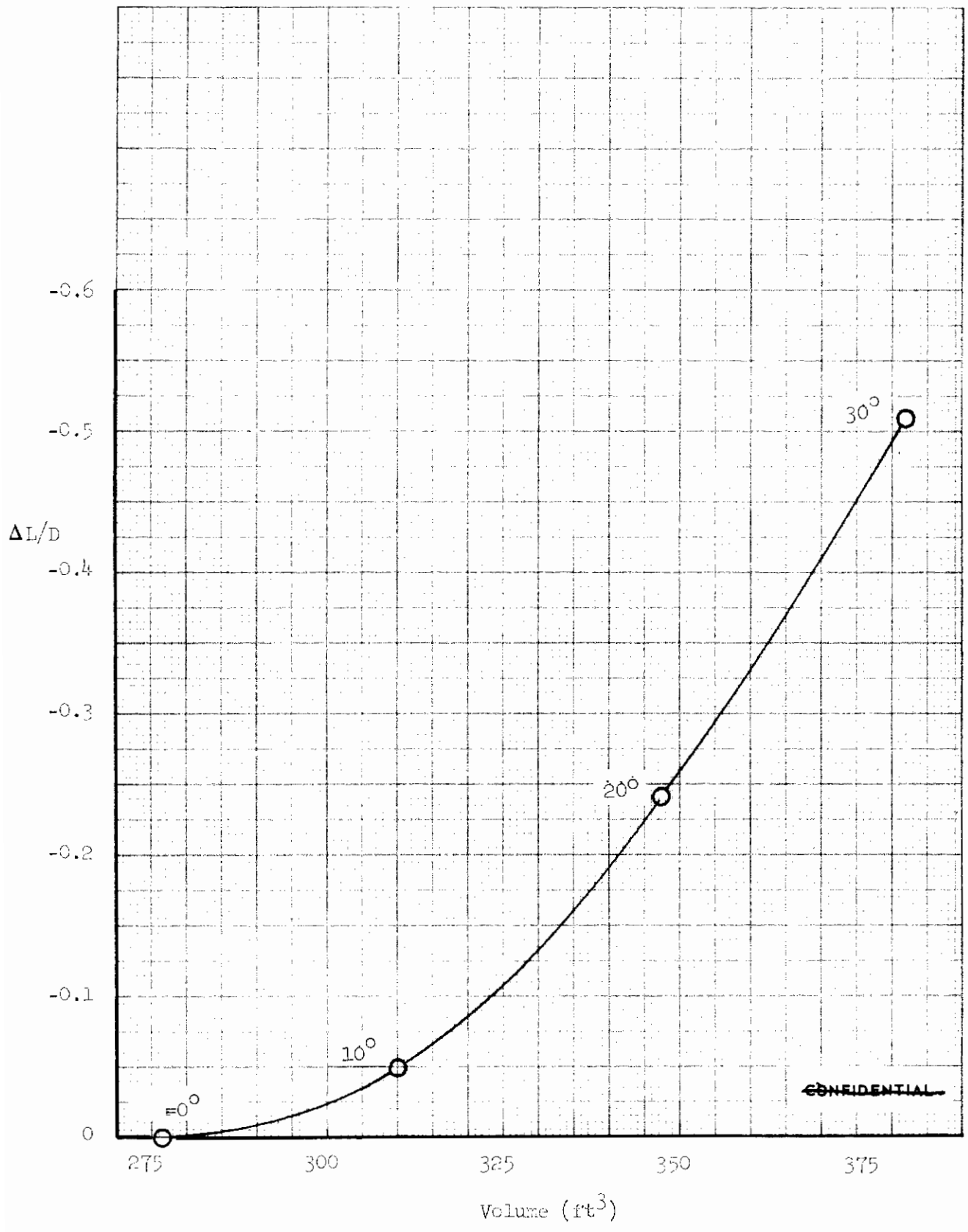
FIGURE 17 (U) EFFECTIVE DIHEDRAL ANGLE TRADE

57

F-5

M = .26
L = 48 (IN.)
τ = 5°
RN = 1.7 x 10^6 (FT)
(UNTRIMMED)

F-5 BASE POINT*
CAMBERED FIN RAMPS

*BASED ON LOCKHEED
WIND TUNNEL TESTS

$(C_D)_{L/D_{MAX}}$

$\bar{S}_{base}$
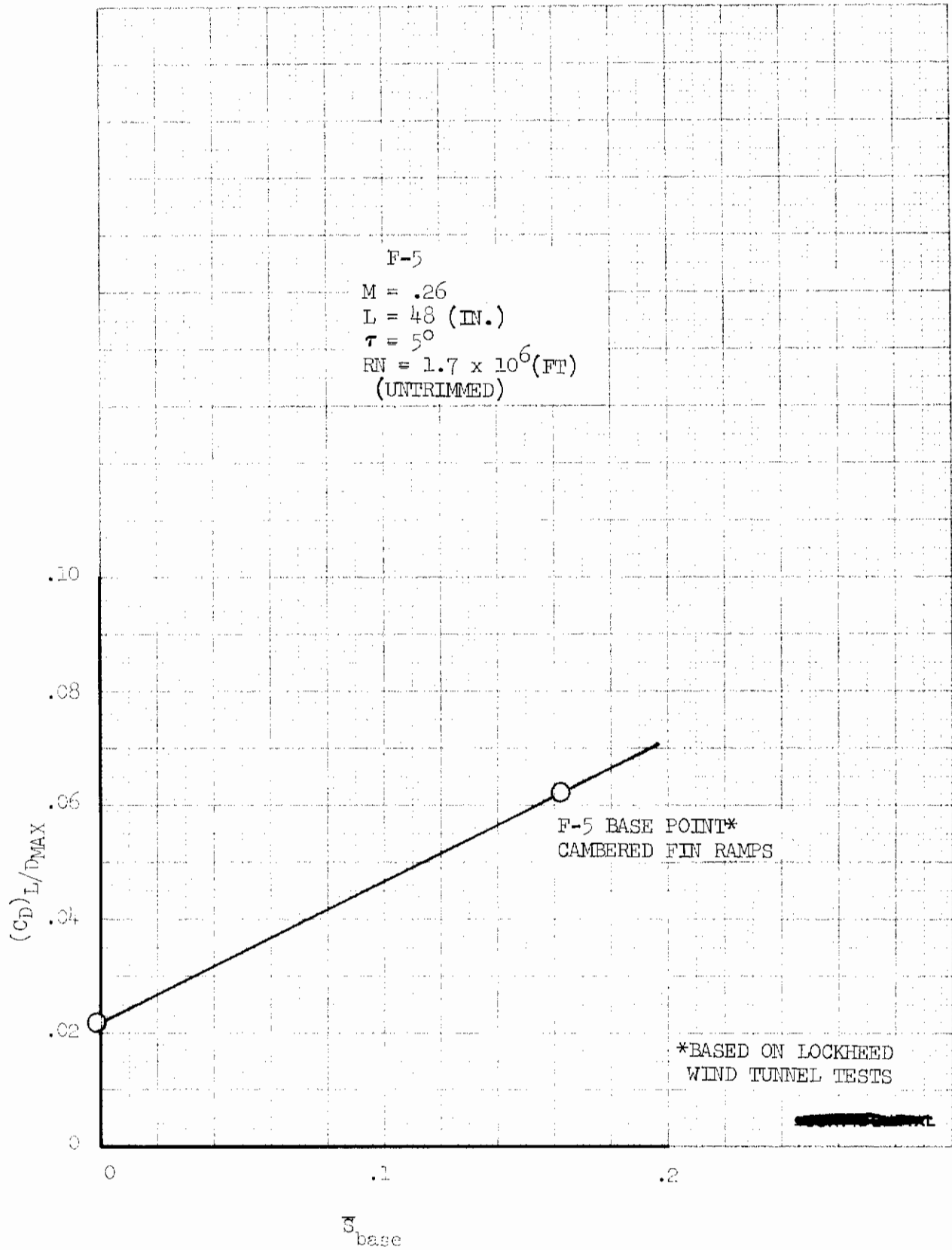
FIGURE 18 (U) EFFECT OF BASE AREA ON SUBSONIC DRAG

58

F-5

M = 20
H = 200,000 (FT)
τ = 5°
K = 25°

F-5 BASE POINT

L/D$_{MAX}$

L (ft)
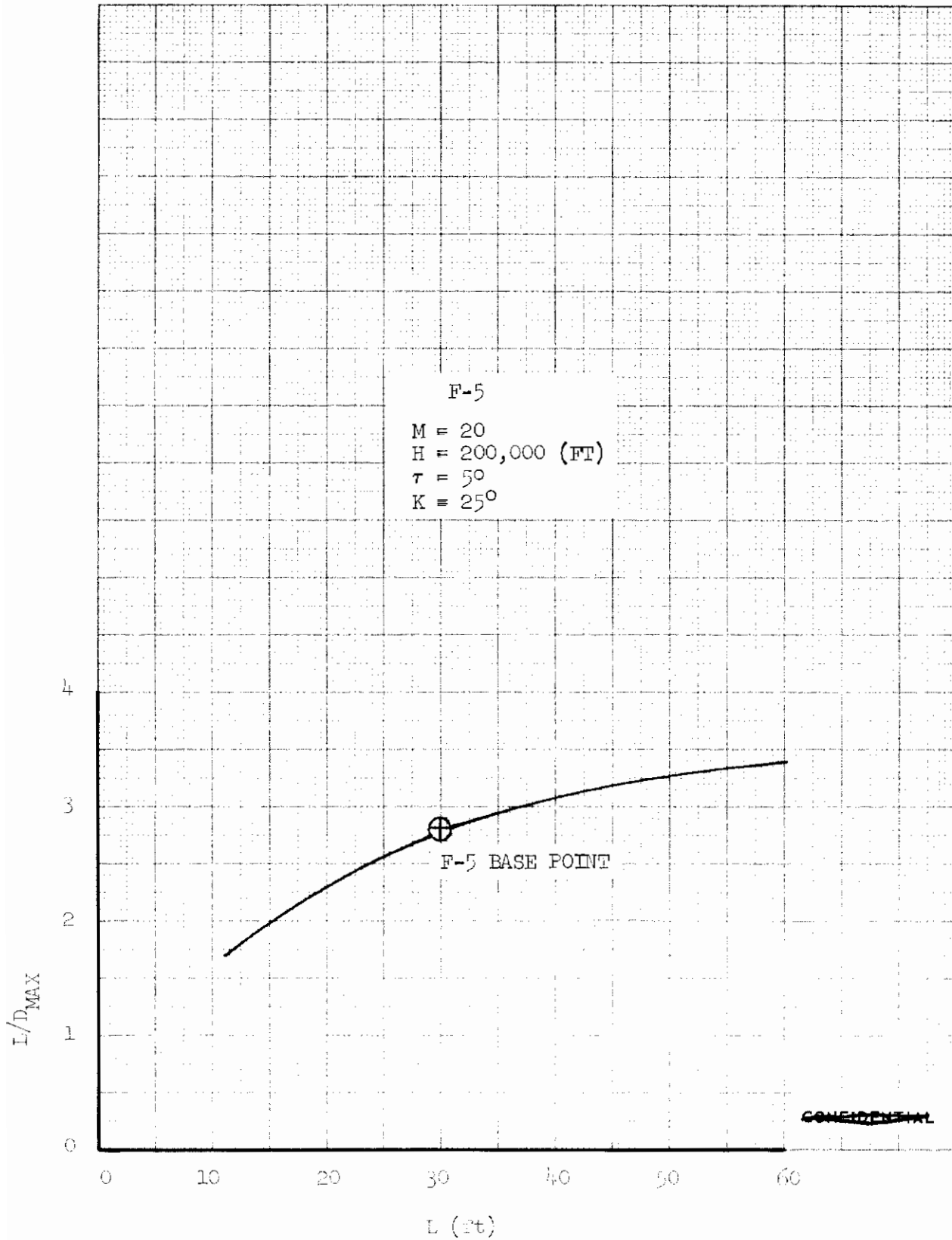
FIGURE 19 (U) VARIATION OF (L/D)$_{MAX}$ WITH VEHICLE LENGTH AT M = 20
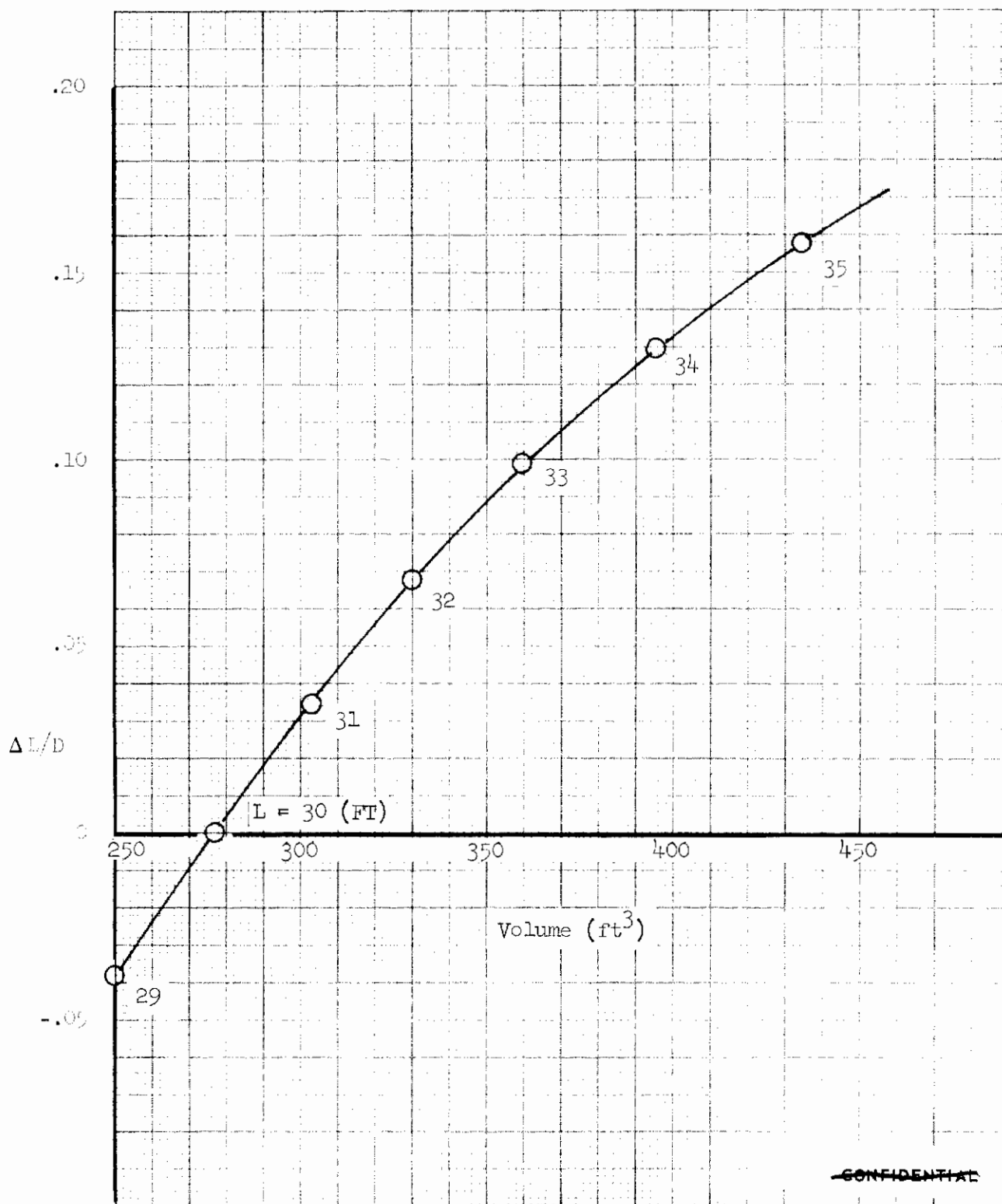
FIGURE 20 (U) LENGTH TRADE
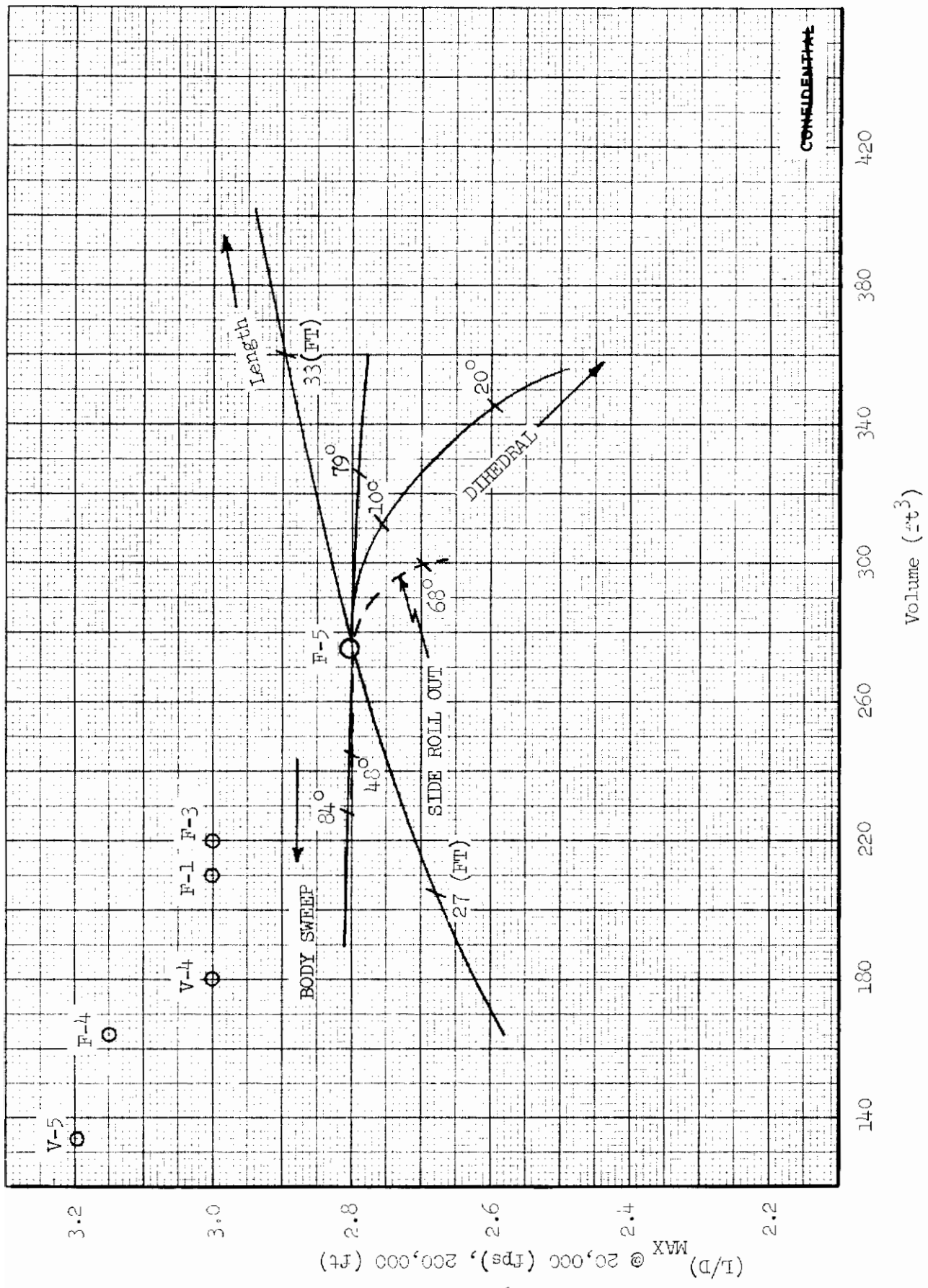
FIGURE 21 (U) VARIATION OF $(L/D)_{MAX}$ WITH VOLUME

F-5
M = 20
H = 200,000 (FT)
L = 30 (FT)
Γ = 5°
K = 25°

4 ─

3 ─

L/D_MAX

F-5 BASE POINT
LER = 1.5 (IN.)

2 ─

1 ─

0 ─

40   60   80

Λ Fin (deg)
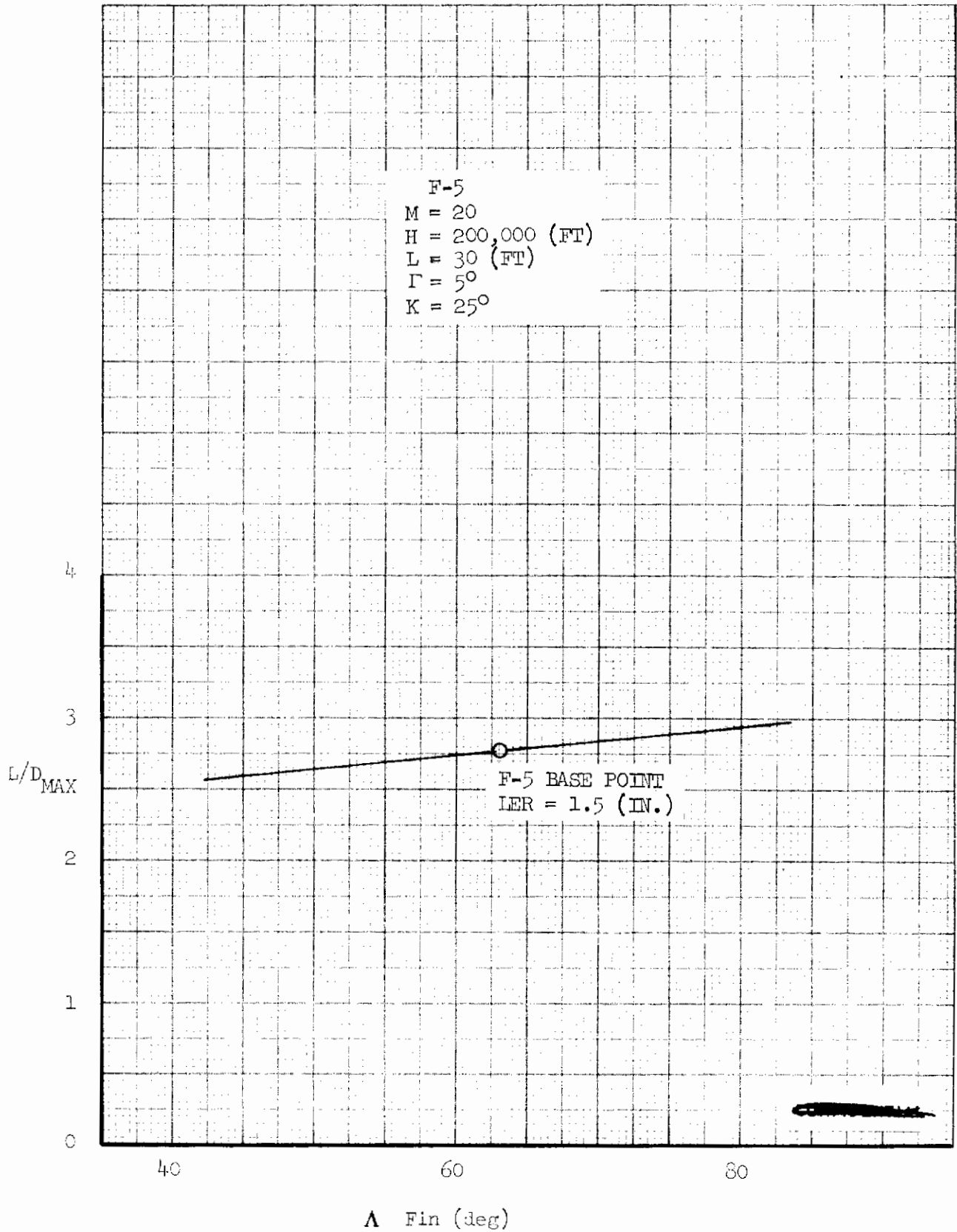
FIGURE 22   (U) VARIATION OF $(L/D)_{MAX}$ WITH FIN SWEEP AT M = 20

F-5
M = 20
H = 200,000 (FT)
L = 30 (FT)
τ = 5°
K = 25°

F-5 BASE POINT

L/D(MAX)

(LER)$_{FINS}$ (in.)
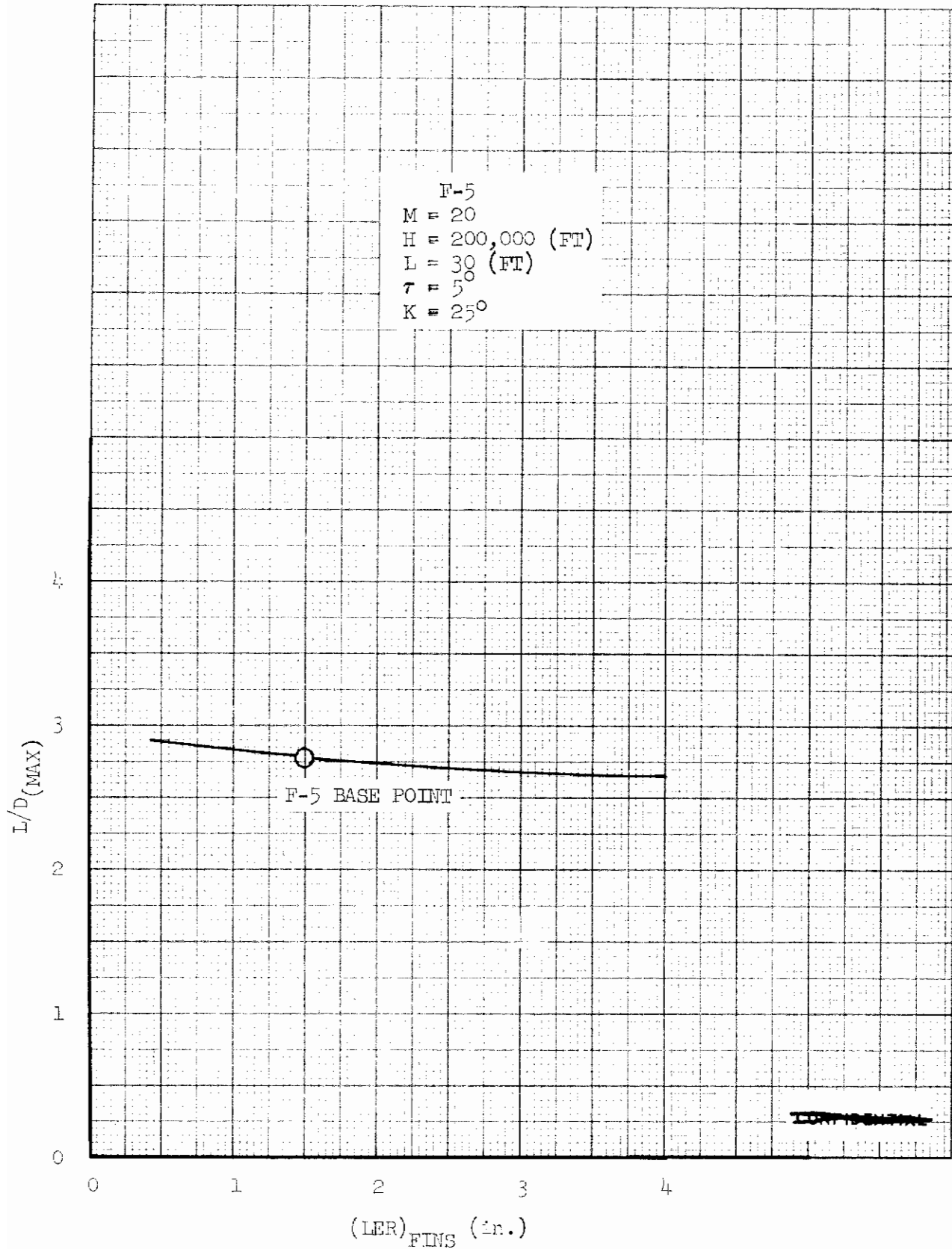
FIGURE 23 (U) VARIATION OF (L/D)$_{MAX}$ WITH FIN LEADING EDGE RADIUS AT M = 20

63
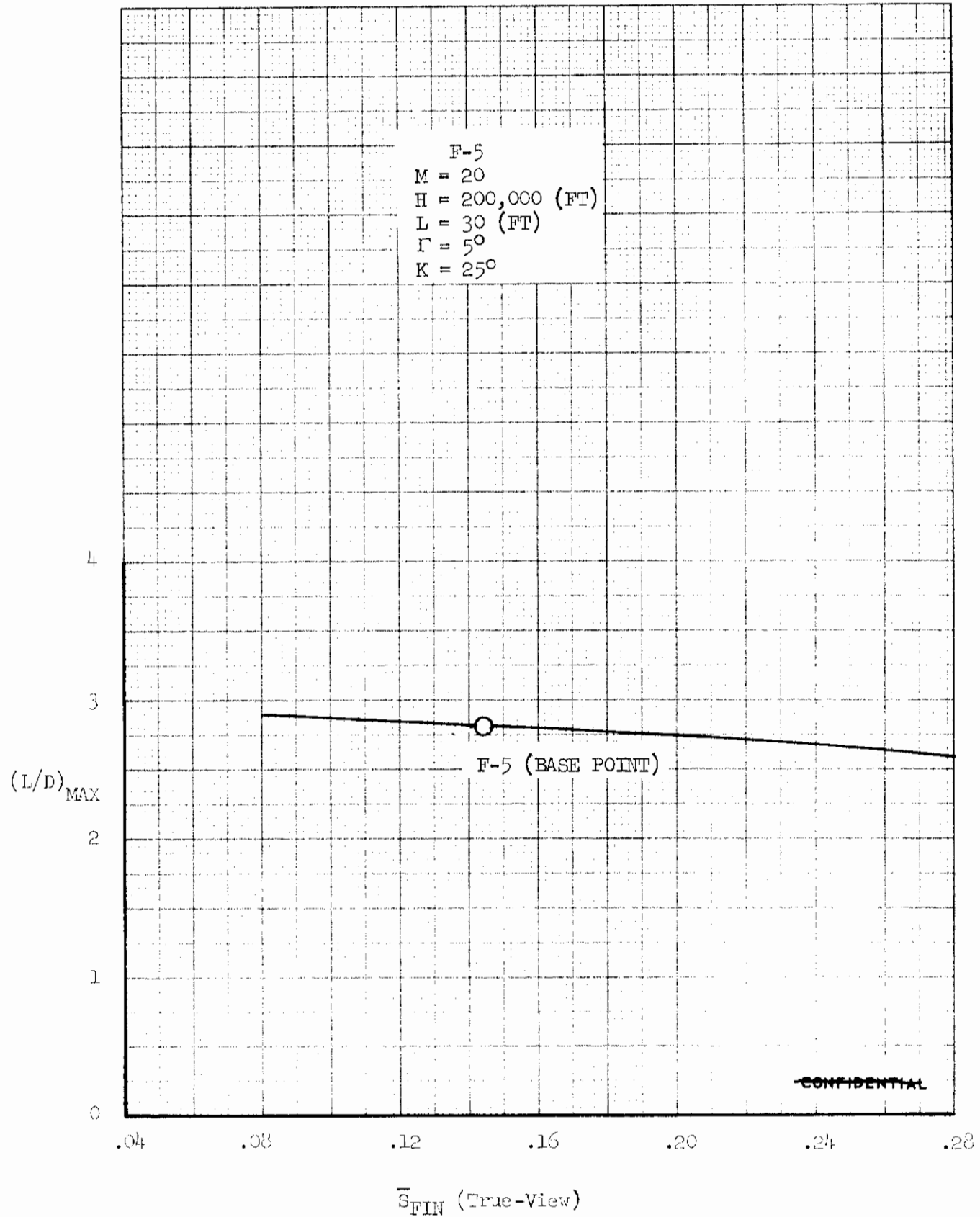
FIGURE 24   (U) VARIATION OF $(L/D)_{MAX}$ WITH FIN SIZE AT M = 20

64
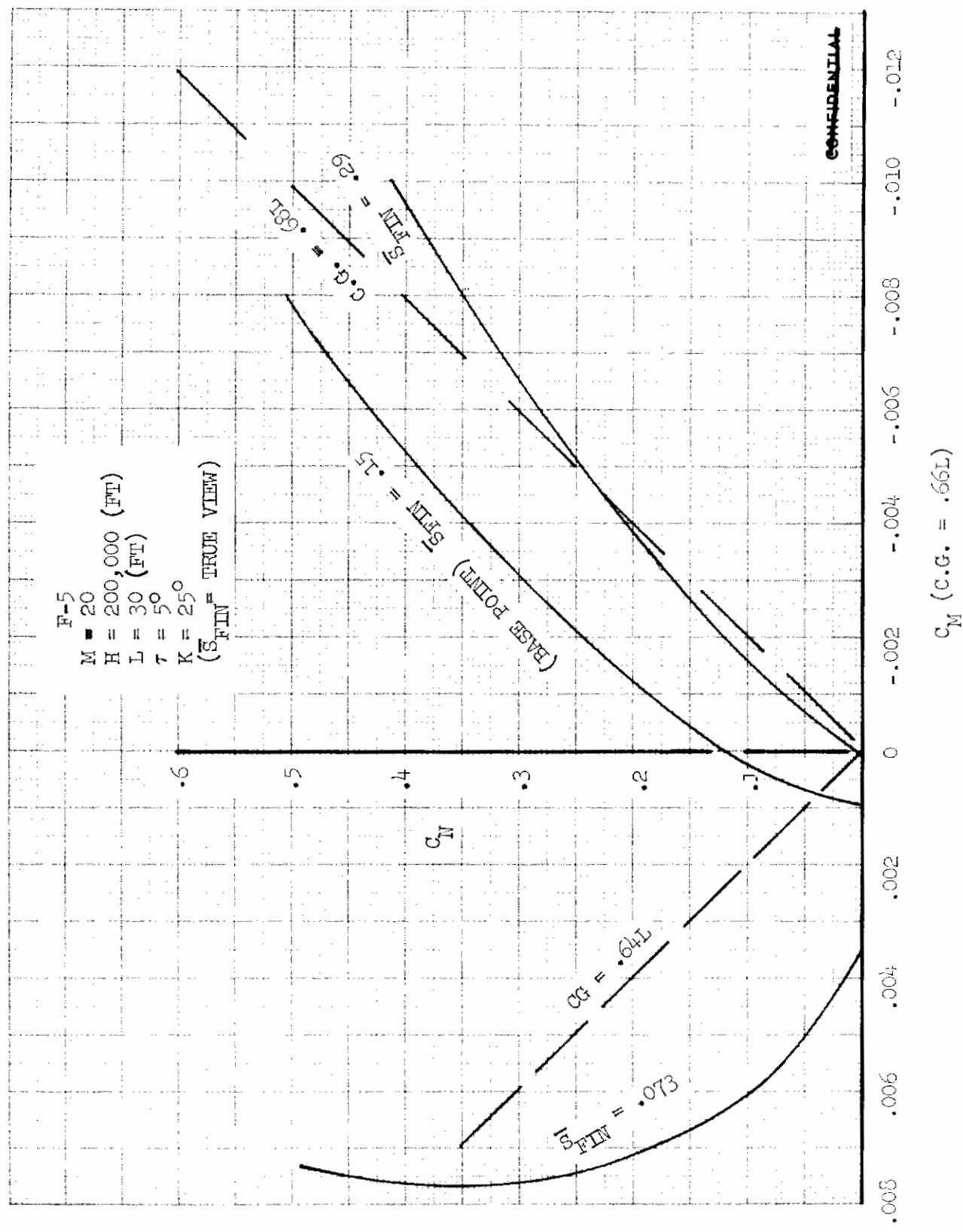
FIGURE 25 (U) VARIATION OF LONGITUDINAL STABILITY WITH FIN SIZE AT M = 20

$\Delta h_2 = 78"$

$\Delta h_1 = 16.5"$

$\vec{F}_{HIGH}$

$\vec{F}_{INT}$

$\vec{F}_{LOW}$

L_D

$D_2 = 23.5"$

$D_3 = 41"$

$D_1 = 35.5"$
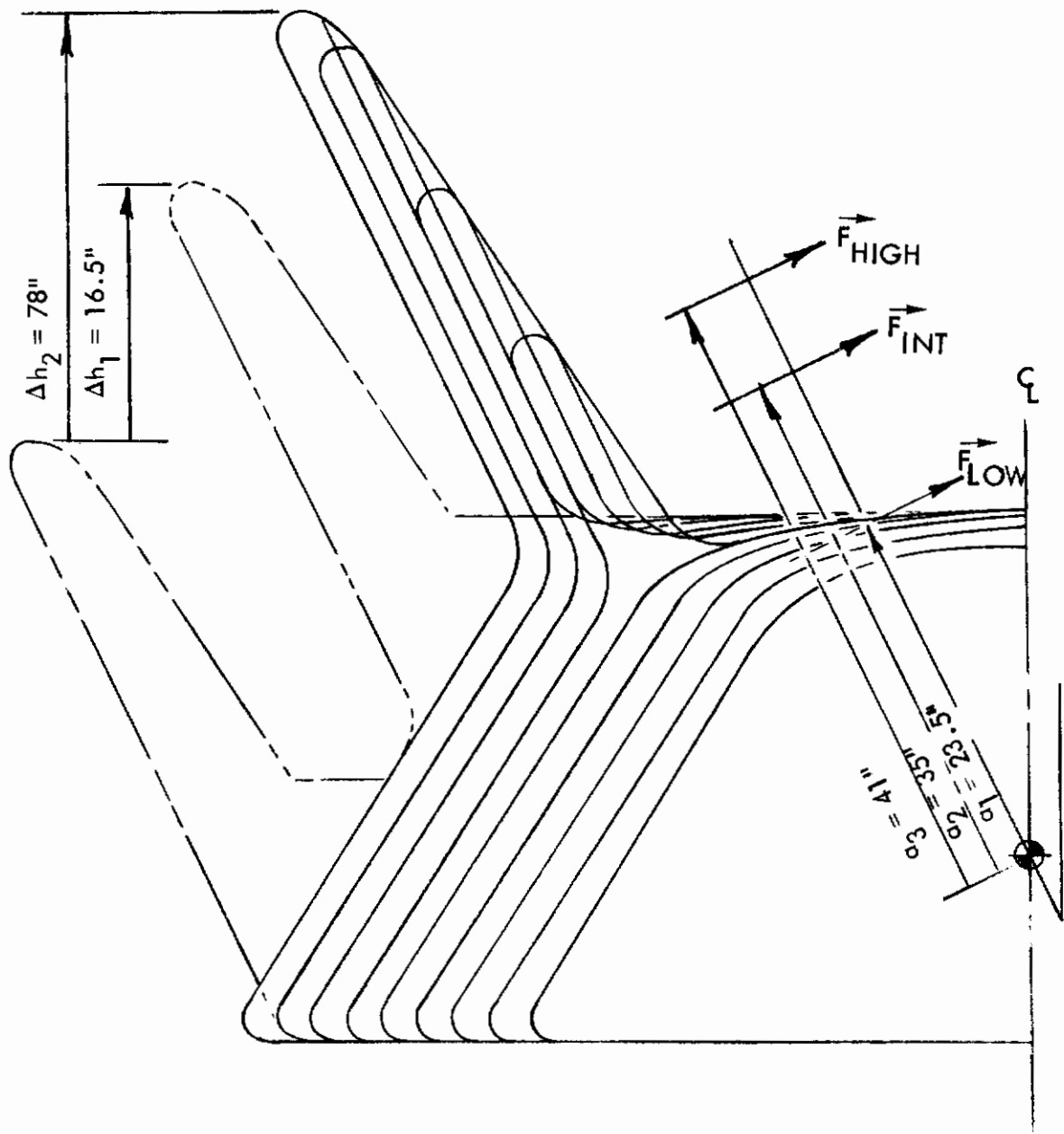
FIGURE 26 (U) MODE OF VERTICAL FIN TRANSLATION

66
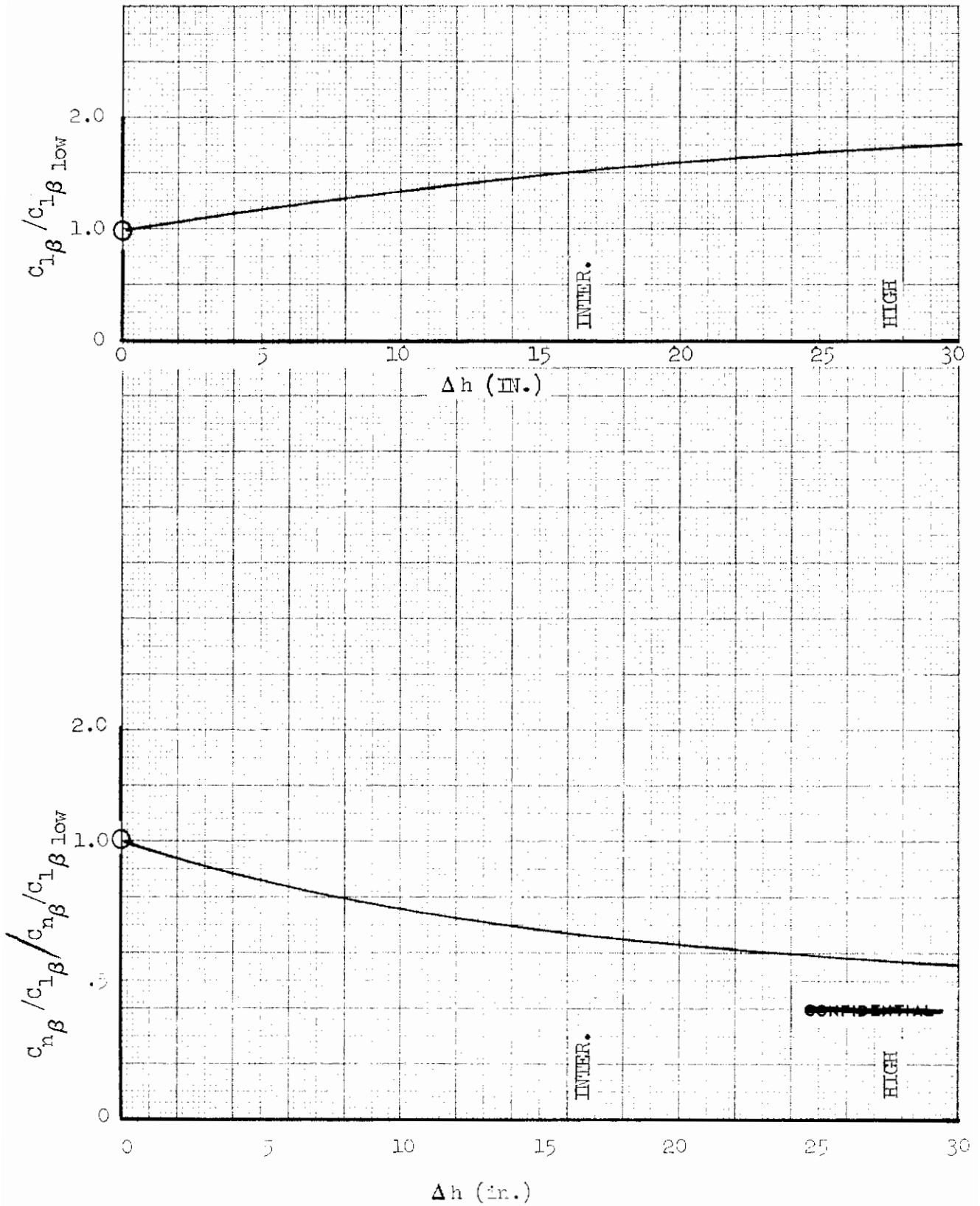
FIGURE 27 (U) VARIATION OF YAW STABILITY WITH FIN GEOMETRY AT M = 20

67

F-5
M = 20
H = 200,000 (FT)
L = 30 (FT)
$\tau = 5^{\circ}$
K = 25°

$\delta_E = 0^{\circ}$

$(L/D)_{MA}$

F-5 BASE POINT

$\overline{S}_{ELE}$
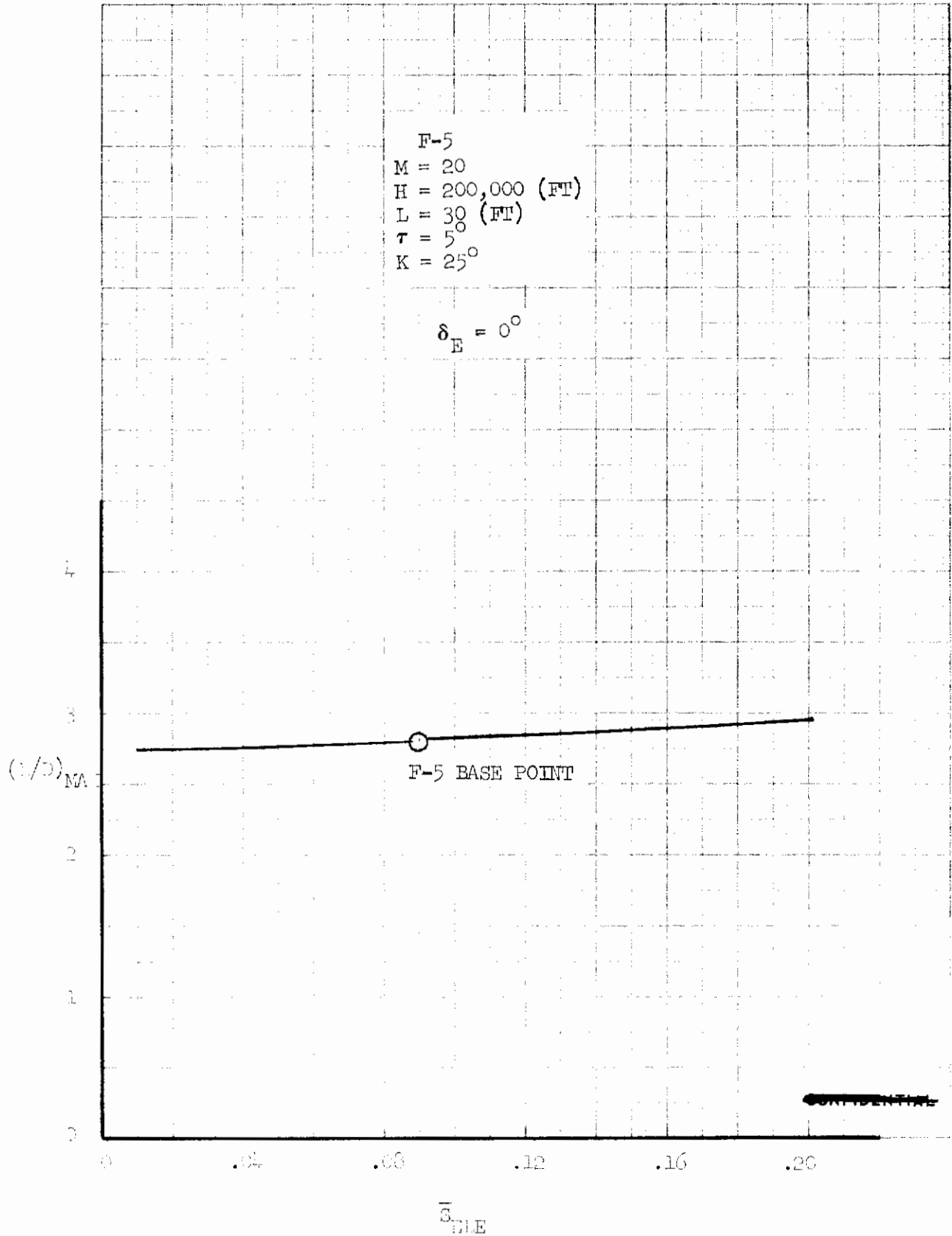
FIGURE 28 (U) VARIATION OF $(L/D)_{MAX}$ WITH ELEVON SIZE AT M = 20 $(\delta_E = 0^{\circ})$

68
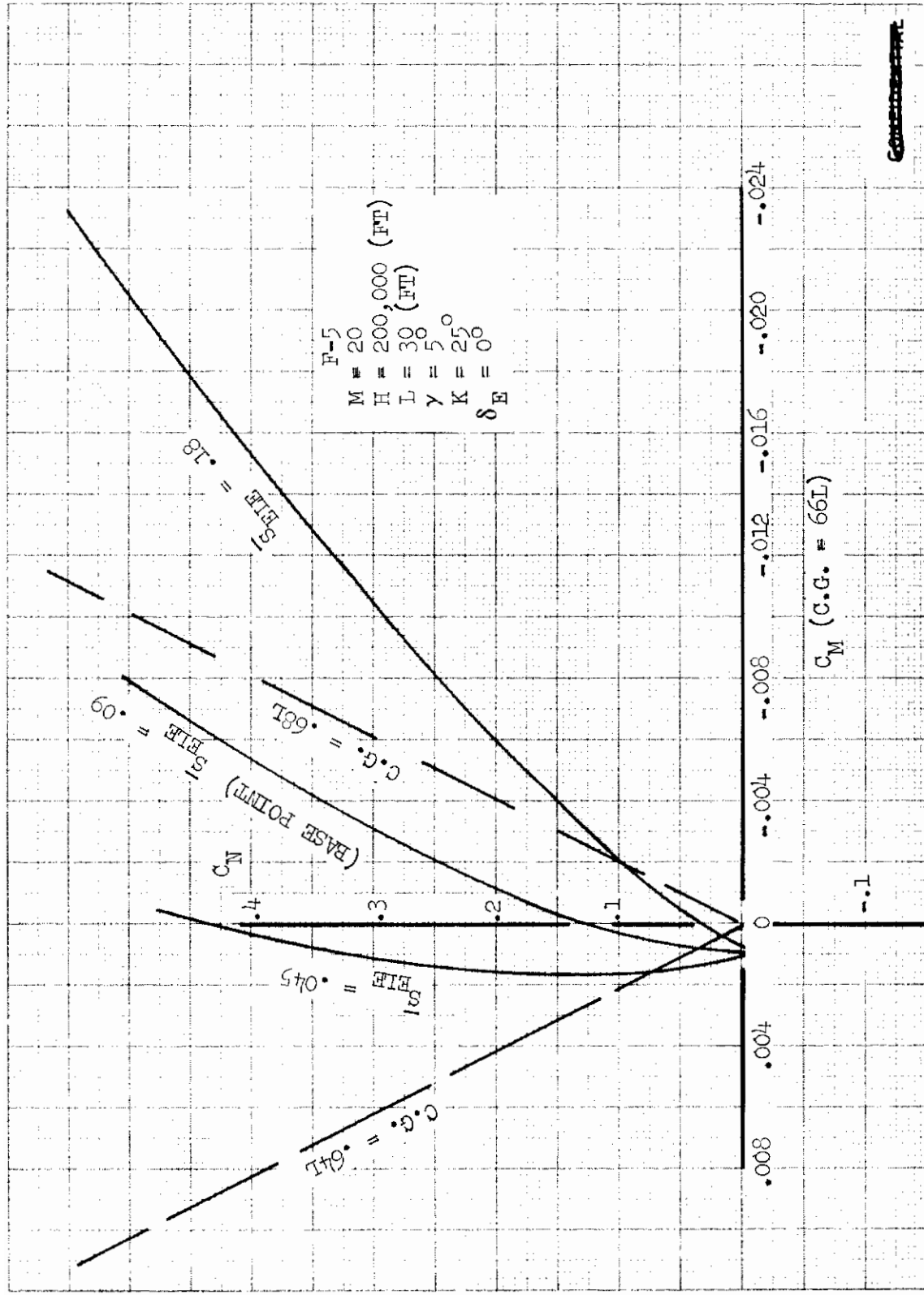
FIGURE 29 (U) VARIATION OF LONGITUDINAL STABILITY WITH ELEVON SIZE AT M = 20 (δ_E = 0°)

69
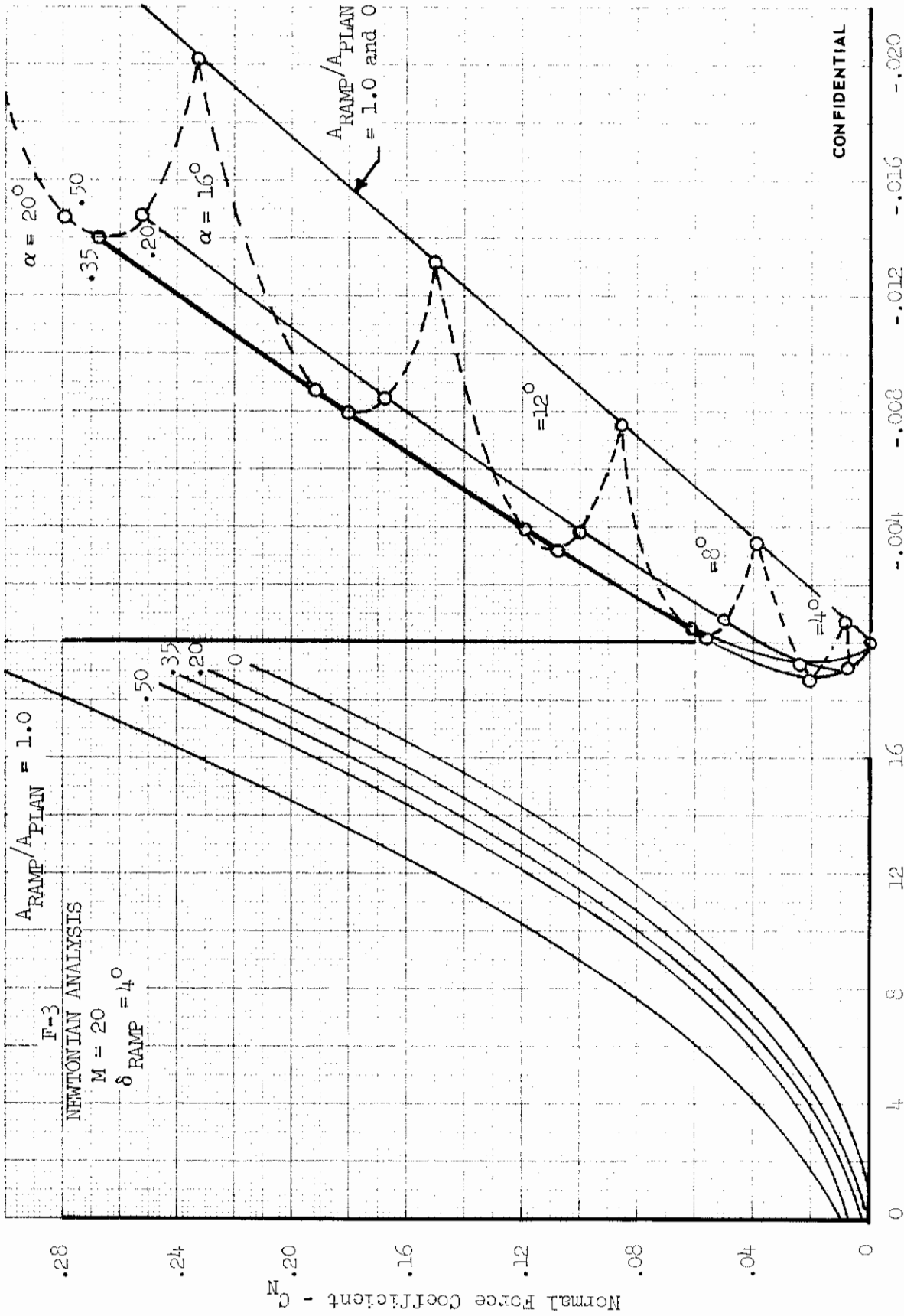
FIGURE 30 (U) VARIATION OF LONGITUDINAL STABILITY WITH LOWER RAMP SIZE AT M = 20

NEWTONIAN FLOW THEORY, K = 2.0
(FLAT BOTTOM F-5, BODY ONLY)

$\alpha = 12^{\circ}$

L/D$_{MAX}$

δ_N (deg)
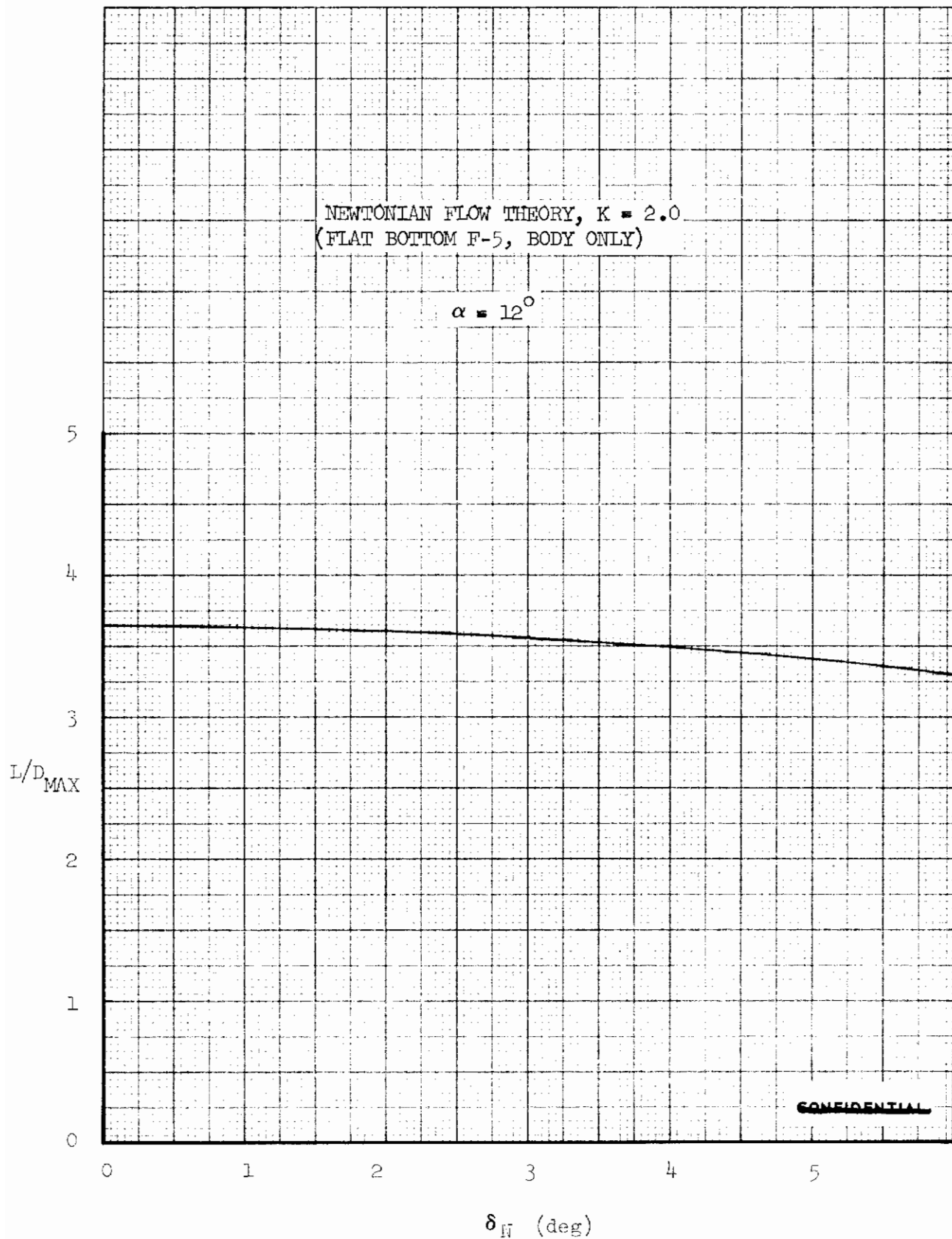
FIGURE 31 (U) EFFECT OF δ_N ON L/D$_{MAX}$

71
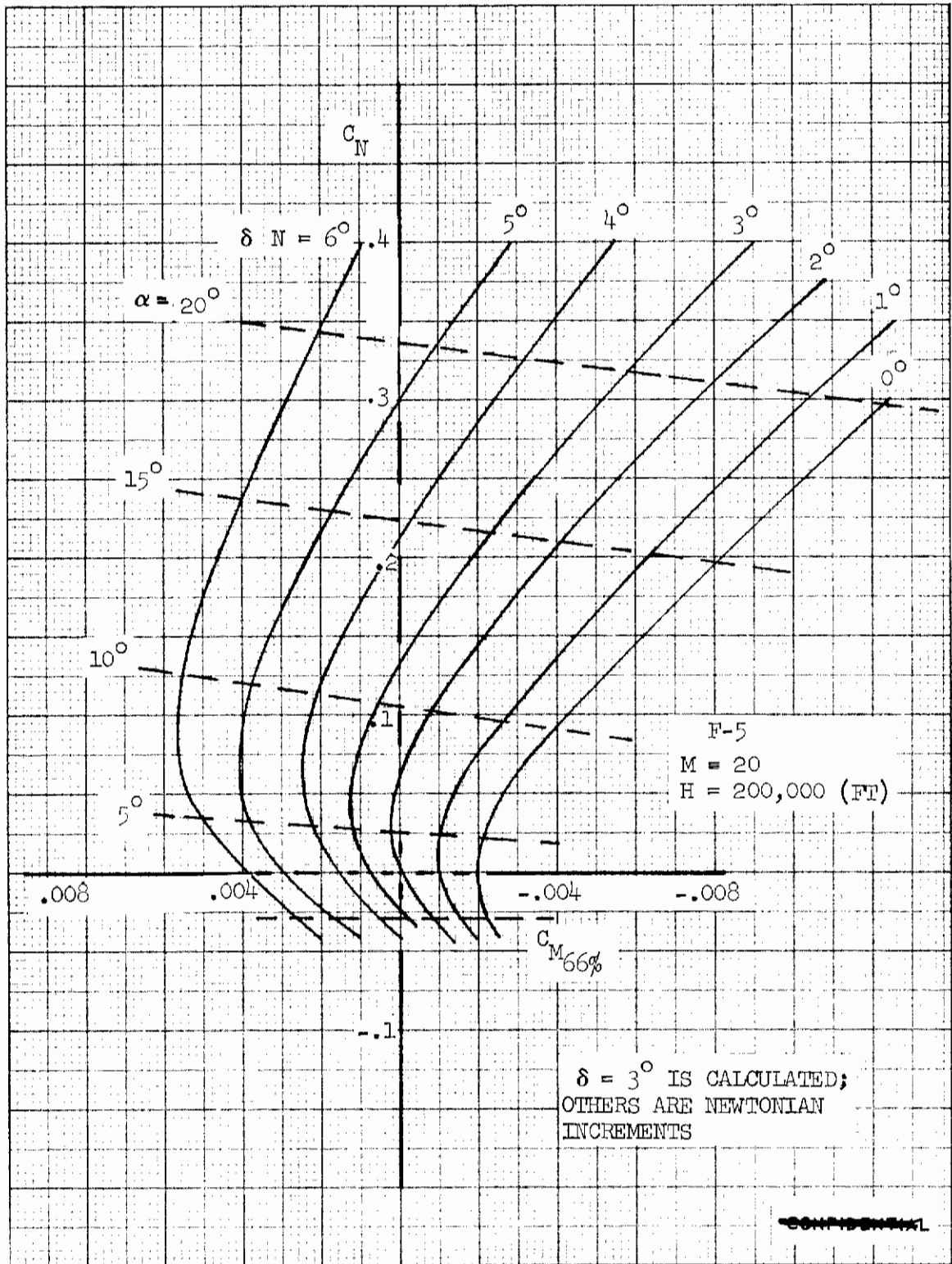
FIGURE 32   (U) EFFECT OF NOSE RAMP VARIATION

72

SERIES "A"

PARAMETRIC VARIATIONS

K_{TE}
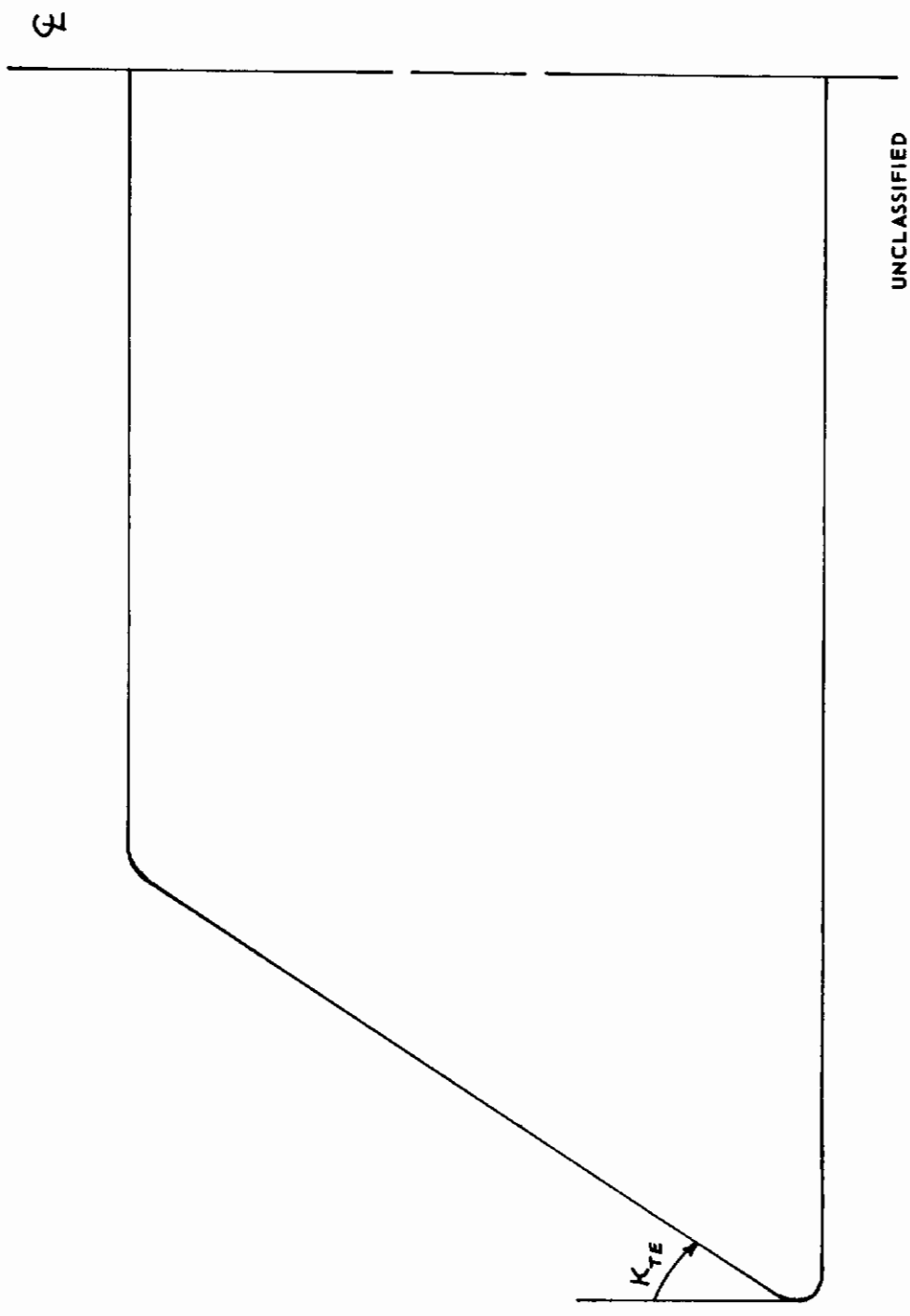
UNCLASSIFIED

FIGURE 33 (U) VEHICLE TRAILING EDGE STATION

(REVERSE SIDE IS BLANK)

FIGURE 34   (U) AFT BODY ALTERNATE NO. 1
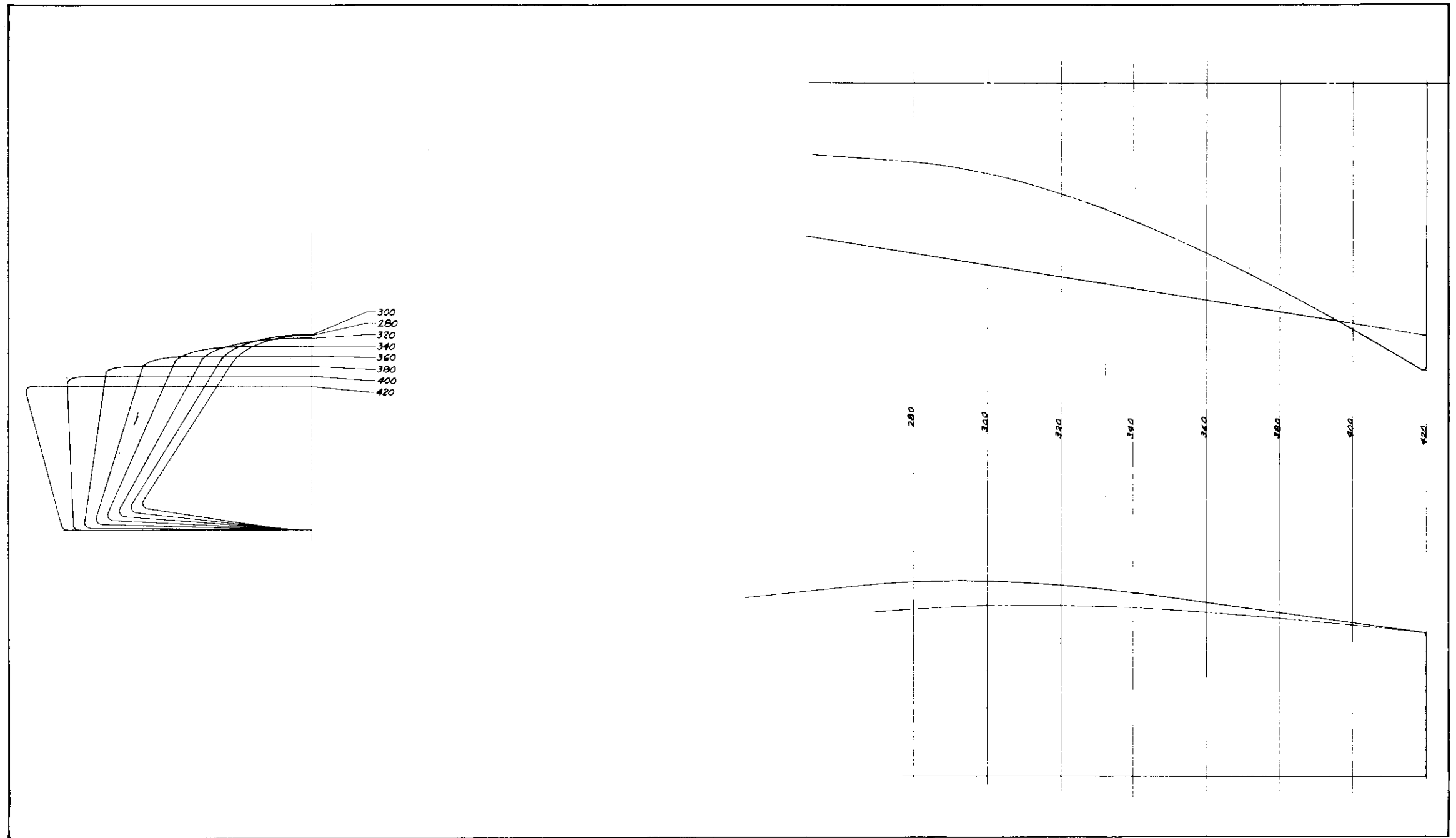
FIGURE 35 (U) AFT BODY ALTERNATE NO. 2
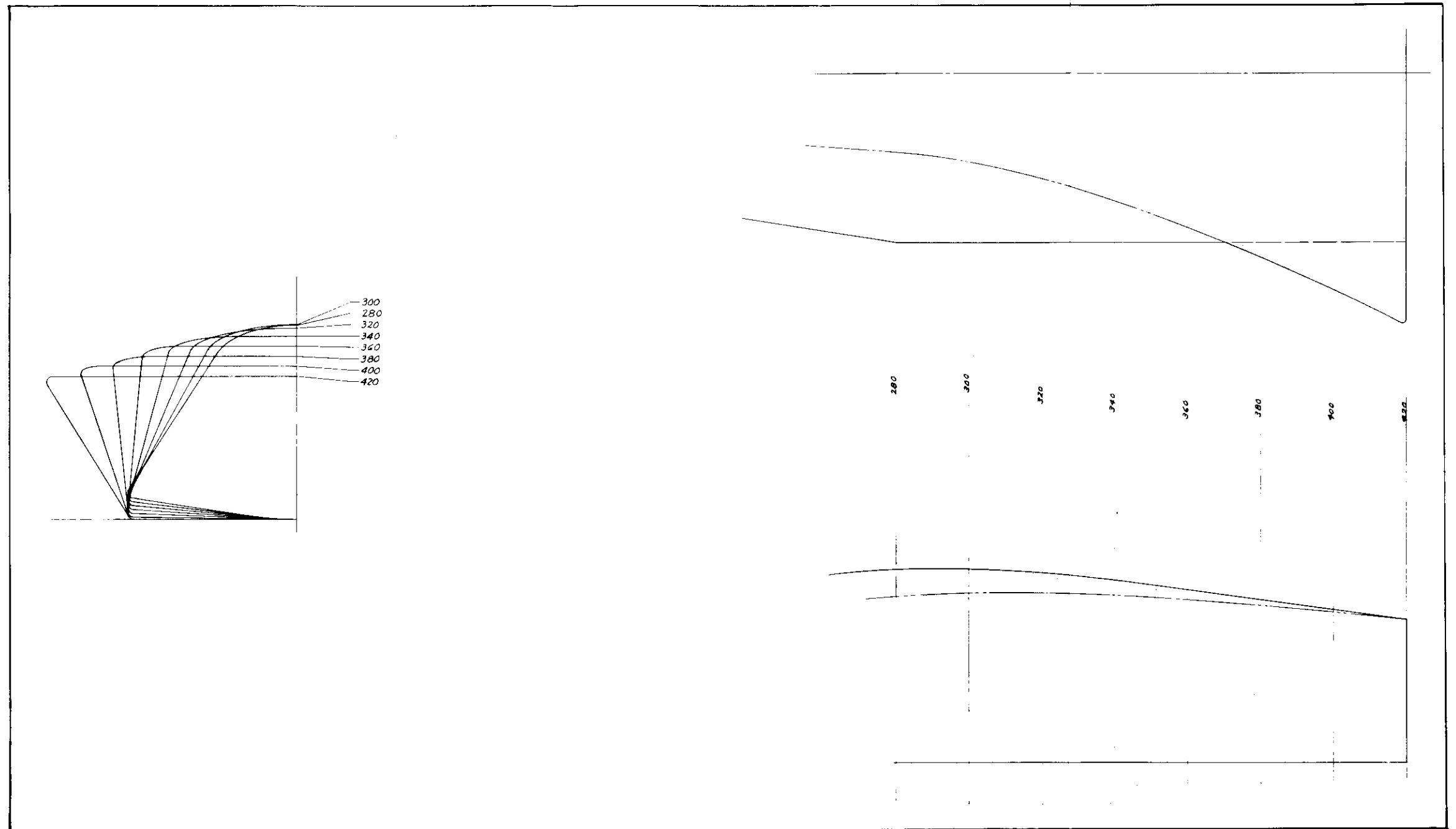
FIGURE 36 (U) AFT BODY ALTERNATE NO. 3
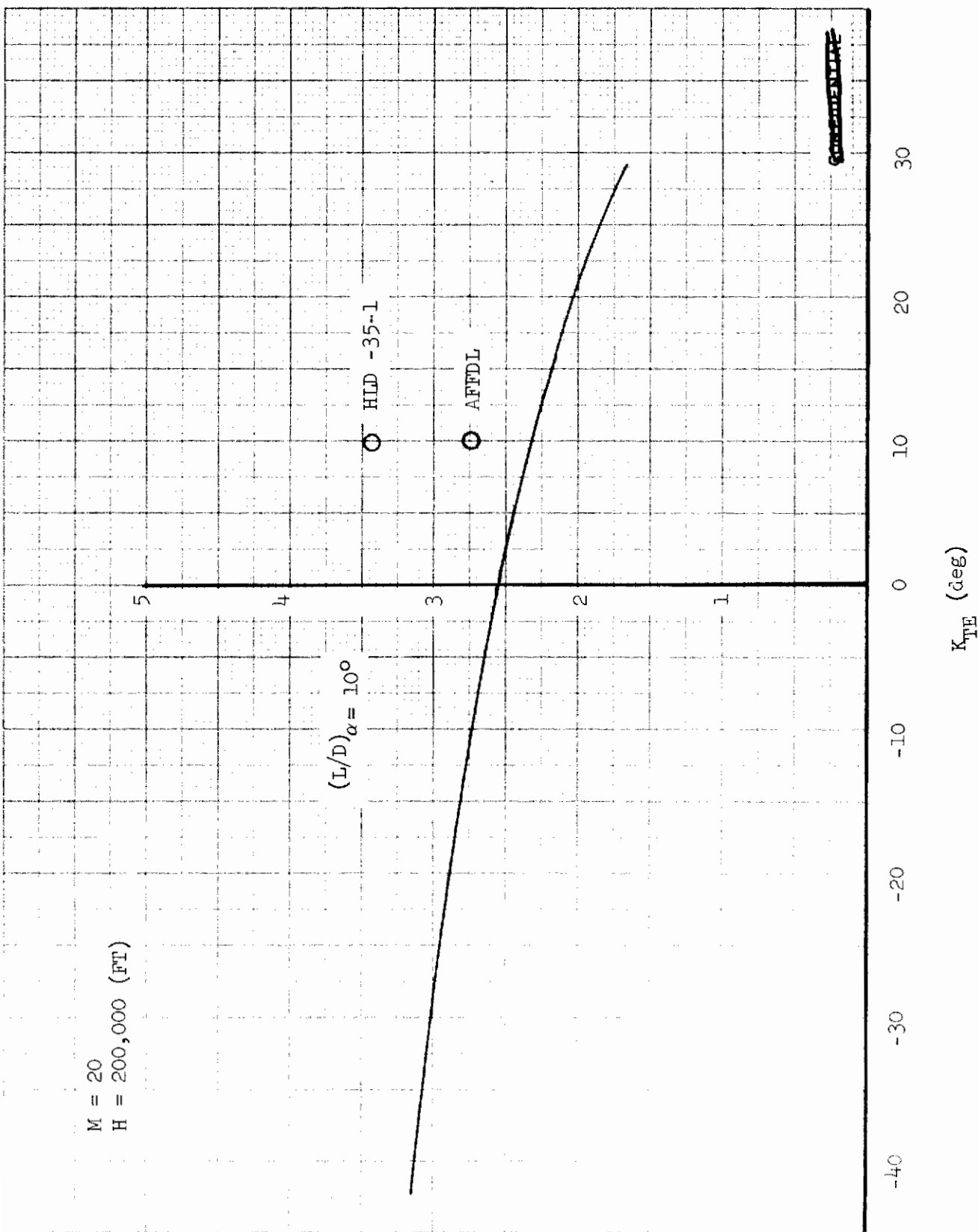
FIGURE 37   (U)   PARAMETRIC VARIATION OF HYPERSONIC L/D WITH AFT BODY CONFIGURATION MODIFICATIONS

81

AFFDL CONFIGURATION
NEWTONIAN FLOW THEORY

C.G. = 0.62L   NO ξ FIN
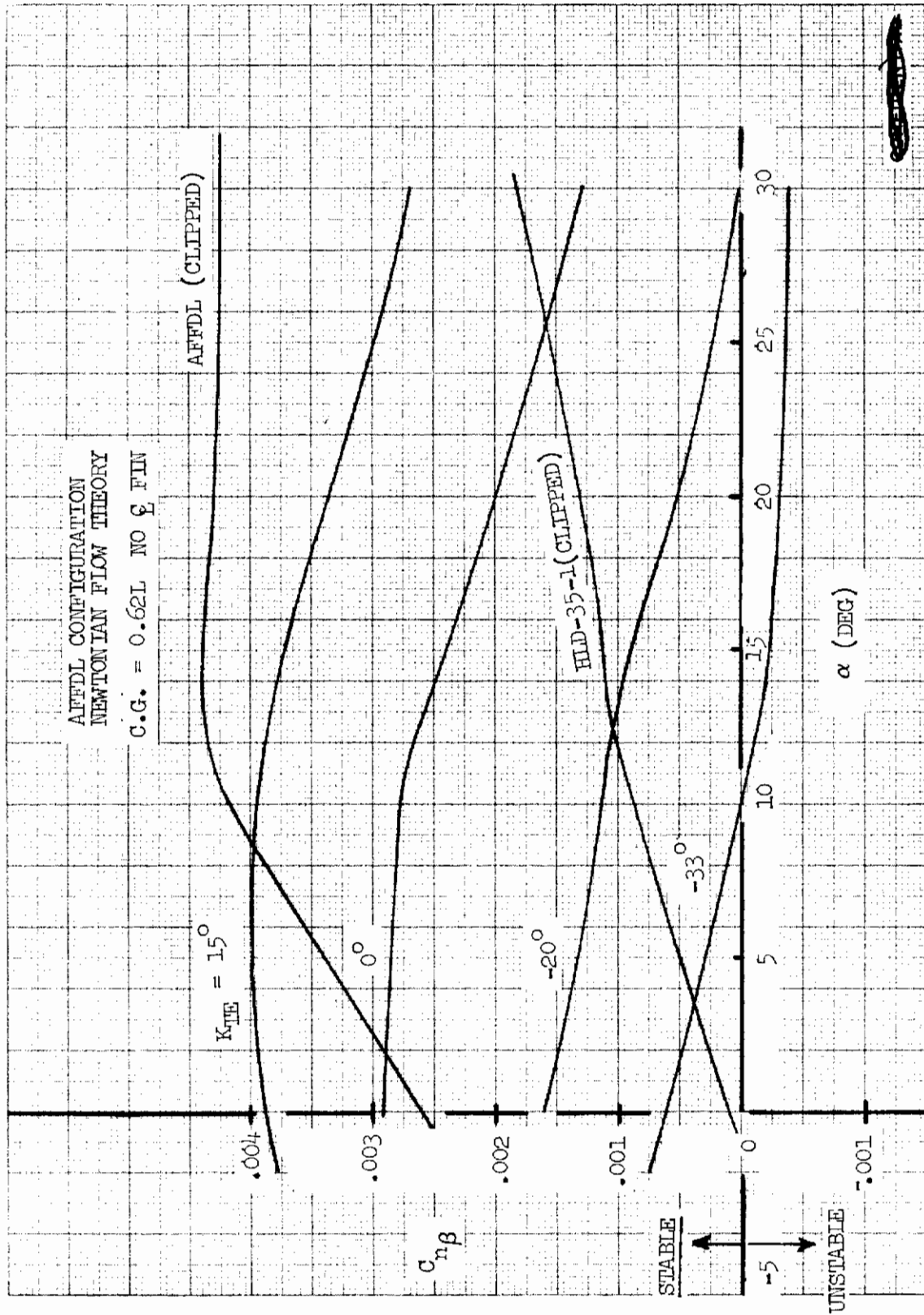
FIGURE 38   (U) VARIATION OF C_{n_β} WITH ANGLE OF ATTACK
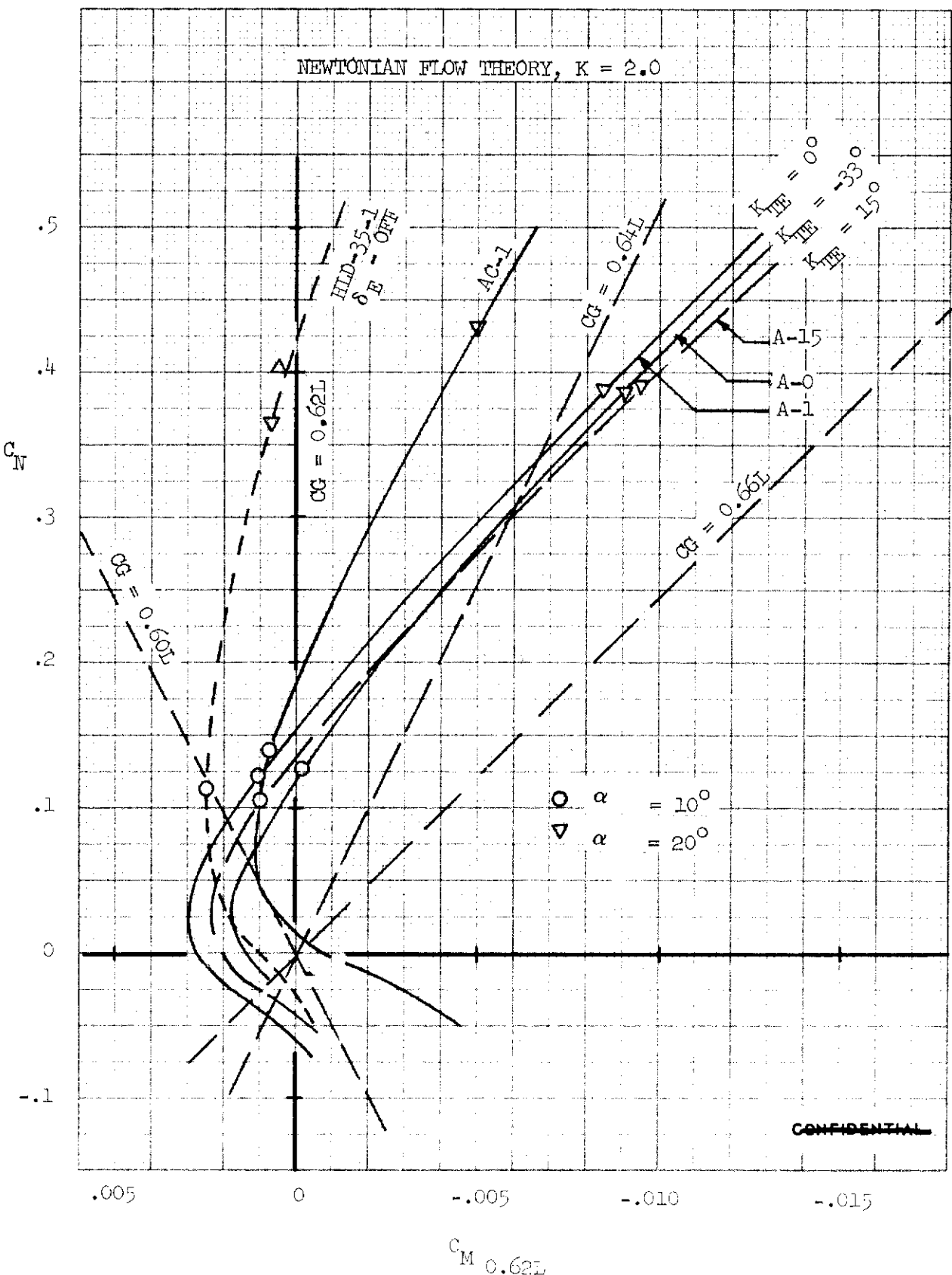
FIGURE 39   (U) VARIATION OF LONGITUDINAL STABILITY
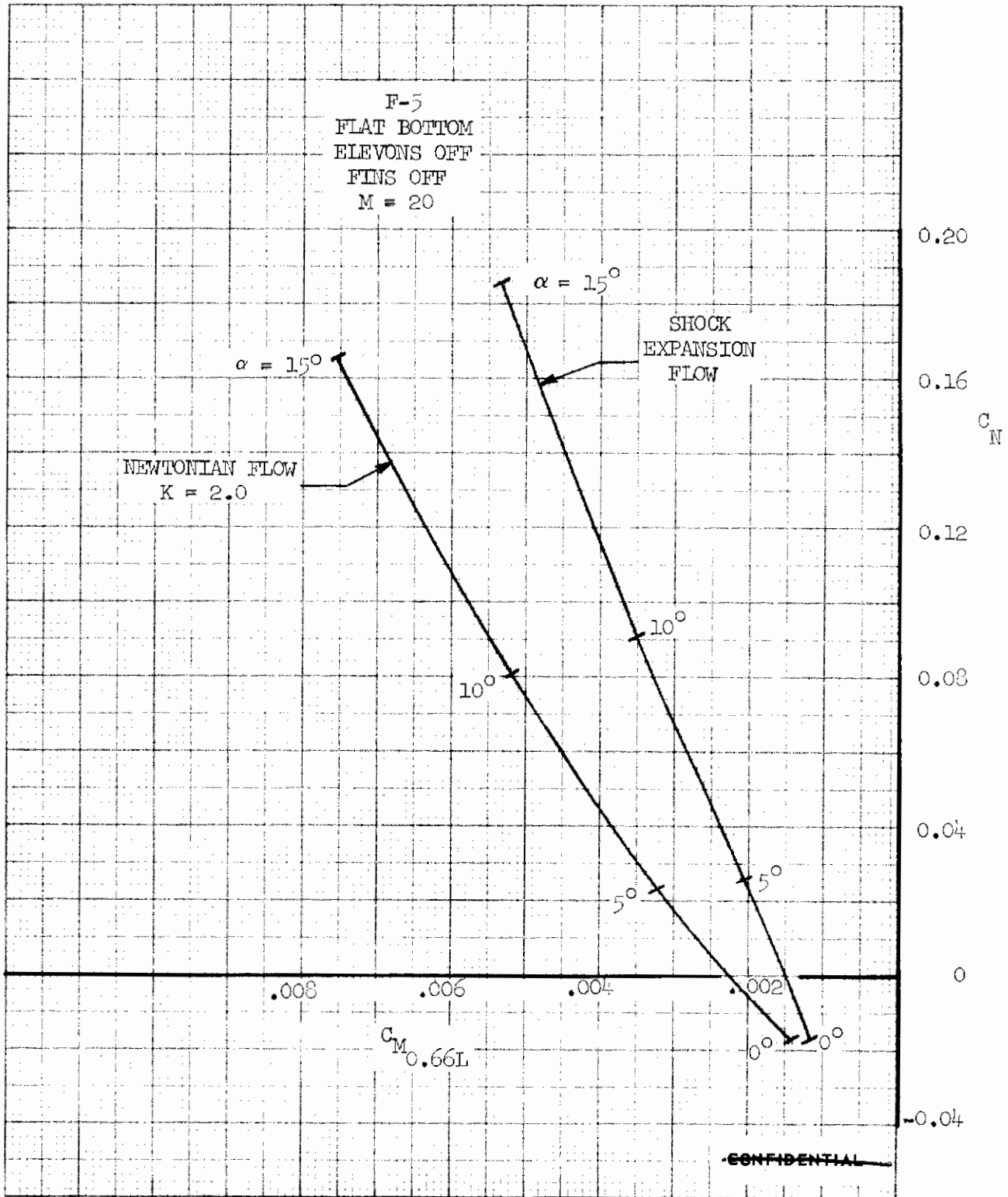
FIGURE 40   (U) LONGITUDINAL STABILITY CHARACTERISTICS OF THE AMR F-5;
            CALCULATED USING NEWTONIAN AND SHOCK-EXPANSION METHODS

84

SERIES "B"

PARAMETRIC VARIATIONS

$T = 5°$, $K = 25°$
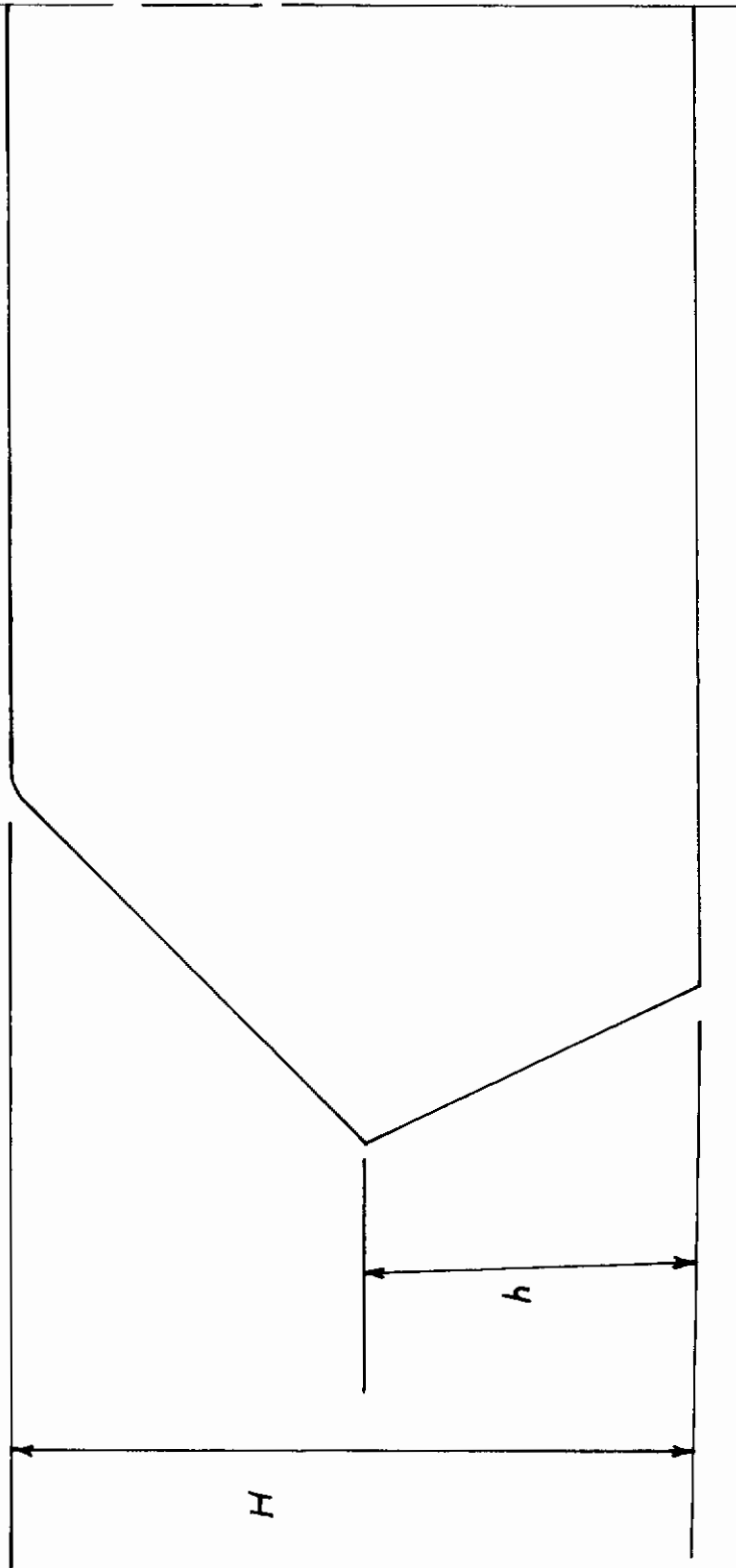
$B_2 \longrightarrow L/H = 0.32$; $B_3 \longrightarrow L/H = 0.48$; $B_4 \longrightarrow L/H = 0.64$ UNCLASSIFIED

FIGURE 41 (U) VEHICLE TRAILING EDGE STATION

CONFIDENTIAL
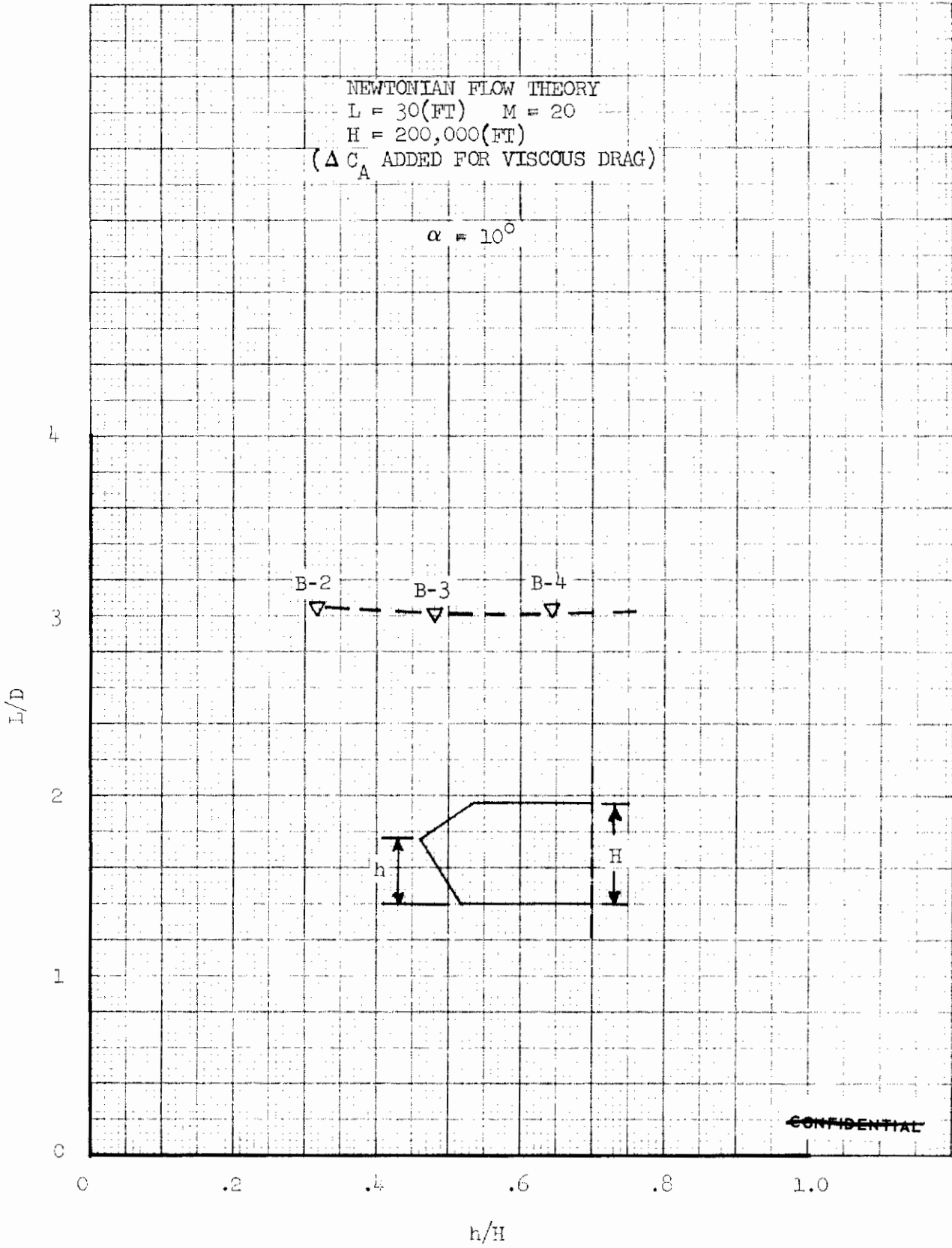
FIGURE 42 (U) VARIATION OF L/D - B-SERIES CONFIGURATIONS

86

CONFIDENTIAL
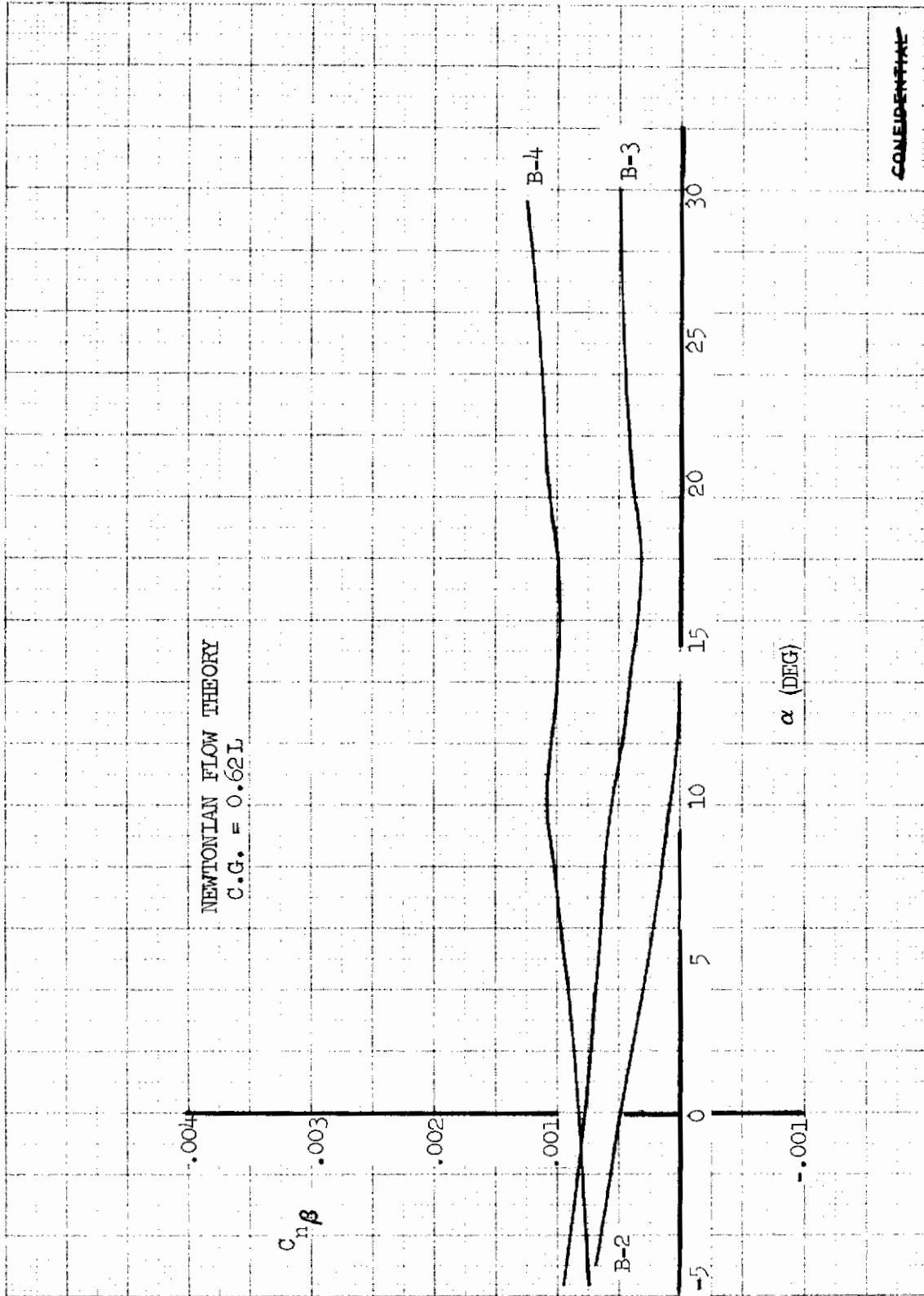
FIGURE 43 (U) VARIATION OF C_{n_β} WITH α - B-SERIES CONFIGURATIONS
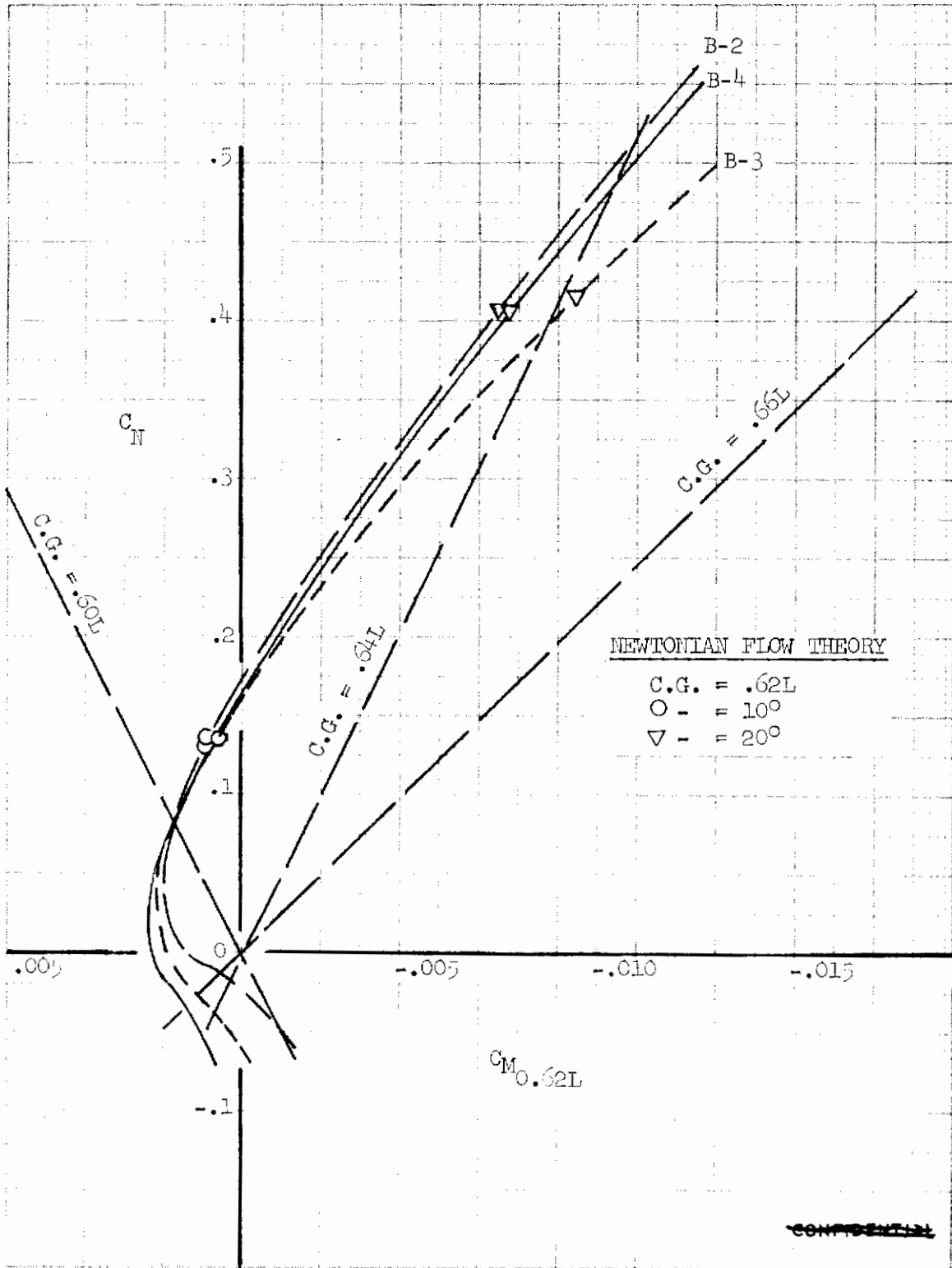
FIGURE 44 (U) VARIATION OF LONGITUDINAL STABILITY - B-SERIES CONFIGURATIONS

SERIES "C"

PARAMETRIC VARIATIONS

(FDL - 5A)

(PLANFORM)

(TRAILING - EDGE)
(STATION)
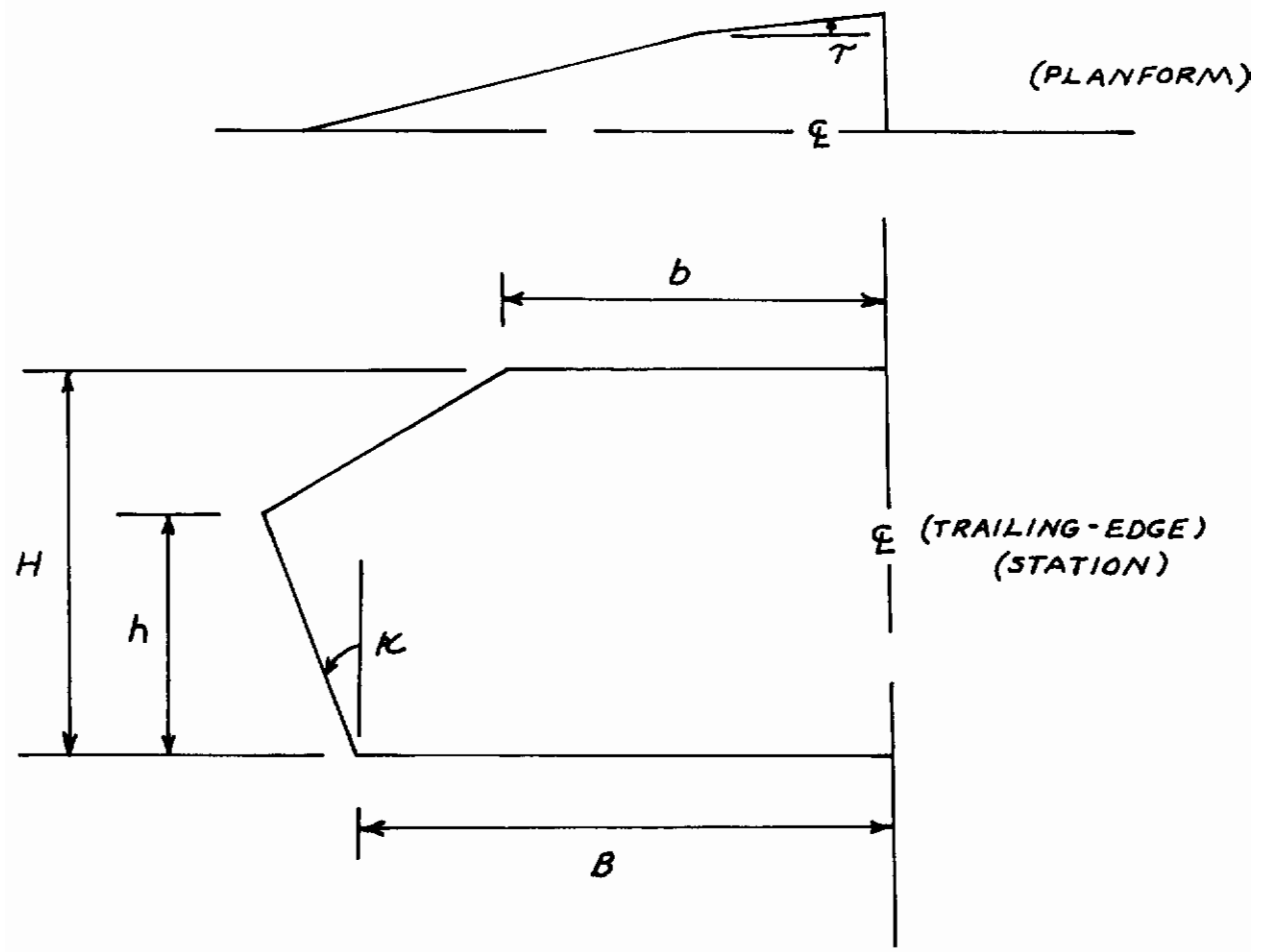
UNCLASSIFIED

FIGURE 45 (U) DEFINITION OF PARAMETRIC VARIABLES
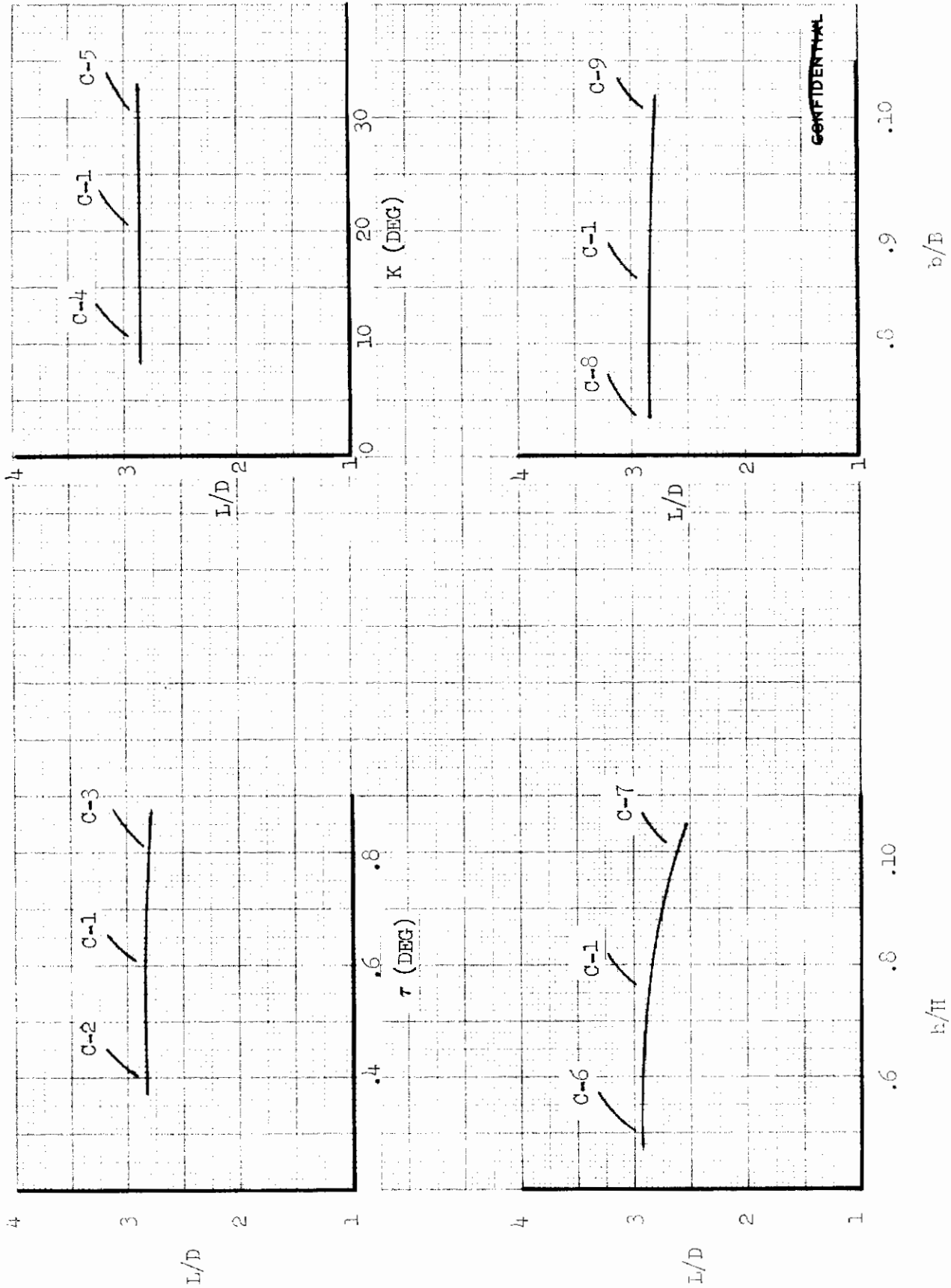
FIGURE 46 (U) VARIATION OF L/D FOR PARAMETRIC CHANGES TO THE FDL-JA CONFIGURATION
(α = 10 deg ; M = 20; h = 200,000 ft ; L = 30 ft)
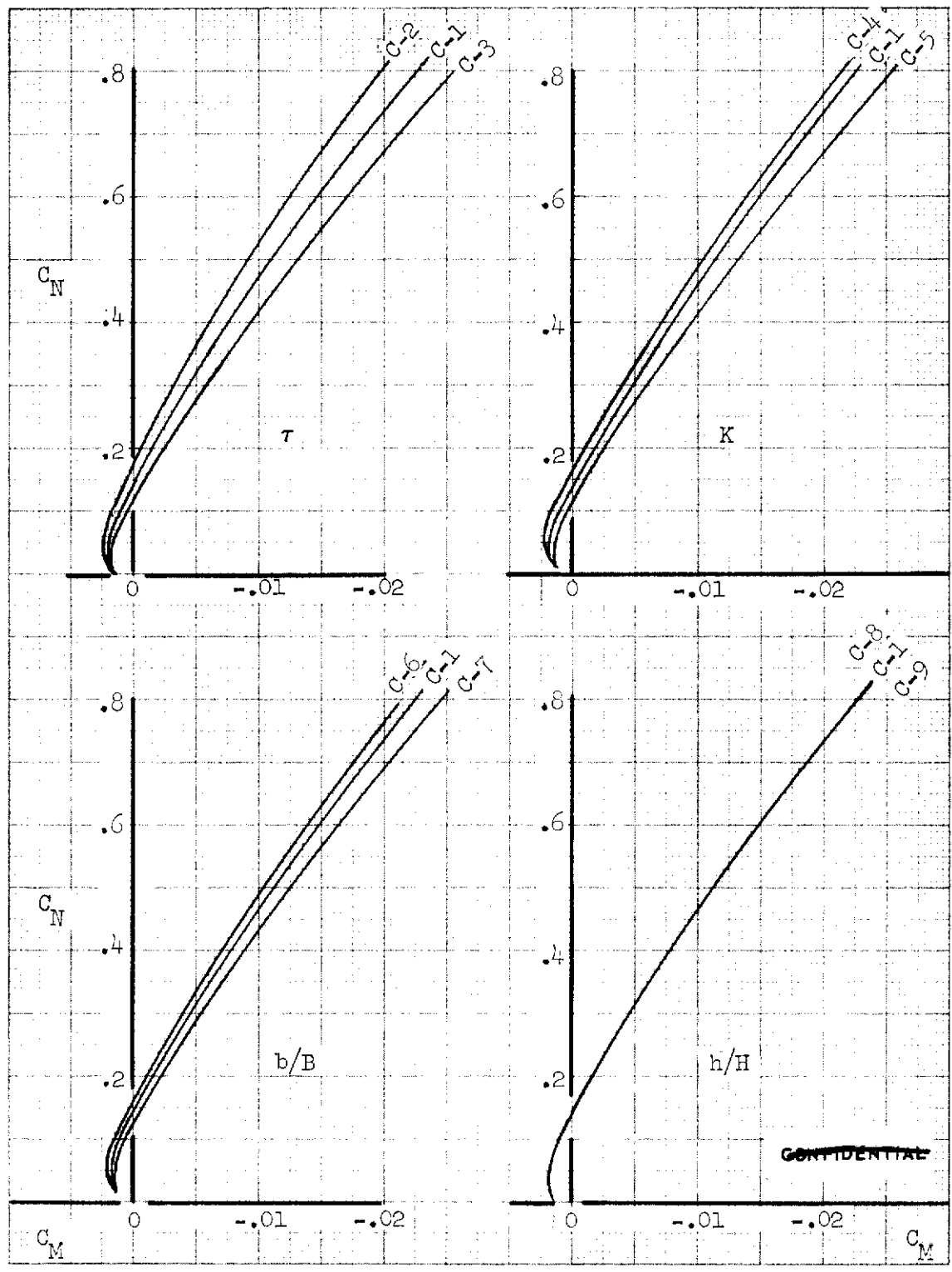
FIGURE 47 (U) VARIATION OF LONGITUDINAL STABILITY FOR PARAMETRIC CHANGES
TO THE FDL-5A CONFIGURATION (NEWTONIAN FLOW; C.G. = 0.64L)

91
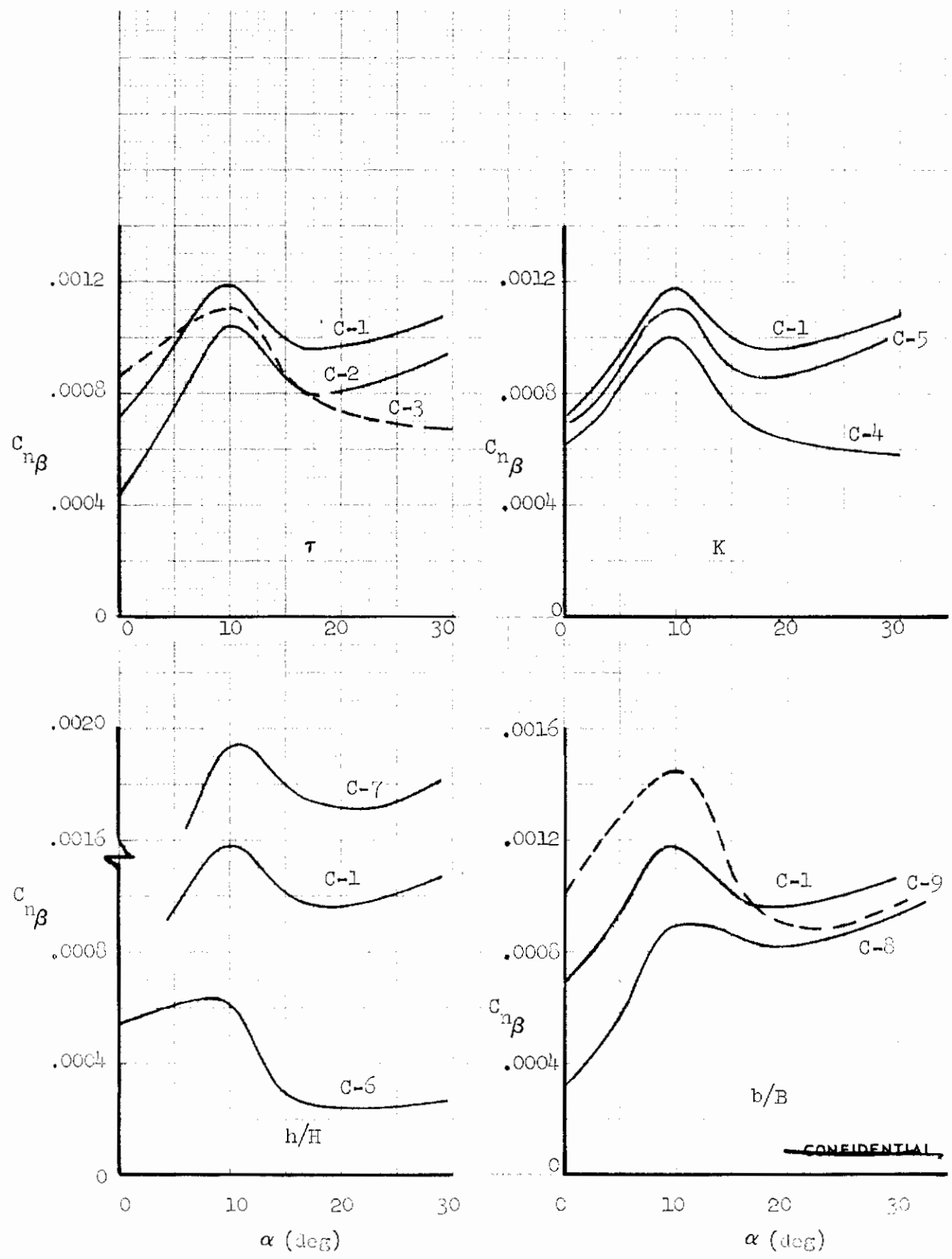
FIGURE 48   (U) VARIATION OF DIRECTIONAL STABILITY FOR PARAMETRIC CHANGES TO THE FDL-5A CONFIGURATION (NEWTONIAN FLOW; CG = 0.69L)

92
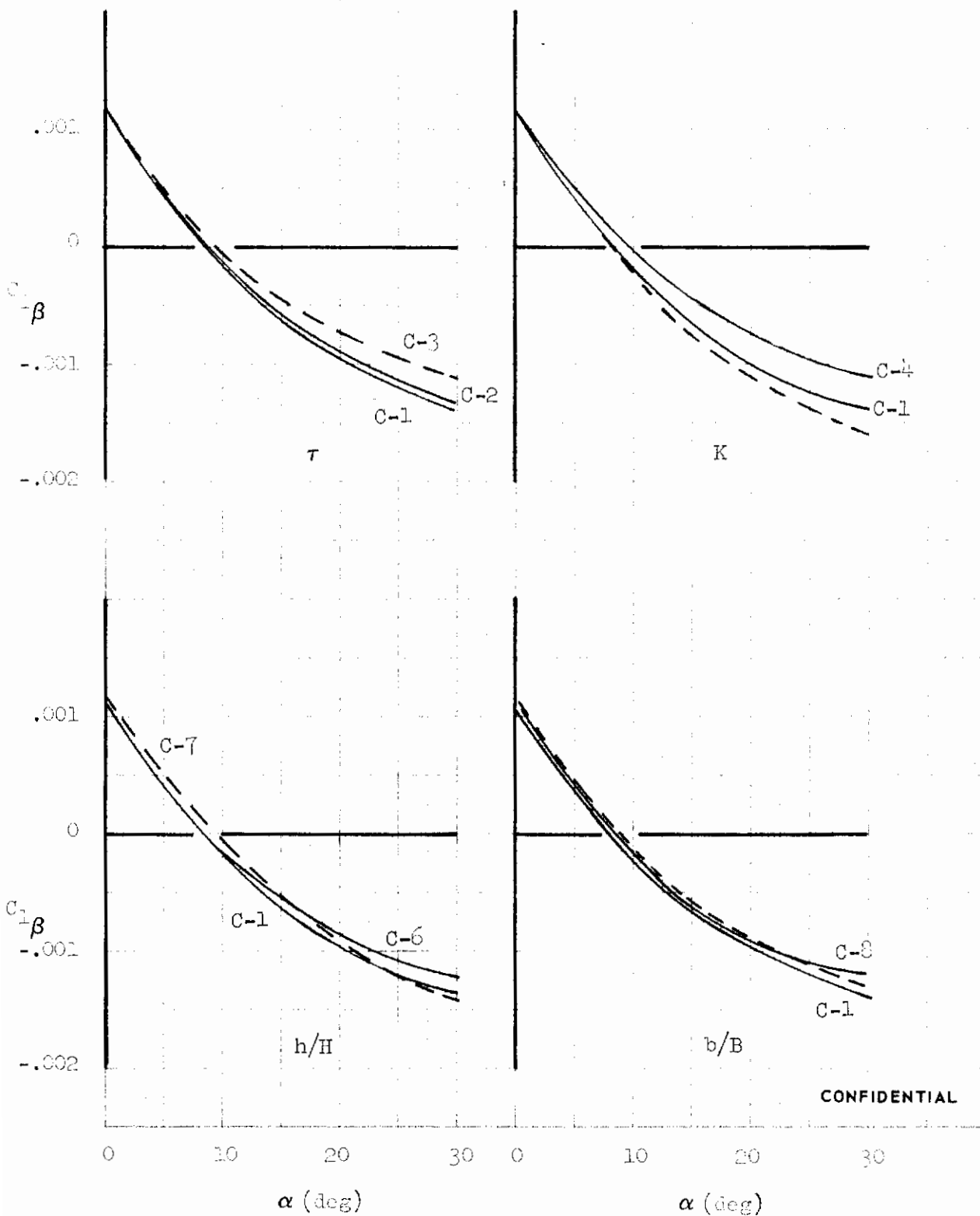
FIGURE 49   (U) VARIATION OF THE ROLL PARAMETER FOR PARAMETRIC CHANGES
TO THE FDL-5A CONFIGURATION (NEWTONIAN FLOW)

93
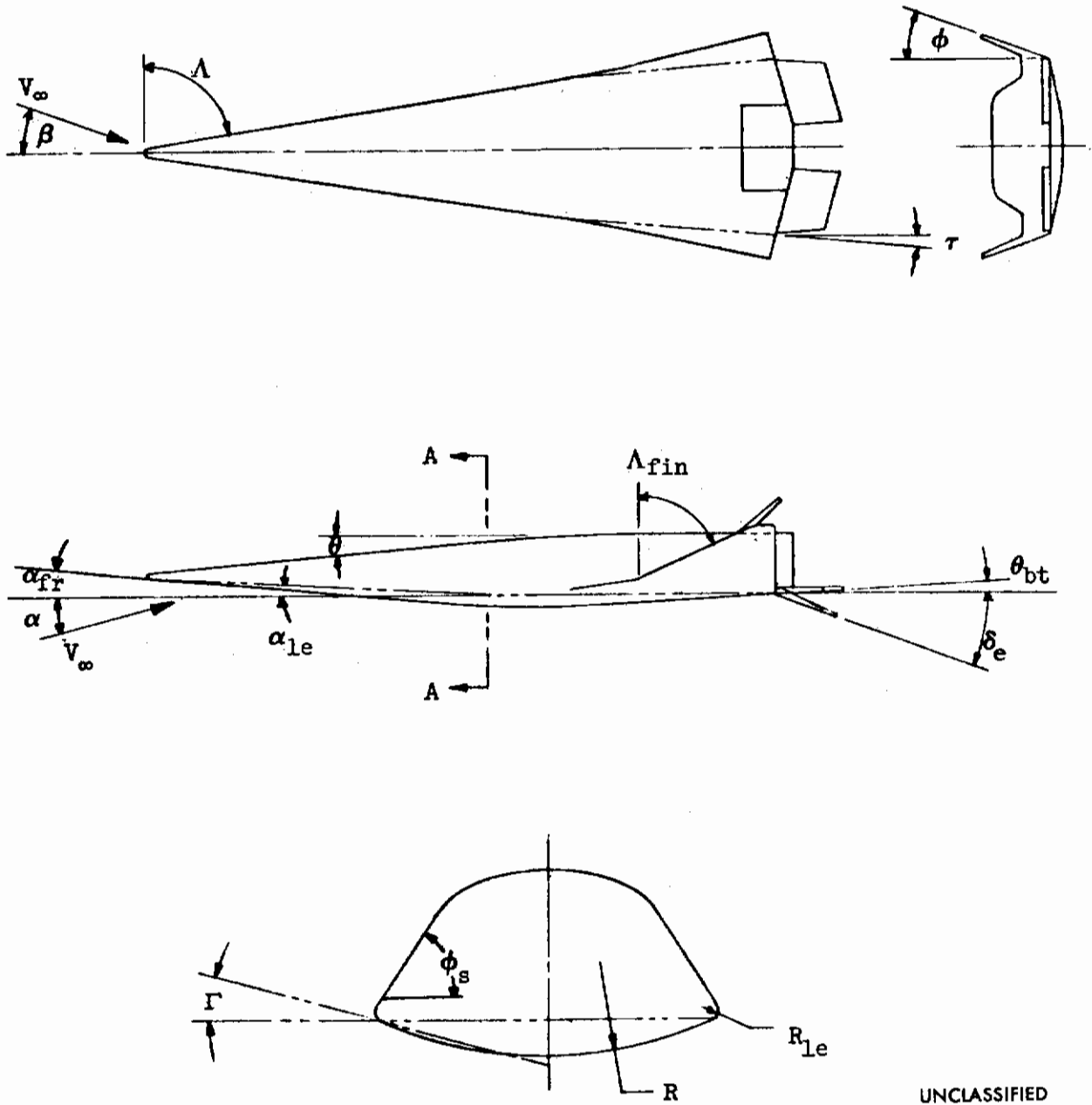
UNCLASSIFIED

FIGURE 50 (U) AEROTHERMODYNAMIC CONFIGURATION PARAMETERS

LOCKHEED
CALIFORNIA COMPANY

$V_\infty = 21,000 (\text{FPS}) \qquad H = 200,000 (\text{FT}) \qquad \alpha = 10^\circ$

$R = 1. \; (\text{IN.})$
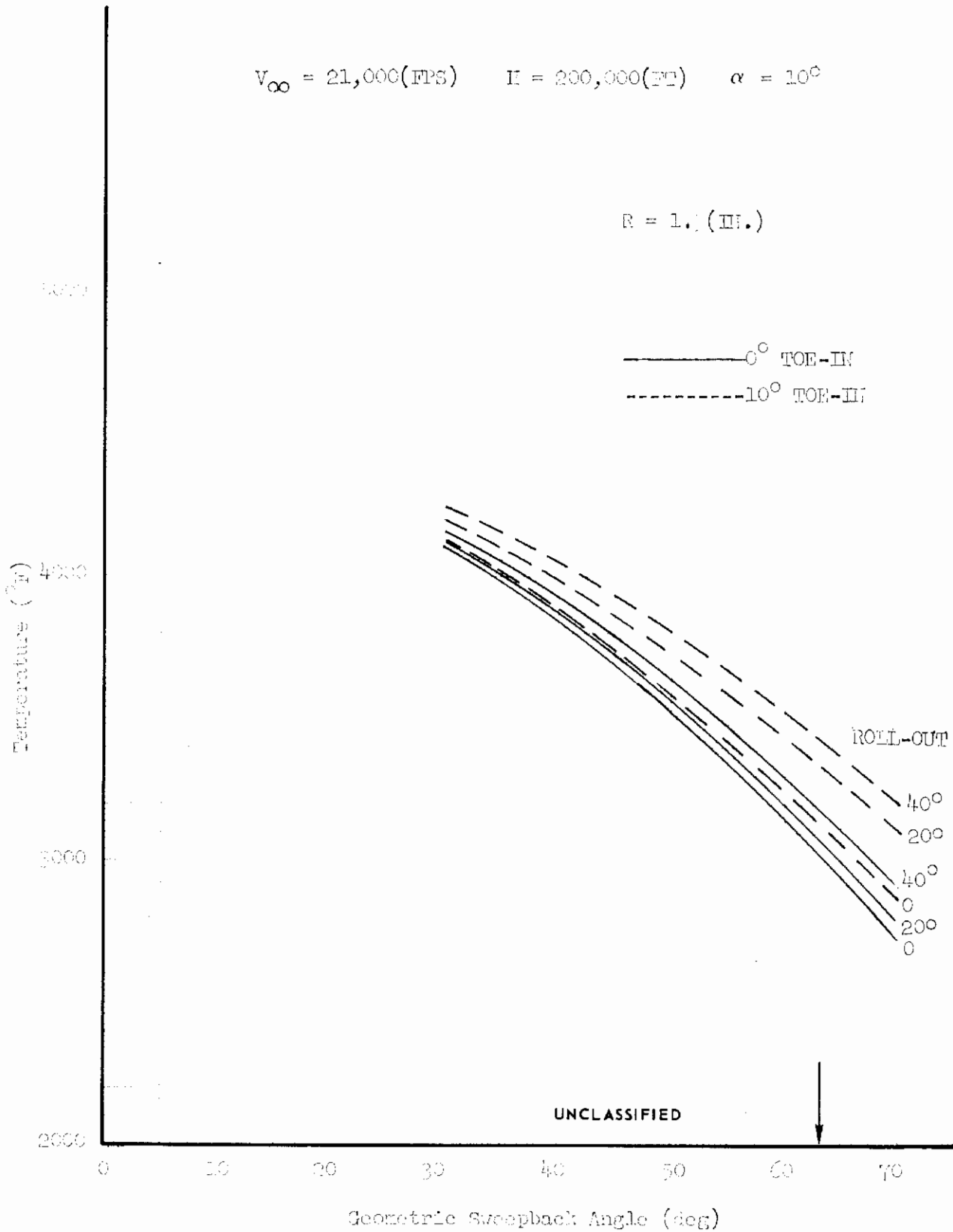
—————— 0° TOE-IN
- - - - - - 10° TOE-IN

FIGURE 51 (U) EFFECT OF SWEEP-BACK, ROLL-OUT, AND TOE-IN ON FIN STAGNATION LINE TEMPERATURES

95
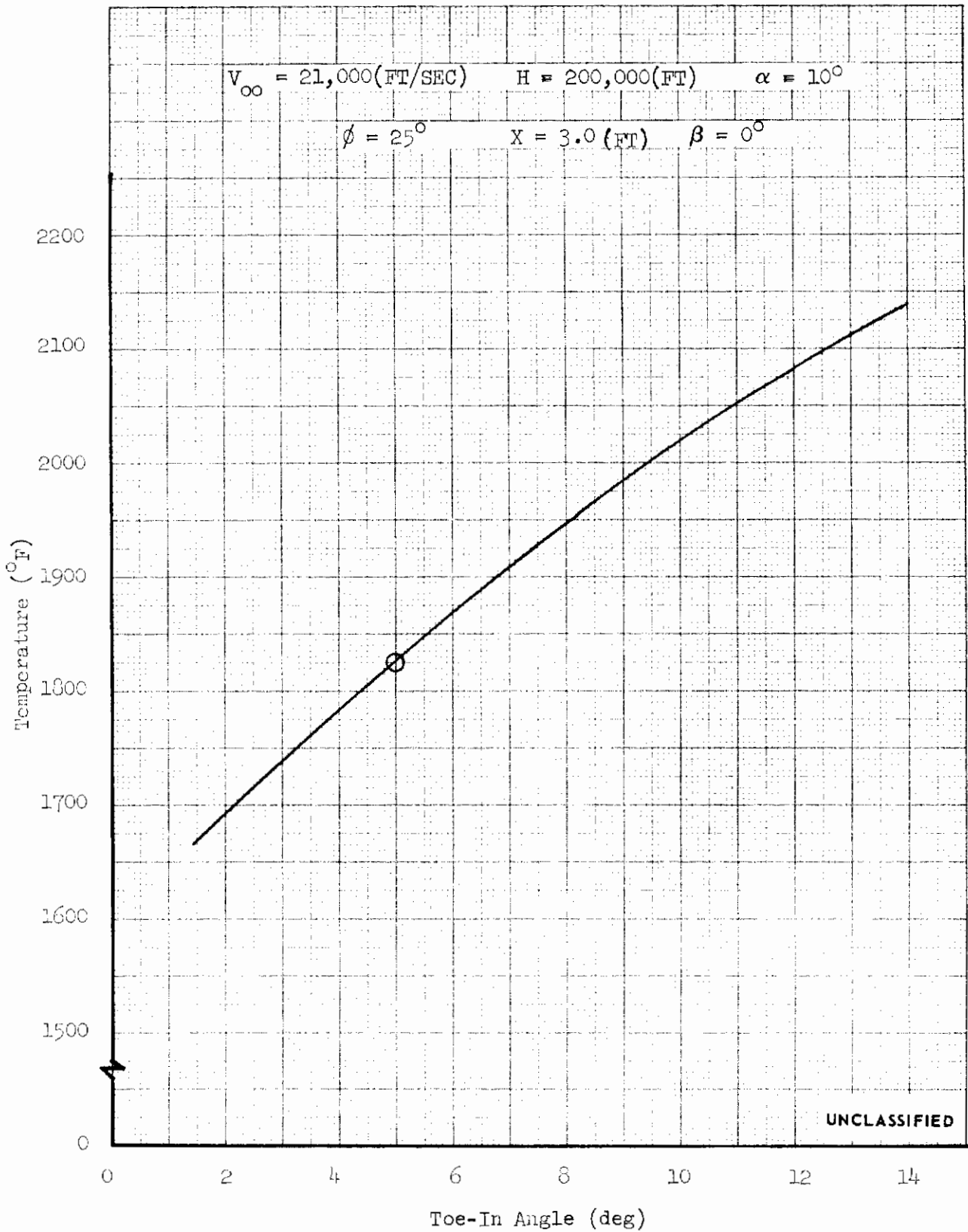
FIGURE 52 (U) EFFECT OF TOE-IN ANGLE ON FIN OUTBOARD PANEL TEMPERATURE

96

$V_\infty = 21,000 \text{ (FT/SEC)}$ $H = 200,000 \text{ (FT)}$ $\alpha = 10°$

$\tau = 5°$ $X = 3.0 \text{(FT)}$ $\beta = 0°$

UNCLASSIFIED

Fin Roll-Out Angle (deg)
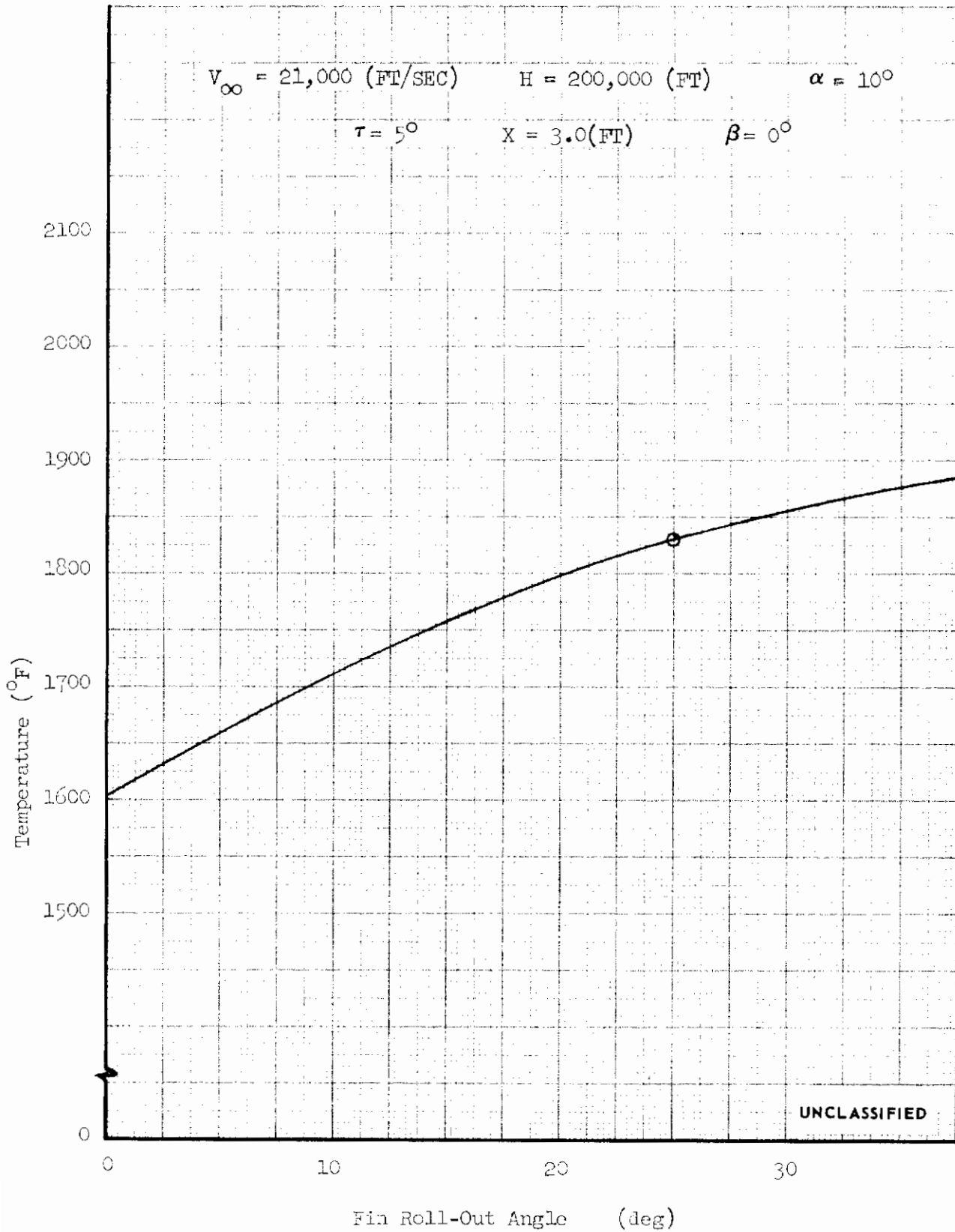
FIGURE 53 (U) EFFECT OF ROLL-OUT ANGLE ON FIN OUTBOARD PANEL
TEMPERATURE

97
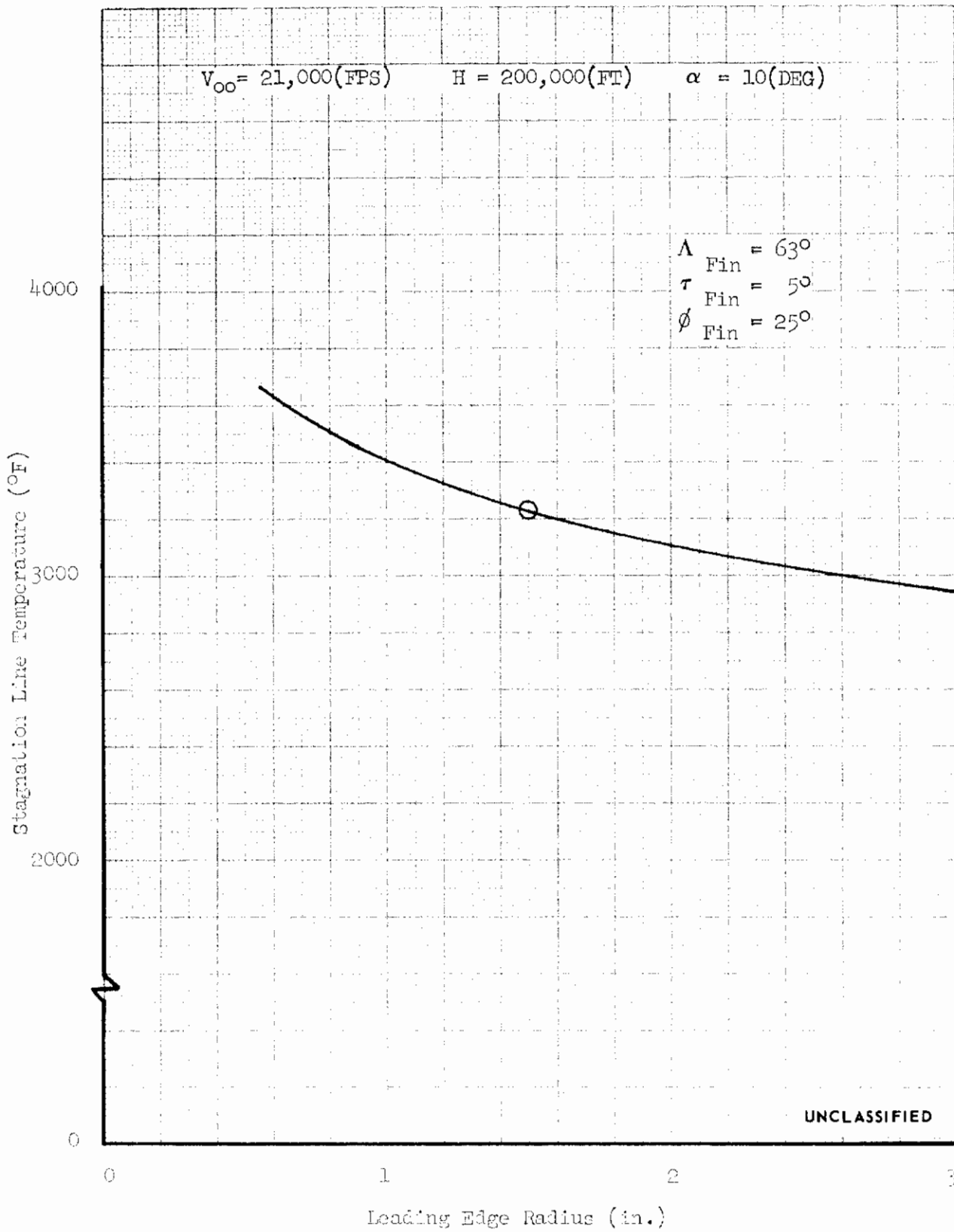
FIGURE 54 (U) EFFECT OF LEADING EDGE RADIUS ON FIN STAGNATION LINE
TEMPERATURES

98

$V_{oo} = 21,000(\text{FPS})$ $H = 200,000(\text{FT})$ $\alpha = 10(\text{DEG})$

$R = 1.5(\text{IN.})$
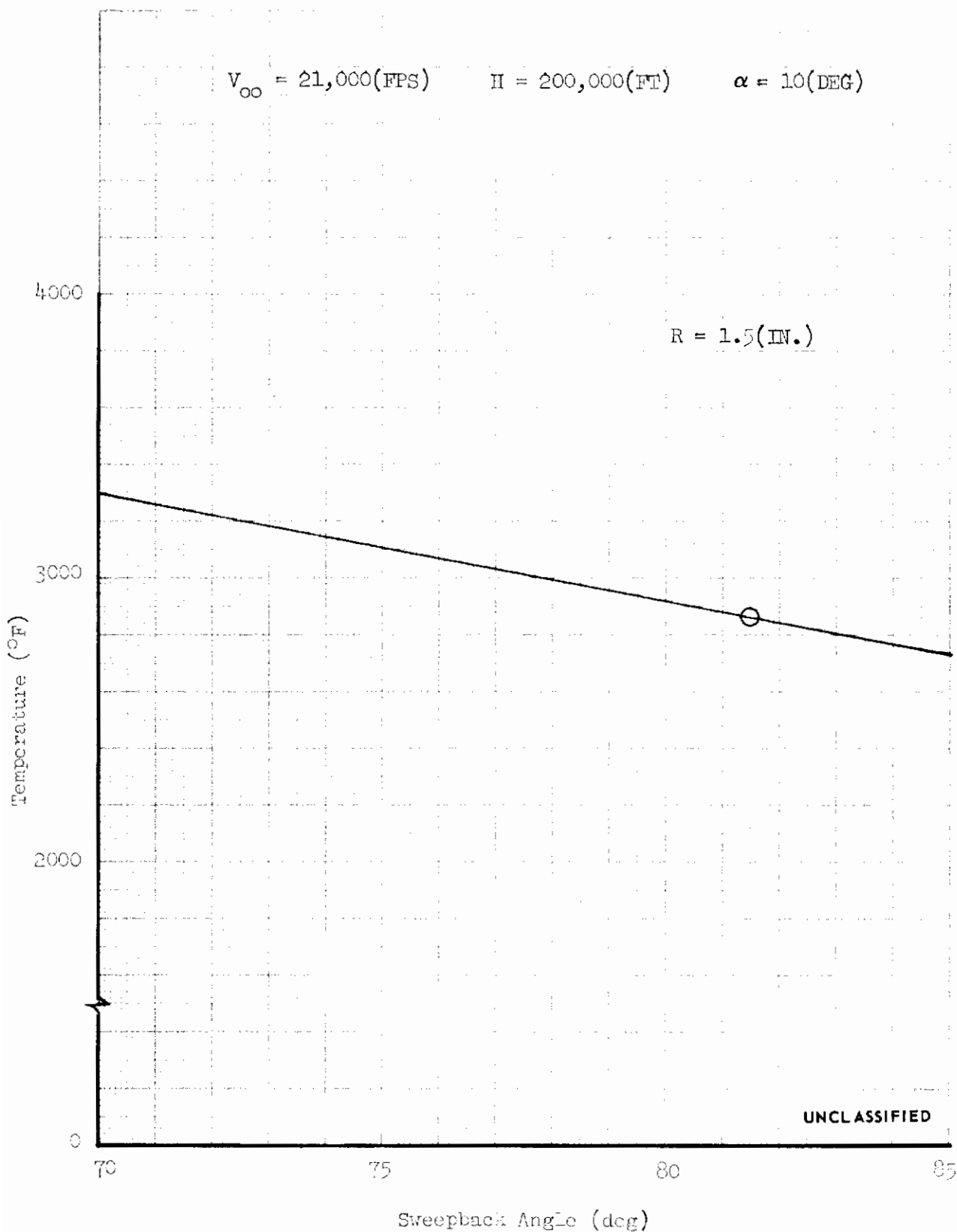
FIGURE 55   (U) EFFECT OF BODY SWEEPBACK ON LEADING EDGE STAGNATION LINE
TEMPERATURES

99
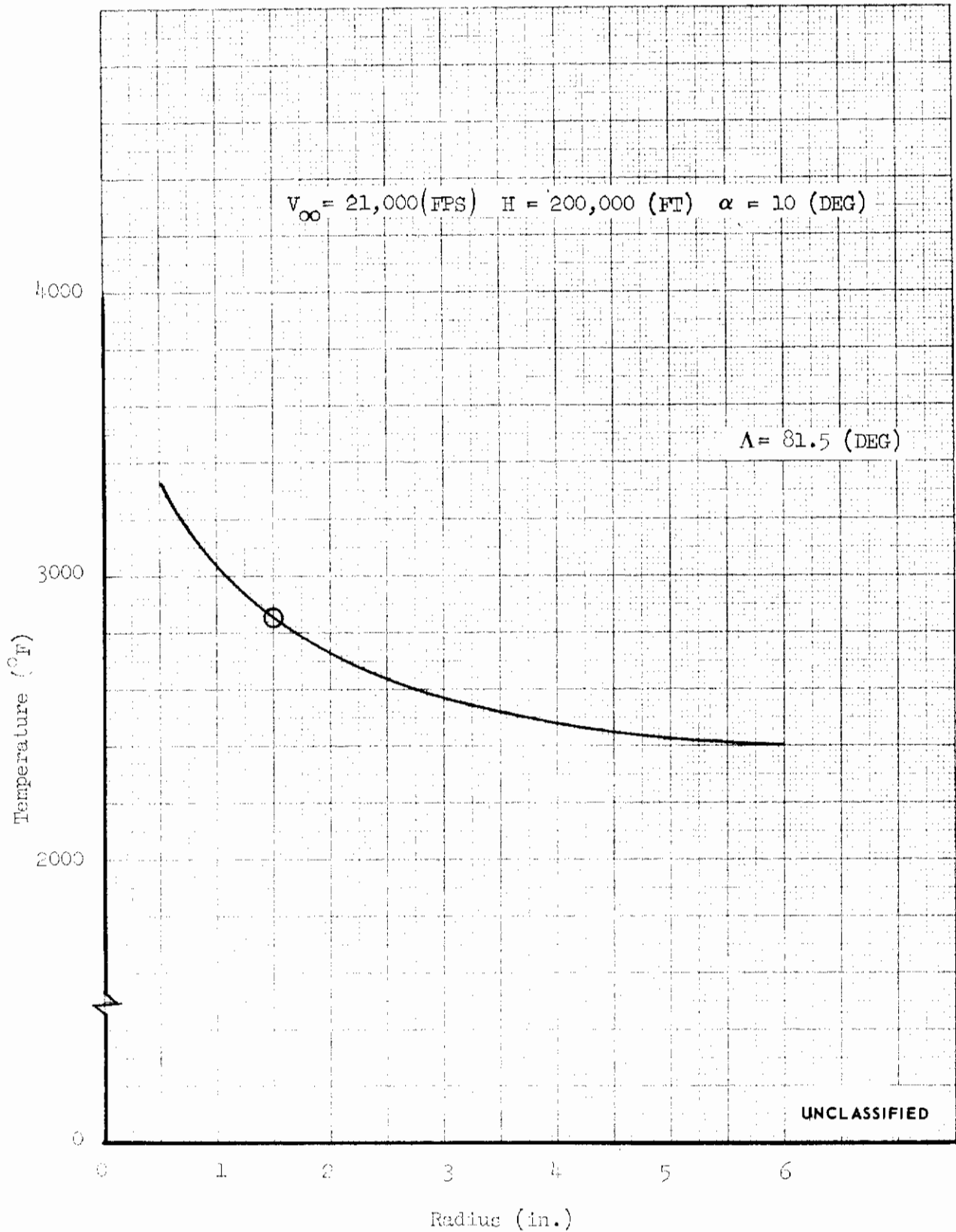
FIGURE 56 (U) EFFECT OF BODY LEADING EDGE RADIUS ON STAGNATION LINE TEMPERATURES

100
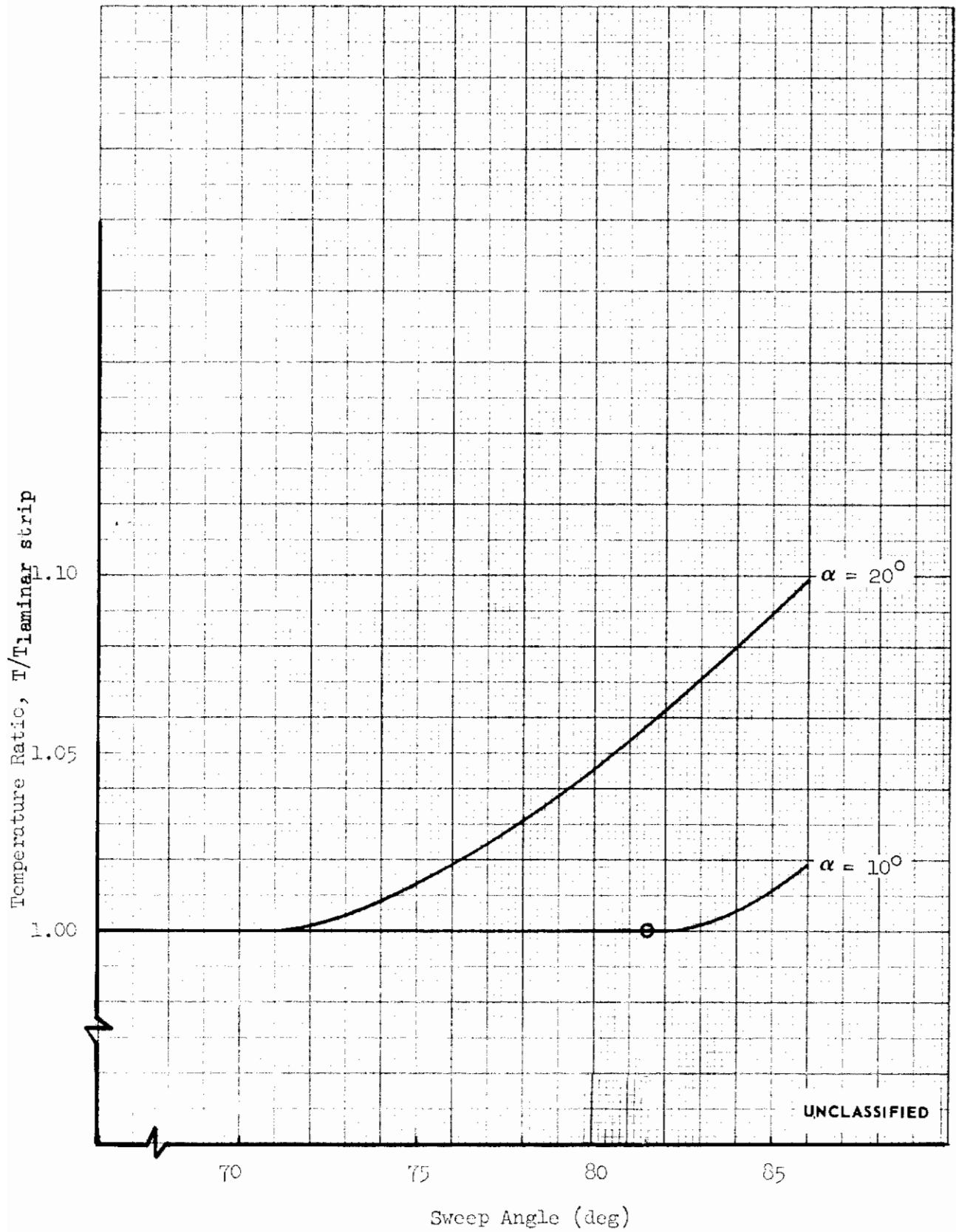
FIGURE 57   (U) EFFECT OF BODY SWEEPBACK ANGLE ON FORWARD RAMP LOWER
SURFACE CENTERLINE TEMPERATURES

101

$V_{oo} = 21,000$ (FPS)

$H = 200,000$ (FT)
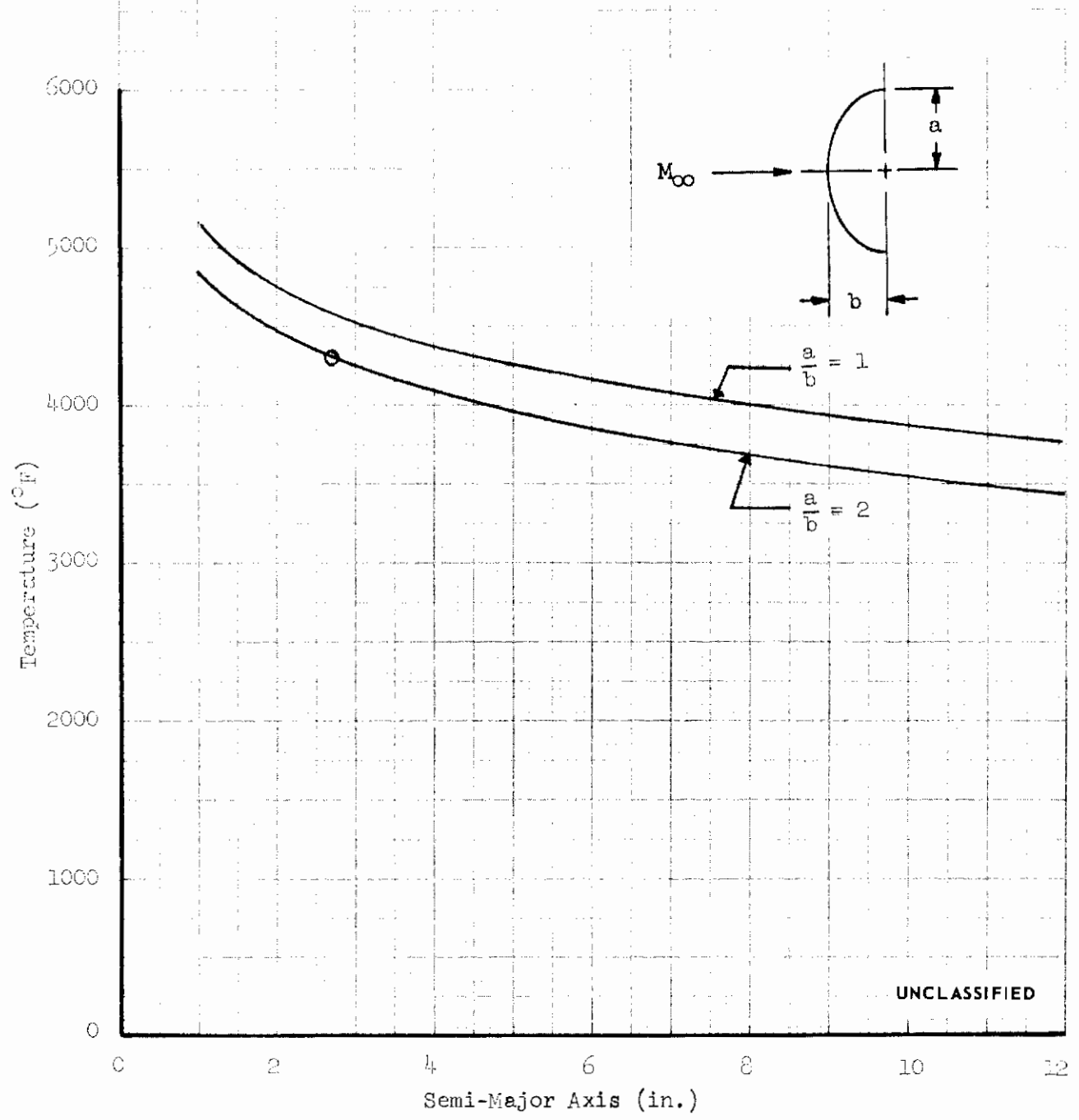
FIGURE 58 (U) EFFECT OF NOSE RADIUS ON STAGNATION POINT TEMPERATURES

102
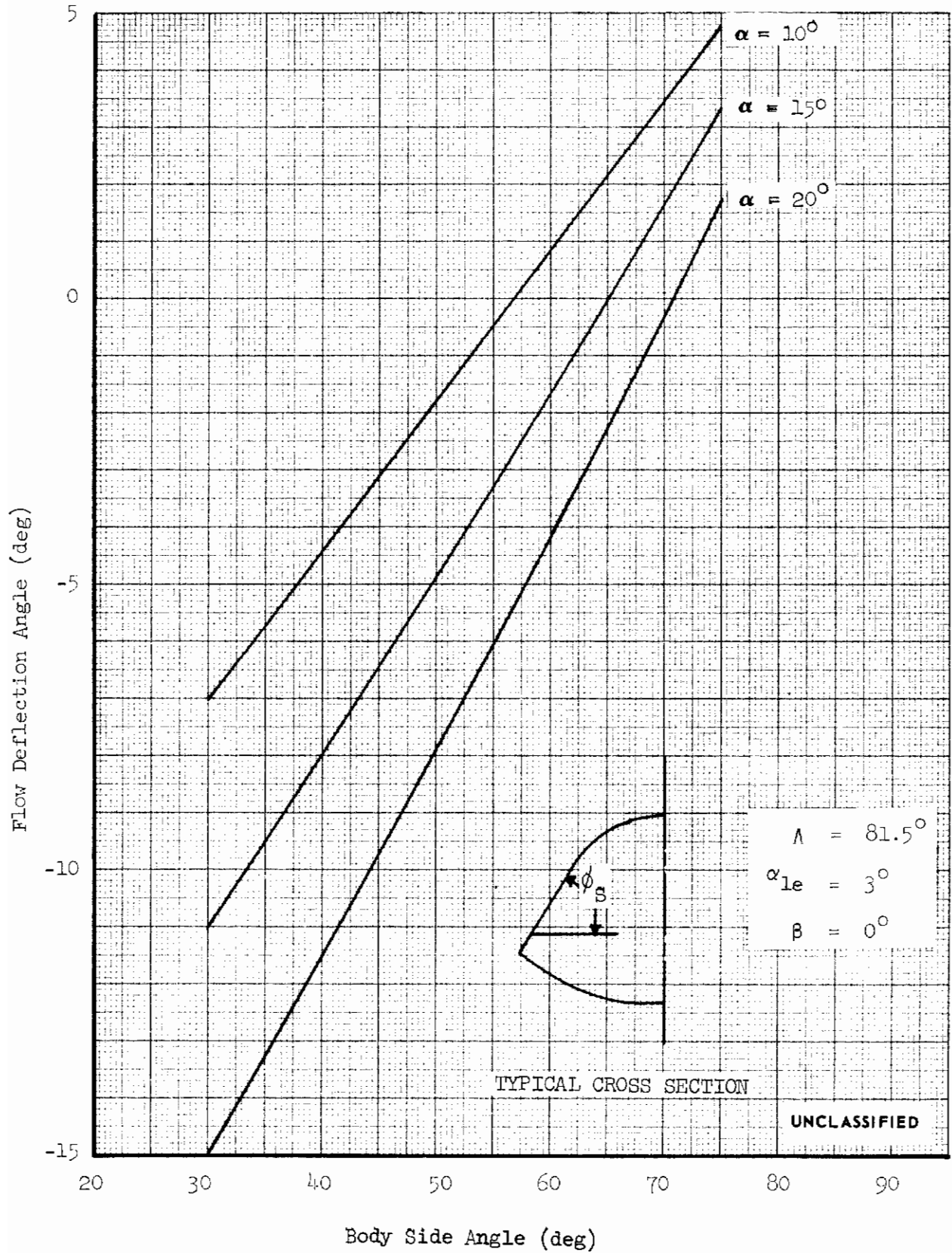
FIGURE 59 (U) EFFECT OF BODY SIDE ANGLE ON SIDE PANEL FLOW DEFLECTION ANGLE

103
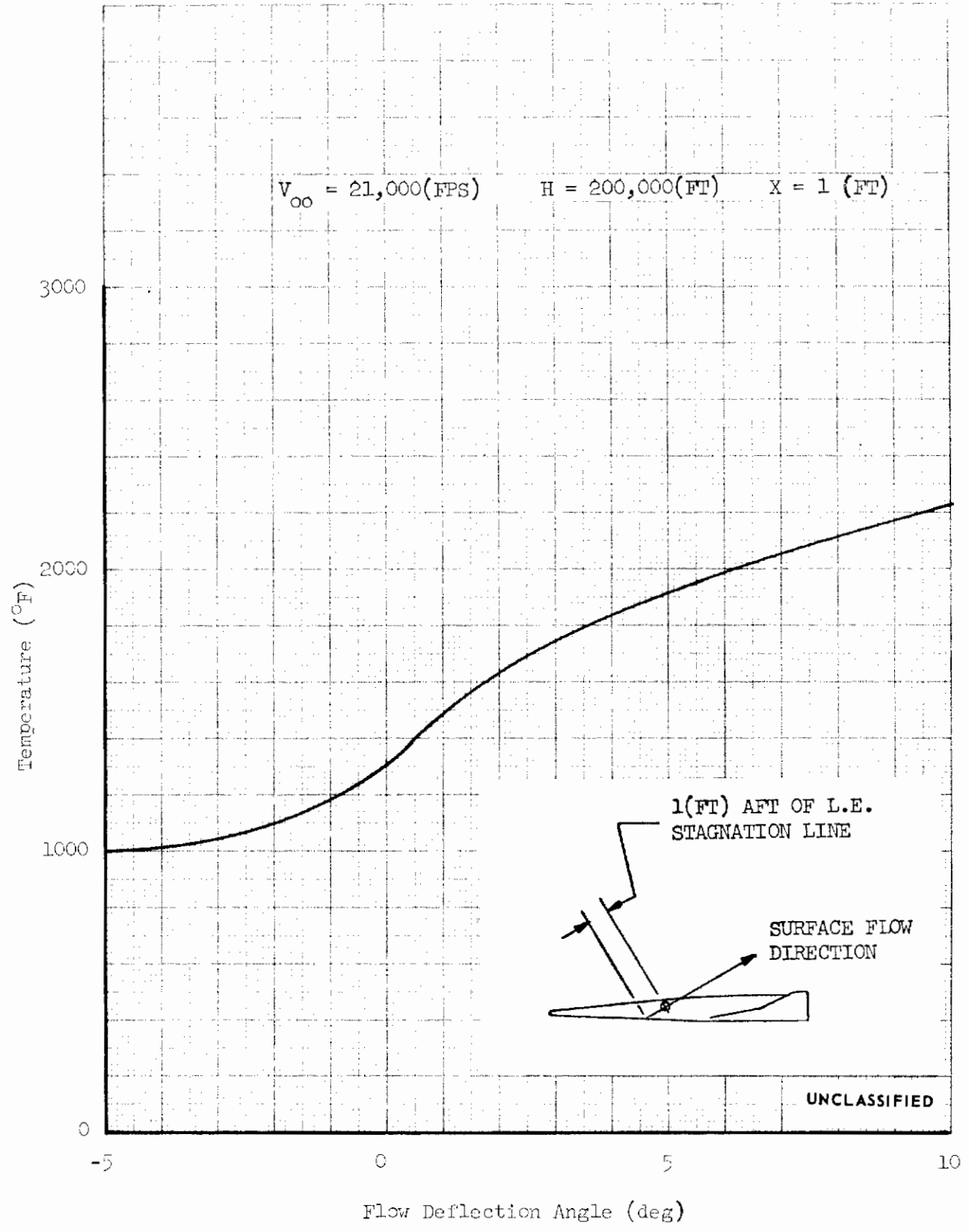
FIGURE 60   (U) EFFECT OF FLOW DEFLECTION ANGLE ON SIDE PANEL SURFACE
TEMPERATURES

104
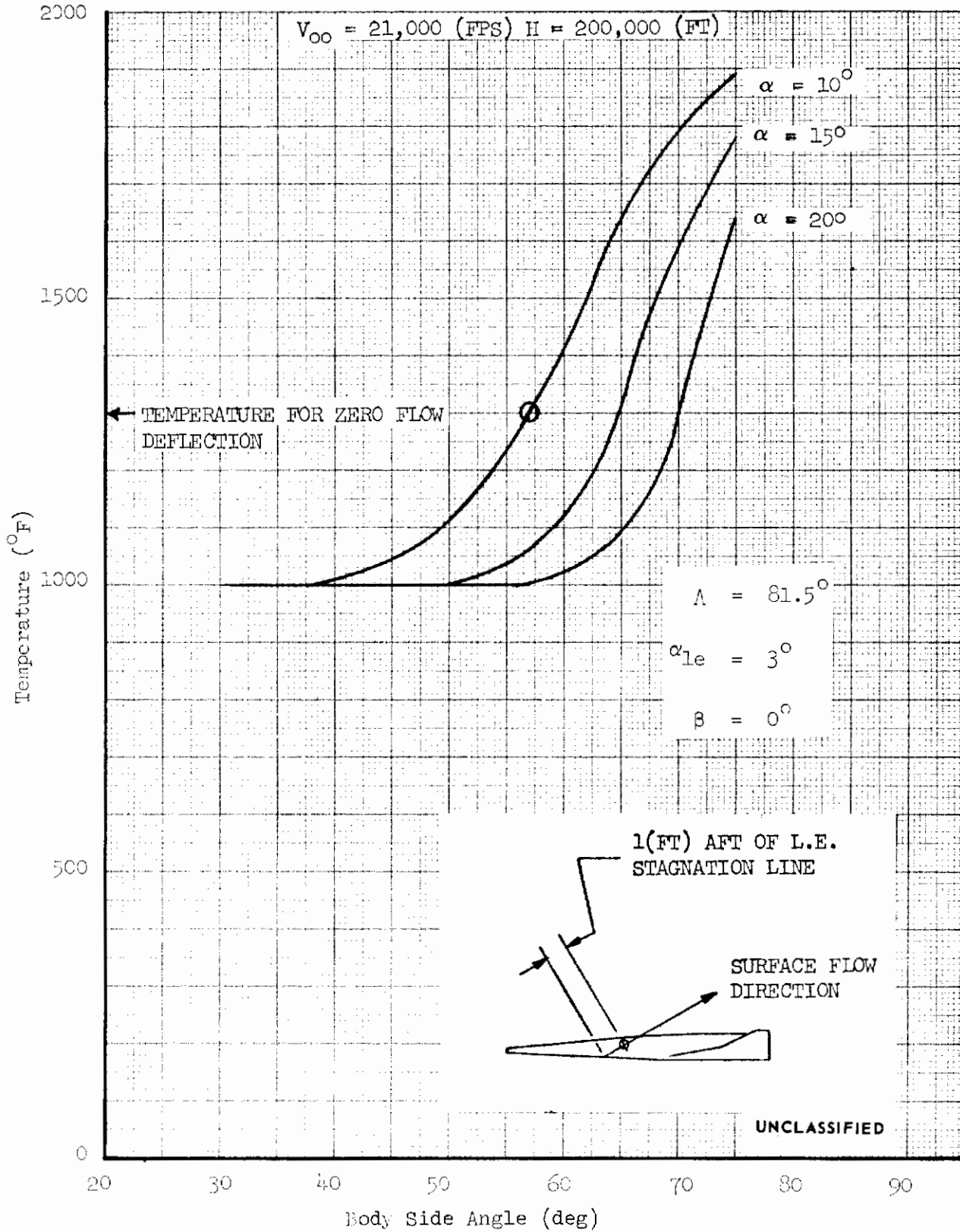
FIGURE 61 (U) EFFECT OF BODY SIDE ANGLE ON SIDE PANEL SURFACE
TEMPERATURES

105
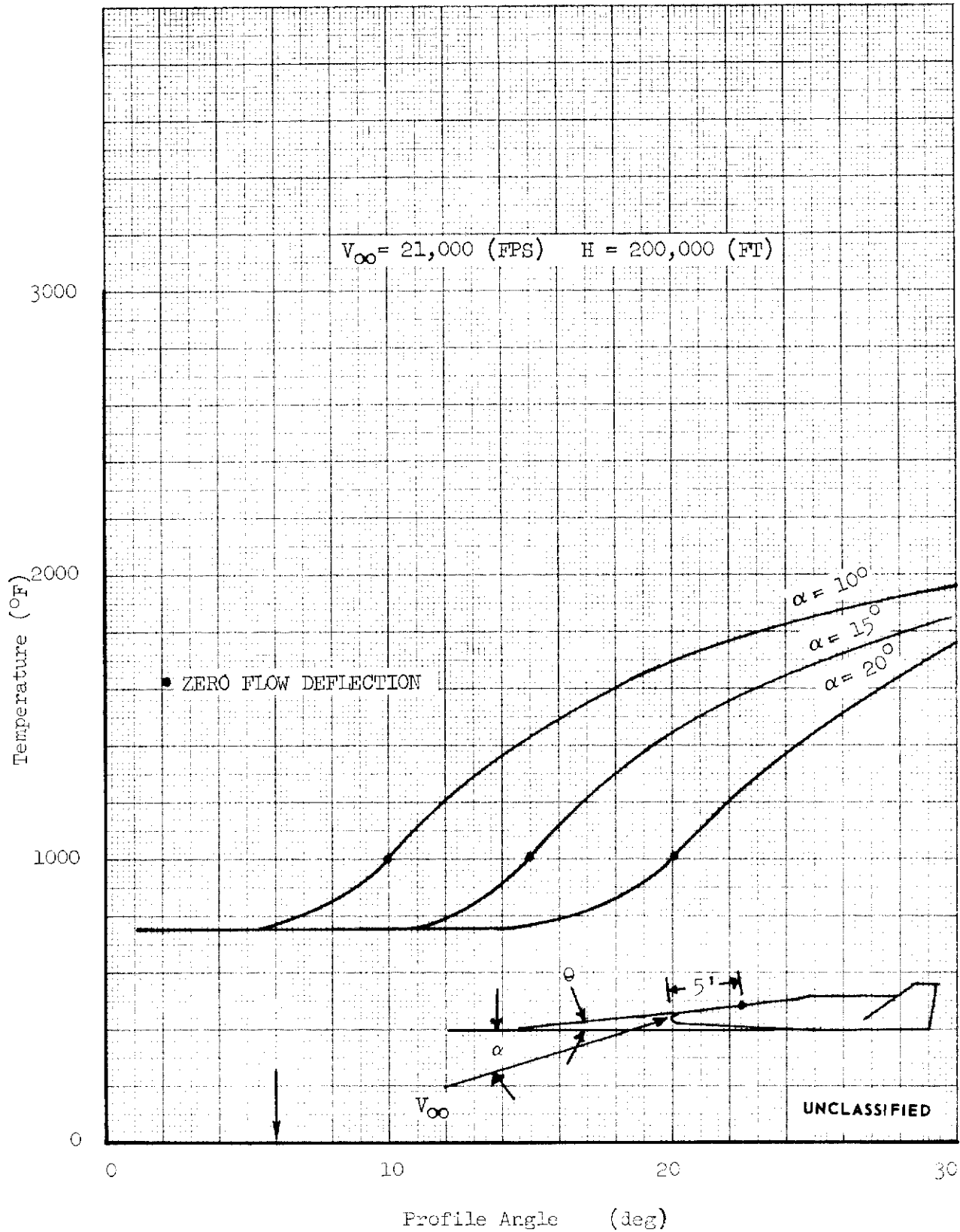
FIGURE 62 (U) EFFECT OF PROFILE ANGLE ON THE UPPER FOREBODY CENTERLINE TEMPERATURES

106
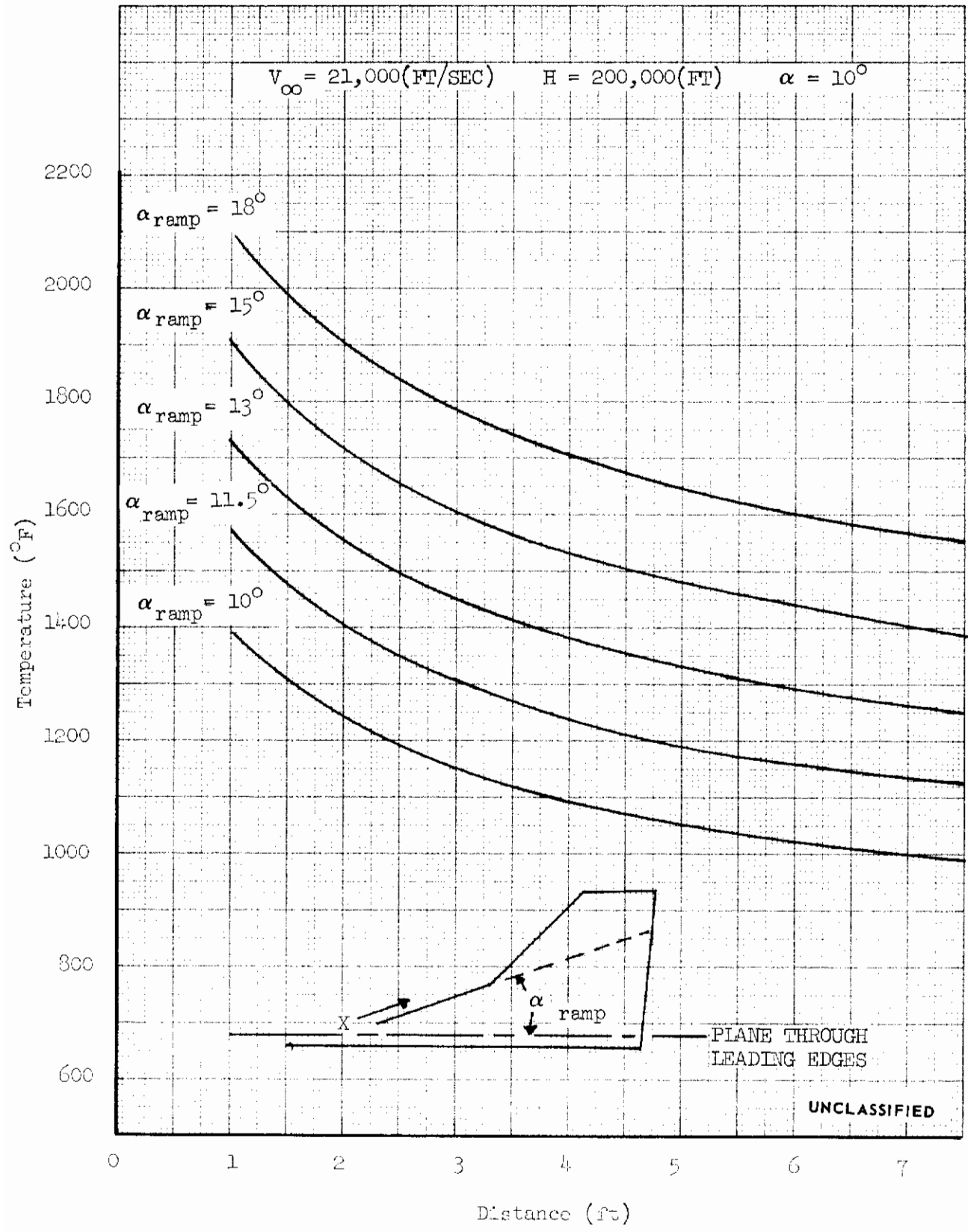
FIGURE 63   (U) EFFECT OF FIN RAMP ANGLE ON UPPER SURFACE TEMPERATURES

107
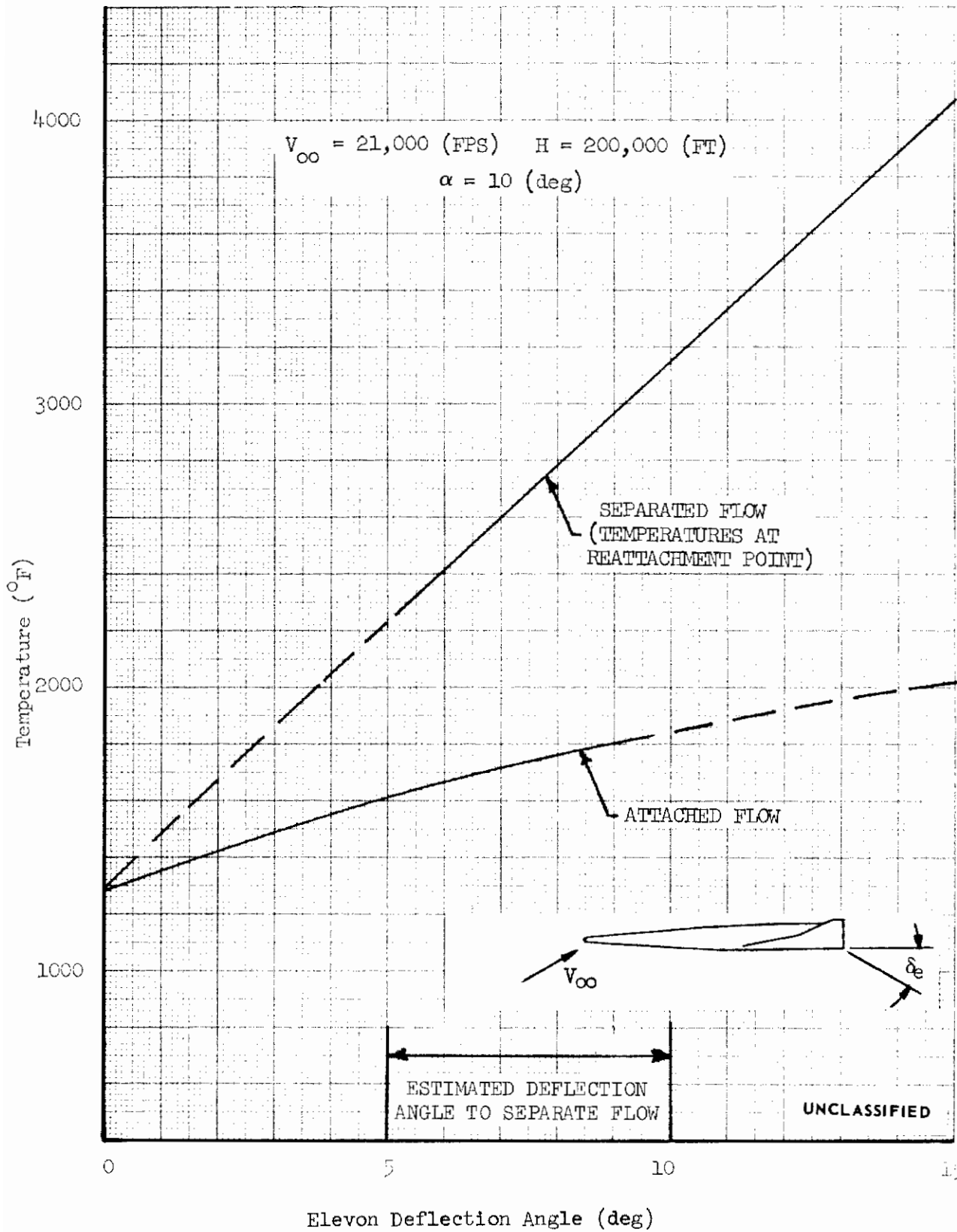
FIGURE 64 (U) EFFECT OF DEFLECTION ANGLE ON MAXIMUM ELEVON TEMPERATURES

108

$V_\infty = 21,000(\text{FPS}) \qquad H = 200,000(\text{FT}) \qquad \alpha = 10(\text{DEG})$

$R = 1.5(\text{IN.})$
$\Lambda = 81.5(\text{DEG})$
$\alpha_{\text{eff}} = \alpha + \alpha_{\text{lc}}$
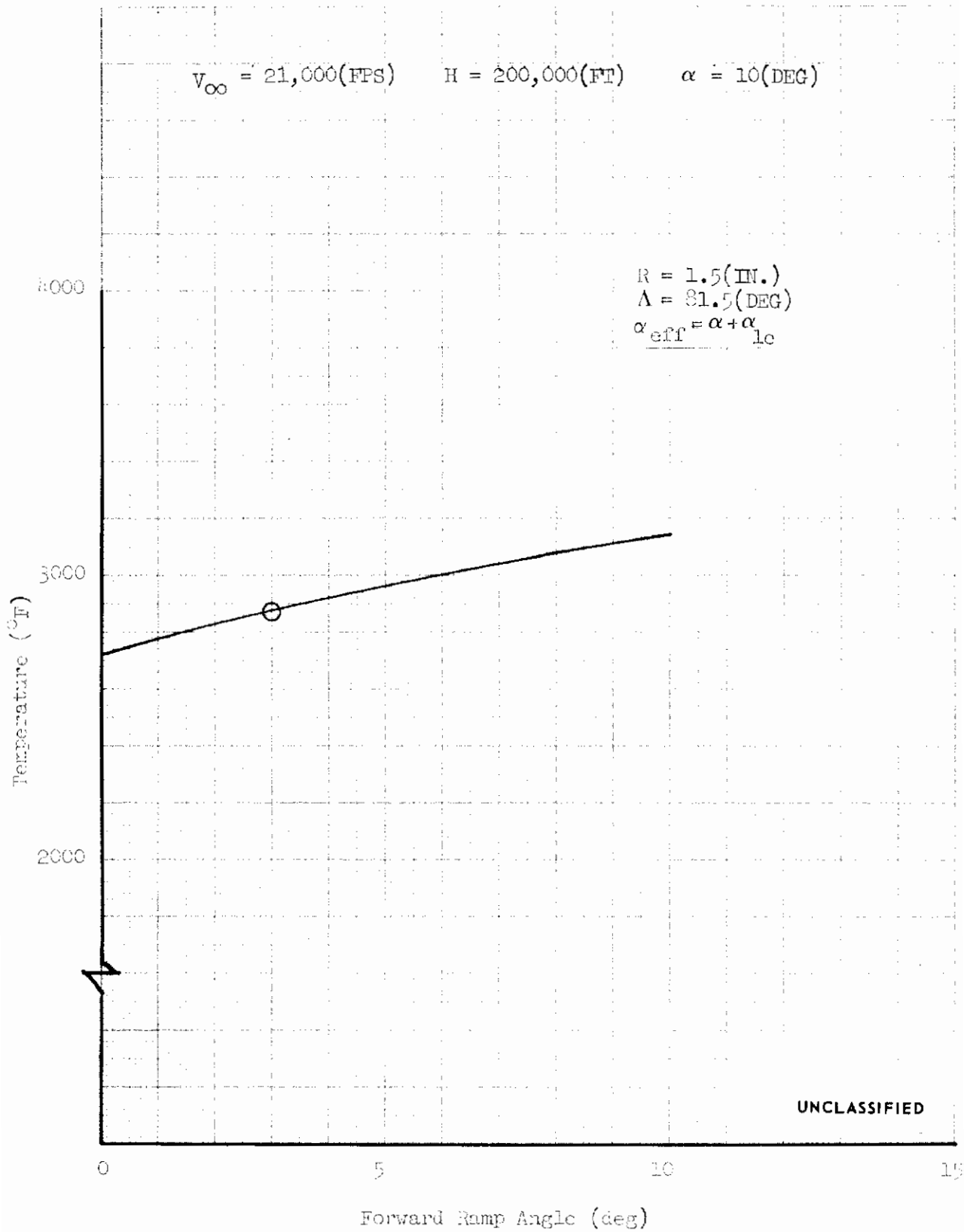
FIGURE 65 (U) EFFECT OF FORWARD RAMP ANGLE ON BODY LEADING EDGE
STAGNATION LINE TEMPERATURES

109
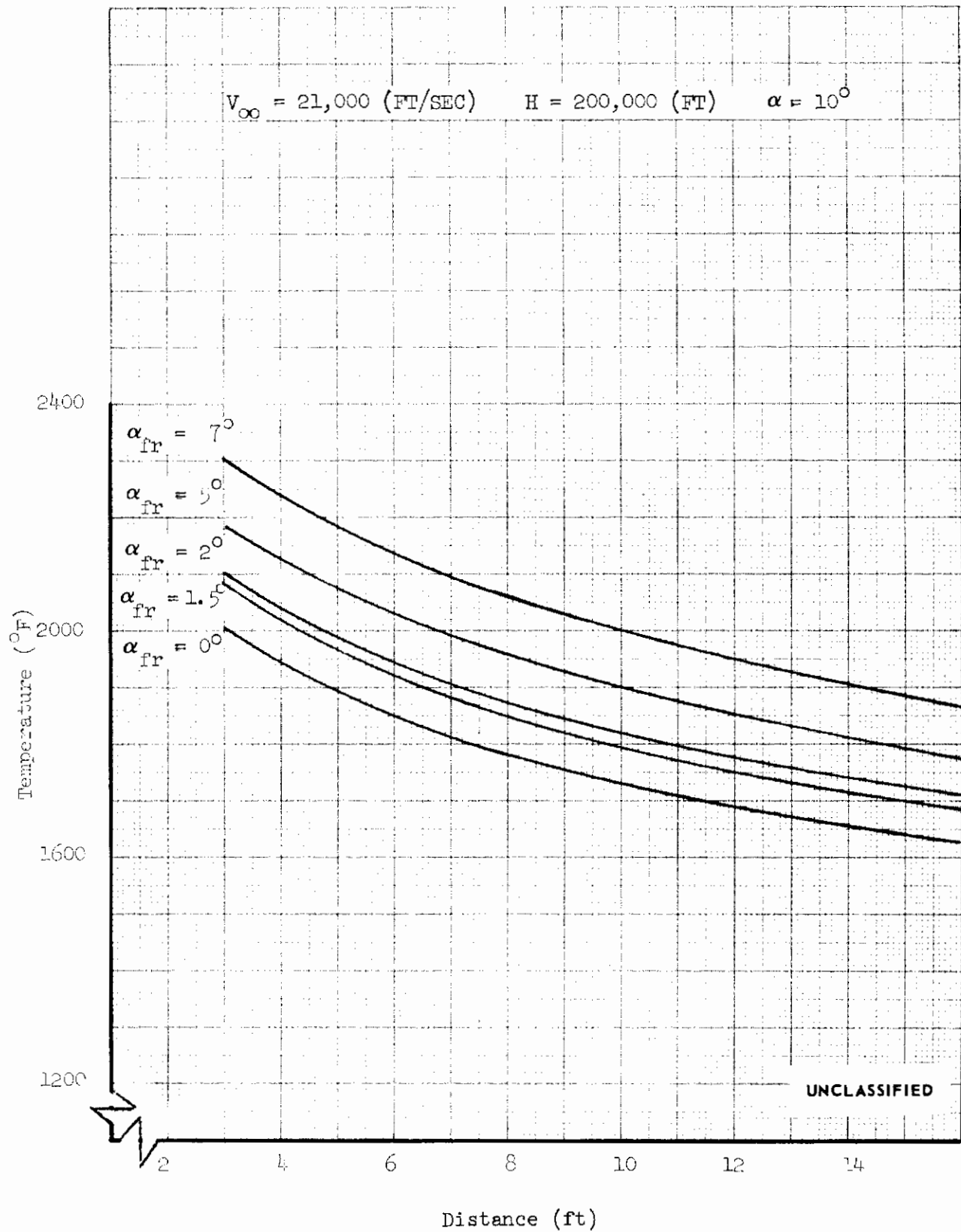
FIGURE 66   (U) EFFECT OF FORWARD RAMP ANGLE ON CURVED LOWER SURFACE
CENTERLINE TEMPERATURE

110
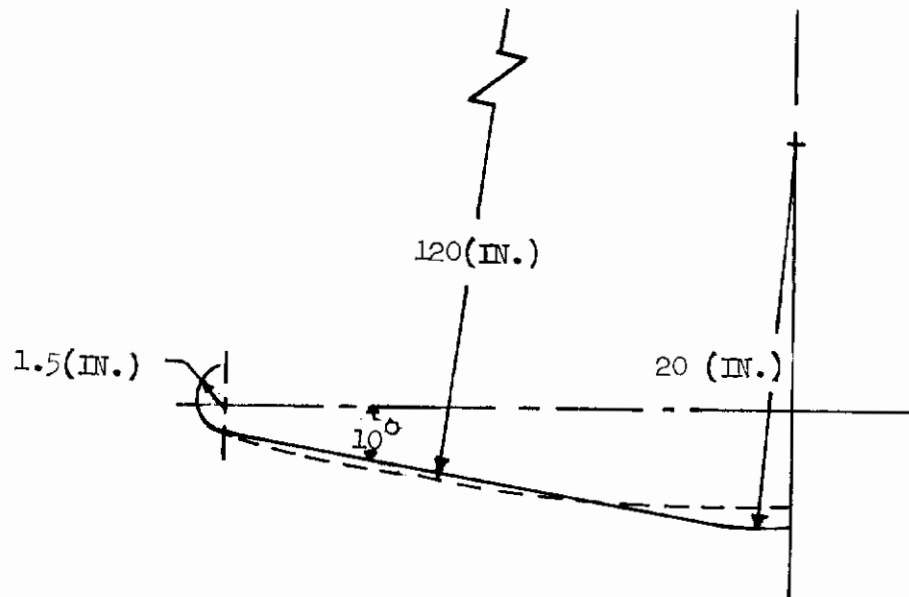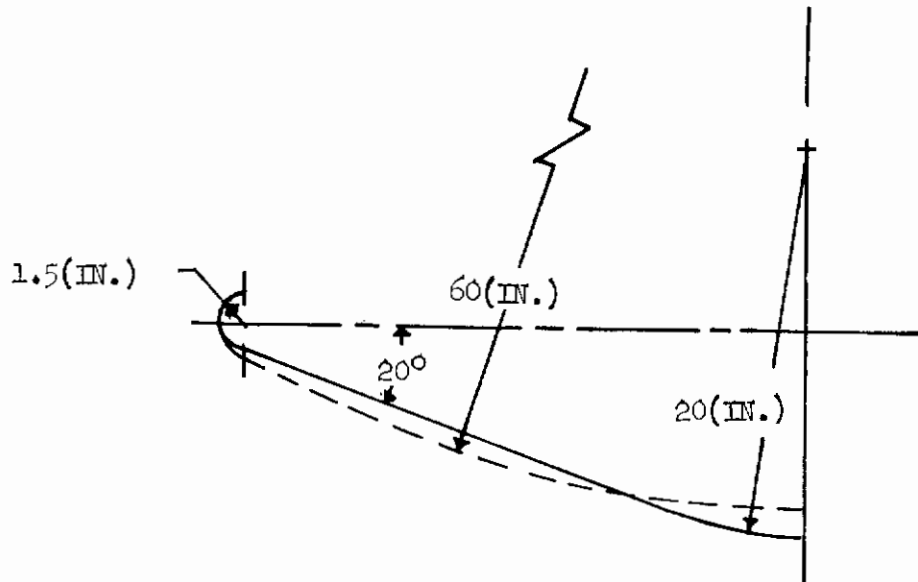
FIGURE 67 (U) LOWER SURFACE CONFIGURATIONS

111
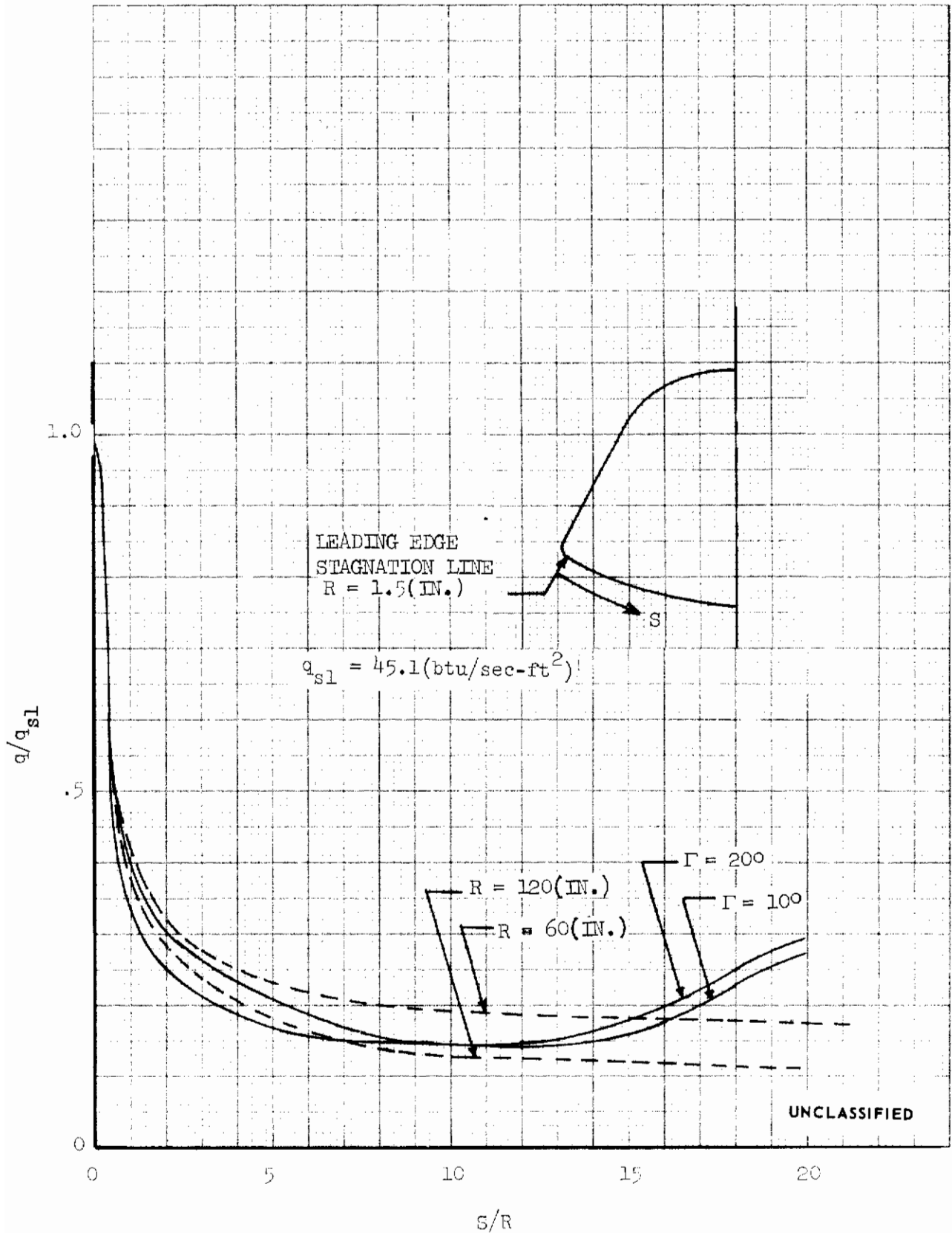
FIGURE 68 (U) COMPARISON OF HEATING DISTRIBUTIONS ON CURVED AND DIHEDRALED LOWER SURFACES, V_∞ = 21,000 FT/SEC, H = 200,000 FT, LAMINAR FLOW α = 10°

112
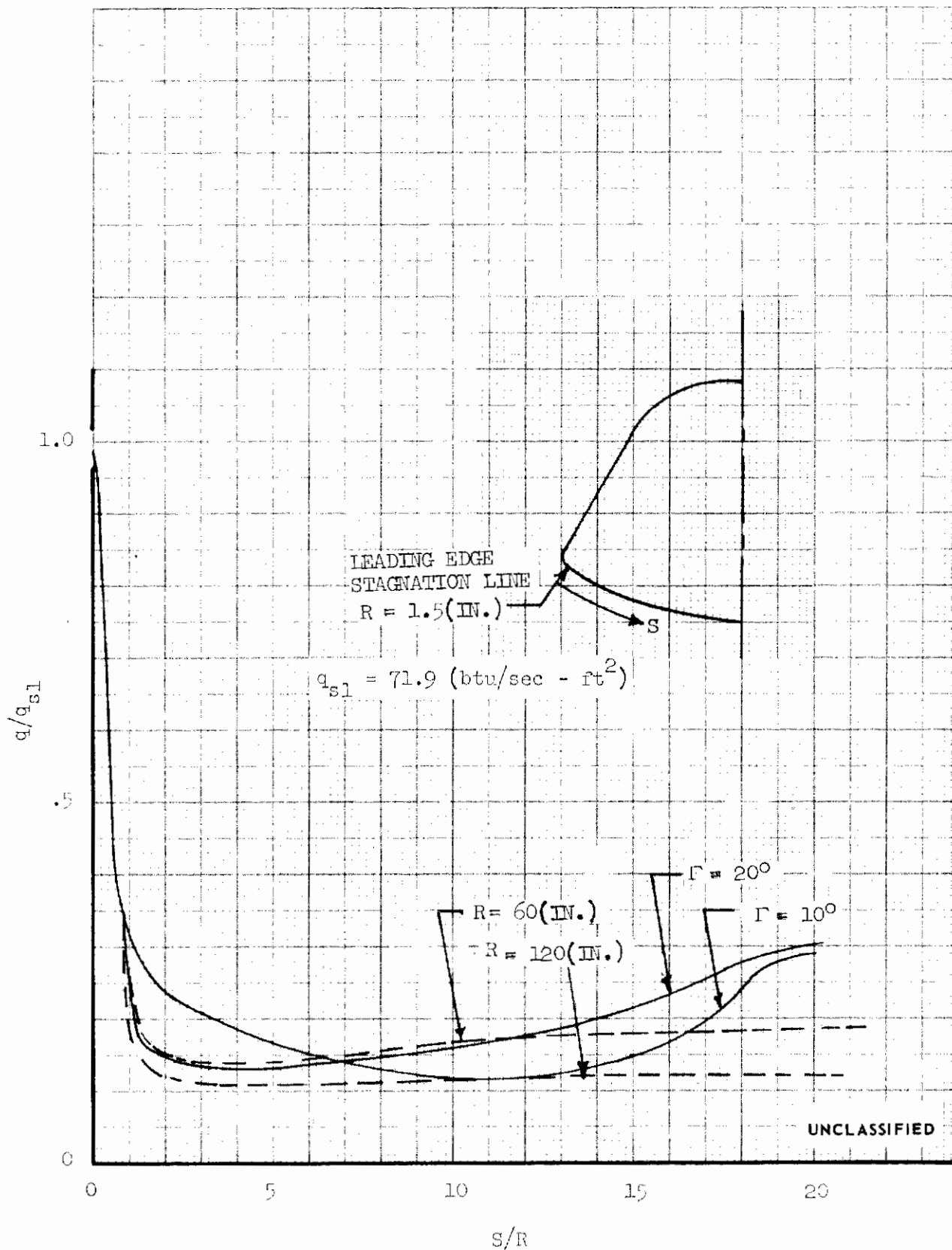
FIGURE 69 (U) COMPARISON OF HEATING DISTRIBUTIONS ON CURVED AND
DIHEDRALED LOWER SURFACES, V_∞ = 21,000 FT/SEC,
H = 200,000 FT, LAMINAR FLOW α = 20°

113
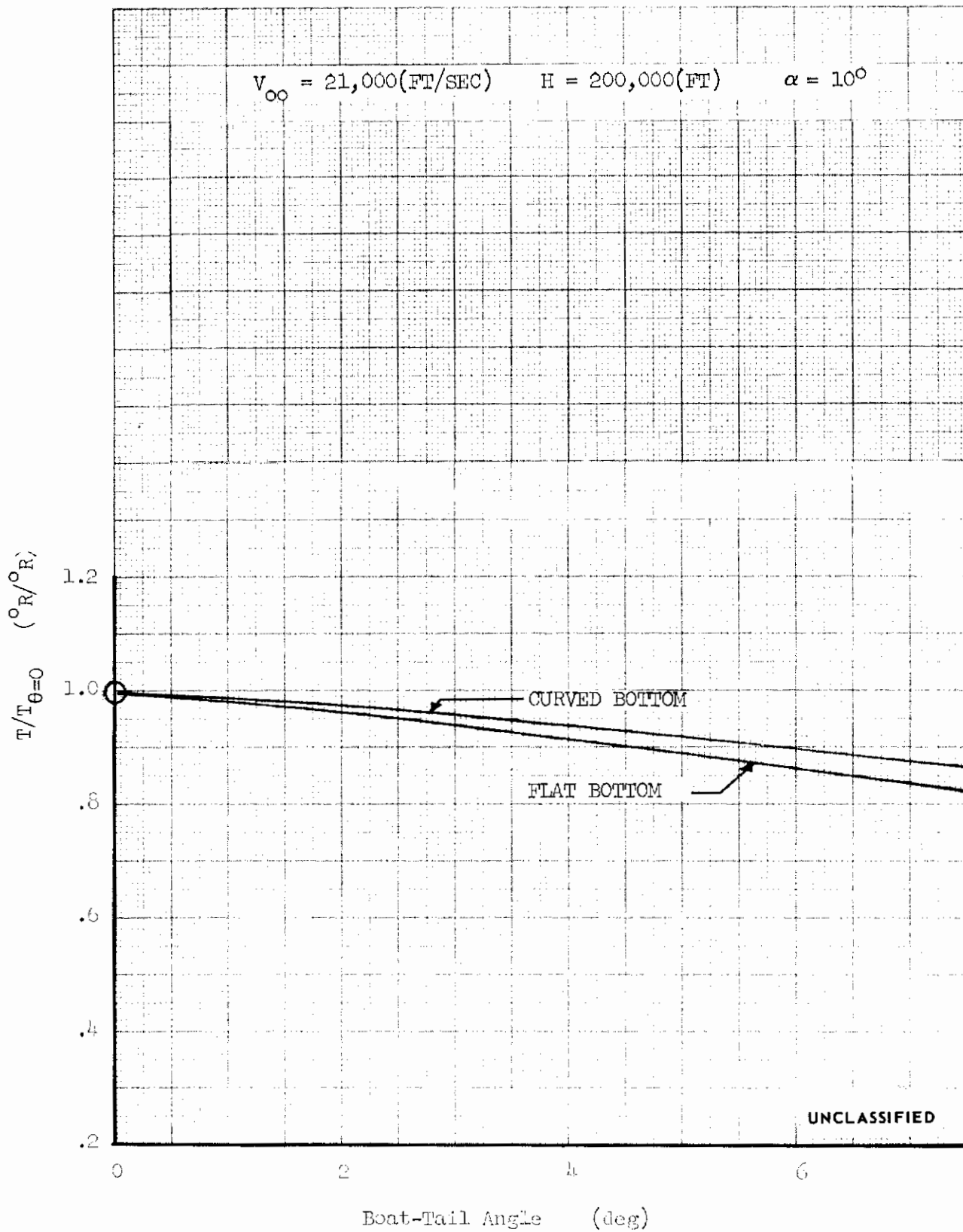
FIGURE 70   (U) EFFECT OF LOWER SURFACE BOAT-TAIL ANGLE ON AFT
LOWER SURFACE TEMPERATURE

114
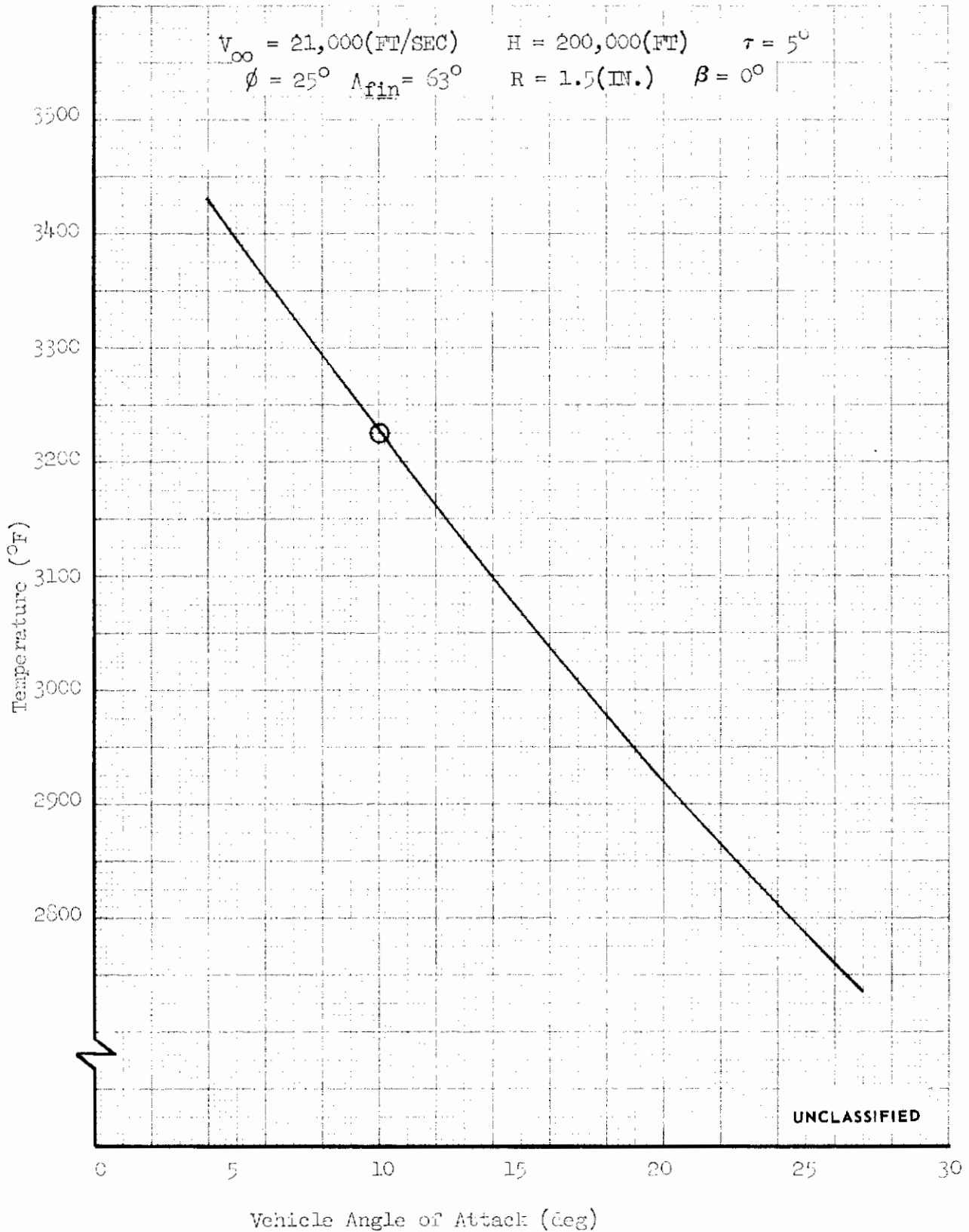
FIGURE 71 (U) EFFECT OF ANGLE OF ATTACK ON FIN LEADING EDGE STAGNATION
LINE TEMPERATURES

115
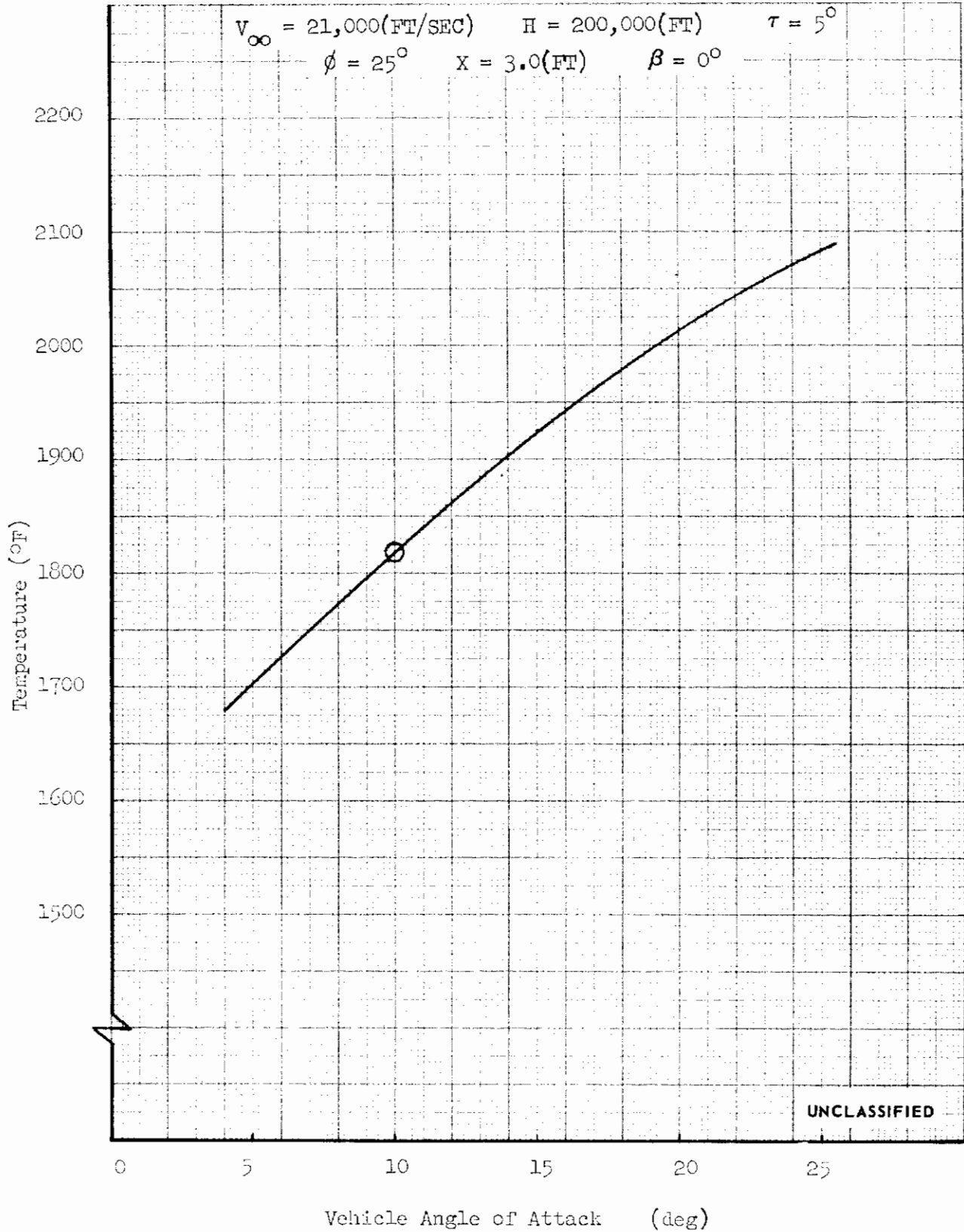
FIGURE 72 (U) EFFECT OF VEHICLE ANGLE OF ATTACK ON FIN OUTBOARD
PANEL TEMPERATURE

116

$$V_\infty = 21,000 (\text{FT/SEC}) \qquad H = 200,000 (\text{FT})$$
$$\Lambda = 81.5^\circ \qquad R = 1.5 (\text{IN.}) \qquad \beta = 0^\circ$$

Temperature (°F) vs. Effective Angle of Attack (deg)
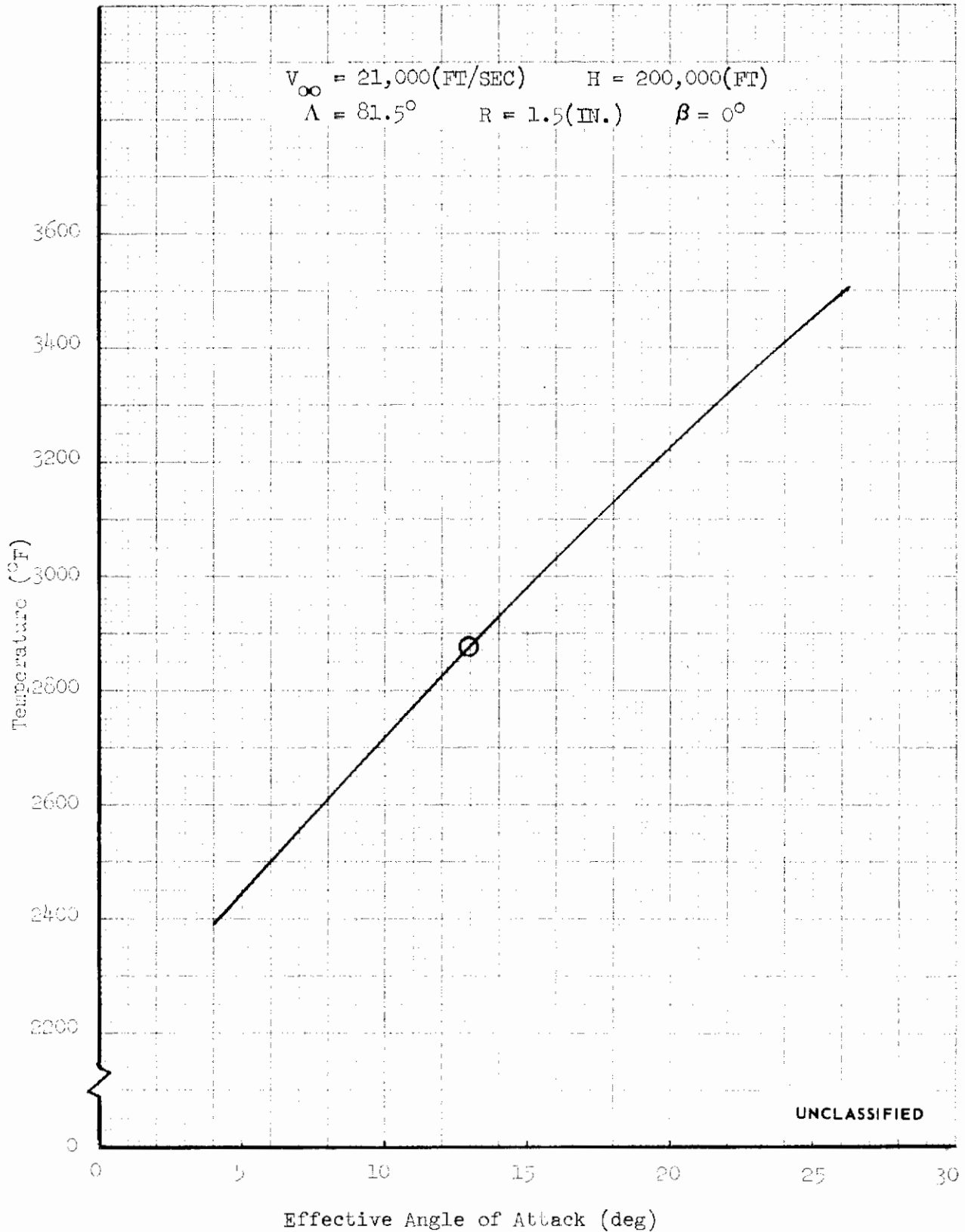
UNCLASSIFIED

FIGURE 73   (U) EFFECT OF ANGLE OF ATTACK ON BODY LEADING EDGE STAGNATION
LINE TEMPERATURE

117

$V_\infty = 21,000 (\text{FPS}) \quad H = 200,000 (\text{FT})(\text{LAMINAR FLOW})$
$V_\infty = 18,000 (\text{FPS}) \quad H = 180,000 (\text{FT})(\text{TURBULENT FLOW})$
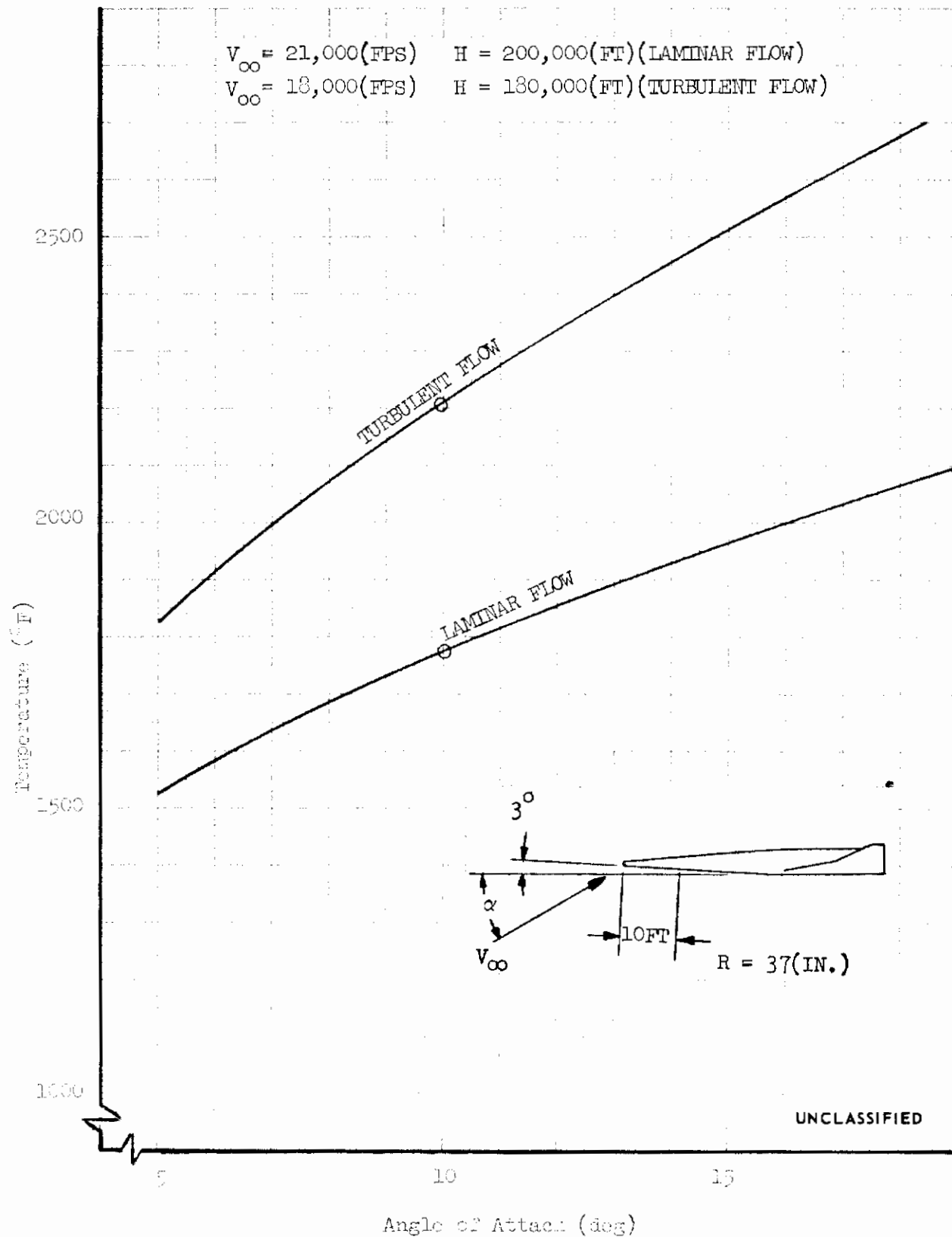
FIGURE 74 (U) EFFECT OF ANGLE OF ATTACK ON LOWER SURFACE CENTERLINE TEMPERATURES

118

$$V_\infty = 21,000 (\text{FT/SEC}) \qquad H = 200,000 (\text{FT}) \qquad \alpha = 10^\circ$$
$$\tau = 5^\circ \quad \Lambda_{fin} = 63^\circ \qquad \emptyset = 25^\circ \qquad R = 1.5 (\text{IN.})$$
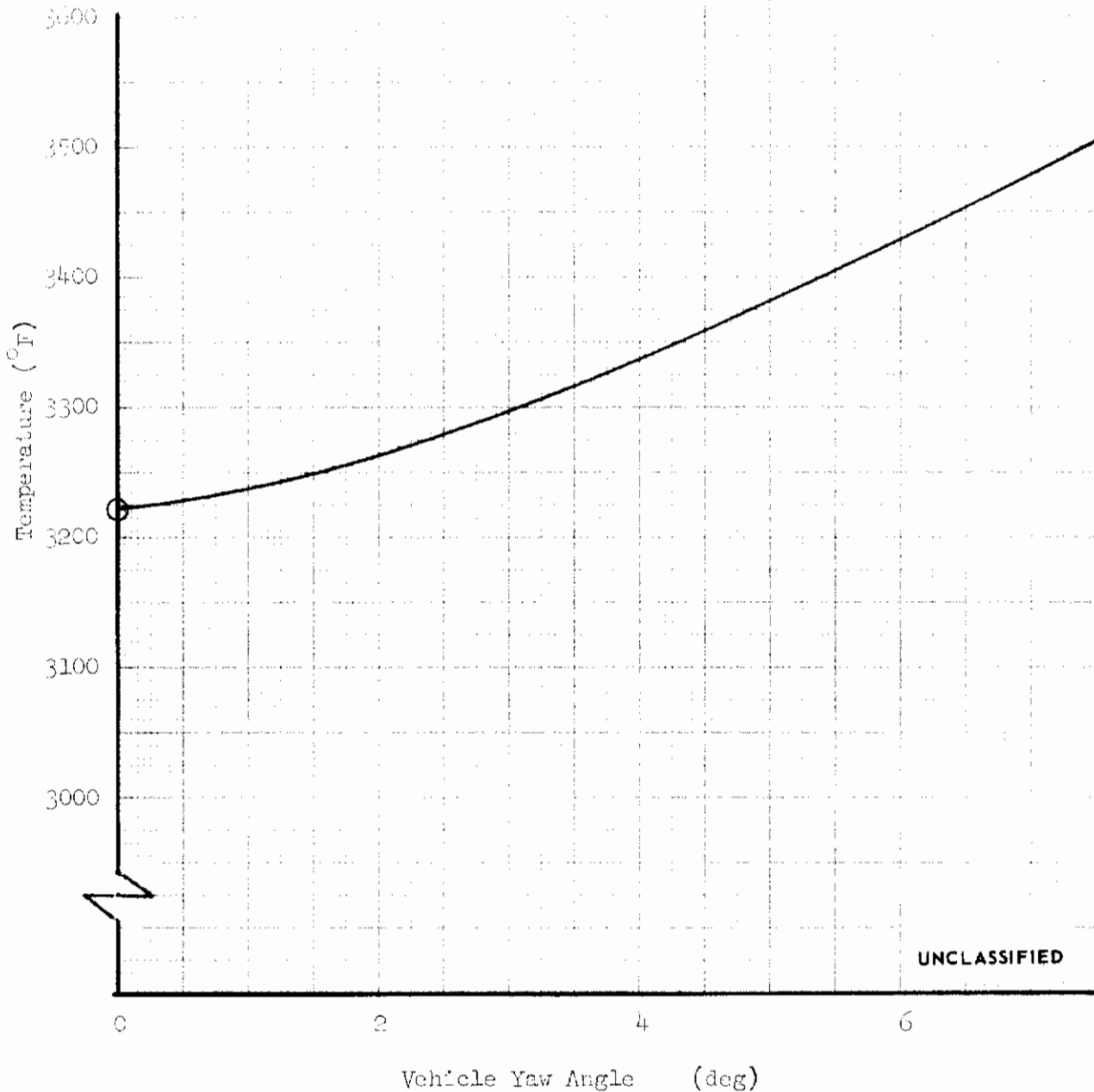
FIGURE 75 (U) EFFECT OF YAW ANGLE ON FIN LEADING EDGE STAGNATION LINE TEMPERATURE

119
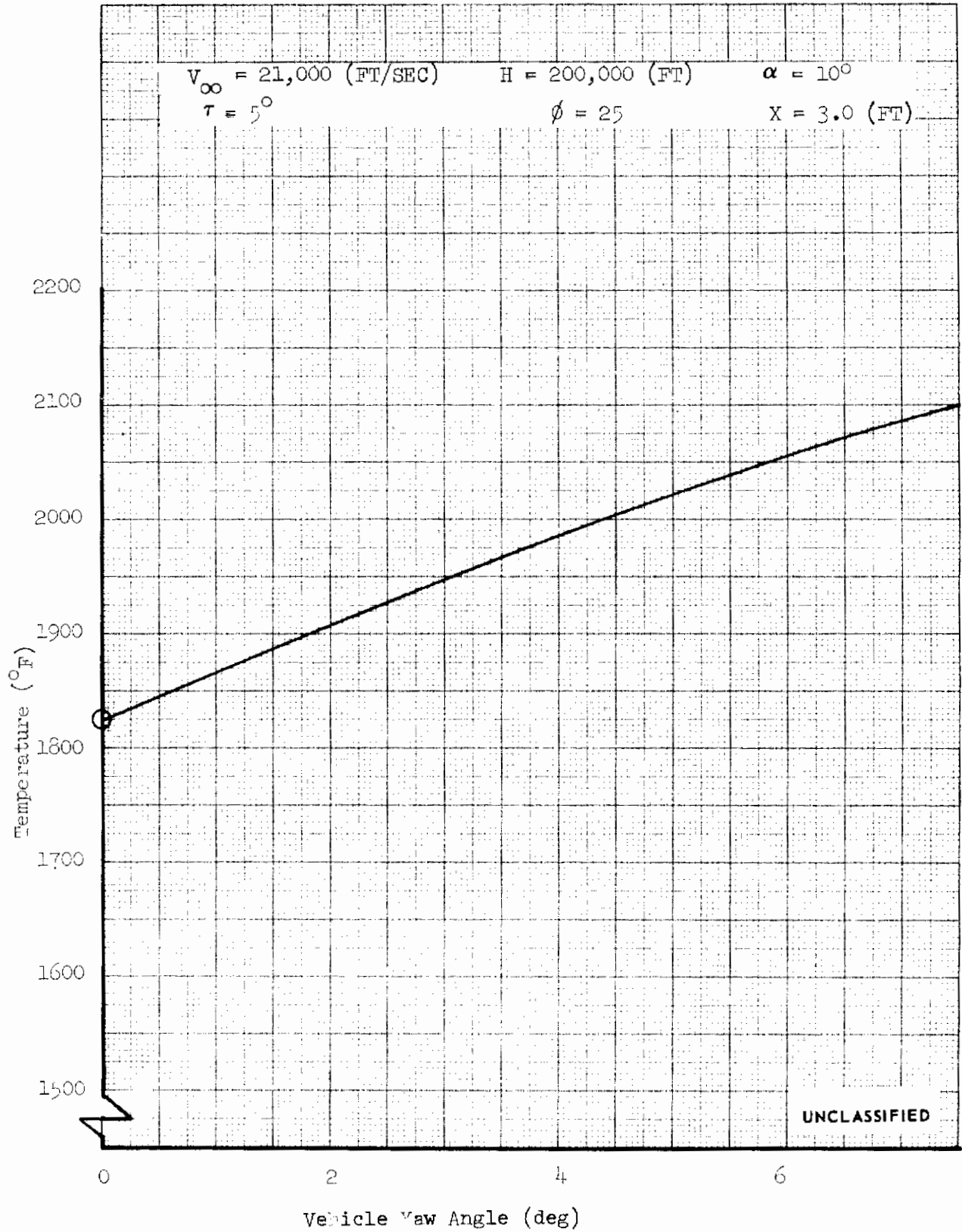
FIGURE 76 (U) EFFECT OF VEHICLE YAW ANGLE ON FIN OUTBOARD PANEL
TEMPERATURE

120
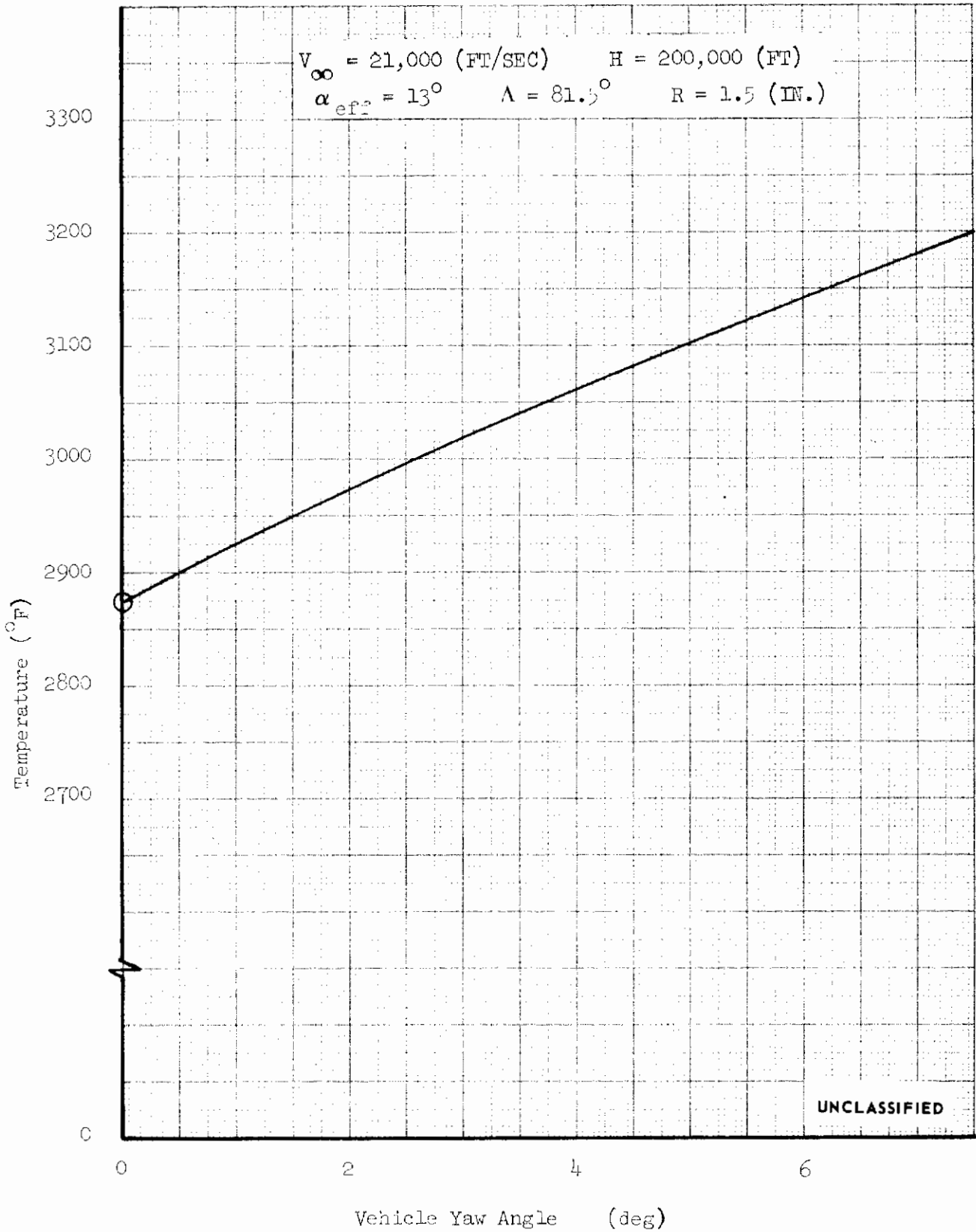
FIGURE 77 (U) EFFECT OF YAW ANGLE ON BODY LEADING EDGE STAGNATION
LINE TEMPERATURE

121
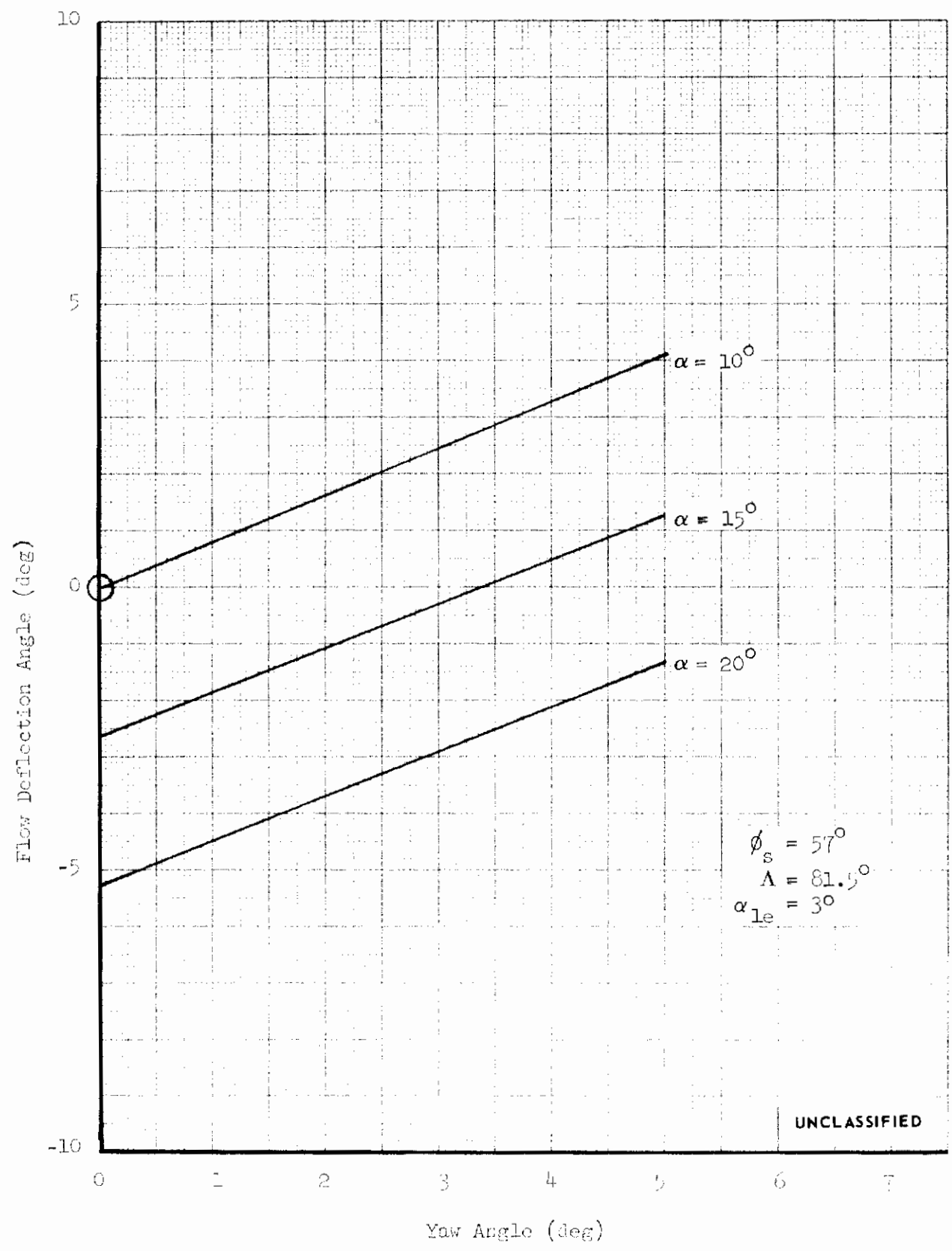
FIGURE 78 (U) EFFECT OF YAW ANGLE ON BODY SIDE PANEL FLOW DEFLECTION ANGLE
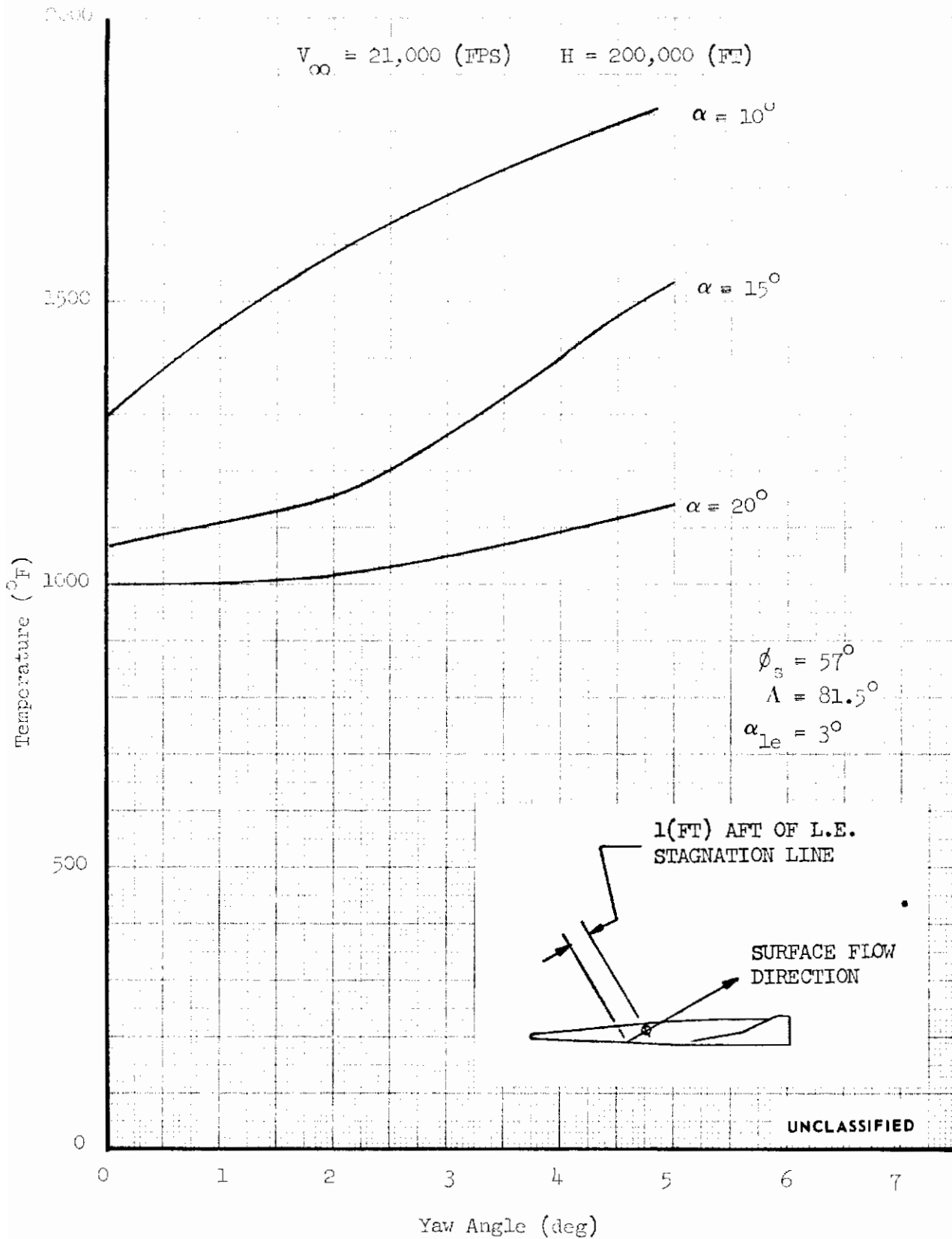
FIGURE 79 (U) EFFECT OF YAW ANGLE ON BODY SIDE PANEL TEMPERATURES

123
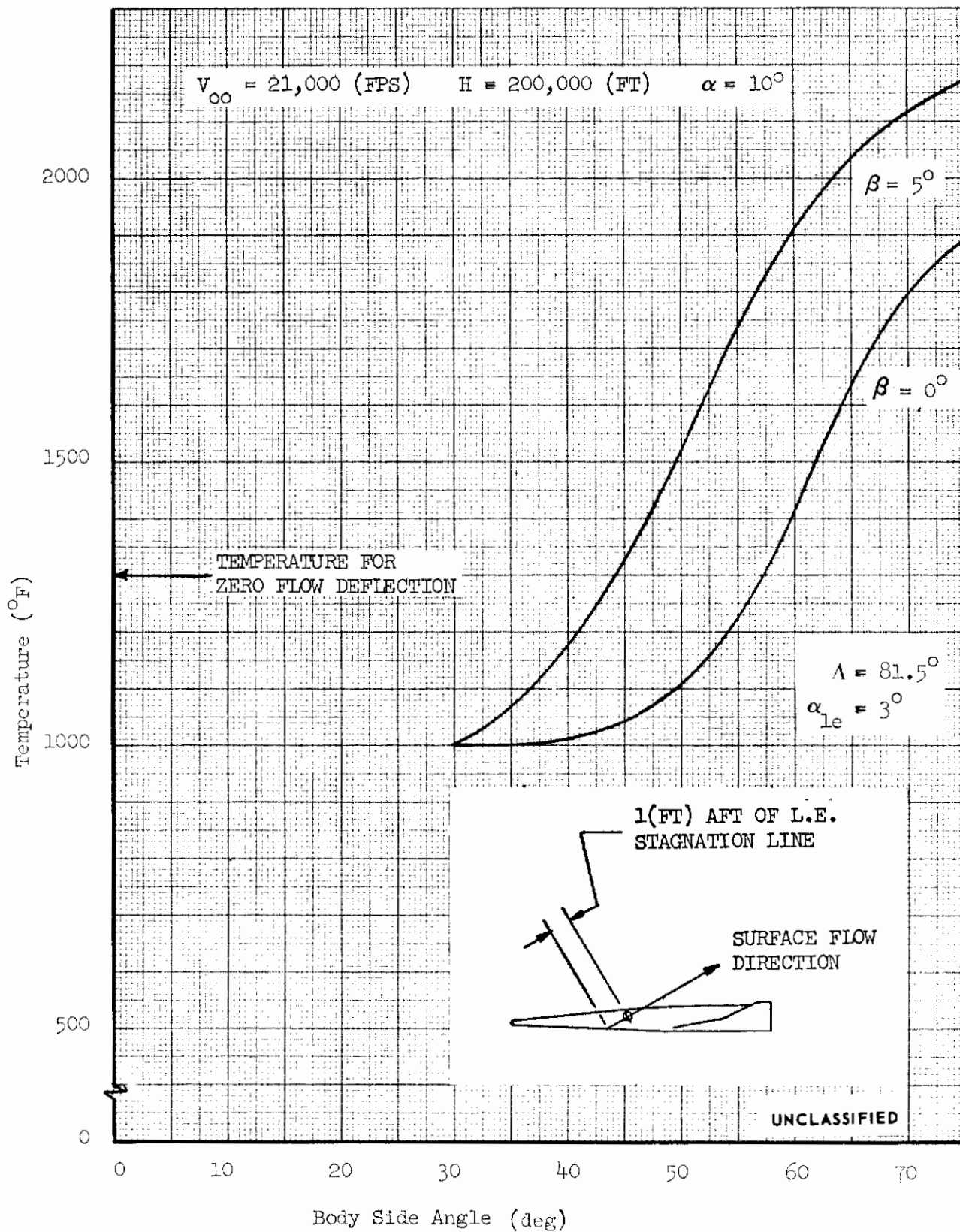
FIGURE 80 (U) EFFECT OF BODY SIDE ANGLE AND YAW ANGLE ON SIDE
PANEL SURFACE TEMPERATURES

124
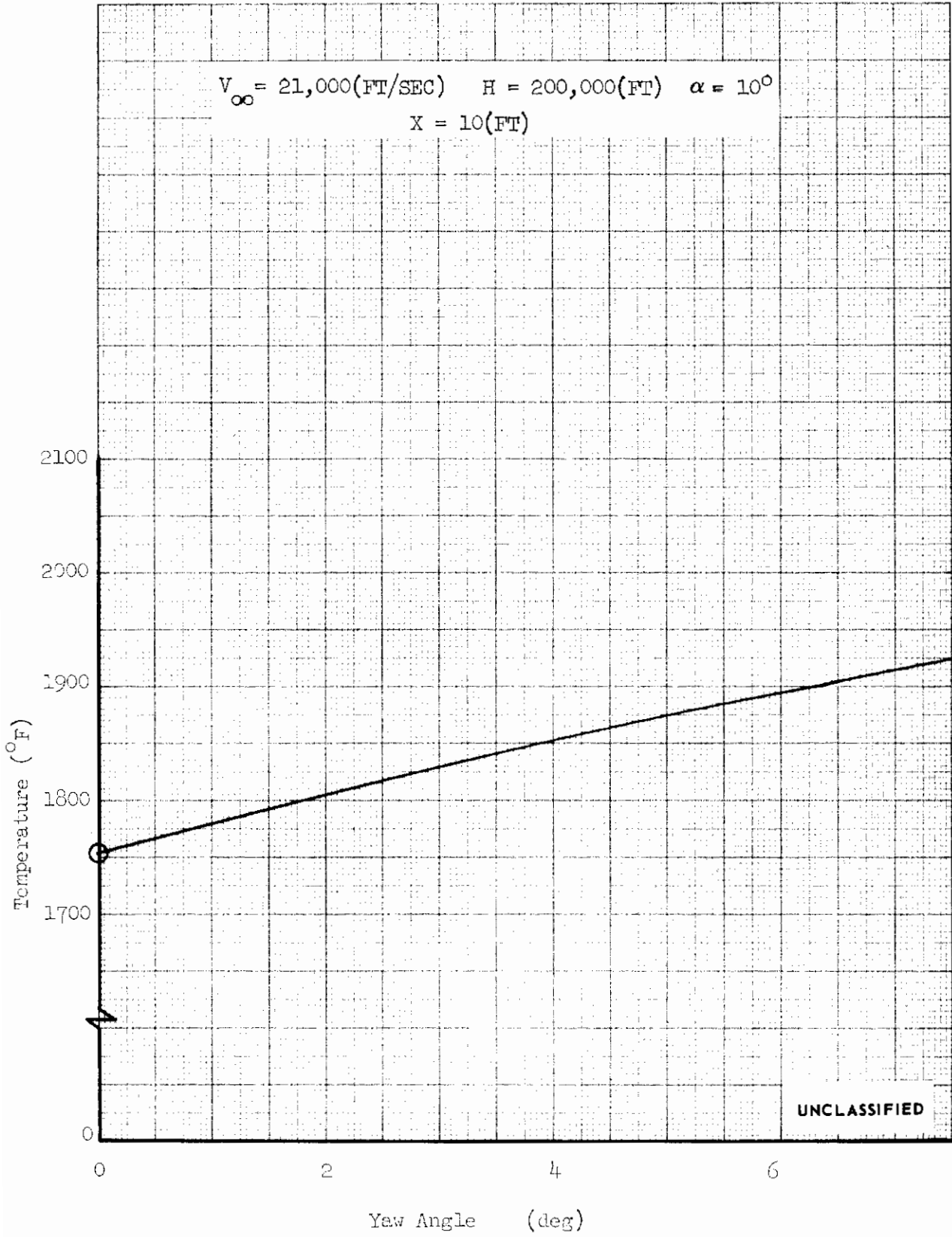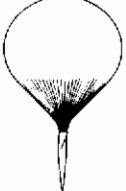
FIGURE 81   (U) EFFECT OF VEHICLE YAW ON FLAT BOTTOM LOWER SURFACE
             TEMPERATURE

125

HORIZONTAL LANDING			
HORIZONTAL LANDING WITH THRUST			
PARACHUTE AND DERIVITIES	LANDING SHOCK ATTENUATION		
	WATER RECOVERY		
	AIRSNATCH		
	PARACHUTE REEL		
	RETRO-ROCKET		
PARAVULCOON			
ROTOR SYSTEM			
VARIABLE GEOMETRY			

UNCLASSIFIED

FIGURE 82   (U) ALTERNATE RECOVERY TECHNIQUES
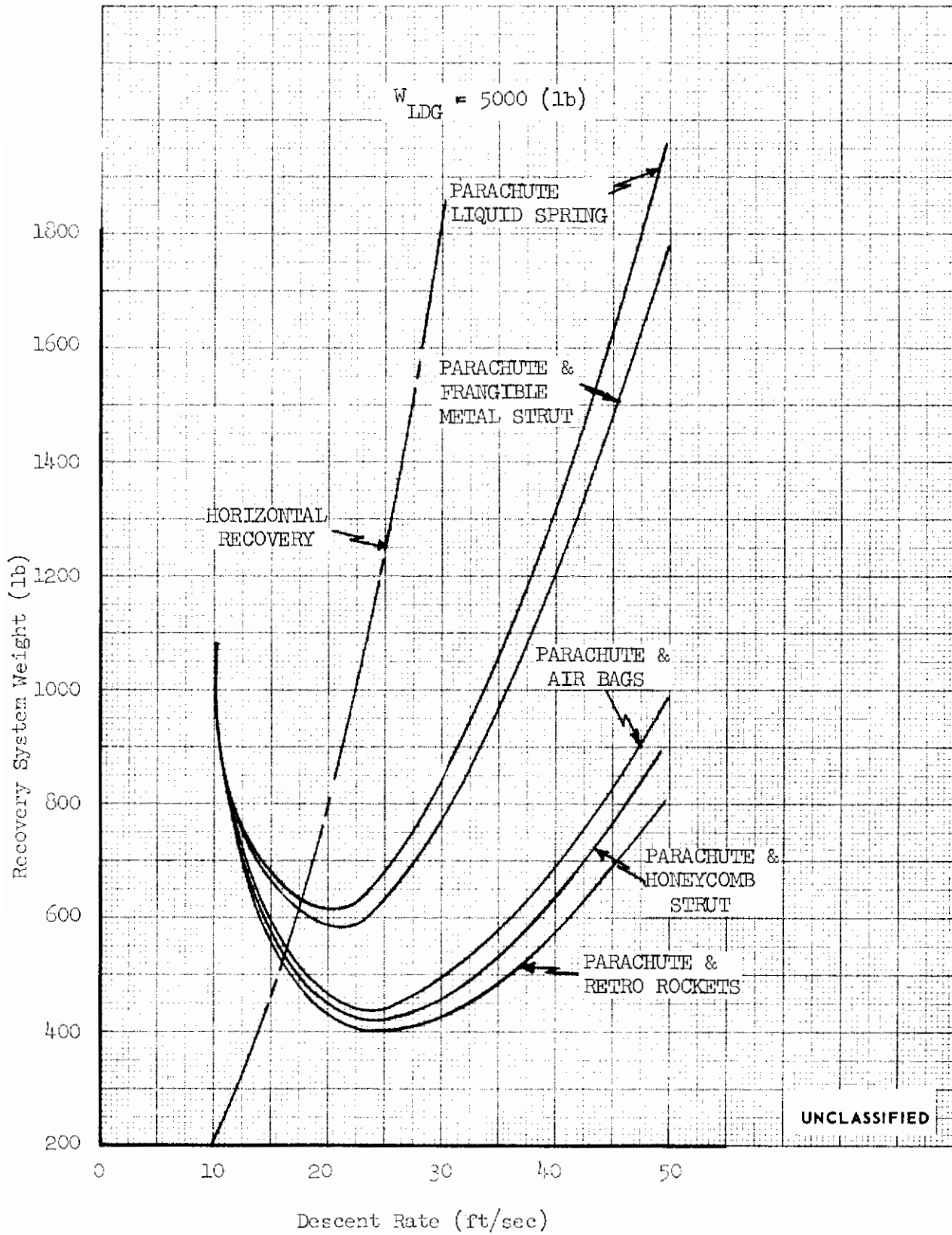
UNCLASSIFIED

FIGURE 83   (U) TOTAL RECOVERY SYSTEM WEIGHT

127
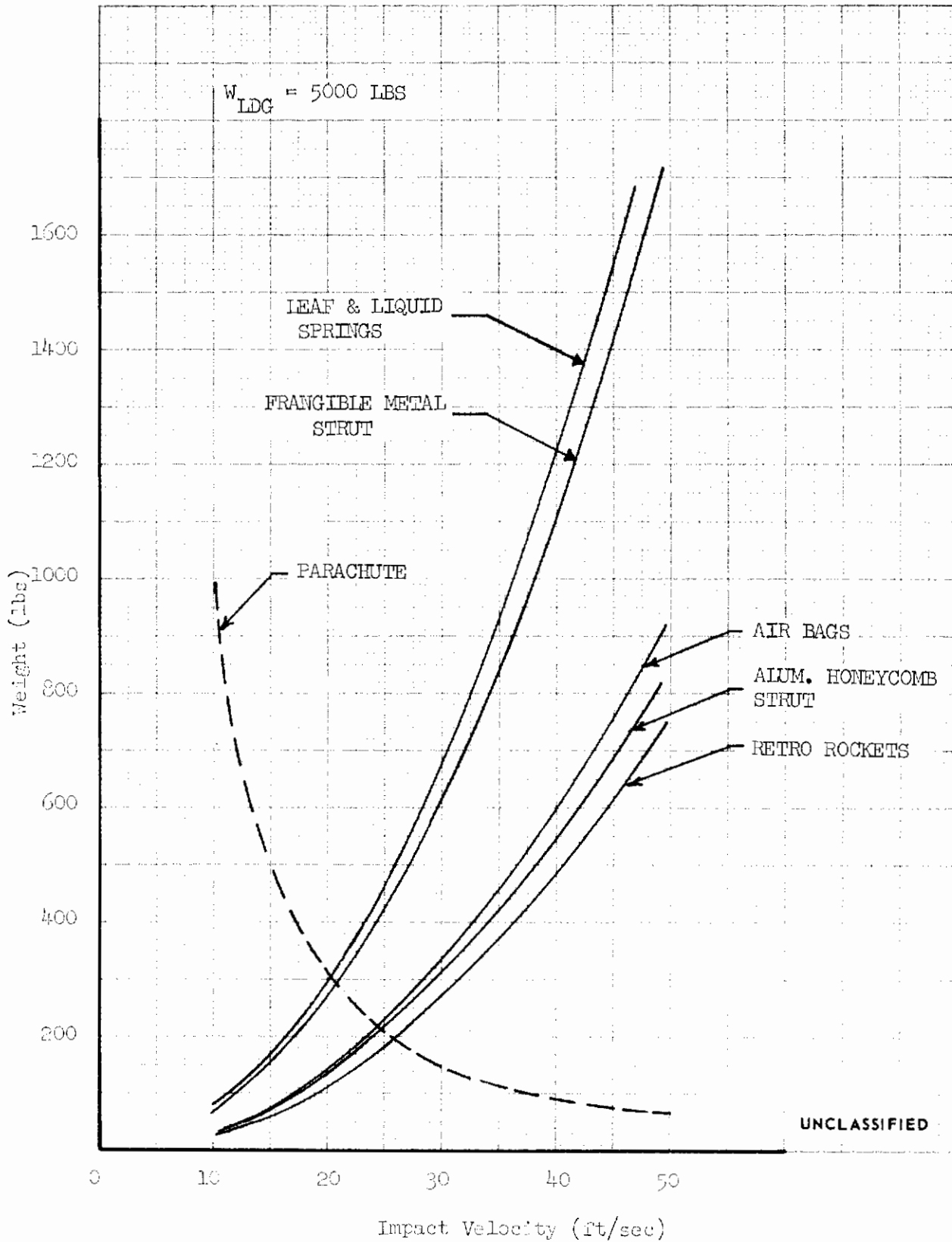
FIGURE 84   (U) PARACHUTE AND ATTENUATION SYSTEM WEIGHT

128
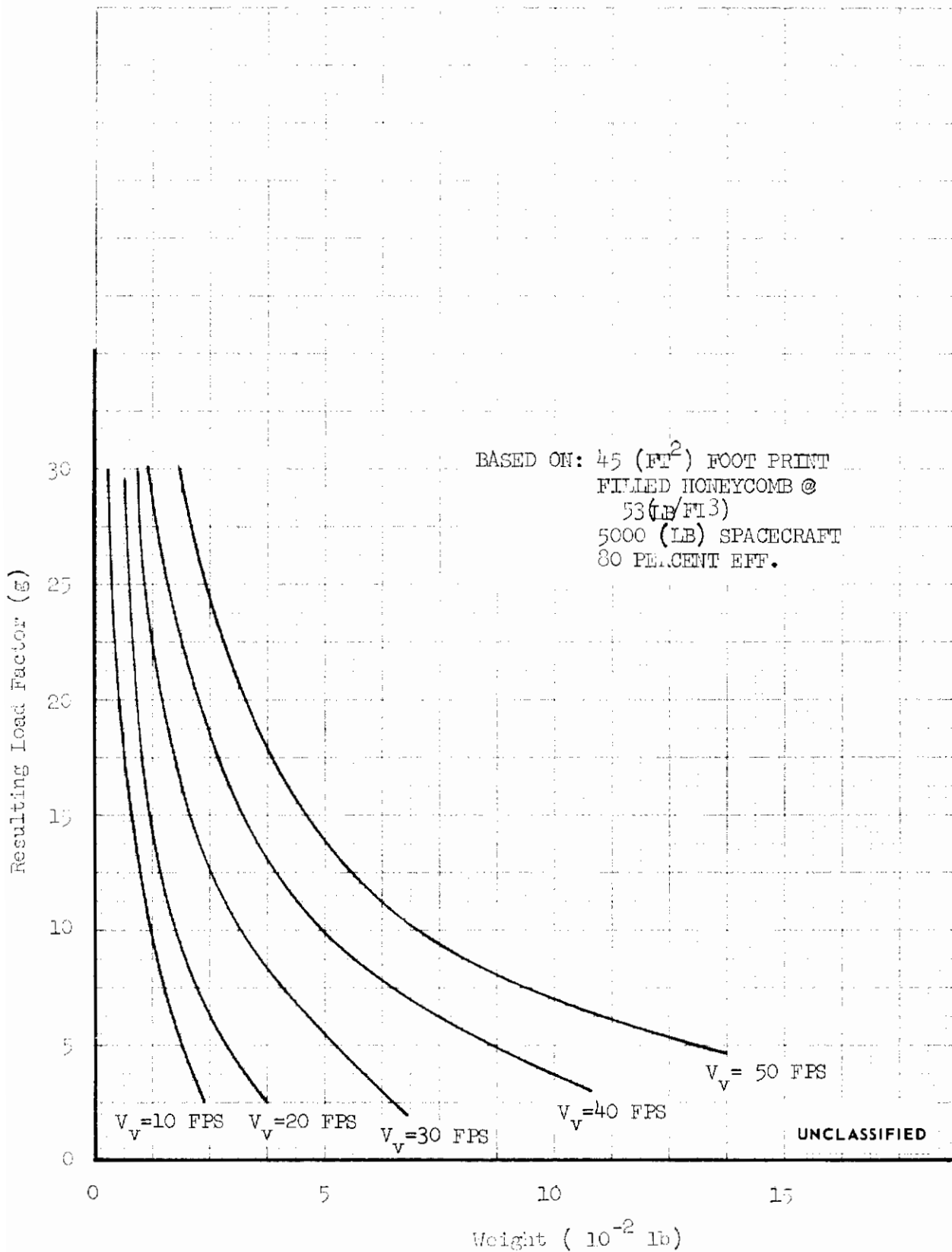
FIGURE 85 (U) CRUSHABLE ATTENUATION

129
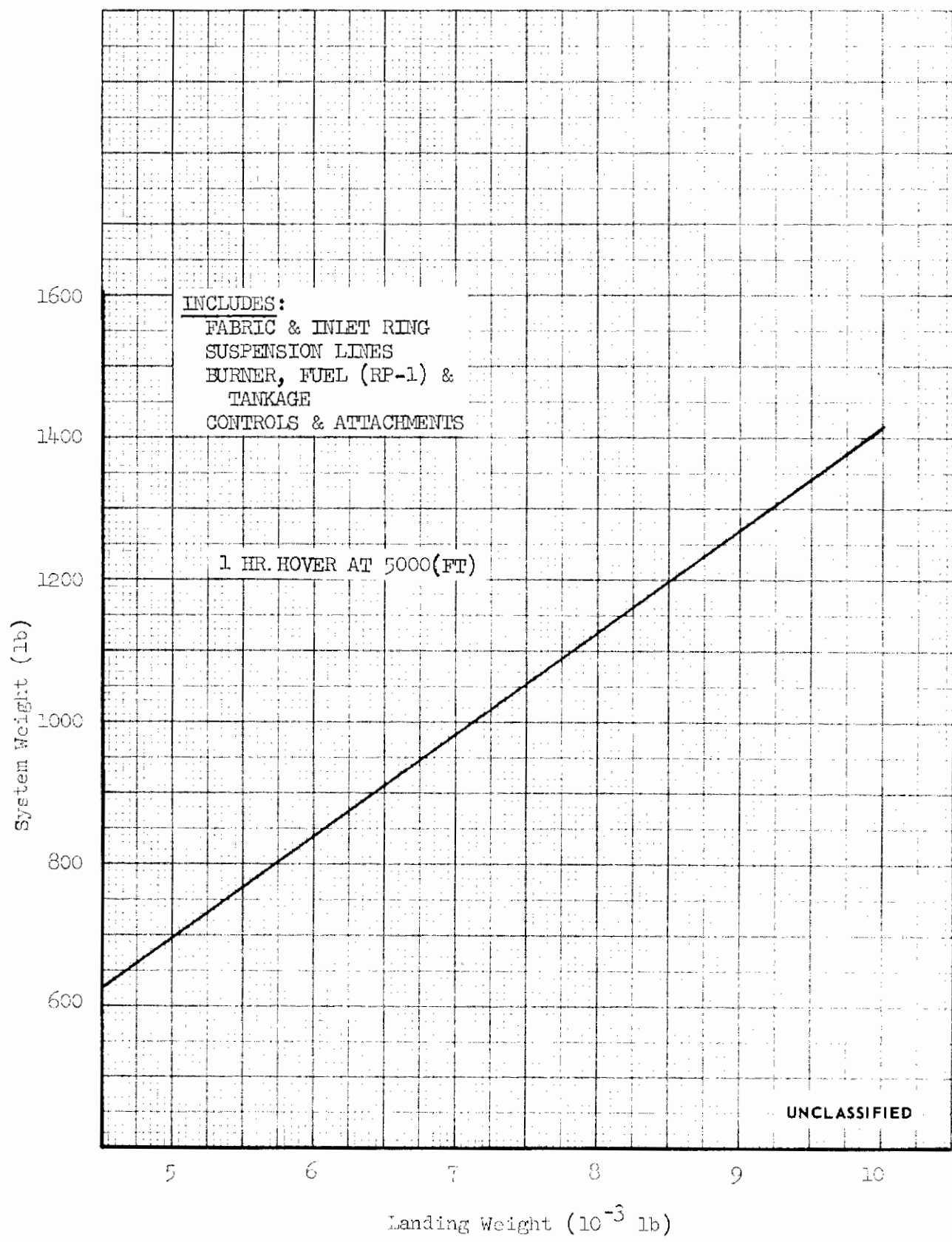
FIGURE 86   (U) PARAVULCOON WEIGHT

130
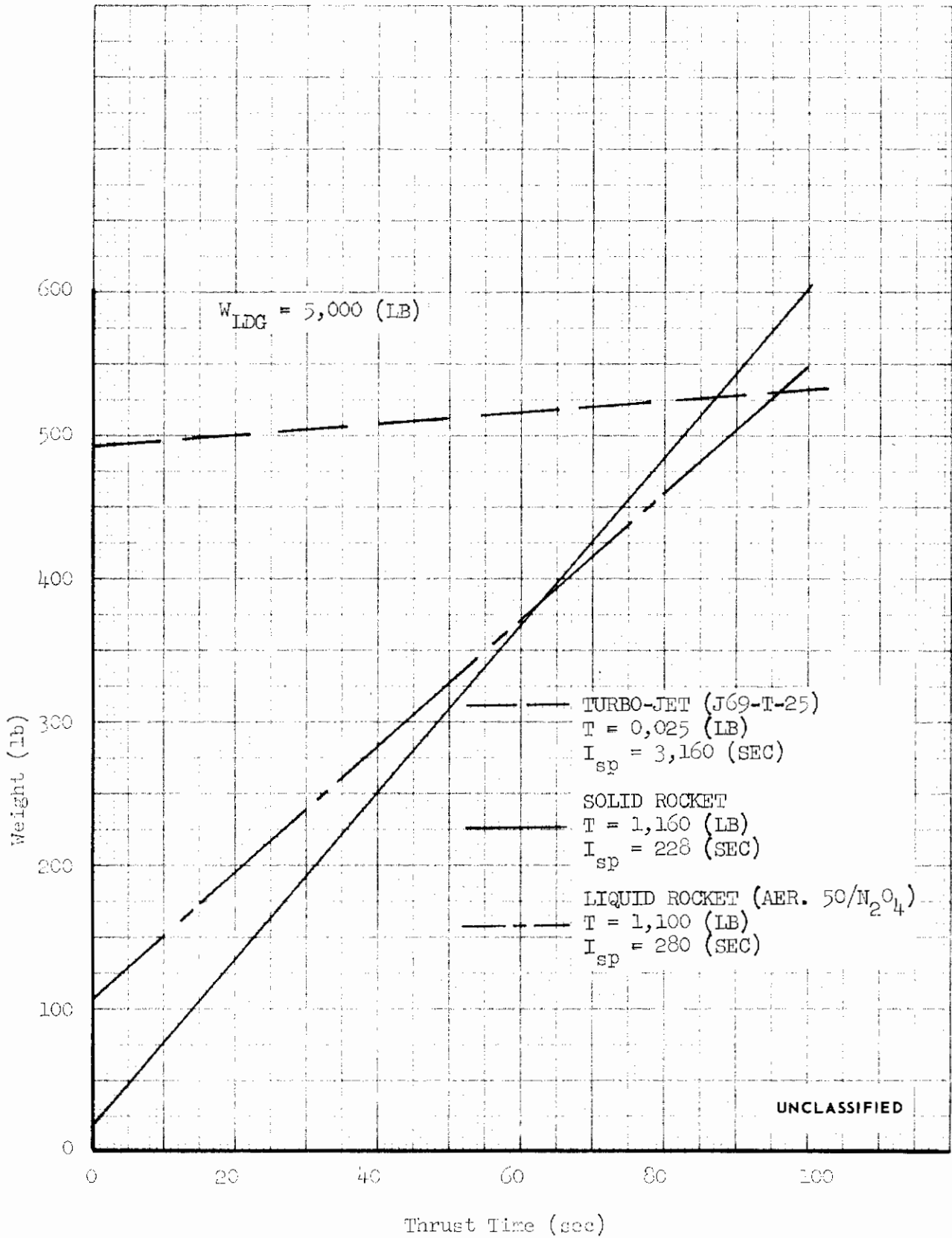
FIGURE 87   (U) PROPULSION SYSTEM WEIGHT (INSTANT L/D)

131
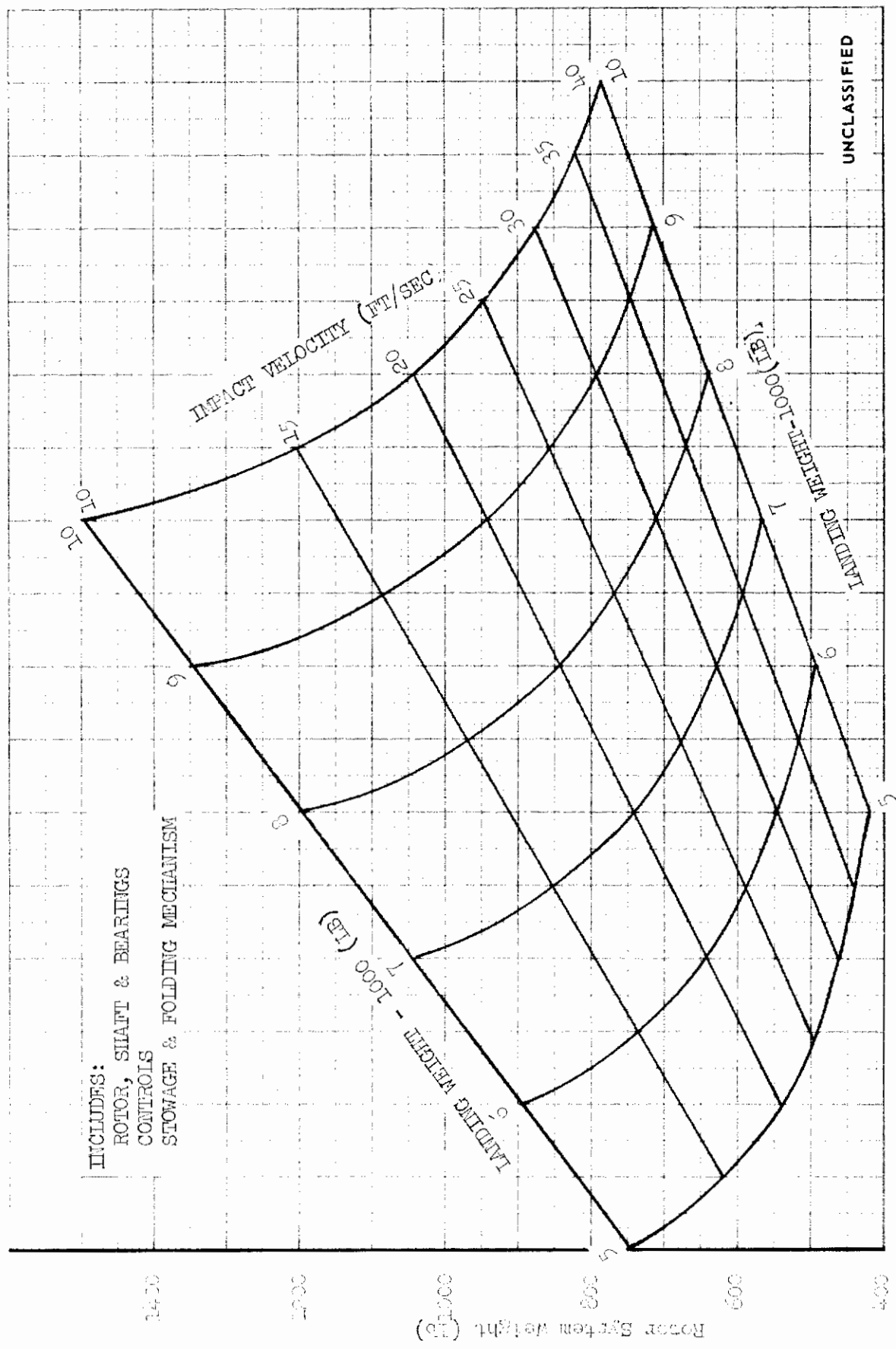
FIGURE 88   (U) ROTOR RECOVERY SYSTEM WEIGHT
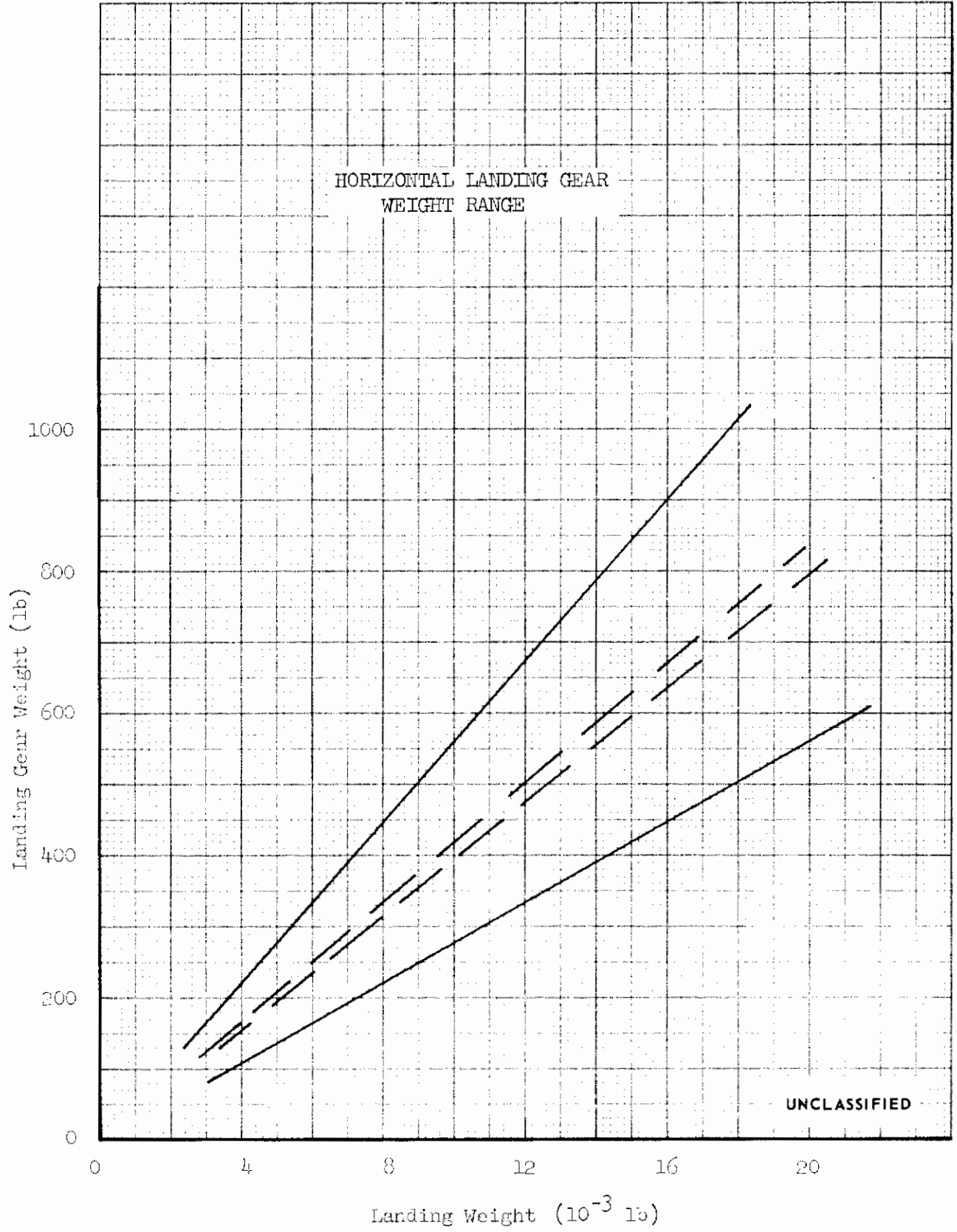
132

HORIZONTAL LANDING GEAR
WEIGHT RANGE

FIGURE 89 (U) RANGE OF ANALYZED AMR HORIZONTAL LANDING GEARS WEIGHT
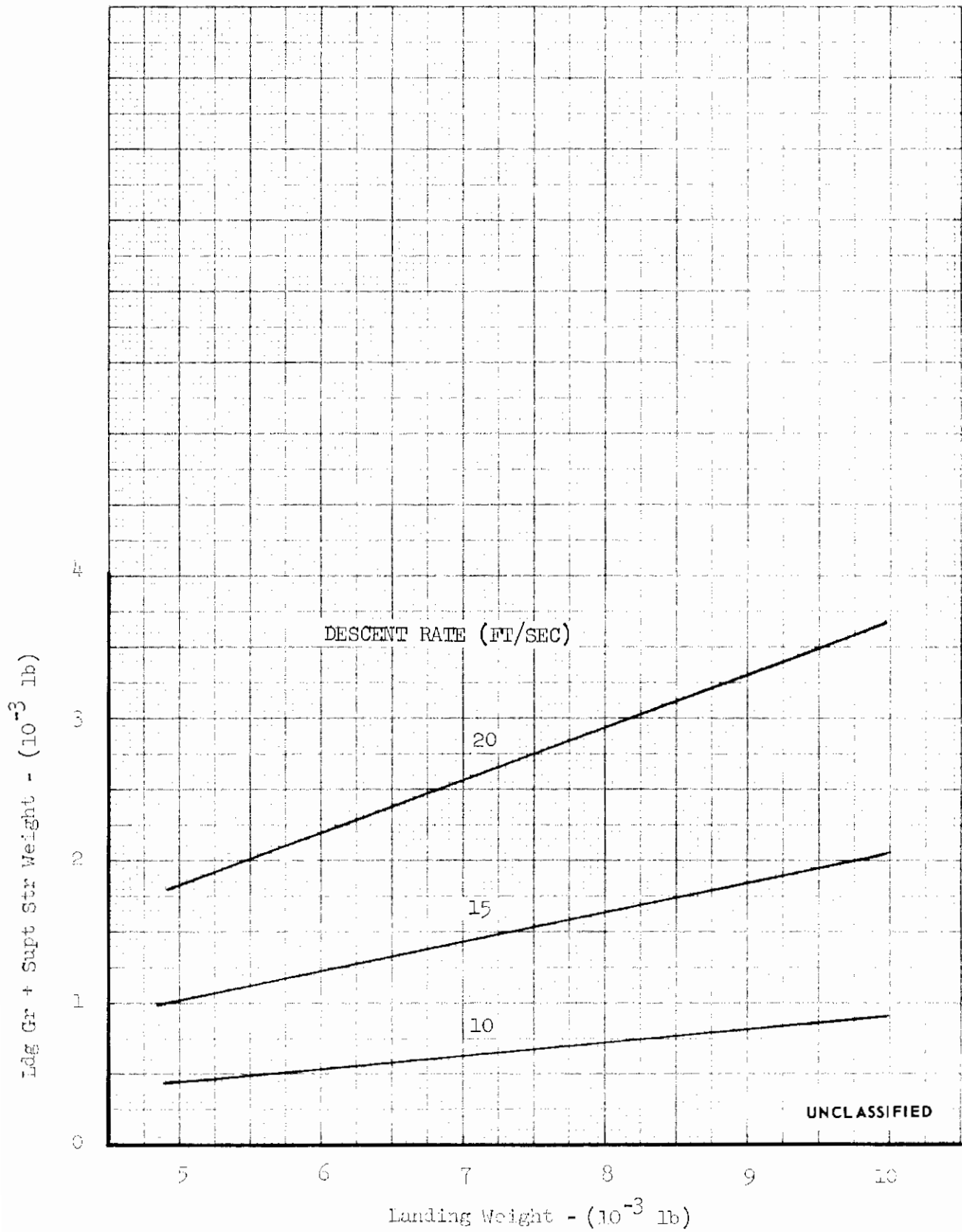RANGE FOR AIRCRAFT HORIZONTAL LANDING GEARS

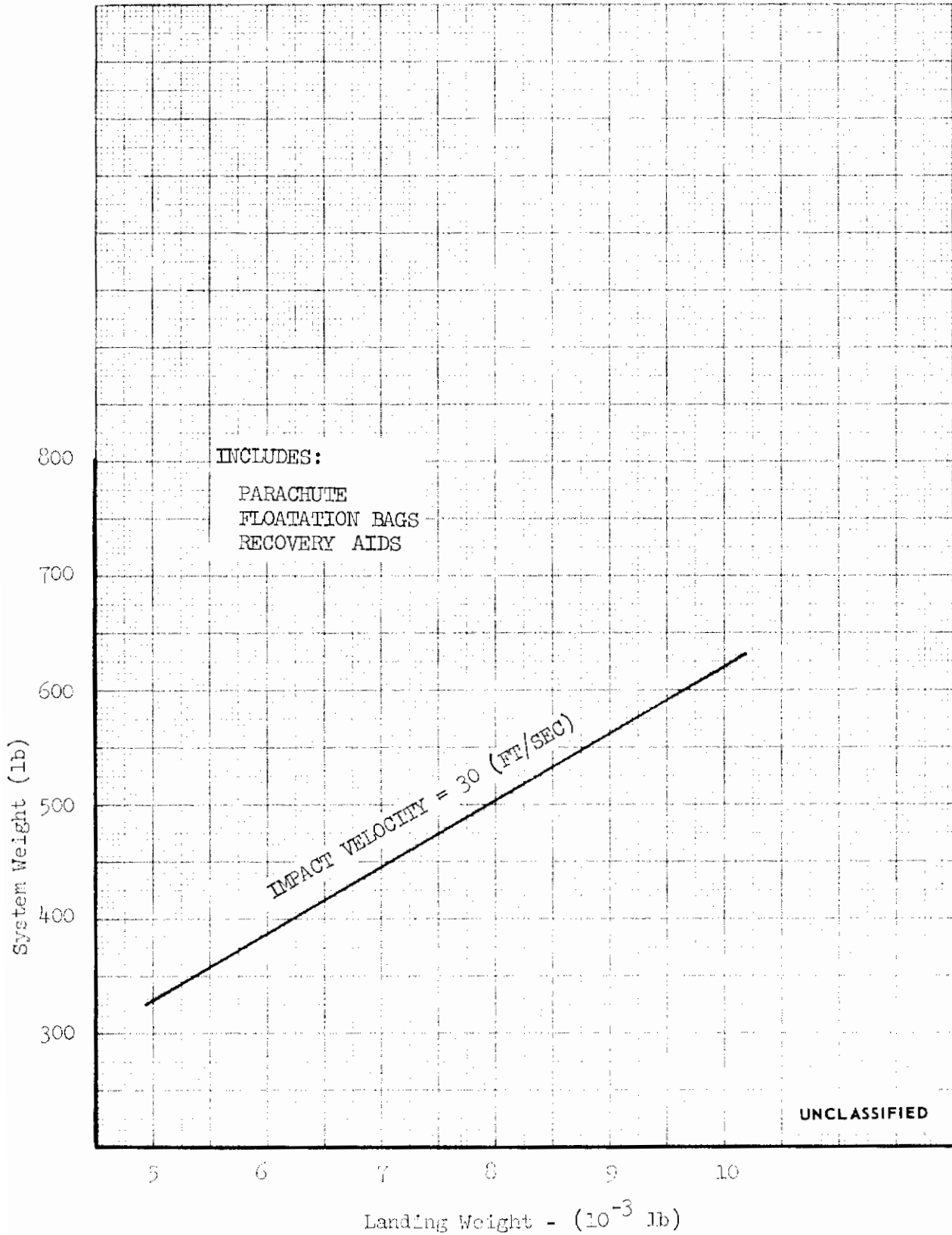133

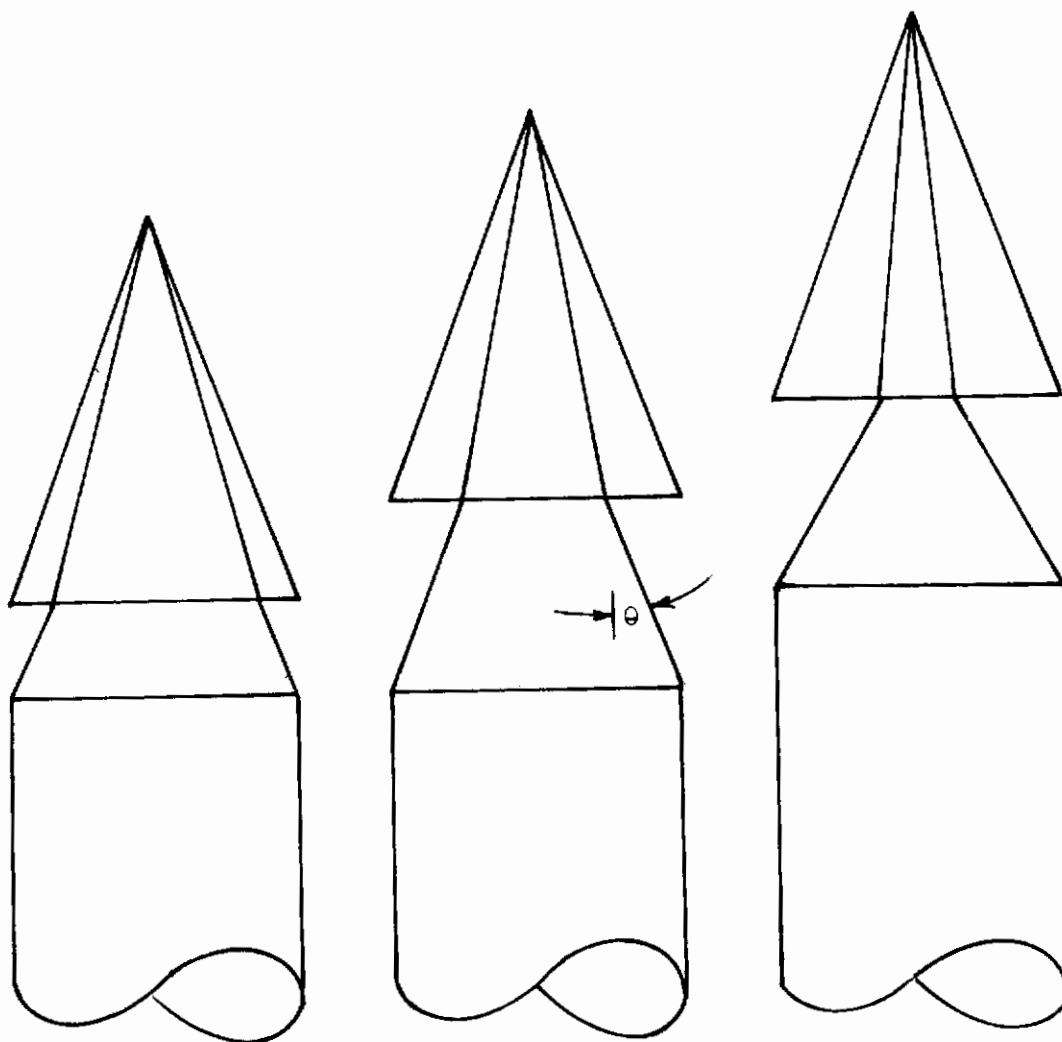FIGURE 90   (U) LANDING GEAR PLUS SUPPORT STRUCTURE WEIGHT

134

INCLUDES:

PARACHUTE
FLOATATION BAGS
RECOVERY AIDS

IMPACT VELOCITY = 30 (FT/SEC)

System Weight (lb)

Landing Weight - $(10^{-3}$ lb)

UNCLASSIFIED

FIGURE 91   (U) WATER RECOVERY SYSTEM

135

FIGURE 92 (U) VARIATION OF TRANSITION SECTION SIZE WITH PAYLOAD
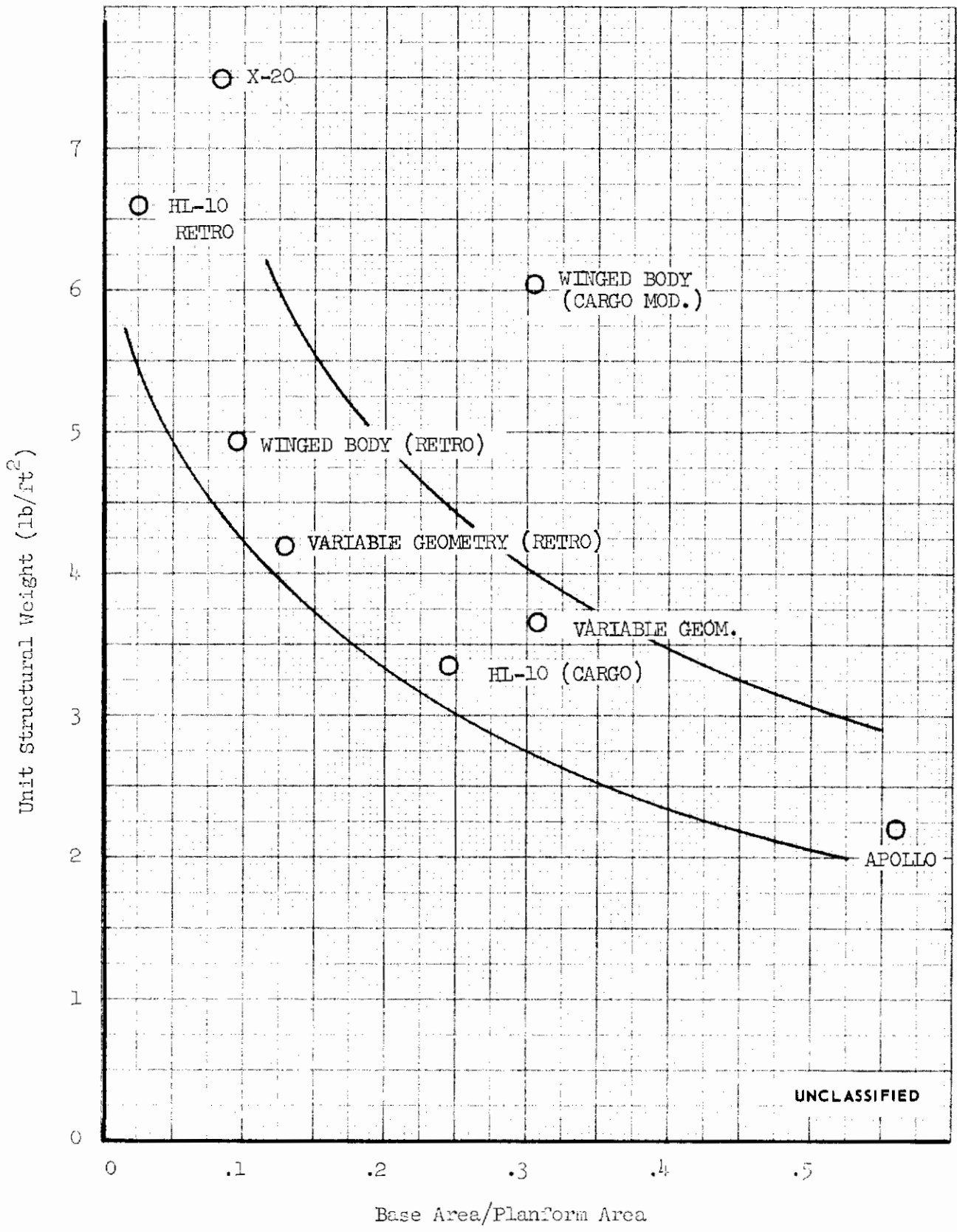BASE AREA, θ = CONSTRUCTION

136

FIGURE 93 (U) VARIATION OF TRANSITION SECTION UNIT STRUCTURAL WEIGHT
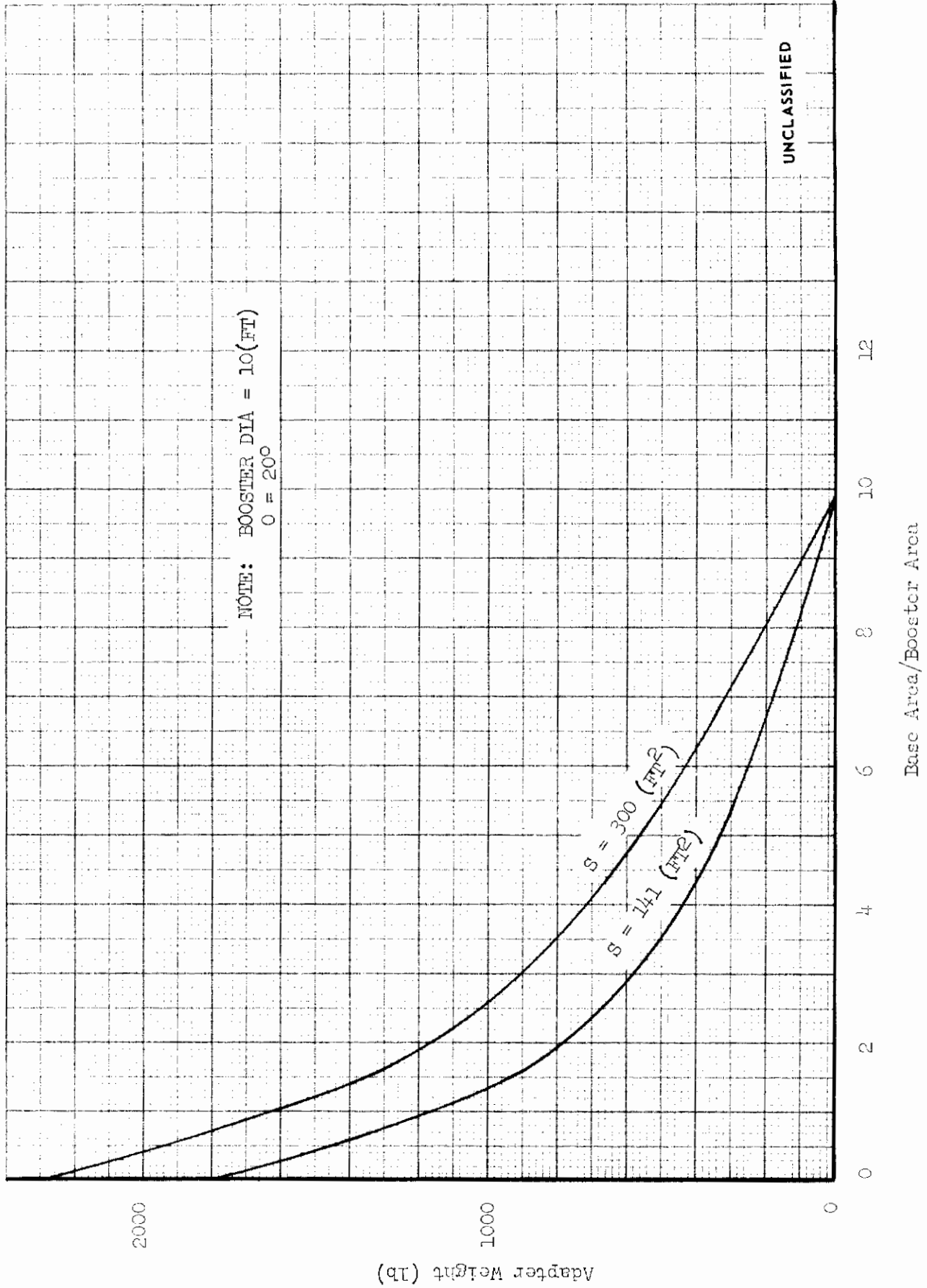WITH BASE AREA-TO-PLANFORM AREA RATIO

137

FIGURE 94 (U) ADAPTER WEIGHT VARIATION WITH BASE AREA-TO-BOOSTER AREA RATIO - 10 FT. DIA. BOOSTER
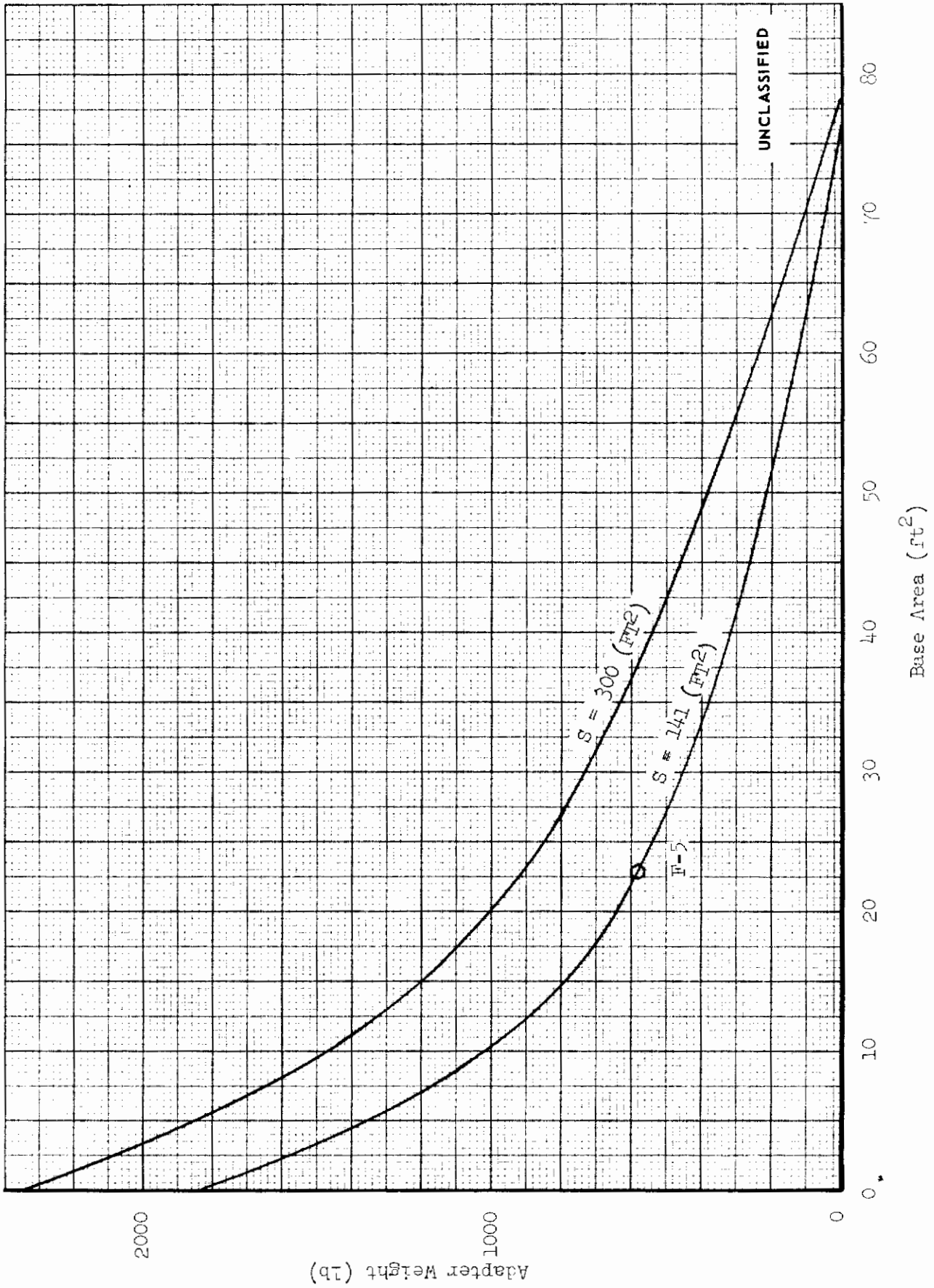
138

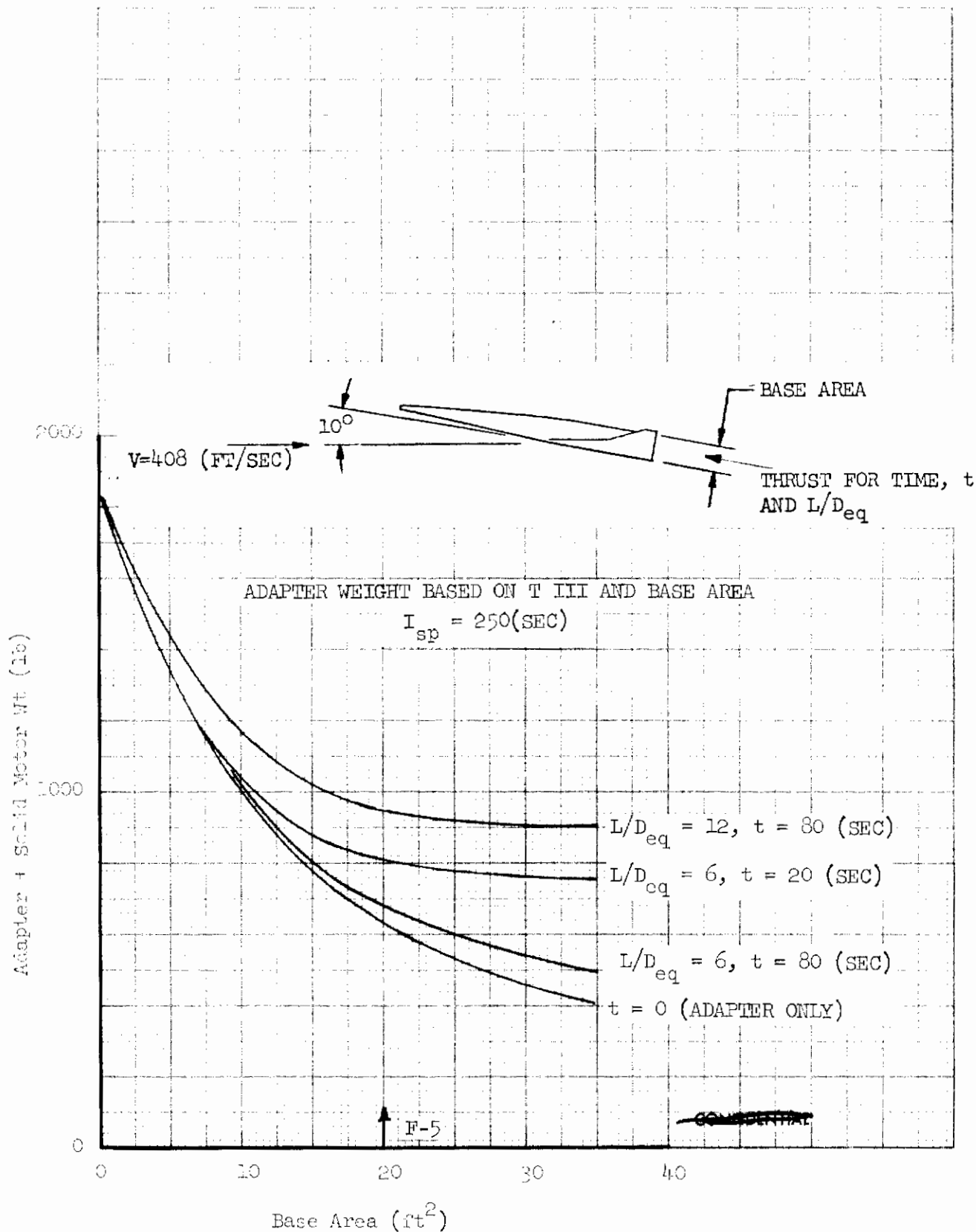FIGURE 95 (U) ADAPTER WEIGHT VARIATION WITH PAYLOAD BASE AREA - BOOSTER DIA - 10 (FT)

FIGURE 96   (U) LANDING WEIGHT PENALTY

140

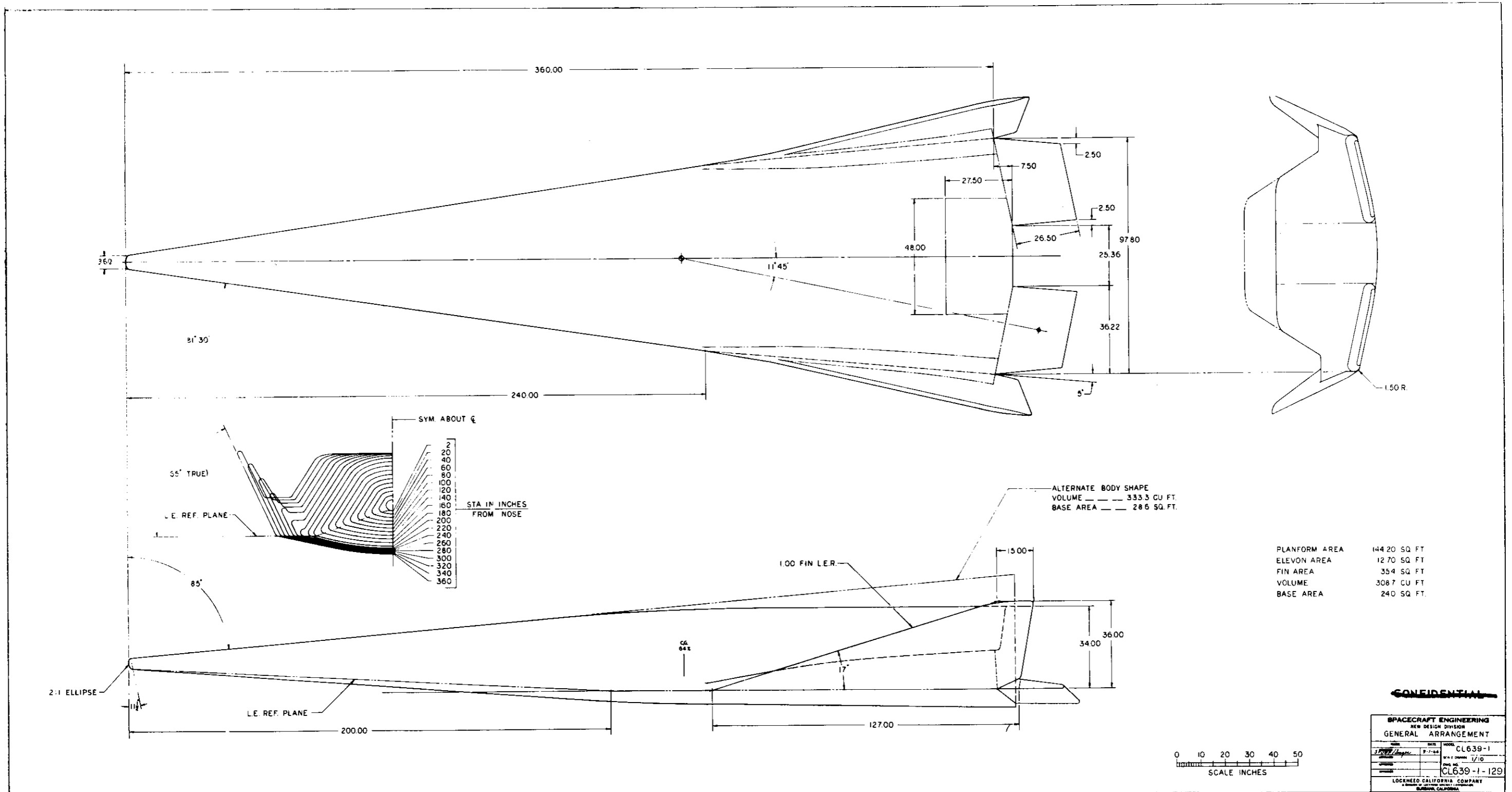FIGURE 97   (U) HLD-35-1 GENERAL ARRANGEMENT

141

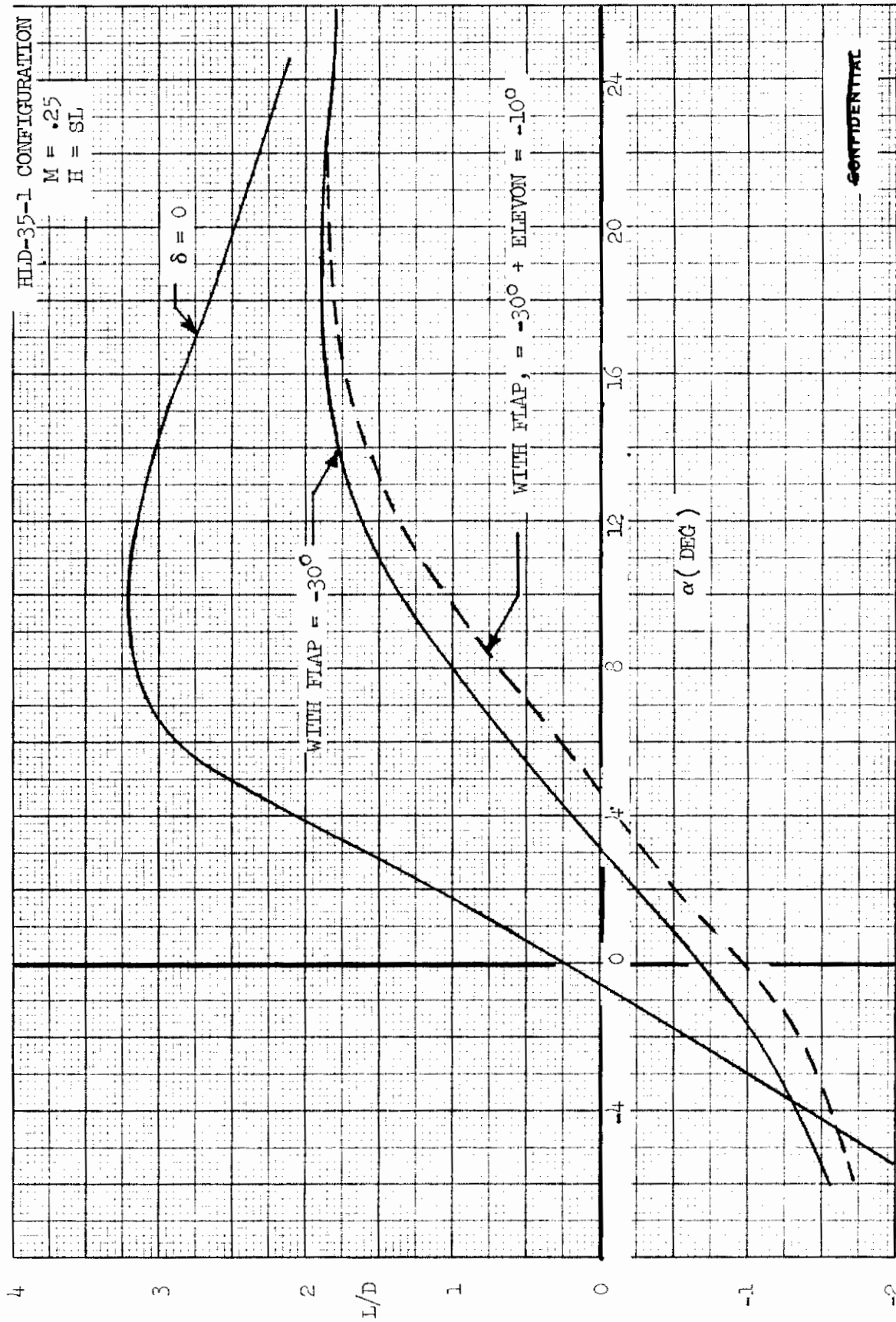(REVERSE SIDE IS BLANK)

FIGURE 98   (U) VARIATION OF TEST CONFIGURATION L/D WITH ANGLE OF ATTACK (M = .25)

143
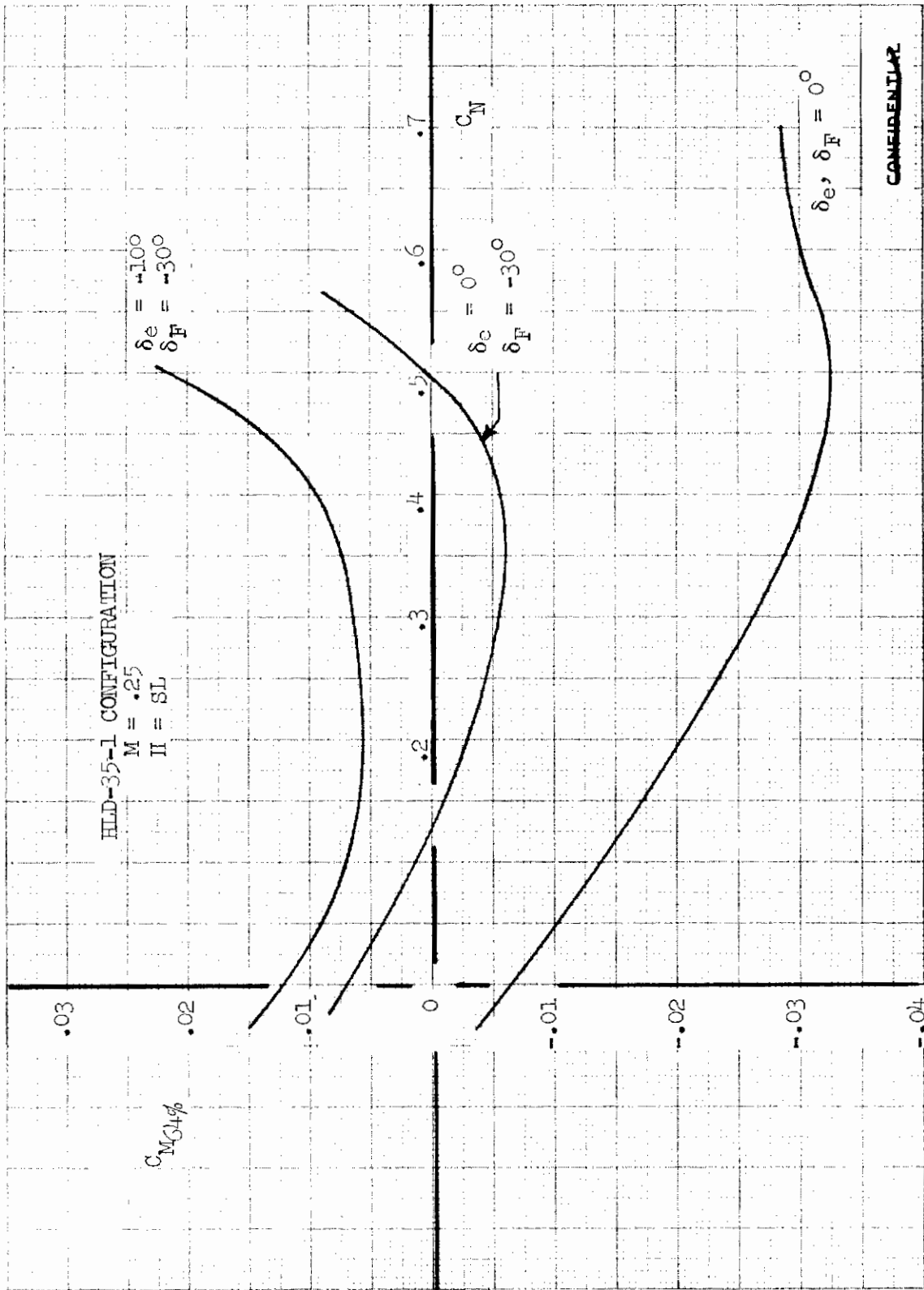
FIGURE 99   (U) TEST CONFIGURATION LONGITUDINAL STABILITY (M = .25)

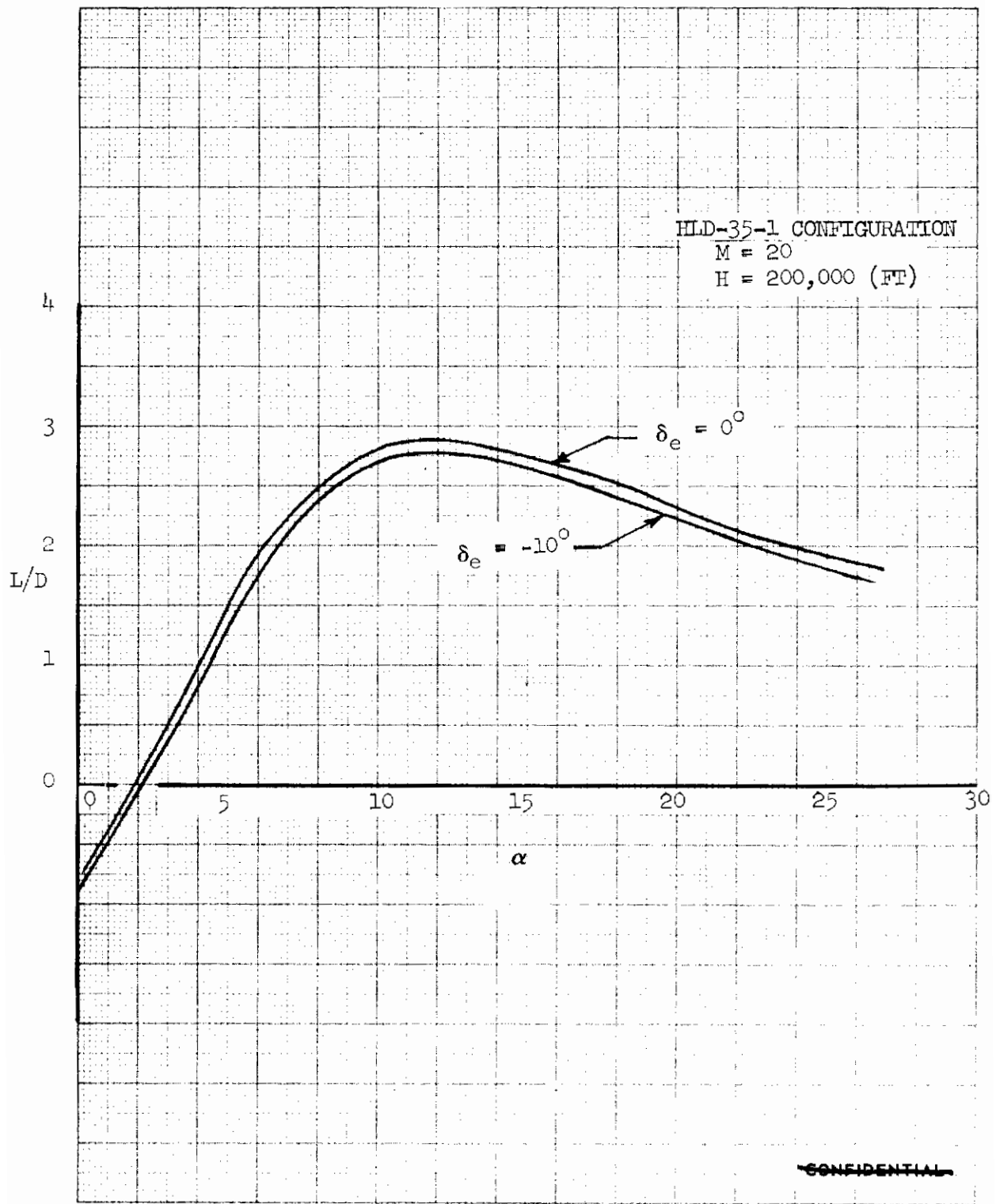FIGURE 100 (U) TEST CONFIGURATION VARIATION OF L/D WITH ANGLE
OF ATTACK (M = 20)

145
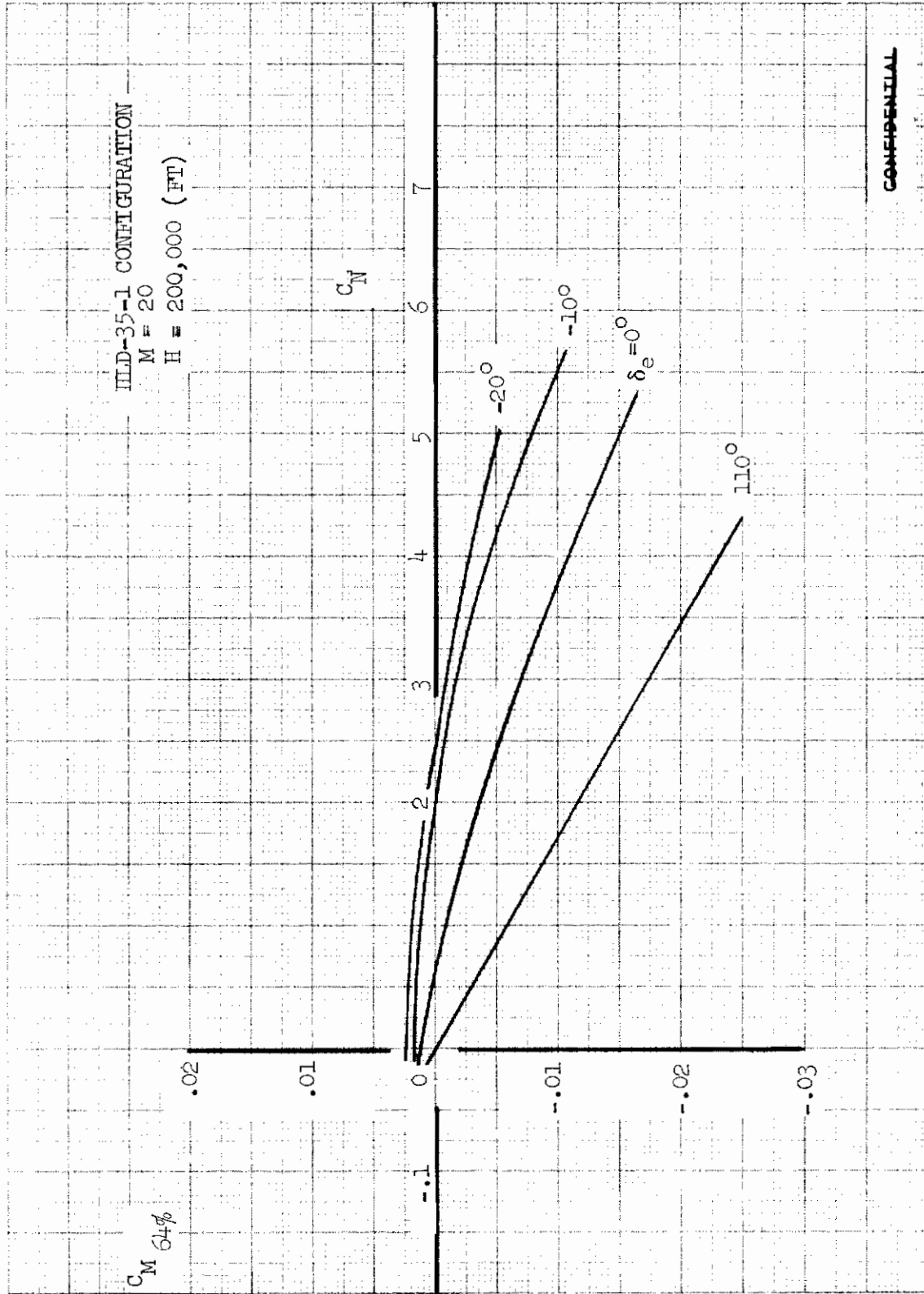
FIGURE 101 (U) TEST CONFIGURATION LONGITUDINAL STABILITY (M = 20)
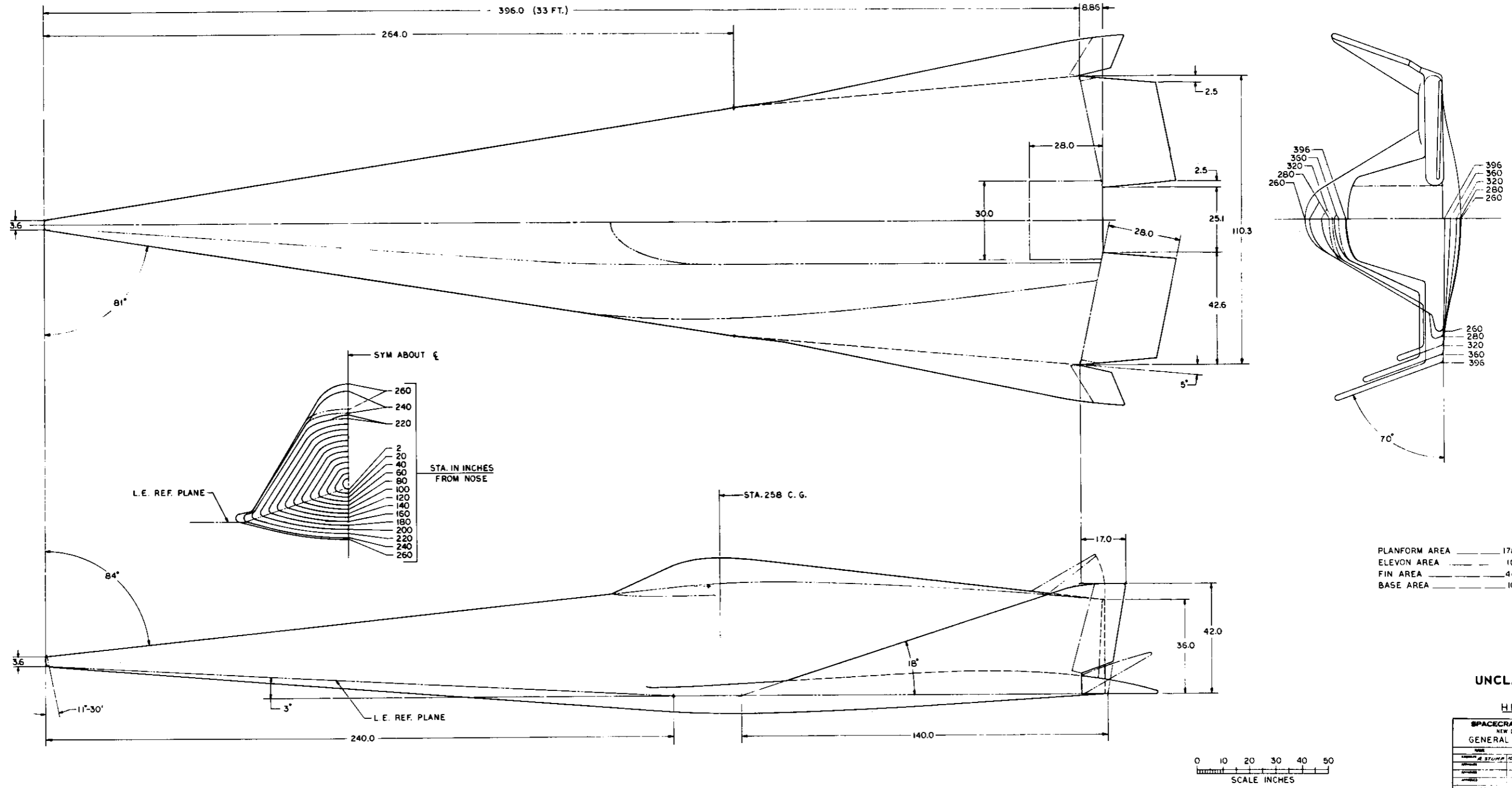
FIGURE 102 (U) HLD-35-2 GENERAL ARRANGEMENT

(REVERSE SIDE IS BLANK)
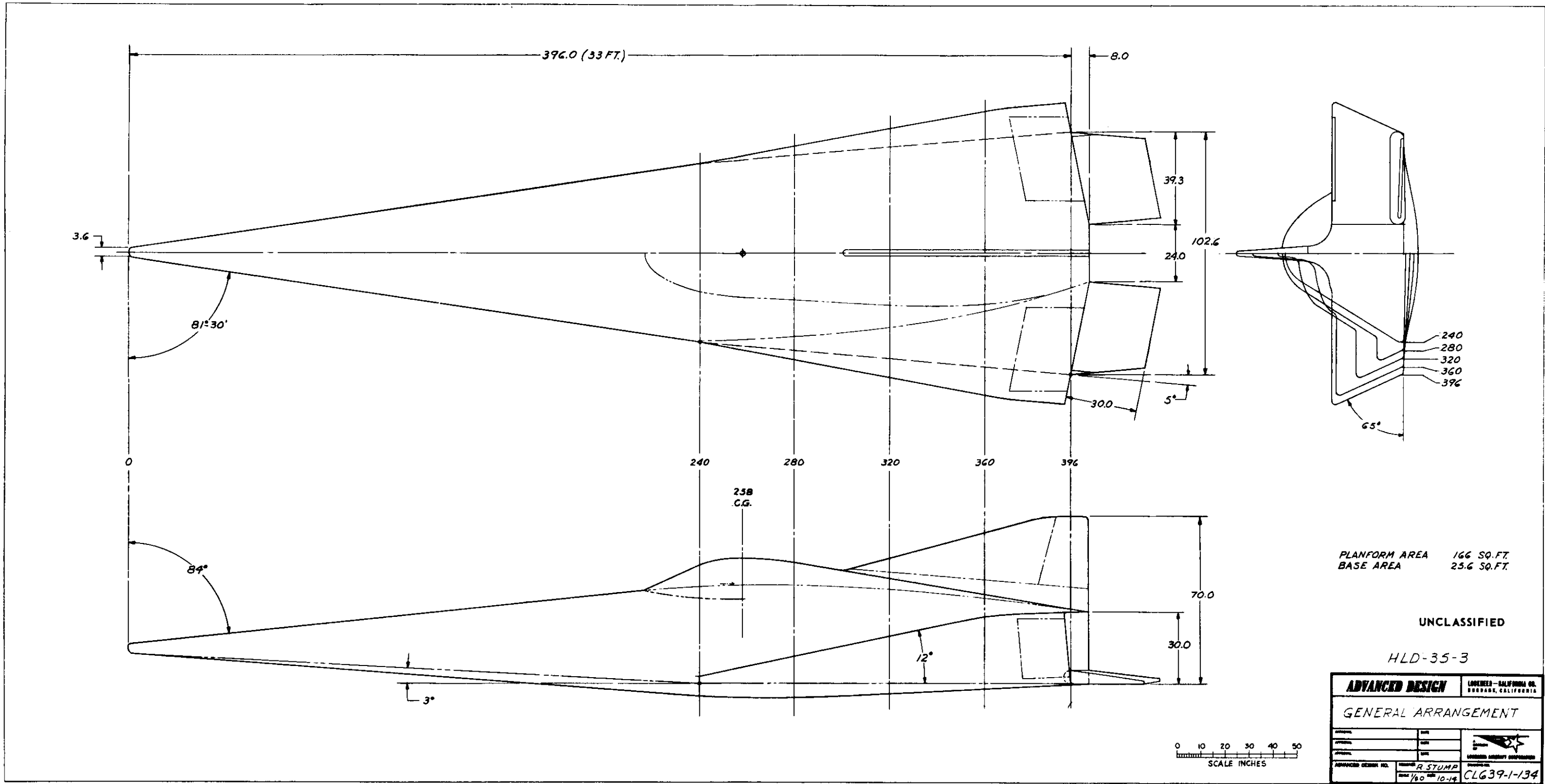
FIGURE 103 (U) HLD-35-3 GENERAL ARRANGEMENT

Contrails
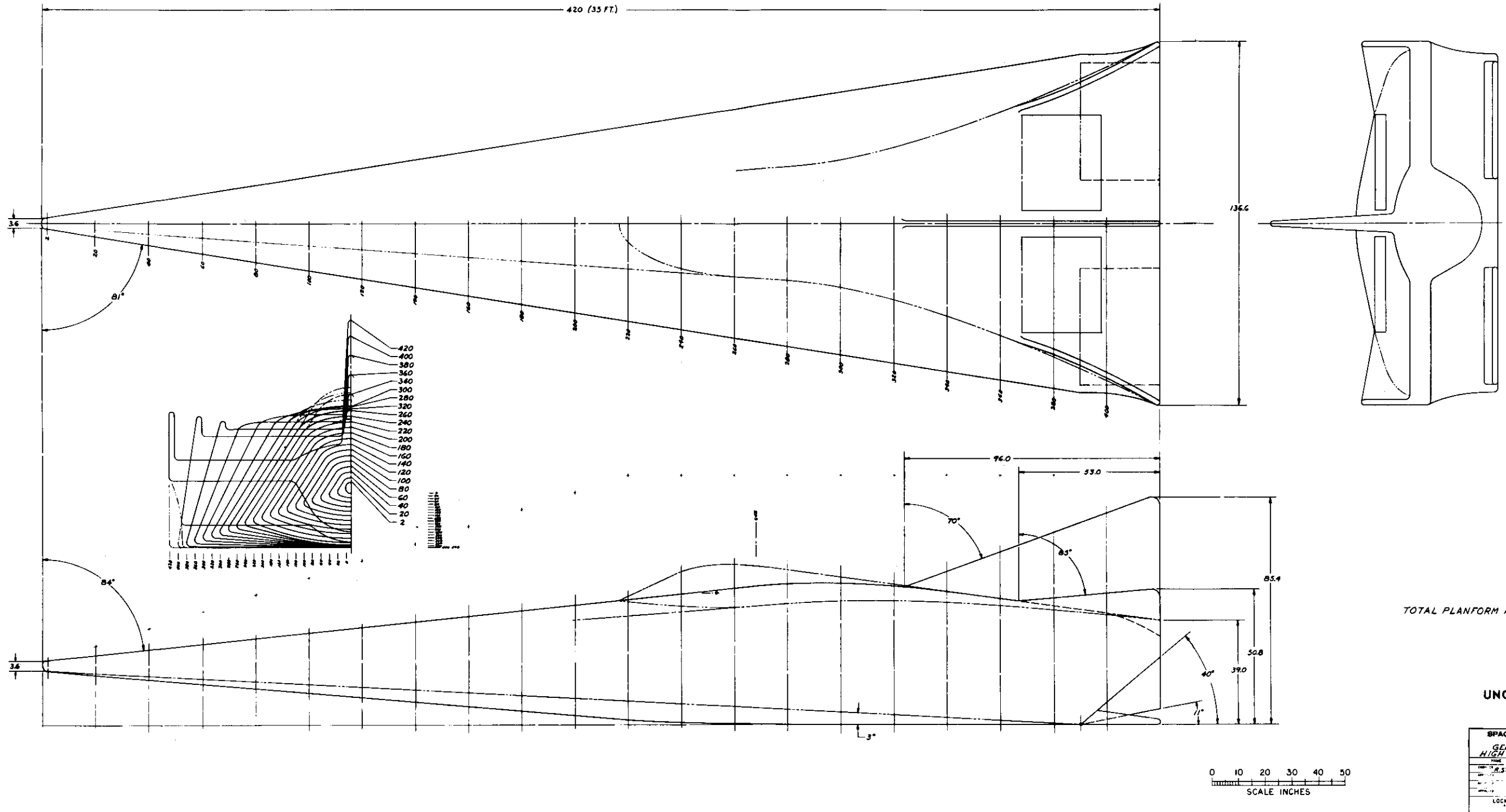
FIGURE 104 (U) GENERAL ARRANGEMENT HIGH L/D
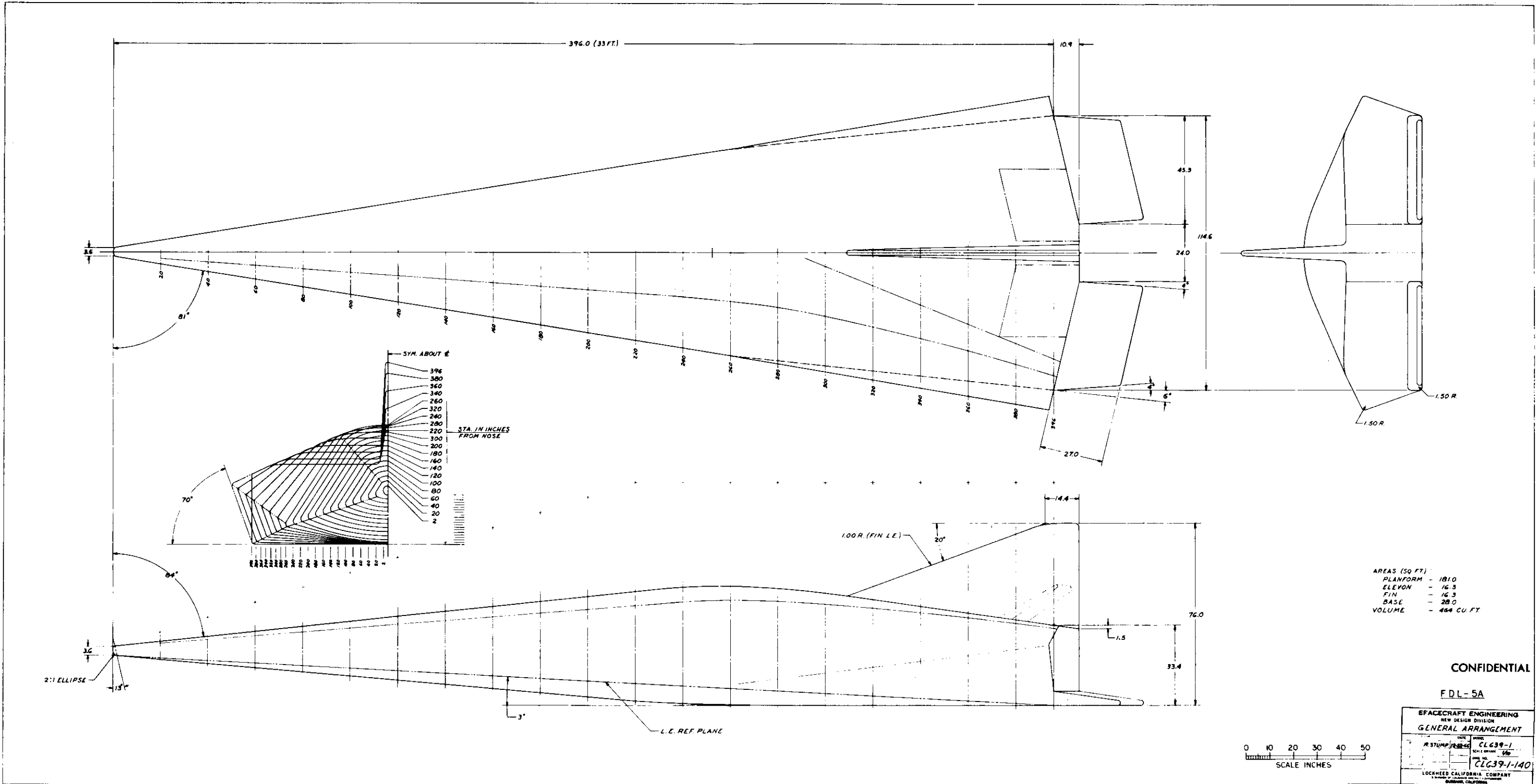LIFTING BODY - 35 FT

(REVERSE SIDE IS BLANK)

FIGURE 105   (U) FDL-5 GENERAL ARRANGEMENT

DOCUMENT CONTROL DATA - R&D

(Security classification of title, body of abstract and indexing annotation must be entered when the overall report is classified)

1. ORIGINATING ACTIVITY (Corporate author)	2a. REPORT SECURITY CLASSIFICATION
Lockheed Aircraft Corporation Burbank, California	CONFIDENTIAL
	2b. GROUP 4

3. REPORT TITLE

Preliminary Design and Experimental Investigation of the FDL-5A Unmanned High L/D Spacecraft - Part II, Parametric Configuration Development and Evolution

4. DESCRIPTIVE NOTES (Type of report and inclusive dates)

Final Report - (1 July 1966 through 31 March 1968)

5. AUTHOR(S) (Last name, first name, initial)

Ehrlich, Carl F. and Guard, Frederick L.

6. REPORT DATE	7a. TOTAL NO. OF PAGES	7b. NO. OF REFS
March 1968	143	19

8a. CONTRACT OR GRANT NO.	9a. ORIGINATOR'S REPORT NUMBER(S)
Contract No. AF 33(615)-5241	LR 21204
b. PROJECT NO. 1366	LAC/619516
c.	9b. OTHER REPORT NO(S) (Any other numbers that may be assigned this report)
d.	AFFDL-TR-68-24 Part II

10. AVAILABILITY/LIMITATION NOTICES

This report is subject to special export controls and each transmittal to foreign governments or foreign nationals may be made only with prior approval of the Air Force Flight Dynamics Laboratory (FDMS) Wright-Patterson Air Force Base, Ohio 45433

11. SUPPLEMENTARY NOTES	12. SPONSORING MILITARY ACTIVITY
	Air Force Flight Dynamics Air Force Systems Command Wright Patterson Air Force Base, Ohio 45433

13. ABSTRACT

The derivation of two volumetric efficient high L/D entry vehicles is described. Parametric trades in the areas of aerodynamics and aerothermodynamics are discussed and selected parameters are identified. Alternate modes of vehicle recovery are described and the effect on vehicle design determined. The evolution of the FDL-5 configuration selected for wind tunnel testing is described through the presentation of a series of intermediate configurations.

14. KEY WORDS	LINK A		LINK B		LINK C	
	ROLE	WT	ROLE	WT	ROLE	WT
* High L/D Entry Vehicles						
* FDL-5 Configuration						
* Vehicle Recovery						
* Aerodynamics						
* Aerothermodynamics						

INSTRUCTIONS

1. ORIGINATING ACTIVITY: Enter the name and address of the contractor, subcontractor, grantee, Department of Defense activity or other organization *(corporate author)* issuing the report.

2a. REPORT SECURITY CLASSIFICATION: Enter the overall security classification of the report. Indicate whether "Restricted Data" is included. Marking is to be in accordance with appropriate security regulations.

2b. GROUP: Automatic downgrading is specified in DoD Directive 5200.10 and Armed Forces Industrial Manual. Enter the group number. Also, when applicable, show that optional markings have been used for Group 3 and Group 4 as authorized.

3. REPORT TITLE: Enter the complete report title in all capital letters. Titles in all cases should be unclassified. If a meaningful title cannot be selected without classification, show title classification in all capitals in parenthesis immediately following the title.

4. DESCRIPTIVE NOTES: If appropriate, enter the type of report, e.g., interim, progress, summary, annual, or final. Give the inclusive dates when a specific reporting period is covered.

5. AUTHOR(S): Enter the name(s) of author(s) as shown on or in the report. Enter last name, first name, middle initial. If military, show rank and branch of service. The name of the principal author is an absolute minimum requirement.

6. REPORT DATE: Enter the date of the report as day, month, year; or month, year. If more than one date appears on the report, use date of publication.

7a. TOTAL NUMBER OF PAGES: The total page count should follow normal pagination procedures, i.e., enter the number of pages containing information.

7b. NUMBER OF REFERENCES: Enter the total number of references cited in the report.

8a. CONTRACT OR GRANT NUMBER: If appropriate, enter the applicable number of the contract or grant under which the report was written.

8b, 8c, & 8d. PROJECT NUMBER: Enter the appropriate military department identification, such as project number, subproject number, system numbers, task number, etc.

9a. ORIGINATOR'S REPORT NUMBER(S): Enter the official report number by which the document will be identified and controlled by the originating activity. This number must be unique to this report.

9b. OTHER REPORT NUMBER(S): If the report has been assigned any other report numbers *(either by the originator or by the sponsor)*, also enter this number(s).

10. AVAILABILITY/LIMITATION NOTICES: Enter any limitations on further dissemination of the report, other than those imposed by security classification, using standard statements such as:

(1) "Qualified requesters may obtain copies of this report from DDC."

(2) "Foreign announcement and dissemination of this report by DDC is not authorized."

(3) "U. S. Government agencies may obtain copies of this report directly from DDC. Other qualified DDC users shall request through

_____."

(4) "U. S. military agencies may obtain copies of this report directly from DDC. Other qualified users shall request through

_____."

(5) "All distribution of this report is controlled. Qualified DDC users shall request through

_____."

If the report has been furnished to the Office of Technical Services, Department of Commerce, for sale to the public, indicate this fact and enter the price, if known.

11. SUPPLEMENTARY NOTES: Use for additional explanatory notes.

12. SPONSORING MILITARY ACTIVITY: Enter the name of the departmental project office or laboratory sponsoring *(paying for)* the research and development. Include address.

13 ABSTRACT: Enter an abstract giving a brief and factual summary of the document indicative of the report, even though it may also appear elsewhere in the body of the technical report. If additional space is required, a continuation sheet shall be attached.

It is highly desirable that the abstract of classified reports be unclassified. Each paragraph of the abstract shall end with an indication of the military security classification of the information in the paragraph, represented as *(TS)*, *(S)*, *(C)*, or *(U)*.

There is no limitation on the length of the abstract. However, the suggested length is from 150 to 225 words.

14. KEY WORDS: Key words are technically meaningful terms or short phrases that characterize a report and may be used as index entries for cataloging the report. Key words must be selected so that no security classification is required. Identifiers, such as equipment model designation, trade name, military project code name, geographic location, may be used as key words but will be followed by an indication of technical context. The assignment of links, roles, and weights is optional.